IN-PROCESS WELD QUALITY MONITORING TECHNIQUES

FOR RESISTANCE-SPOT WELDS

by

SABYASACHI BHATTACHARYA

A Thesis Submitted in Fulfilment of

the Requirement for the Degree of

Doctor of Philosophy

Faculty of Engineering,

The University of Aston in Birmingham,

DECEMBER 1972

SUMMARY

Dynamic resistance and thermal condition of the weld are the two process parameters which are monitored and related to weld quality of resistance-spot welds in mild steel.

The investigation reported in Part I is concerned with measurement and application of dynamic or instantaneous resistance of spot welds. Thus, an electronic instrumentation system has been designed which computes dynamic resistance. The results of investigation show that the pattern of variation exhibited by the instantaneous resistance of a spot weld is indicative of the state of nugget growth and therefore can be used in monitoring weld quality.

In Part II of the dissertation thermal condition of the weld is related to the state of nugget growth. The thermal condition of the weld, in this instance, is assessed from the monochromatic radiant emission from the weld surface, thermal radiation from the weld being collected through an aperture at the electrode tip.

In addition, a mathematical equation has been developed for initial static resistance of the weldment; also, probable forms of equations relating dynamic resistance and time are suggested. It is also demonstrated that the classical ψ-θ theorem is a more reliable basis for deriving any relationship connecting weld voltage and weld temperature.

CONTENTS

PART II

WELD QUALITY MONITORING BY DETECTING THERMAL

RADIATION FROM THE WELD

ACKNOWLEDGEMENTS

APPENDICES

PUBLICATIONS

1.　"Temperature Measurement of Resistance Spot Welds,"
S. Bhattacharya and D.R.Andrews, Welding and Metal
Fabrication, 1969, 37, 448-49.

2.　"Resistance Weld Quality Monitoring,",
S. Bhattacharya and D.R.Andrews - Paper presented at the
Conference on Steel Sheet and Strip Welding, Kenilworth,
March 1972, and subsequently published in the Sheet Metal
Industries, 1972, 49, 460-66.

LIST OF ILLUSTRATIONS

LIST OF SYMBOLS

A = Area of emitting surface.

A_c = Gain of the amplifier in the current branch.

A_v = Gain of the amplifier in the voltage branch.

A_x, A_y, A_z = Radius of macroscopic area of contact.

a_c = Radius of each microcontact.

a_m = Derived constant defined by optical pass-band.

b_1, b_2 = Derived constants defined by optical pass-band.

c_1 = First radiation constant.

c_2 = Second radiation constant.

d_t = Electrode tip diameter.

e_c = Output voltage of the current branch.

e_v = Output voltage of the voltage branch.

E_o = Output voltage of the instrumentation system used in measuring dynamic resistance.

$F, F(L)$ = Fraction or numerical coefficient in radiant power calculations over finite waveband.

F_λ = Transmittance of optical filter.

I_1, I_2 = Photocurrent output.

i_D = Detector output current.

i_w = Instantaneous welding current.

j = Operator "j".

k_a = Attenuation constant.

k_D = Constant for the signal processing system in radiation detection.

k_m = Constant defined by monochromatic pass-band.

k_θ = Fraction (of radiant flux) determined by angle θ.

k_T = Toroid constant.

L = Optical band-width.

M = Mutual Inductance.

M_a = Macroscopic area of contact.

n_c = Total number of microcontacts.

p = Heaviside operator.

R_B = Bulk resistance.

R_T = Total static resistance.

R_x, R_y, R_z = Constriction resistance.

R_D, R_2, R_1 = Response of detection system.

R_{cc} = Constriction resistance in copper side of the contact.

R_{cs} = Constriction resistance in steel sice of the contact.

r_t = Weld resistance in the region of the initial trough of the
   dynamic resistance curve, or trough resistance.

r_w, r_w' = Instantaneous resistance of weld.

S_λ = Detector responsivity.

T = RC time constant(in Part I); temperature (in Part II).

T_1, T_2, T_3, T_4 = Temperature.

T_a = Ambient temperature.

T_c = Maximum contact temperature.

T_u = Ultimate temperature.

T_{s1}, T_{s2}, T_{s3} = Surface temperature.

t, t' = Time or Weld Time.

t_s = Thickness of steel sheet.

t_λ = Transmissivity of optical medium.

V_c = R.M.S. value of contact voltage.

V_w = R.M.S. value of weld voltage.

v_t = Instantaneous output voltage of toroid.

v_w = Instantaneous weld voltage.

W_1, W_2, W_3 = Hemispherical spectral radiant intensity.

$W(\lambda,T)$ = Hemispherical spectral radiant intensity corresponding to wavelength λ and temperature T.

D^*_λ = Normalized detectivity, read as "dee-star lambda".

ϵ_λ = Spectral emittance.

$\lambda, \lambda_0, \lambda_1, \lambda_2$ = Wavelength of thermal radiation.

ρ_c = Resistivity of copper.

ρ_s = Resistivity of steel.

σ = Stefan-Boltzmann radiation constant.

ω = Angular frequency.

$\mu_\theta, (\mu_\theta)_k$ = Some critical material property influencing dynamic resistance characteristics.

1. GENERAL INTRODUCTION

1.1 Inspection and Testing of Spot Welds

In the automobile and aircraft industries, resistance-spot welding is a well established production method. Over the years, various methods of inspecting the reliability of spot welds have been devised. More recently, however, the safety requirements of motor cars manufactured and marketed in the United States call for more stringent measures to ensure reliability of fabrication methods. The safety requirements for the aircraft industry have always been strict, and will become even more demanding with the advent of larger and faster aircraft in the near future. Thus, inspection of spot welded joints for 'quality' and consistent 'quality control' under production conditions will be of greater importance in the years to come. In the context of testing or inspection of spot welds, the term 'quality' will be used to mean 'suitability for service', involving, as it invariably does, an occasional misuse or overload. The term 'quality control', in this context, will be used to denote 'maintenance of an agreed quality'.

Spot welds can be tested for quality using destructive as well as non-destructive methods. Both macro-examination and the tension-shear test, commonly employed for destructive testing, give comparatively positive indications of weld quality. However, in metal fabrication industries, where the spot welding process is to be used as a reliable production technique, objections to the destructive methods of inspection stem from the following reasons:

(a) The tension-shear test is not always suitable unless the shape and size of the work-piece falls within certain limits; the macro-etch test can be carried out only with a small number of specimens from a production batch, because of the time involved in such tests.

(b) No corrective action can be undertaken during the welding operation, and it becomes necessary to incorporate an additional testing or inspection stage in the production line.

The aim of a suitable technique for inspection of spot welds by non-destructive means should be to provide an indication of the quality of the weld during welding, so that no additional inspection at a later stage is necessary as a routine measure. The term 'monitoring', in this context, will be used to denote such in-process techniques of non-destructive inspection. Any physical phenomenon, observable as a manifestation of the physical processes during a spot weld and which can be correlated to the formation of a weld nugget, may find potential application in weld-quality monitoring. In the present context, any consistent indication signifying the state of development of a nugget may be termed a 'process parameter'.

Whether a closed-loop system, where weld quality can be controlled within agreed limits of acceptance by automatic adjustment of the welding variables, is desirable or not may be a moot point; it will, however, be generally agreed that development of a simple and dependable monitoring system, where the progress of nugget growth is indicated by a suitable process parameter, is the first step towards realization of more complex systems.

1.2 Survey of Monitoring Techniques

A brief survey of the more important techniques of weld-quality monitoring is given in the following paragraph.

The fact that some relationship exists between the state of development of weld nugget and the pattern of variation exhibited by the electrical resistance of the weld has been known to the researchers in the field for some time; investigation in this respect was carried

out by   several researchers[1,2,3,4,5] with a view to establishing

some correlation between the pattern of resistance variation and the

growth of weld nugget. Similar investigations[6,7,8] were also under-

taken in attempts to relate weld voltage or electrode voltage to nugget

growth. Recently, attention has been drawn to the fact that the thermal

expansion of the work-piece can be detected as a relative movement of

one electrode with respect to the other, and monitoring techniques have

been developed[9,10] employing the 'expansion' principle. Inspection of

welded joints produced by processes other than spot welding by ultra-

sonic techniques has been in existence for some time; in recent years,

however, ultrasonic techniques have been developed[11,12,13] for in-

process monitoring of resistance-spot welds. Although varying degrees

of success have been claimed for the monitoring techniques cited above,

some confusion still exists as to the selection of the most reliable

technique under industrial conditions.

1.3 Objectives of the Present Investigation and Outlines
   of the Dissertation

Research work, in this instance, was carried out using low-carbon

mild steel, and single resistance-spot welds were mainly considered for

this purpose. The principal objective of the present research was to

investigate the application potential of two process parameters -

(a) electrical resistance of the weld, and (b) thermal condition of the

weld, in weld-quality monitoring. The main body of the dissertation is

divided into two parts, Part I and Part II. The electrical resistance

of the weld is used as a process parameter in developing the monitoring

technique described in Part I; in Part II, monitoring techniques are

developed utilizing the thermal condition of the weld as a process

parameter.

The investigation undertaken in Part I had the following objectives:

1. To develop an electronic instrumentation system whereby the instantaneous or dynamic resistance of the weld can be computed from the weld voltage and welding current, and obtained directly as a voltage signal.

2. To investigate the effects of altering the welding variables such as welding current, weld time, electrode force, and other conditions influencing the weld.

3. To outline a technique whereby dynamic resistance can be utilized in monitoring weld quality.

The electronic instrumentation system designed for computing dynamic resistance is discussed in detail in Section 5. It is shown in Section 6 that the pattern of dynamic resistance variation can be interpreted in terms of the development of weld nugget. Again, in Section 7, it is shown that the pattern of dynamic resistance variation is modified by the selection of the welding variables and other external conditions. Thus, the welding variables can be selected correctly within a narrow band for the production of a good weld, and the completion of a good weld in mild steel can be predicted from the characteristic shape of the dynamic resistance curve. Finally, in Section 8, some simple techniques are outlined whereby the dynamic resistance characteristic can be utilized for initial selection of welding variables and in in-process monitoring of weld quality.

The second half or Part II of the dissertation introduces a distinctly different concept of monitoring weld quality. Since attainment of a suitably high temperature by the weldment in the immediate vicinity of the electrodes is an essential requirement for

the production of a good weld, it is natural to assume that some indication of the thermal condition of the bulk metal bounded by the electrode tips may be used as a process parameter in monitoring weld formation. The investigation reported in Part II had the following objectives:

(i)   To devise practical methods of collecting and detecting thermal radiation from the weld.

(ii) To develop electronic detection systems whereby an indication representative of the thermal condition of the weld may be obtained according to the principles of radiation pyrometry.

(iii) To obtain experimental results so that the effects of altering the welding variables and other external conditions can be related to the signal recorded as an output of the detection systems referred to in (ii).

The technique of collecting thermal radiation through a minute aperture at the electrode tip, for visual observation as well as photoelectric detection, is developed in Section 10. The underlying theory relating monochromatic emission from the weld surface and the progress of nugget formation is given in Section 11. In Sections 12 and 13, the various electronic detection techniques employing photo-electric detectors are discussed. Finally, in Section 14, it is shown that the pattern of monochromatic radiant intensity variation of the radiation emitted by the weld surface is modified by the choice of the welding variables and other external conditions. The monochromatic radiant emission from the weld surface can, therefore, be utilized in monitoring weld quality.

Separate introductory Sections are included in Part I and Part II, along with an appropriate summary of conclusions in each case. The

analysis and interpretation of experimental results are qualitative
for most part of the dissertation, since exact values of any monitored
indication are of little use unless the specification of the weld are
defined precisely within narrow limits. Macro-examination and tension-
shear tests were used for testing weld quality, the results of such
destructive tests being compared with the monitored indication revealed
by the dynamic resistance characteristics of Part I and the monochro-
matic emission characteristics of Part II. The main objective in
analysing and interpreting the recorded characteristics was to show that
a relationship existed between weld quality and the pattern of variation
exhibited by the monitored process parameters, namely dynamic resistance
and monochromatic radiant intensity.

A short review of certain theoretical aspects in spot welding is
presented in Section 15. Thus, a mathematical equation is derived which
expresses the initial static resistance of the weldment in terms of the
resistivity and thickness of the work-piece, resistivity of the electrode
material and the diameter of the electrode tips; by analogy with
Van der Waal's equation of state for real gases, the probable form of a
mathematical equation relating dynamic resistance and time, for a good
weld in mild steel and other materials, is also suggested.

In Section 16, the concluding Section, the various process para-
meters of potential application in monitoring weld quality are compared
and contrasted. It is shown that the relationship connecting weld
voltage and weld temperature is more reliable when derived on the basis
of the classical $\psi-\theta$ theorem, and that Archer's equation[6] relating
weld voltage and weld temperature has some serious drawbacks and lacks
the rigour of similar equations based on the $\psi-\theta$ theorem.

Variation in spectral emittance of the weld surface due to different surface conditions, material properties, and change in temperature introduces a certain amount of inaccuracy in the indicated output of a monitoring system based on monochromatic radiant power measurements. It is therefore suggested in Section 16 that an improved monitoring system can be developed by applying the principle of bichromatic response ratio measurement.

The relationship between electrical and thermal conductivity of metallic conductors, the constriction resistance of a circular area of contact, and the classical ψ-θ theorem are dealt with in Appendices 1, 2 and 3 respectively. The radiation laws and the basic principles of radiation pyrometry are outlined in Appendix 4. Certain features of the photodetectors, the light-guide, and the optical filter, employed in the design of the various detection systems are included in Appendix 5.

The terminology used in the Welding Handbook[14] and the Resistance Welding Manual[15] is adhered to, in most cases, in describing and defining various terms in resistance-spot welding. Other terms and letter symbols, used in the dissertation, are mostly in accordance with the SI system of units. Graphical symbols used in electronic diagrams are, in most cases, in accordance with the appropriate British Standard specifications*. In expressing numerical values of physical quantities, the SI unit is followed by the older unit within parenthesis.

---

* B.S.3939, 1966 with subsequent additions at later dates.

2.   WELDING MACHINE, ELECTRODES, AND MATERIALS UNDER INVESTIGATION

2.1   Welding Machine and Electronic Control Unit

A 10 kVA bench SPOT/PROJECTION welder in conjunction with an
electronic control unit was used in the present investigation; both
the machine and the electronic control unit are manufactured by the
British Federal Welder and Machine Company Limited. The British
Federal type S5SW/1 electronic control unit provides synchronous timing
control and phase-shift heat control[16]. 'Squeeze' time, weld time,
'hold' or 'forge' time and 'off' time can be selected as a specific
number of cycles of the supply frequency by setting the appropriate
knobs of the electronic control unit; similarly, by setting the 'weld
heat' control knob, phase-shift control of welding current can be
achieved. A British Federal current meter was used in conjunction
with a toroid to measure welding current. The current meter registers
the r.m.s. value over the half-cycle during which maximum welding
current flows through the weld; the current read from the current
meter is termed the "peak r.m.s." current.

The electrode pressure can be set by adjusting the air-pressure
control valve mounted on the machine. The static electrode force was
measured by a statimeter*, and the calibration graph of Figure 2.1 is
plotted for various values of air pressure. Thus the electrode force
corresponding to any pressure gauge reading can be read from the cali-
bration graph.

The open-circuit voltage of the transformer secondary can be
selected by the rotary tap switch mounted on the side of the machine.

---

* The statimeter is made by Holden and Hunt Limited.

The positions marked 1 to 8 on the tap switch are in the order of increasing open-circuit voltage.

2.2 Electrodes

Sciaky tiptrodes* were used as electrodes in the experimental investigation. A typical Sciaky tiptrode is made of two parts - the electrode body and the tip, the electrode tip being held in position by means of a retaining ring. A detailed diagram of a tiptrode is shown in Figure 2.2. For the investigation of Part II, it was necessary to bore holes in the electrode holder; consequently, the electrodes were not water-cooled for the present investigation.

Experimental investigation, in most cases, was conducted using tiptrodes with 4.76 mm (0.1875 in.) diameter tips, except in where the diameter of the electrode tip was the variable.

2.3 Materials under Investigation

For the present investigation, low-carbon mild steel containing less than 0.1% carbon was used. One millimetre or 0.039 in. thick specimen coupons, measuring 102 mm (4 in.) x 25.4 mm (1 in.), were prepared from 20 S.W.G. mild steel stock, for a major part of the experimental work. In most cases, the specimen coupons were rubbed with a piece of dry cloth before they were offered to the electrodes; any additional surface preparation is specified otherwise. For a single spot weld, the two specimen coupons were overlapped such that the area of overlap was a square defined by the width of the coupons. Before initiating a weld, the specimen coupons were held together under pressure by bringing the top electrode down. The quality of welds

---

* 'Tiptrode' is the trade name of special electrodes marketed by Sciaky Electric Welding Machines Limited.

was tested according to the established procedures[14] of tension-shear test and macro-etch test. In the absence of any well-defined specifications for weld quality, acceptability of a weld was arbitrarily decided from destructive tests and related to the monitored indication.
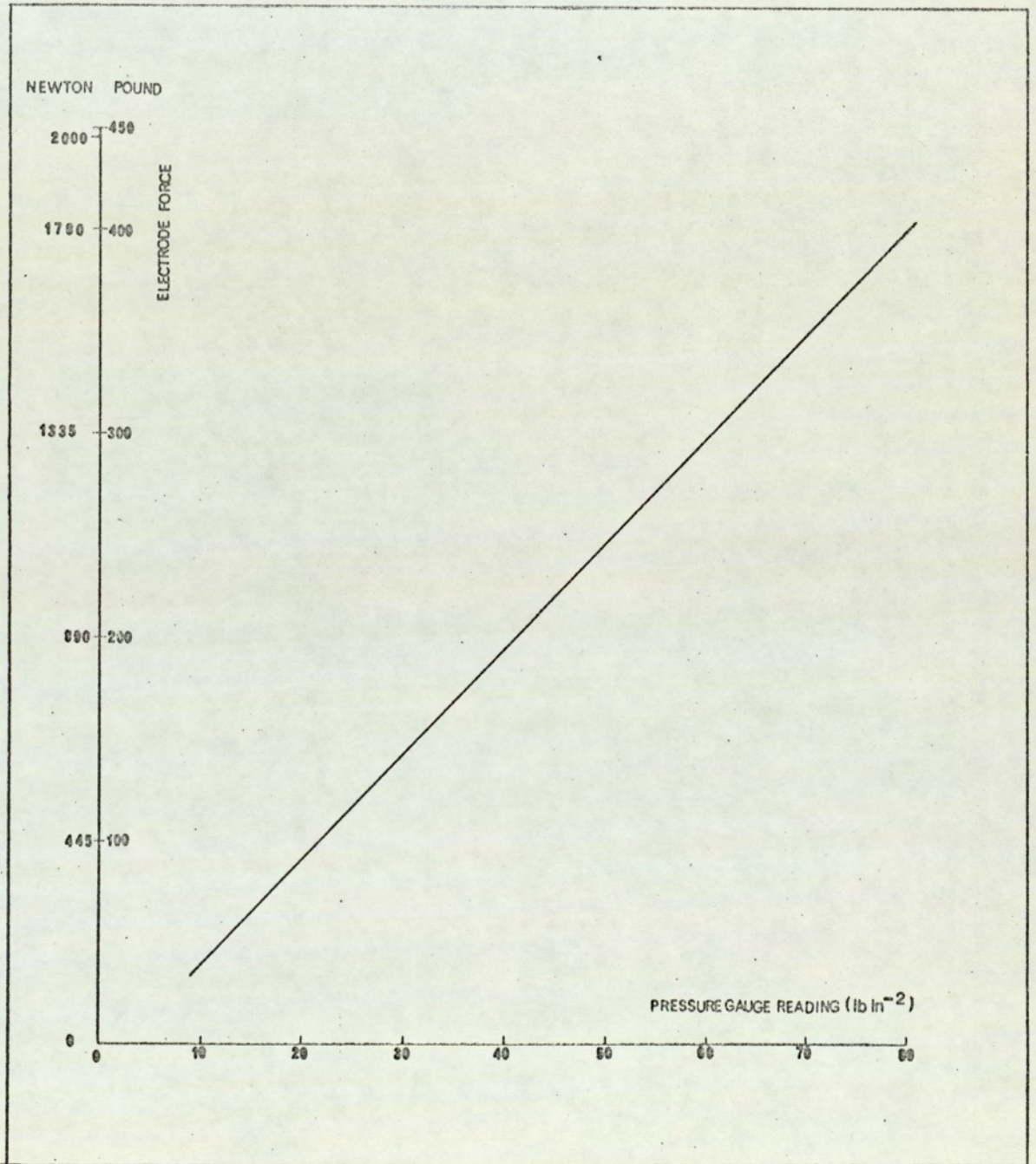
FIG. 2.1. Pressure Gauge Calibration Graph.

1- Steel Retaining Ring

2 - Rubber Ring.

Diameters

a = 4.76 mm. ($\frac{3}{16}$ in.).

b = 9.5 mm.

c = 17.5 mm.

---

d = 5.6 mm.

e = 9.5 mm.

f = 9.5 mm.

g = 25.4 mm.

h = 2 mm.

j = 44.4 mm.

Diameters

A = 17.5 mm.

B = 19 mm.

C = 25.4 mm.

D = 52 mm.

E = 8 mm.

(a)

(b)

FIG. 2.2. Sciaky Tiptrode.

(a) General Construction, Full Size;

(b) Sectional View, Twice Full Size.

PART I

DYNAMIC RESISTANCE MEASUREMENT AND ITS

APPLICATION IN MONITORING WELD QUALITY

3. <u>INTRODUCTION AND LITERATURE SURVEY</u>

The rate of heat generation in a resistance-spot weld is in accordance with the principle of Joule heat generation in a resistive element, and therefore, the electrical resistance of the weld is an important parameter governing the progress of weld nugget formation. The term 'instantaneous' or 'dynamic' resistance refers to the quotient $\frac{v_w}{i_w} = r_w$, where v_w and i_w represent instantaneous values of weld voltage and welding current respectively; weld voltage, in this context, may be defined simply as the voltage drop across the weldment. The dynamic resistance of the weld is modulated by the process itself during welding. In contrast, the static resistance offered by the specimen coupons held together under pressure, in the absence of any welding current, is a combination of the bulk resistance of the work-piece and constriction or contact resistance of the electrode-to-sheet and sheet-to-sheet contacts. Although the initial static resistance can and does influence the welding process, it can in no way indicate or characterize the physical process during welding.

Variation of the electrical resistance of spot welds was observed by Hess and Ringer[1], and Hess and Wyant[2], as early as 1939. Hess and Wyant worked with both low carbon mild steel and 18-8 stainless steel; while the dynamic resistance characteristics for mild steel showed some regularity of pattern, the same for stainless steel showed very little consistency to permit any definite correlation between weld quality and dynamic resistance. According to these authors[2] intimate contacts at the sheet-to-sheet and electrode-to-sheet interfaces are established after about a quarter of a cycle from the instant

of initiating the welding current; explanation for the pattern of
dynamic resistance variation exhibited by mild steel is, however, not
complete in the account given by Hess and Wyant.

Tylecote[3] introduced the concept that "minute areas of true
intimate metallic contact" at the interfaces are responsible for the
phenomenon of contact resistance in resistance-spot welding. The
sharp fall in resistance immediately after initiation of the welding
current was explained by Tylecote as a result of "rapid failure of
contact resistance"; evidently, Tylecote refers to the breakdown of
insulation at the sheet-to-sheet and electrode-to-sheet interfaces.
Tylecote, however, did not attempt a rigorous explanation of the
pattern of resistance variation; he concluded from his observation of
initial and final values of weld resistance that these values could
not be related to weld quality.

In 1951, Roberts[4] published an account of his exhaustive work
on resistance variations during spot welding, and the observations made
by Roberts have since been supported by the work of other researchers.
In 1952, VanSciver[5], in a paper presented at the A.I.E.E. 3rd
Conference in Detroit, made the suggestion that the observed variation
in electrical resistance of the weld could be used in monitoring weld
quality. Archer[6] proposed that the weld voltage in itself was an
indication of the state of nugget development, and put forward his idea
of controlling weld quality by constraining the weld voltage within
predetermined limits. The method suggested by Archer is also known as
the "voltage-constraint principle", and is based on the assumption
that there is a consistent relationship between weld voltage and the
ultimate temperature attained by the weld metal.

Complete systems for controlling weld quality were claimed by Paxton and Zeller[17], and Grant[18]; in both instances weld voltage was used as an indication of the physical process. Chuloshinkov and Verdenskii[7], and Lankin[19] seem to have accepted weld voltage as an indication of weld quality without questioning the validity of Archer's[6] equation for the "voltage-constraint principle".

Reference to weld voltage as an indication of weld quality has been made at this juncture, since some confusion exists in relating weld voltage and weld resistance to weld quality. The suggestion made by VanSciver[5] about monitoring weld resistance has been taken by some as being equivalent to monitoring weld voltage. Although weld voltage can be thought of as a function of weld resistance, the equation* derived by Archer[6] in propounding his "voltage-constraint principle" is not wholly admissible.

---

* See Section 16.

4. THEORY AND SIMPLIFYING ASSUMPTIONS IN MEASUREMENT OF DYNAMIC RESISTANCE

4.1 Theory

If the voltage drop across the weld at any instant is known along with the current flowing through the weld, then the electrical resistance of the weld can be calculated from Ohm's law, and expressed as

$$r_w = \frac{v_w}{i_w} \tag{4.1}.$$

In equation (4.1),

v_w = instantaneous voltage drop across the weld,

i_w = instantaneous current through the weld,

r_w = instantaneous or dynamic resistance of the weld.

4.2 Simplifying Assumptions

(i) Strictly speaking, the electrical load offered by the weldment is resistive as well as inductive. The inductive loading is influenced by the Machine geometry and size and material properties of the work-piece. In this instance, the electrical impedance of the work-piece is assumed to be purely resistive. From the typical experimental values cited by Roberts[4], the error in calculating dynamic resistance introduced by such an assumption is in the region of 1%.

(ii) The term 'instantaneous' usually refers to measurements made over very short intervals of time during which the variable may be assumed to remain constant. Theoretically, such periods of time have to be extremely short. Roberts[4] calculated the values of resistance at the instants of peak current during each half-cycle; and more recently, Savage et al[20] found from their work that the dynamic resistance remained constant within each individual half-cycle. Accordingly, instantaneous resistance is defined as the

resistance of the weld computed at the instant of peak current during each half-cycle, and this definition will be used throughout unless specified otherwise.

(iii) The term electrode voltage refers to the voltage developed across the electrodes at any instant during a weld. In contrast, the term weld voltage may be defined as the voltage drop across the weldment such that the voltage drop due to the body resistance of the electrodes is excluded. Precise measurement of weld voltage according to the above definition is very difficult in practice, and in the published literature authors have not adhered to any such strict definition. Under laboratory conditions, the voltage drop across the weld may be obtained by using special probes similar to those used by Hayward[21]. Use of such special probes, however, may not be so convenient under common industrial conditions; therefore, for the present investigation voltage-sensing leads were located at convenient positions on the electrodes. The voltage measured in this manner represents the total voltage across the electrodes, and includes the contact voltage developed across the electrode-to-sheet contacts as well as the voltage drop in the bulk resistance of a part of each electrode. It is assumed that the voltage developed across the specified points on the electrodes is a close approximation of the actual weld voltage; experimental results due to VanSciver[5] and Roberts[4] suggest that such an assumption does not affect the pattern of dynamic resistance variation, and introduces only a small error in the absolute values of weld resistance.

5. ELECTRONIC INSTRUMENTATION SYSTEM FOR COMPUTING DYNAMIC RESISTANCE

5.1 Principle of Operation

With the exception of VanSciver[5] and Hayward[21] the previous workers calculated dynamic resistance from the recorded waveforms of weld voltage and welding current. To explore the potential of dynamic resistance as an indication of weld quality, it is necessary to devise methods so that it may be readily obtained as a meter reading or a recorded trace. Moreover, any possible application of dynamic resistance in controlling weld quality requires that an electrical signal representative of dynamic resistance be available. For the present work, a composite instrumentation system was designed to compute dynamic resistance, the resistance variation being recorded as an analogue voltage signal. Although the instrumentation system developed in this instance was used for spot welds in mild steel only, the system can be employed for investigation in stainless steel and aluminium alloys as well. It is to be noted, however, that the reported[4,22] correlation between weld quality and resistance variation applies to mild steel only.

To obtain the quotient $\frac{\text{weld voltage}}{\text{welding current}}$, d.c. signals proportional to weld voltage and welding current have been used as inputs to an electronic divider; the output of the divider is a voltage proportional to the dynamic resistance of the weld. A block diagram of the instrumentation system is shown in Figure 5.1. The top branch carrying a signal from the electrodes is termed the voltage branch, since it carries the weld voltage signal; similarly, the other branch from the toroid is referred to as the current branch, since it carries a signal proportional to the welding current.

Voltage Branch

The difference of voltages appearing across the electrodes is amplified, and passes through the full-wave precision rectifier circuit; the fluctuating d.c. voltage level e_v at the output of the precision rectifier is an undirectional representation of the a.c. weld voltage.

Current Branch

The output voltage of the toroid is attenuated and integrated; the output of the integrator is then amplified, and is taken through the full-wave precision rectifier. The resulting d.c. voltage e_c at the output of the precision rectifier is an undirectional representation of the welding current.

Divider Stage

The function of the divider stage is to operate on the inputs e_v and e_c and perform division by inverse multiplication. Output of the divider is given by

$$E_0 = -10. \frac{e_v}{e_c} \qquad (5.1),$$

where E_0 = output voltage of the divider, due to the input signals e_v and e_c.

Low-pass Filter

The low-pass filter is introduced to suppress extraneous noise and short-duration oscillations resulting from divider saturation.

5.2 Output Equation of the Instrumentation System

Let v_1, v_2 represent the voltages with respect to ground at the connection points of the voltage-sensing leads. Also, let i_w represent the welding current.

Since the differential amplifier has unity gain, the output of
the differential amplifier stage approximates to $v_w = v_1 \sim v_2$. The
input to the precision rectifier stage, and therefore the d.c. output
of the rectifier stage is given by

$$e_v = A_v \cdot v_w \qquad (5.2),$$

where A_v is a constant and represents the gain-setting of the variable-
gain amplifier in the voltage branch.

For the current branch, the toroid output can be taken as $\dfrac{i_w}{1900}$,

since the toroid constant[23] k_T is 1900 AV^{-1} according to calibration
carried out at the National Physical Laboratory. A fraction k_a of the
toroid output appears at the output of the attenuator network and is
fed into the integrator stage through the voltage follower. Thus, the

input to the integrator is $k_a \cdot \dfrac{i_w}{1900}$. Since the integrator has been

designed to operate with unity gain at 50 Hz, the final output of the
current branch is given by

$$e_c = A_c \cdot k_a \cdot \frac{i_w}{1900} \qquad (5.3),$$

where A_c represents the gain of the variable-gain amplifier in the
current branch.

Substituting for e_v and e_c from equations (5.2) and (5.3),
equation (5.1) can be written as

$$|E_0| = 10 \cdot \frac{A_v \cdot v_w \cdot 1900}{A_c \cdot k_a \cdot i_w} \qquad (5.4),$$

where $|E_0|$ represents the magnitude of the divider output.

Equation (5.4) can be re-arranged as

$$|E_0| = \frac{10 \cdot A_v \cdot 1900}{A_c \cdot k_a} \cdot \left(\frac{v_w}{i_w} \right) \qquad (5.5).$$

Substituting r_w for the quotient $\frac{V_w}{I_w}$, equation (5.5) becomes

$$|E_0| = \frac{1 \cdot 9. \; 10^4 . A_v}{A_c . \; k_a} \cdot r_w \qquad (5.6).$$

In equation (4.1), r_w has been defined as the dynamic resistance of the weld; equation (5.6) therefore gives the relationship between dynamic resistance r_w and the output E_0 of the instrumentation system. Equation (5.6) may be termed the output equation of the instrumentation system shown in Figure 5.1.

Again, from the recorded trace of E_0, dynamic resistance r_w can be calculated by re-arranging equation (5.6). Thus,

$$r_w = |E_0| . \; \frac{A_c . \; k_a}{1 \cdot 9. 10^4 . \; A_v} \qquad (5.7).$$

The low-pass filter mentioned in 5.1 has been neglected for the above derivation; when a low-pass filter with cut-off at 50 Hz is included, the output is to be multiplied by 0.707, such that the output E_0' from the low-pass filter becomes

$$E_0' = 0.707 . \; E_0 \qquad (5.8).$$

5.3 Details of Electronic Circuitry

5.3.1. Differential Amplifier in the Voltage Branch

With the bottom platen of the welding machine connected to 'earth' or 'ground', preliminary investigation showed that there was an appreciable voltage drop between 'ground' and the voltage-sensing lead on the bottom electrode. To obtain the true voltage drop across the electrodes it is necessary to measure the difference in potential at the locations of the voltage-sensing leads. Hence a differential amplifier was used at the input end of the voltage branch.

The differential amplifier shown in Figure 5.2 was designed for unity gain using a Computing Techniques type Dl-2 operational amplifier. The input-output relation of the differential amplifier is given by $e_o = e_1 - e_2$, where e_o is the output voltage for the inputs e_1 and e_2. The 5kΩ logarithmic potentiometer was used for the adjustment of gain.

5.3.2. Attenuator and Voltage Follower

The output from the toroid can be very high and may exceed the limit of maximum permissible voltage to the input of the following stage. Hence, it has been necessary to include an attenuator so that only a small fraction of the toroid output is fed into the integrator. Again, to avoid loading the attenuator circuit, a voltage follower has been included as a buffer amplifier between the attenuator network and the integrator.

The resistance network of the attenuator and the voltage follower are shown in Figure 5.3; the fraction of the toroid output appearing at each output terminal of the attenuator is indicated in each case. A selector switch 'S' was used to select the required fraction of toroid output.

A Computing Techniques type F1-7 operational amplifier was used in the voltage follower circuit. The output voltage e_o of the voltage follower equals the input voltage e_1, and there is no phase inversion.

5.3.3. Integrator

The output v_t of the toroid is given by

$$v_t = -M. \frac{di_w}{dt} \tag{5.9},$$

where M = mutual inductance between the secondary circuit of the machine and the toroid,

and $\dfrac{di_w}{dt}$ = rate of change of welding current i_w. Therefore, to obtain a signal indicative of welding current, it is necessary to integrate the voltage developed in the toroid. From equation (5.9),

$$\int V_t dt = -\int M.\, di_w = -M.i_w \qquad (5.10).$$

Therefore, $\int V_t dt$ is proportional to the welding current i_w. The integrator shown in Figure 5.4 was designed using a Computing Techniques type F1-4 operational amplifier. The output voltage e_o of the integrator is related to its input voltage e_1 by

$$e_o = -\frac{1}{Tp} \cdot e_1 \qquad (5.11).$$

where T = integrator time constant.

and p = the Heaviside operator used in operational amplifier theory.

Replacing operator 'p' by 'jω', equation (5.11) becomes

$$e_o = -\frac{1}{j\omega T} \cdot e_1 \qquad (5.12).$$

The A.C. integrator* of Figure 5.4 is a practical form for implementing the relationship of equation (5.12) in a drift-free manner. Thus, substituting $T = 3.16 \times 10^{-3} s$ and $\omega = 3.14 \times 10^2 s^{-1}$, equation (5.12) becomes

$$e_o = \frac{j}{3.14 \times 10^2 \times 3.16 \times 10^{-3}} \cdot e_1 \qquad (5.13).$$

The denominator in the right-hand side of equation (5.13) approximately equals unity, and the input-output relation of the integrator can be written as

$$\left| e_o \right| = \left| e_1 \right|.$$

---

* "Applications Manual for Operational Amplifiers", Philbrick-Nexus Research.

5.3.4. Variable-gain Amplifiers

True divider operation requires that e_v and e_c of equation (5.1) must be such that $|e_v| \leq |e_c|$; to ensure that $|e_v| \leq |e_c|$, the variable-gain amplifiers of Figures 5.5 and 5.6 were included so that the magnitude of e_v and e_c could be controlled.

The circuit of Figure 5.5 operates as a simple variable-gain amplifier when switch S_1 is closed and switch S_2 is open. With switch S_1 open and S_2 closed, the circuit operates as an adjustable lag circuit, and introduces a phase lag in the output. In this instance, however, the circuit was used as a simple variable-gain non-inverting amplifier, its voltage gain varying from 2 to 5 in unit steps.

The variable-gain non-inverting amplifier of Figure 5.6 used in the current branch had its gain calibrated between 2 and 10 in unit steps.

Computing Techniques type D1-2 operational amplifiers were used in Figures 5.5 and 5.6.

5.3.5. Full-wave Precision Rectifiers

Operation of the divider stage requires d.c. inputs, and therefore the a.c. signals derived from the welding machine were rectified. The full-wave precision rectifier of Figure 5.7 provides a negative-going output waveform; the circuit of Figure 5.8, on the other hand, produces a positive-going full-wave output waveform. The polarities of the two inputs to the divider stage were such that the divider output under these conditions was positive-going. The circuit configuration shown in Figures 5.7 and 5.8 were designed using Computing Techniques type A1-7 operational amplifiers in conjunction with Mullard type OA202 silicon diodes; in both cases the output was a unidirectional representation of the input waveform.

5.3.6. Divider Stage

Initially, a Computing Techniques type M3-2 multiplier unit was used in conjunction with a Dl-2 operational amplifier. In the circuit of Figure 5.9, however, a Philbrick-Nexus type 4450 multiplier unit has been shown in conjunction with a Philbrick-Nexus type QFT-5 operational amplifier; the Philbrick-Nexus type 4450 multiplier unit was found to be more compact and easy to install in the circuit.

The input-output relation of the divider, within the limits of its operation, is given by

$$e_0 = -10. \frac{e_a}{e_b} ,$$

where e_a and e_b represent the inputs to the divider. In fact, the polarities of signals e_a and e_b are such that e_a is always negative-going and e_b is positive-going; since the multiplier type 4450 does not introduce any sign inversion in its output, the output of the divider, with the referred polarities of e_a and e_b, is always positive.

5.3.7. Low-pass Filters

At the instants when the denominator in equation (5.1) goes through zero, the operational amplifier in the divider circuit is overloaded and spurious oscillations appear at the output of the divider stage; in addition, a considerable amount of noise is also present at the output. In order to reduce the level of spurious signals in the recorded trace the output of the divider stage was taken through a low-pass filter. Initially, low-pass active filters with cut-off frequencies at 50 Hz as well as 100 Hz were used. It was, however, found that the 50 Hz low-pass filter produced a clearer recorded trace; hence the dynamic resistance recordings, in most cases, were obtained by using the 50 Hz low-pass filter at the output.

Figures 5.10 and 5.11 show the circuit diagrams of the low-pass filters having cut-off frequencies at 50 Hz and 100 Hz respectively. In each case, the filter was designed to give 3rd order Butterworth response. An Analog Devices type 40JV operational amplifier was used in the circuit of Figure 5.10, a Computing Techniques type F1-4 operational amplifier being used in Figure 5.11. At the cut-off frequency, attenuation was 3db in each case; in other words, the output was 0.707 of the input. Beyond the cut-off frequency the attenuation rate was 60db/decade.

5.3.8. Bound and Null Circuits

'Bounding' means restriction of the output voltage to some assigned maximum, even when the input signal exceeds its assigned full-scale value of either polarity. The circuit diagram (a) in Figure 5.12 shows the zener bound circuit which may be connected parallel to the feed-back loop of the operational amplifier in the divider stage (see Figure 5.9). Inclusion of the bound circuit in the divider stage limits the output swing between +10V and -10V.

Nulling, in this context, refers to partial or complete cancell-ation of a d.c. signal level. The circuit diagram (b) of Figure 5.12 shows a zener nulling network which was used to cancel partially the standing d.c. level at the output of the divider under quiescent con-ditions. With the zener nulling network introduced between the divider output and the low-pass filter, dynamic resistance can be recorded using a more sensitive range of the recording instrument. The zener nulling network only shifts the d.c. level of the recorded signal, the general pattern of the recorded trace remaining unaltered.

5.3.9. Balancing or Trimming for Zero Offset

In circuits employing operational amplifiers, it is frequently necessary to set the output to zero for zero input condition; initial balancing or trimming for zero offset voltage was achieved, in most cases, by introducing an external voltage at the appropriate terminal of the operational amplifier. In the relevant circuit diagrams of Section 5, the potentiometer lead going to the 'balance' or 'trim' terminal of the operational amplifier is indicated by the letter T.
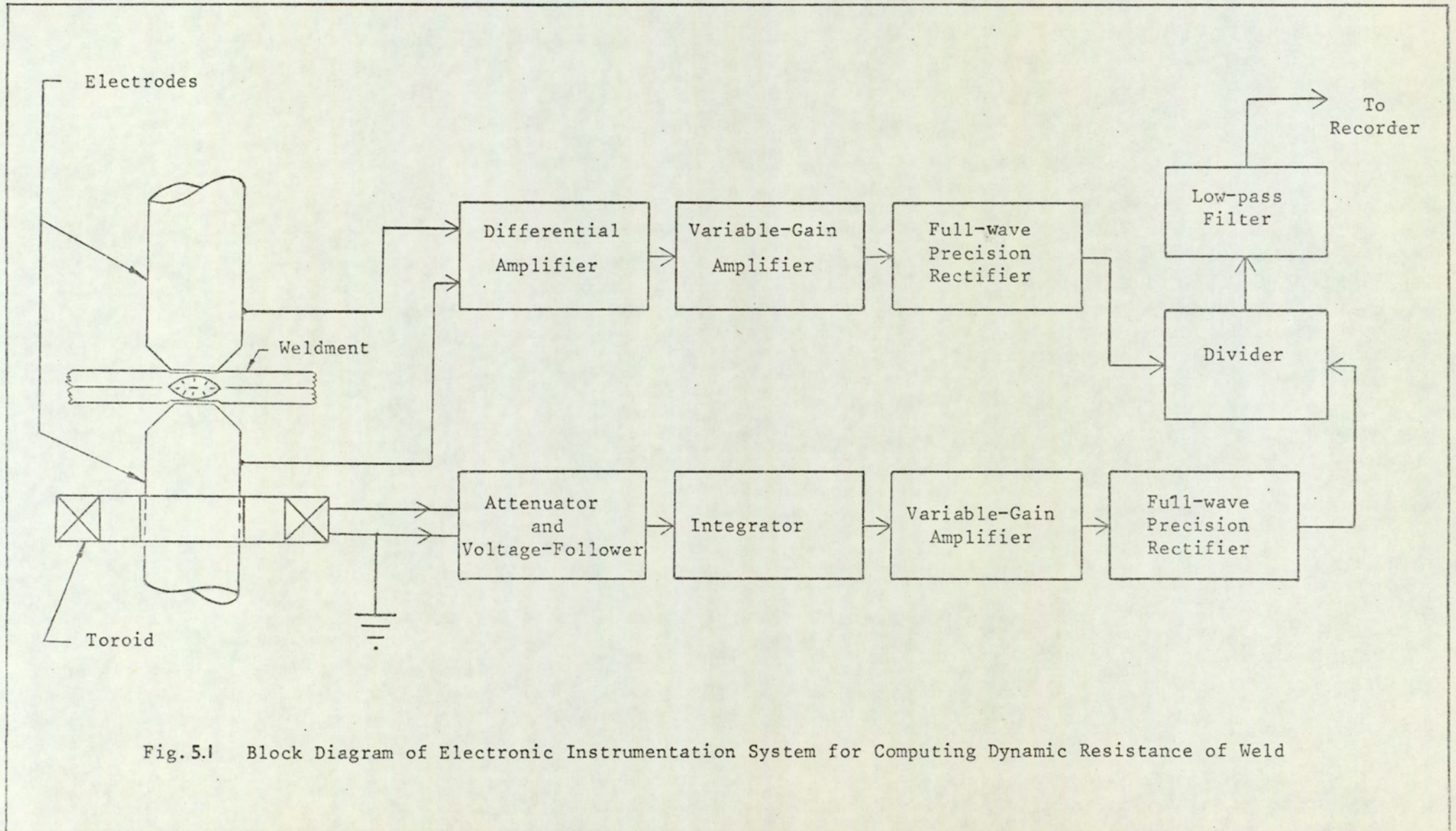
Fig. 5.1   Block Diagram of Electronic Instrumentation System for Computing Dynamic Resistance of Weld
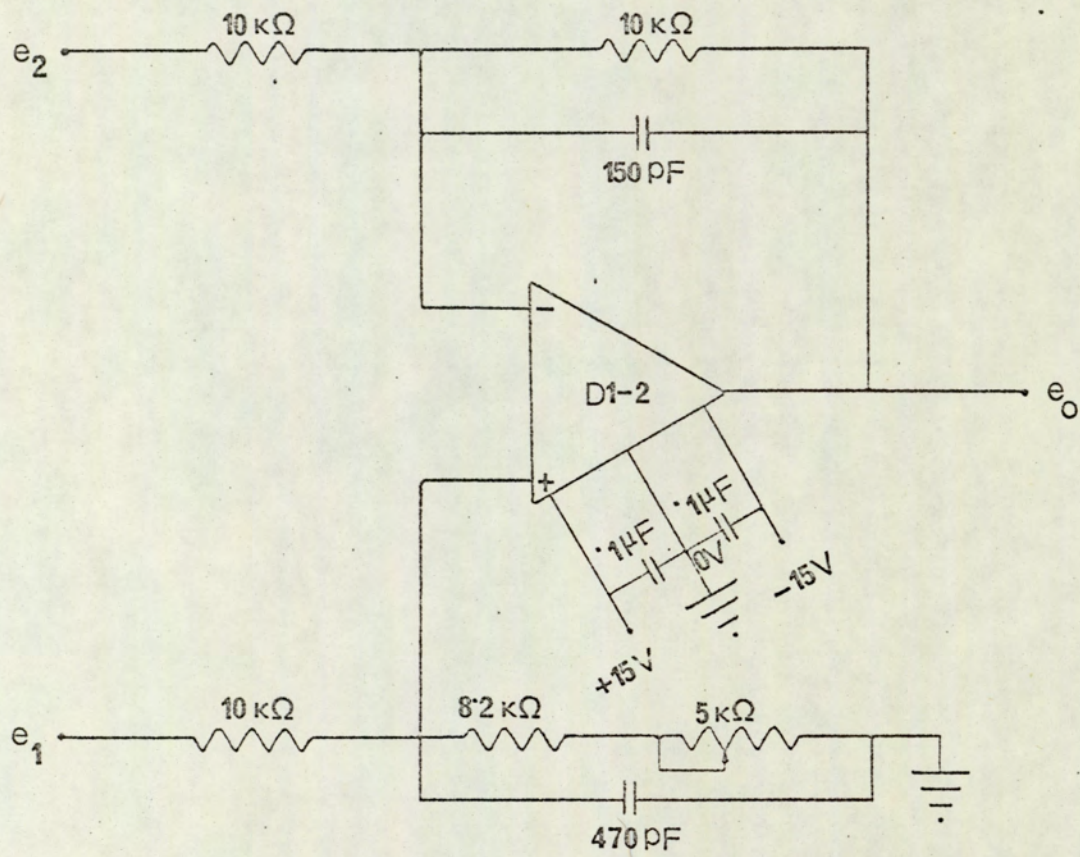
FIG. 5.2. Differential Amplifier Circuit for Voltage Branch
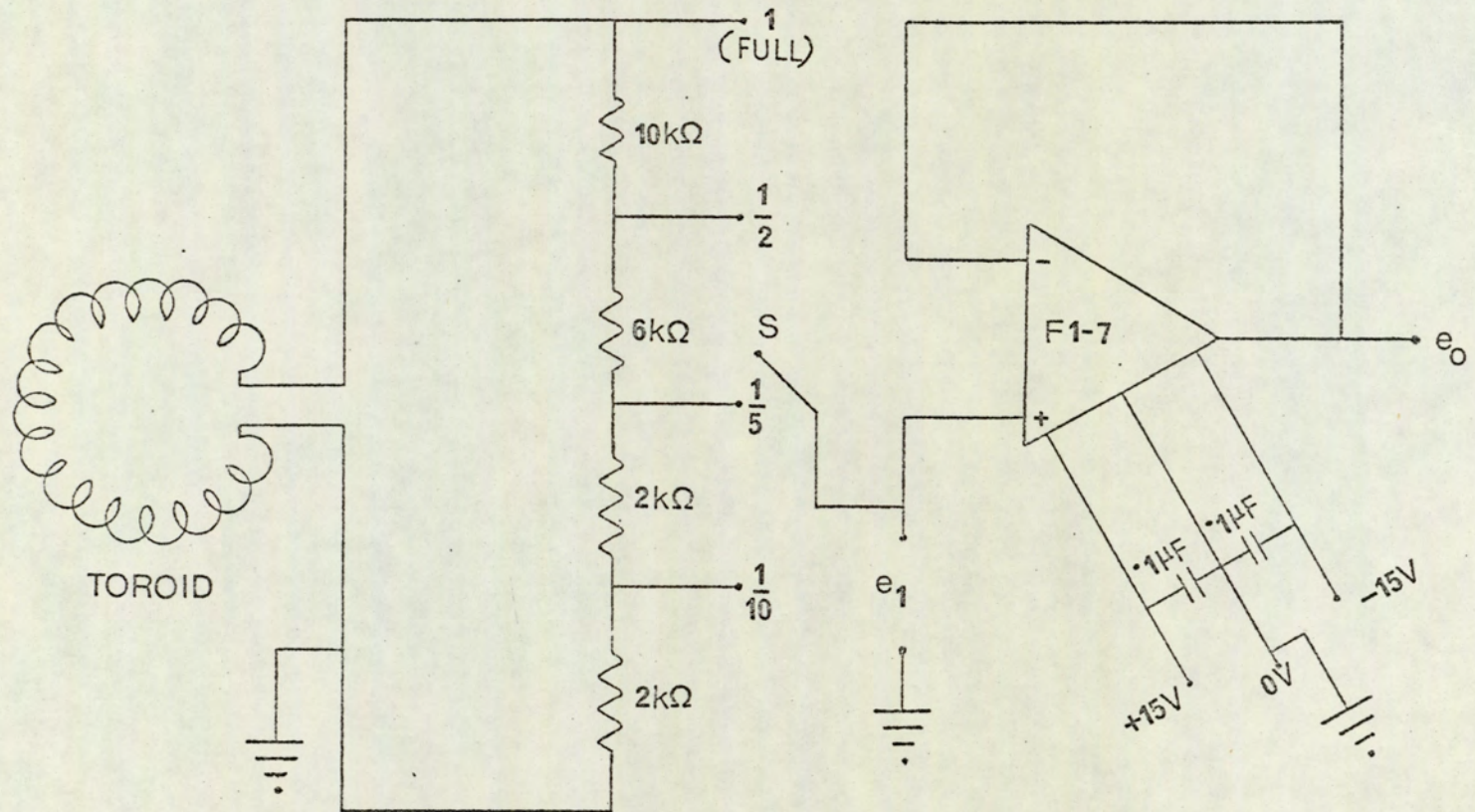
FIG. 5.3. Attenuator and Voltage Follower
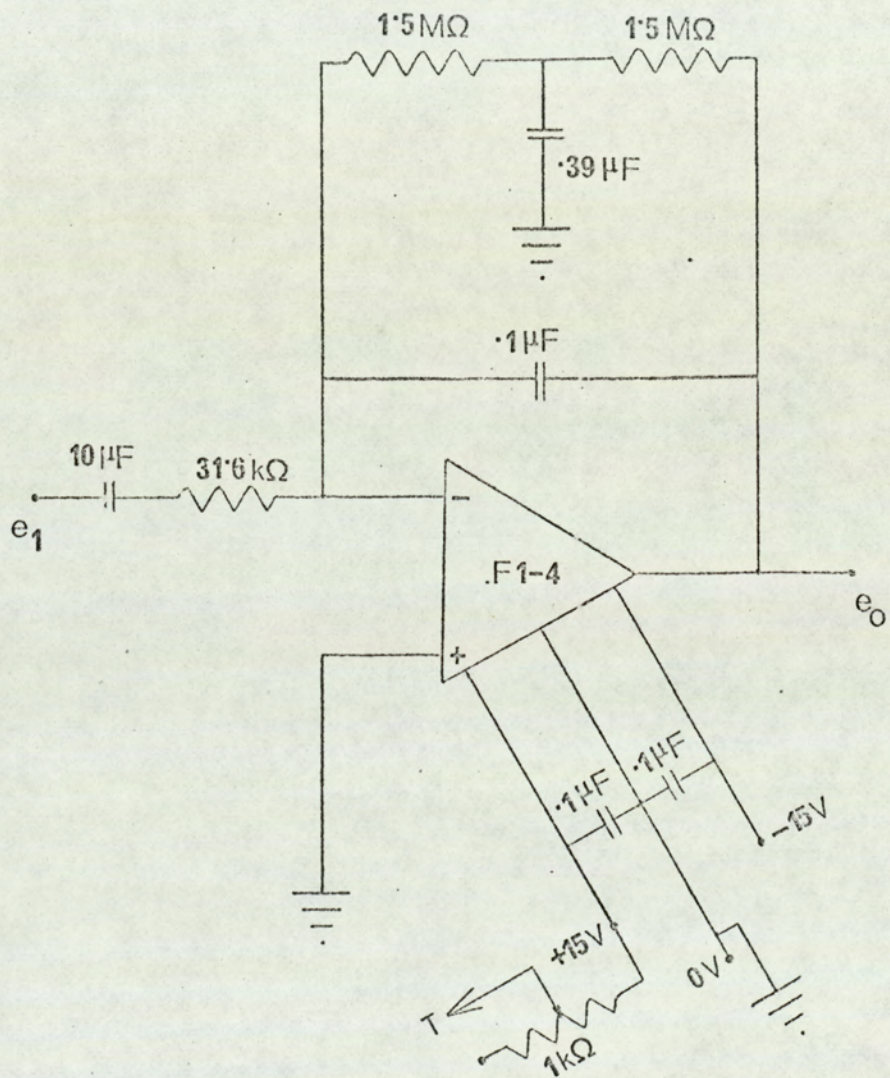
FIG. 5.4 Circuit Diagram of A.C Integrator
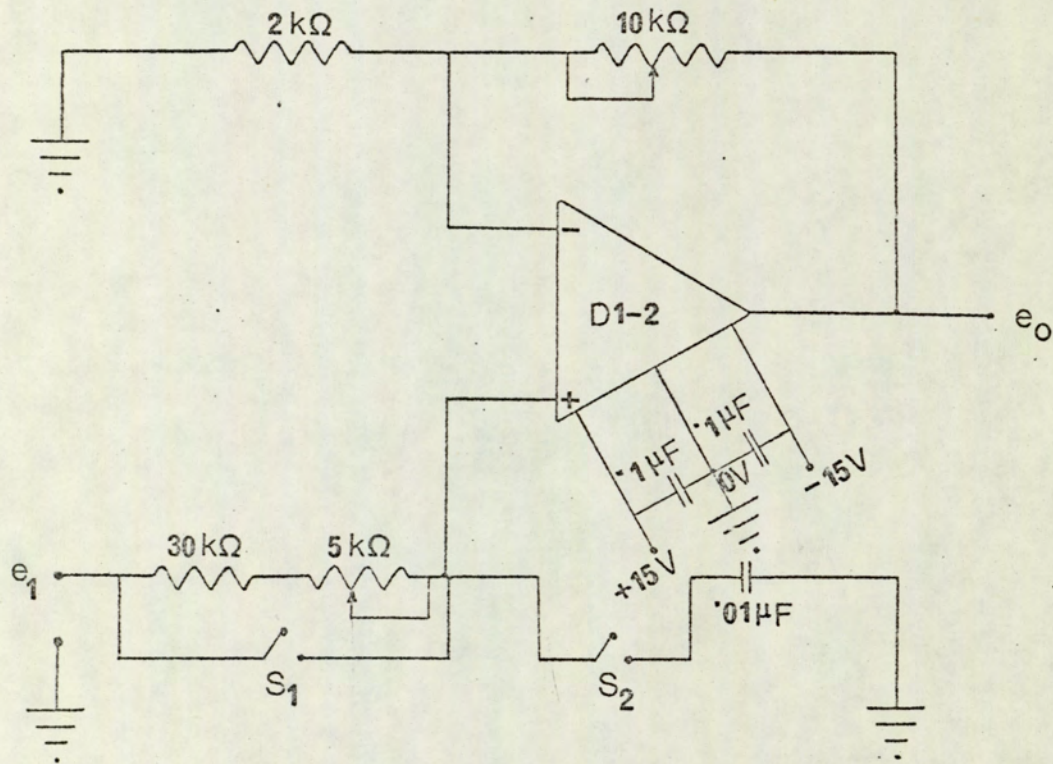
FIG. 5.5. Variable-gain Amplifier with Adjustable Phase-lag
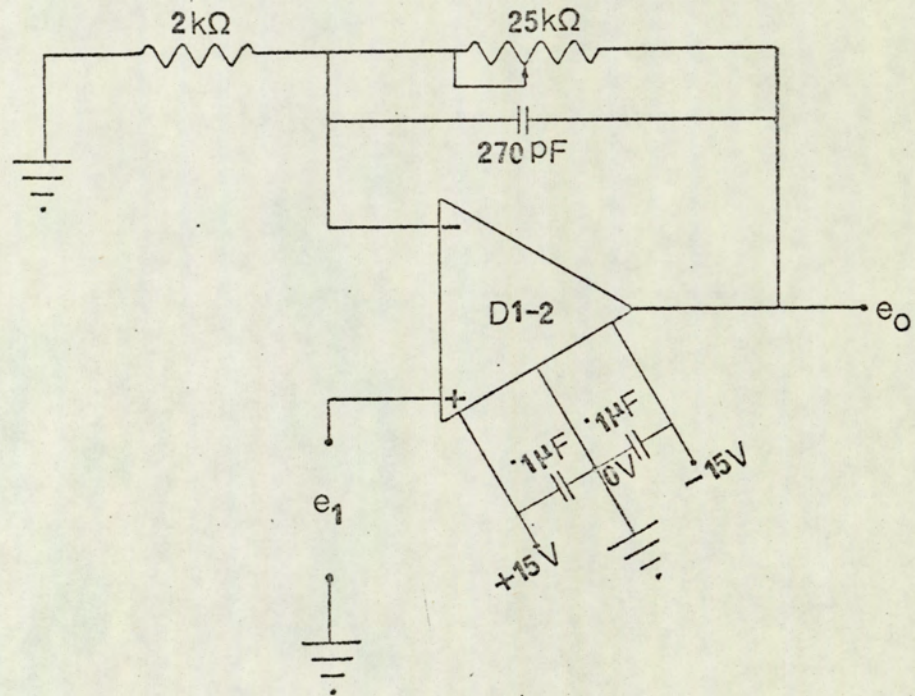
FIG. 5.6.   Variable-gain Amplifier for Current Branch
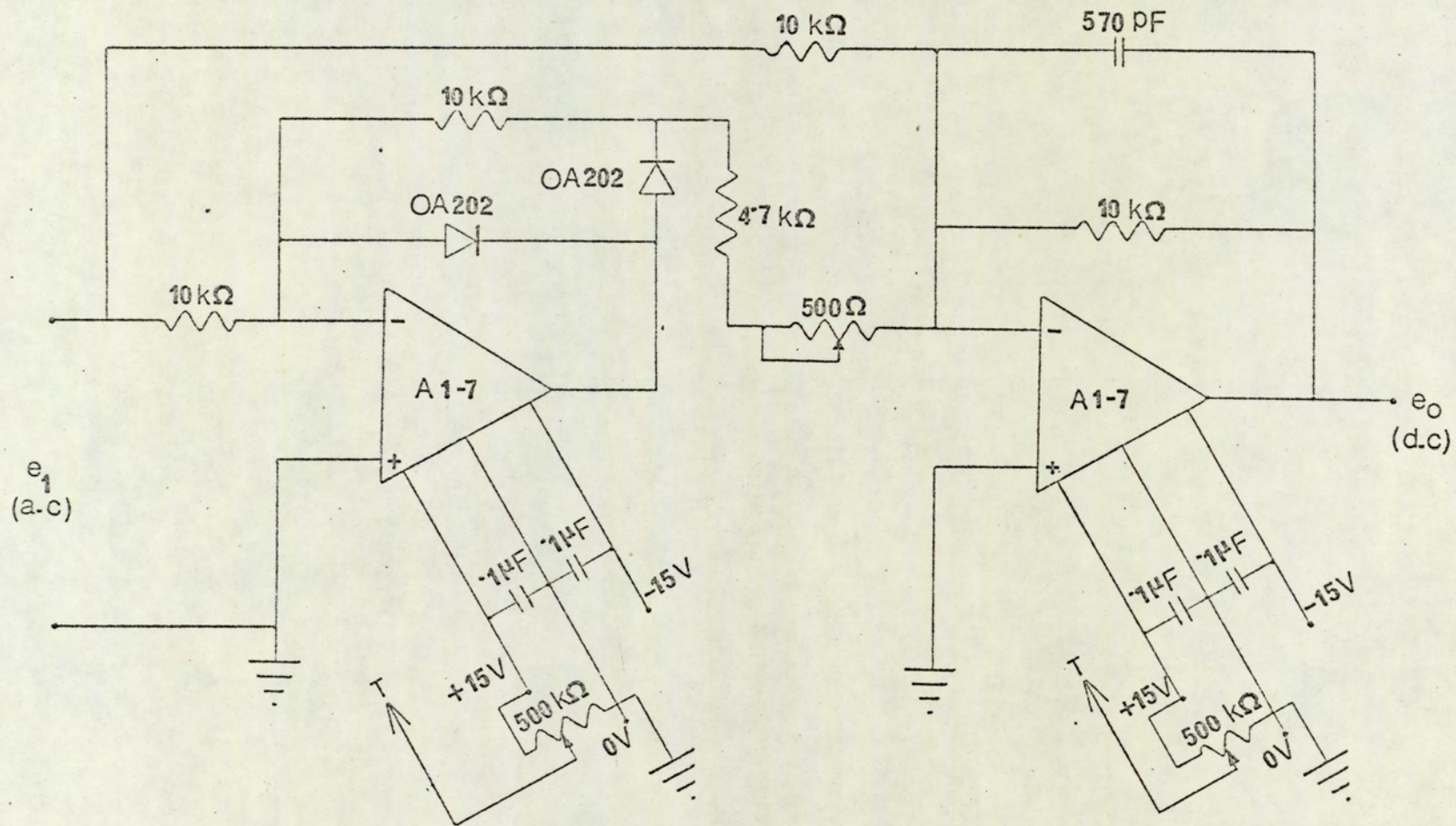
FIG. 5.7. Full-wave Precision Rectifier for Voltage Branch.
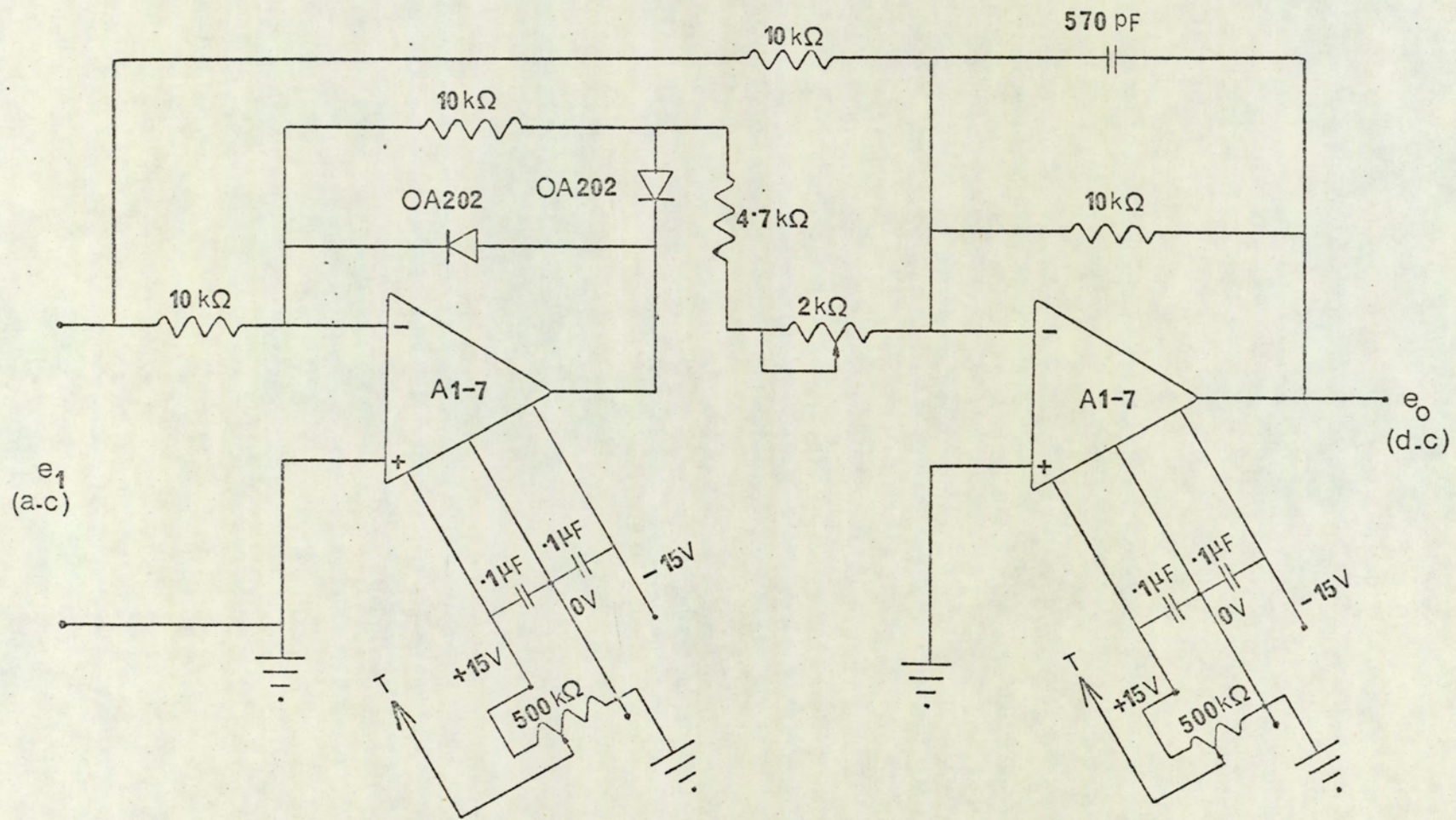
FIG. 5.8. Full-wave Precision Rectifier for Current Branch.
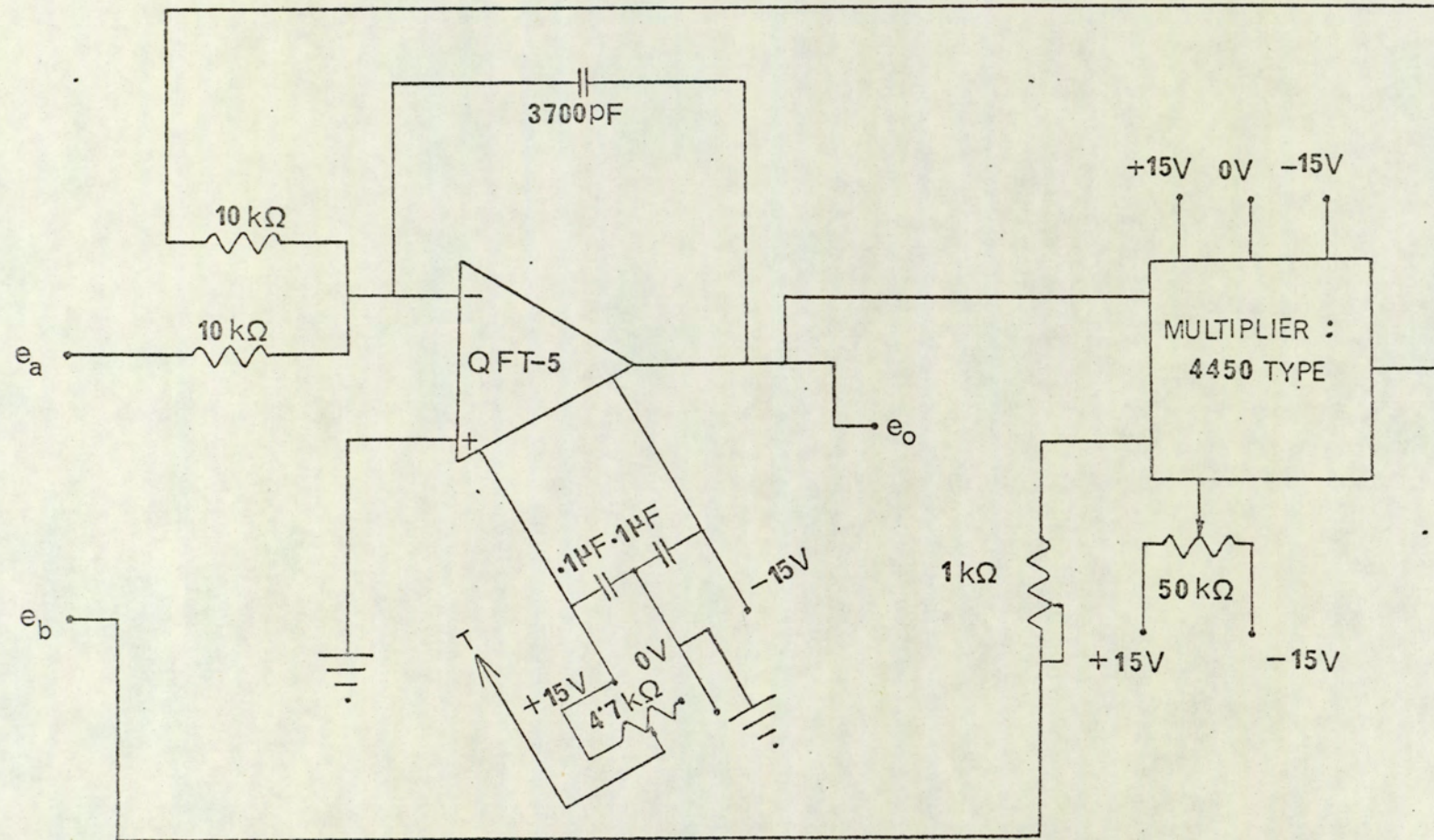
FIG. 5.9. Divider Circuit.
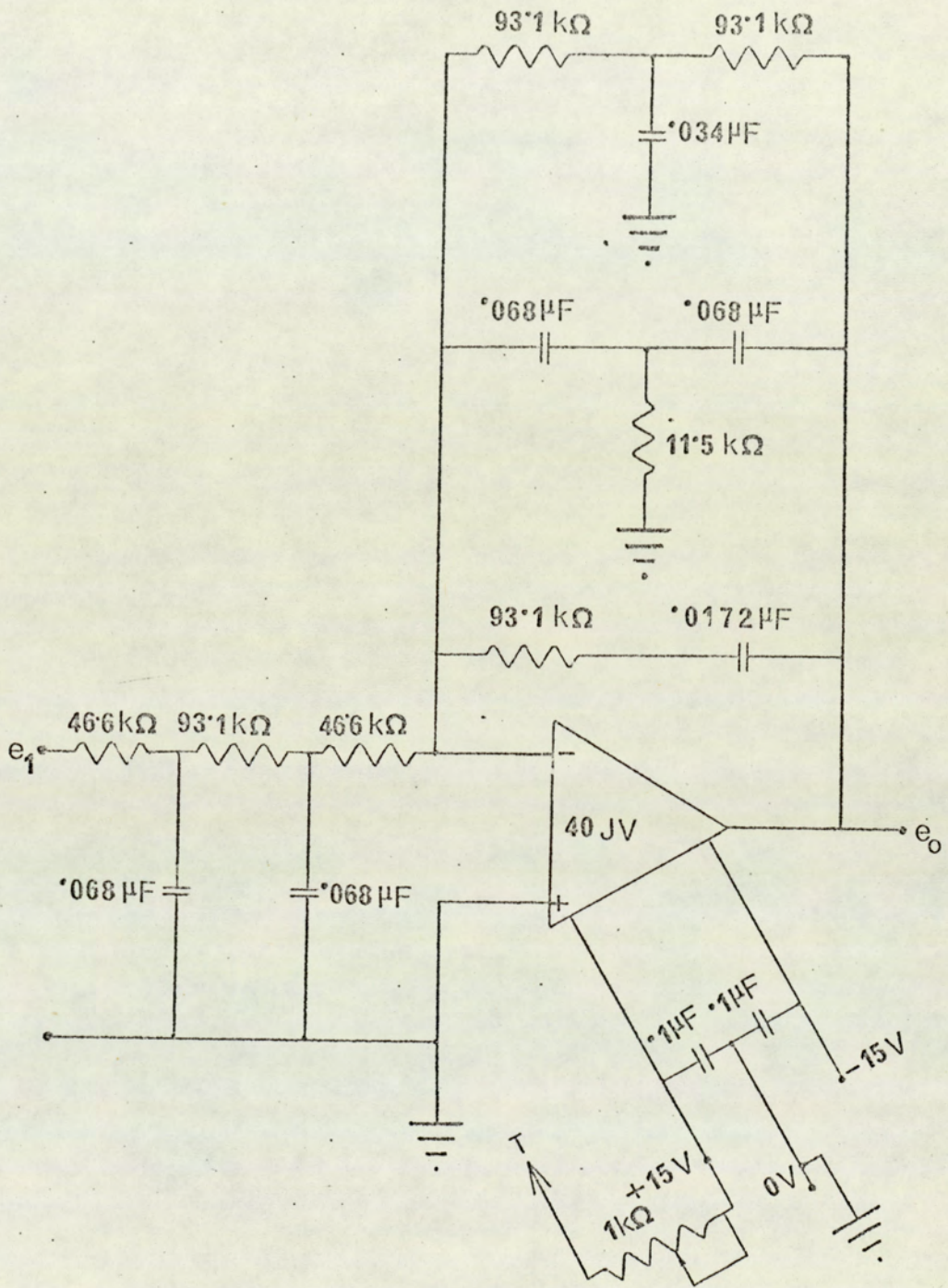
FIG. 5.10.   Low-pass Active Filter with 50 Hz Cut-off Frequency.
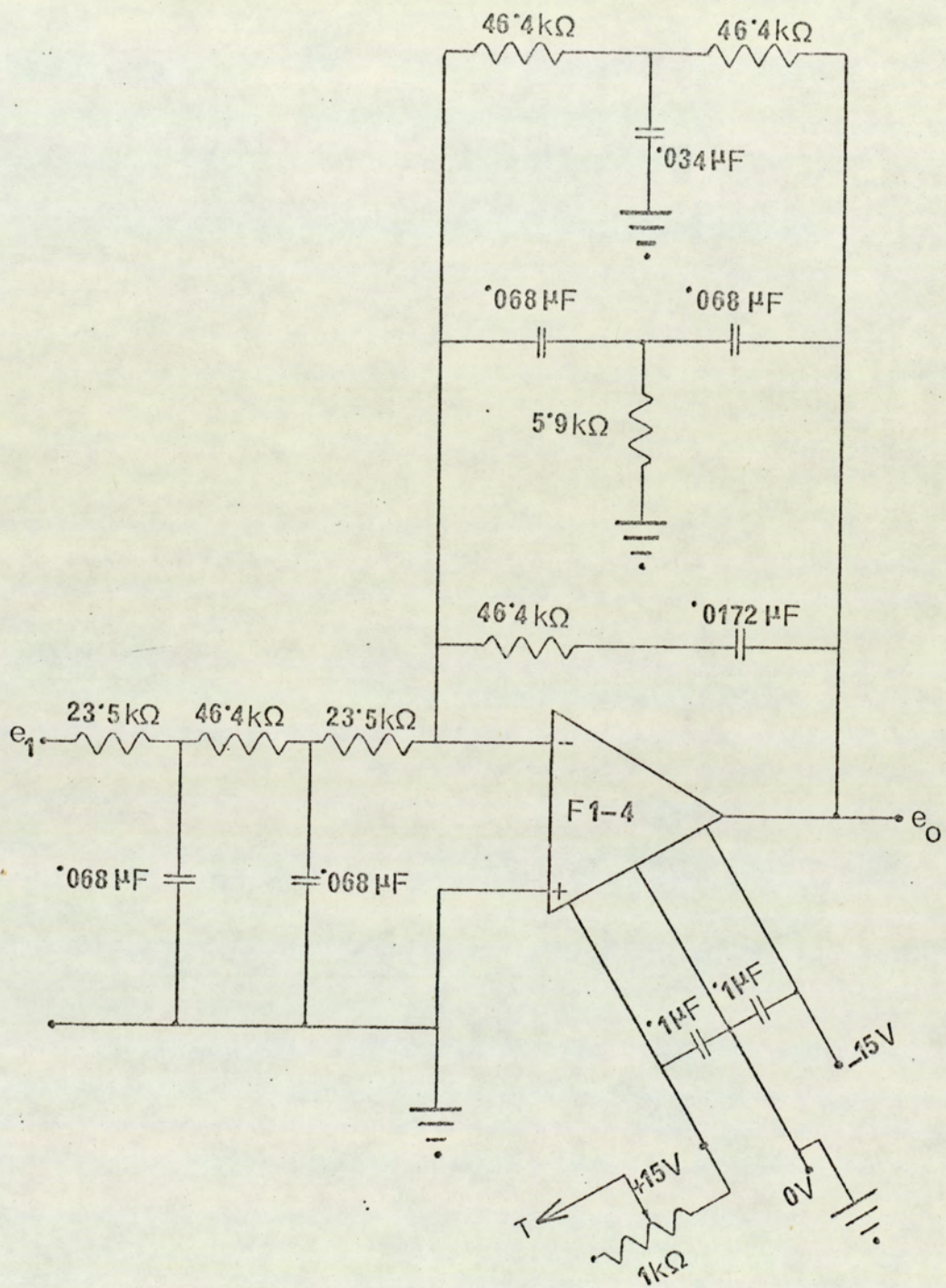
FIG. 5.11   Low-pass Active Filter with 100 Hz Cut-off Frequency

OA 202

9·1 V ZENER

OA 202

1kΩ

To Inverting Input
of QFT-5.

To Output
of QFT-5.

a

5·1 V ZENER

Divider

Low-pass
Filter

Recorder

10kΩ

b
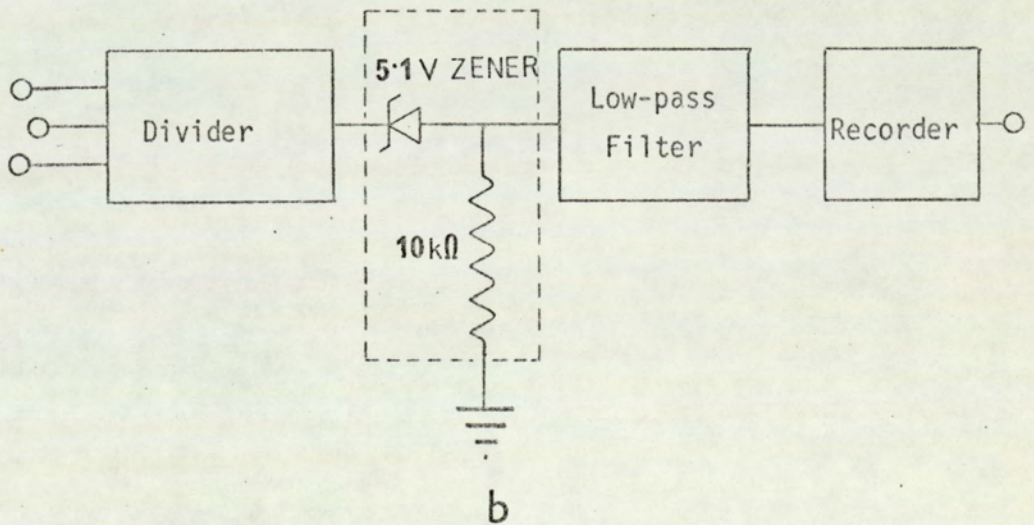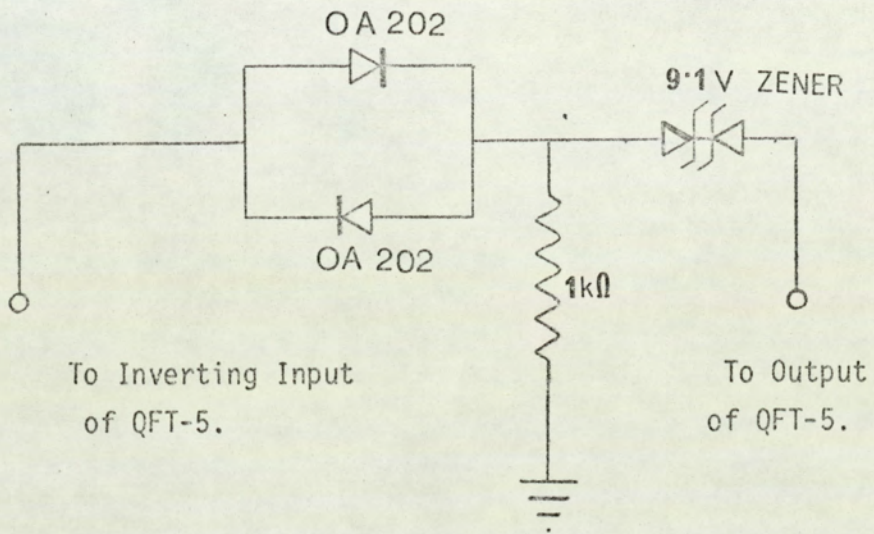
FIG. 5.12. Bound and Null Circuits

(a) Zener Bound Circuit.

(b) Zener Null Circuit.

6.   TYPICAL RECORDINGS OF CURRENT, VOLTAGE AND RESISTANCE -
      THEIR ANALYSIS AND INTERPRETATION

6.1. Recorded Traces of Welding Current and Weld Voltage

6.1.1. A.C.Waveforms

Typical recordings of the a.c. waveform of welding current and
weld voltage are shown in Figure 6.1. The current waveform is shown
in the recorded trace (a). The attenuator ratio was set to 1/5 so that
only 1/5th of the total toroid output was fed to the integrator, and
trace (a) was recorded as the output of the integrator.

Trace (b) is the weld voltage trace and was obtained by connecting
the oscillomink recorder to the output of the differential amplifier
stage.

A closer inspection of the weld voltage trace shows an upward-
going 'spike' at the end of each negative half-cycle, the interval
between two successive half-cycles being separated by a 'dead period'.
The mutual inductive coupling between the voltage-sensing leads and
the secondary circuit of the welding transformer is believed[4] to be
responsible for such distortion of the voltage waveform. The current
waveform, on the other hand, is seen to be comparatively smooth and
free from such distortions during the 'dead periods'; it may be con-
cluded that the integrator behaves as a low-pass filter and eliminates
any sharp-rising edge in the current waveform.

6.1.2. Voltage and Current Traces after Full-wave Rectification

The waveforms of welding current and weld voltage after full-wave
rectification are shown in Figure 6.2. The output of the precision
rectifier stage in the current branch is recorded as the upper trace in
both (a) and (b) of Figure 6.2. Similarly, the lower trace in both (a)

and (b) is the full-wave rectified voltage trace and was obtained as the output of the precision rectifier stage in the voltage branch. The peak r.m.s. current registered by the current meter is shown for both (a) and (b); the peak r.m.s. current, in this context, is defined as the r.m.s. value measured over the half-cycle during which welding current reaches its highest value. In (a), the peak r.m.s. current is 5300 A, and the recorded traces are for low-current conditions in 20 S.W.G. mild steel; the r.m.s. current in (b), however, is 6800 A, and the recorded traces represent the high-current conditions.

The following observations are made from an inspection of the recorded traces of Figure 6.2.

(i) Apparent amplitude modulation in the current and voltage traces

A close inspection of the patterns of variation exhibited by welding current and weld voltage reveals that the peaks of alternate half-cycles increase (or decrease) in a repetitive manner. Thus, the voltage and current traces appear to have a 50 Hz amplitude modulation superposed on the patterns of voltage and current waveforms after full-wave rectification. It is suggested that the increase or decrease during alternate half-cycle is caused by unequal current-conducting properties of the two ignitrons in the primary circuit of the welding machine. Any slight unbalance in the precision rectifier circuit enhances this effect on the recorded traces.

(ii) Voltage 'peak' and current 'valley'

The voltage trace in (b) is seen to go through a 'peak'; a 'valley' corresponding to the voltage 'peak' occurs in the current trace. A similar effect, although less prominent, can be seen in (a).

6.1.3. Voltage and Current Traces after Half-wave Rectification

In order to eliminate the effect of unequal current conduction by the two ignitrons, voltage and current traces were also obtained after half-wave rectification, and are shown in Figure 6.3. The upper trace in (a), (b), (c) and (d) represents the half-wave rectified current, and was obtained by connecting the recorder to the output of the first stage of the precision rectifier circuit in the current branch. The lower trace in each case represents weld voltage, and was obtained as the output of the first stage of the precision rectifier circuit in the voltage branch. The reversed polarity of the recorded signals in Figure 6.3, relative to those in Figure 6.2, can be explained from the principle of operation of the precision rectifier circuits.

The characteristic 'peak' in the voltage trace and the 'valley' in the current trace, noted in Figure 6.2, are seen much more clearly in the recorded traces of Figure 6.3. The voltage and current traces in (a) of Figure 6.3 are due to a peak r.m.s. current of 5300 A; the recorded traces in (b) and (d) correspond to a peak r.m.s. current of 6800 A. To demonstrate the 'peak' and 'valley' effects more clearly, the voltage and current traces in (d) were obtained with a recorder speed of 10 centimetre/second. It can also be seen from the recordings of Figure 6.3 that the 'peak' in the voltage trace and 'valley' in the current trace become more prominent as the current increases. The traces in (c) are due to a splash weld. The splash weld is seen to be characterised by a sharp drop following the 'peak' in the voltage trace; the current trace shows a sudden 'rise' corresponding to the sharp 'drop' in the voltage trace.

Except for the recorded traces in (d) of Figure 6.3, the recorder speed was set to 20 centimetre/second for Figures 6.1 through 6.3; the

recording head, in all cases, was set at the 20 mm position. For the recorded traces shown in Figures 6.2 and 6.3, the electronic instrumentation system was set as below.

Voltage Branch Gain - 2

Current Branch Gain - 5

Attenuation Ratio of Toroid Output - 1/5.

In addition, the following machine settings were used.

Transformer Tapping - Number 6.

Electrode Force - 1.55kN (350 lbf) corresponding

to 70 lb/in^2 on the Pressure Gauge.

Weld time - 15 Cycles.

6.2. Adjustments of the Instrumentation System for Recording Dynamic Resistance Traces

The following adjustments were carried out in setting up the instrumentation system before resistance traces were recorded.

(a) Offset Balancing

To minimize error in the divider output, it is necessary to null the offset voltage appearing at the inputs to the divider circuit in the absence of any incoming signal. All the various stages of the instrumentation system, in the voltage branch as well as in the current branch, can be individually nulled for zero offset by means of the respective balance or trim potentiometers. It was, however, found that if the differential amplifier and variable-gain amplifier in the voltage branch were nulled for zero offset, then nulling of the following stages was not so critical; similarly, when the integrator and the variable-gain amplifier in the current branch were nulled for zero offset, then offset adjustment of the remaining stages was not necessary.

(b) <u>Adjustment of the Divider Stage</u>

The divider stage was set up for true divider-mode operation by using external sinusoidal signals. Thus, an externally derived 50 Hz sinusoidal signal was fed simultaneously into the input of the variable-gain amplifier in each branch, and the gain of each variable-gain amplifier was adjusted so that the peak of the full-wave rectified output in each case was 10V. Ideal gain factor of the divider stage was initially set by adjusting the 50kΩ potentiometer of the multiplier unit so that the correct input-output relation of the divider was obtained according to equation (5.1). Finer adjustment cf the divider stage was achieved by adjusting the 1kΩ optional trim potentiometer of the multiplier unit and the 4.7 kΩ trim potentiometer of the QFT-5 operational amplifier.

It was found that inclusion of the bound circuit in the feedback loop of QFT-5 made little difference to the output when the denominator had a finite non-zero value.

(c) <u>Selection of Attenuation Factor</u>

Selection of the correct attenuation factor is important for two reasons. Firstly, because the input to the integrator is to remain within the maximum input voltage limit of the operational amplifier; secondly, because true divider operation requires that $e_v \leq e_c$ in equation (5.1). The value of e_c was measured by recording the output of the precision rectifier in the current branch, and the attenuation factor was so selected that $e_c \leq 10V$, when the gain was set at 5 in the current branch.

(d) <u>Selecting Gain of the Variable-gain Amplifiers</u>

For the desired range of current values appropriate to the specific experimental conditions, the voltage and current traces were

recorded after full-wave rectification. The gain factor of each variable-gain amplifier was then adjusted to ensure that, (i) the peak values of both e_v and e_c remained between 8V and 10V, and that (ii) $e_v \leq e_c$.

6.3 Typical Dynamic Resistance Recordings

Some typical recordings of dynamic resistance are shown in Figure 6.4. The upper trace in (a) represents dynamic resistance obtained as the direct output of the divider stage without any zener nulling; the lower trace represents welding current, and is used as a reference trace to indicate the beginning and end of weld time. During each 'dead period' the voltage and the current signals pass through zero; thus the inputs e_v and e_c to the divider tend to zero (see equation (5.1)). During these 'dead periods' the divider is called upon to perform the operation $\frac{0}{0}$ according to equation (5.1). Since the ratio $\frac{0}{0}$ is mathematically indeterminate, positive feedback results in overloading of the operational amplifier and spurious signals are superimposed on the dynamic resistance trace, as shown in (a). Spurious oscillations may also result when the divider inputs are such that a finite numerator and a very small denominator occur in equation (5.1).

Recorded traces in (b) of Figure 6.4 are dynamic resistance traces, and were obtained after taking the divider output through a zener nulling network and an active low-pass filter in each case. The resultant phase inversion due to the inclusion of the active low-pass filters is evident from a comparison of the dynamic resistance traces in (a) and (b) of Figure 6.4. The upper trace in (b) was obtained after taking the divider output through the null network and a low-pass filter with cut-off frequency at 50 Hz; the lower trace in (b) was recorded after passage through the null network and a 100 Hz low-pass filter. In comparison with the dynamic resistance trace shown in (a), the recordings of (b)

are free from spurious signals. The recorded trace obtained with the 50 Hz low-pass filter presents a clearer pattern and is preferred to that obtained with the 100 Hz low-pass filter.

6.4. Interpretation of Dynamic Resistance Characteristic as an Indication of Nugget Growth.

By joining the small peaks in the contour of the upper trace in (b) of Figure 6.4, the smooth resistance curve of Figure 6.5 is drawn*. The corresponding curves of weld voltage and welding current are redrawn as (a) and (c) respectively in Figure 6.5. It is to be noted that curve (b) of Figure 6.5 is drawn in the positive quadrant and thus appears inverted in relation to the recorded traces of dynamic resistance shown in Figure 6.4.

The dynamic resistance curve of Figure 6.5 is divided into regions labelled (I) (II) (III) and (IV) by dotted lines α, β and γ; an arbitrary zero has been chosen for the r_w-axis to specify the origin of the reference axes.

The region labelled (I) represents the initial period of transient conditions immediately after initiating the welding current. When the primary side of the welding machine is switched on, the full open-circuit voltage of the transformer secondary appears across the electrodes. However, because of the existence of insulating films[24] at the electrode-to-sheet and sheet-to-sheet contacts, momentarily no current flows in the secondary circuit; moreover, the inductance of the secondary circuit tends to retard the immediate growth of current. Following the principle of electrical breakdown of contact insulation developed by Holm[24], a

---

* In fact, the redrawn curves are shown here after magnification.

finite minimum voltage is necessary to cause initial breakdown of the insulating films at the electrode-to-sheet and sheet-to-sheet interfaces. Thus, prior to the instant marked α there is no appreciable current flow through the weldment, although a finite voltage builds up across the electrode. Under these conditions, the divider output in accordance with equation (5.1), is given by

$$E_0 = -10. \frac{F}{\delta} \qquad (6.1)$$

where F in the numerator is of finite value and δ tends to zero. Thus, accurate divider operation is no longer possible, and the operational amplifier in the divider circuit is overloaded. Although the overload recovery time of the operational amplifier in the divider circuit is of the order of a few milliseconds, the response of the recorder is such that only the recovery from the overload condition is recorded in the oscillomink trace. Accordingly, no finite value of dynamic resistance is recorded before the instant α ; the portion of the dynamic resistance characteristic before α has been extrapolated as a broken line in curve (b) of Figure 6.5.

Appreciable current flow through weldment commences at the instant marked α , and dynamic resistance is seen to increase over the region labelled (II). During the period of initial nugget formation, a bridge of base metal connecting the specimen coupons is gradually established, and may be termed the 'metallic constriction' of the weld; the development of the nugget takes place around this metallic constriction. The increase in dynamic resistance over this region may be accounted for by the increase in resistance of the bulk metal due to temperature rise; partial transformation of the base metal from a solid to a liquid phase adds to this effect and may bring about a much larger increase[25,26] in electrical resistance.

At the instant β , dynamic resistance reaches its maximum and
then falls gradually along the contour of region (III). Decrease
in dynamic resistance during the period labelled (III) can be attributed
to two major factors - (i) growth of a metallic bond at the sheet-to-
sheet interface, and (ii) a substantial increase in the electrode-to-
sheet contact area because of plastic deformation of the weld metal at
high temperatures. Redrawn curves of weld voltage and welding current,
shown as (a) and (c) in Figure 6.5, indicate that the 'peak region' of the
voltage curve and the 'valley region' of the current curve are centred
around the line β .

The decrease in dynamic resistance is continued beyond γ in the
region labelled (IV); the gradient of fall in resistance value is,
however, much less compared to that in region (III). During the period
labelled (IV), the metallic bond already in existence is subjected to a
kind of heat treatment, and most of the heat generated in the work-piece
is conducted away to the electrodes and the surrounding metallic mass.
Referring to the voltage and current curves of Figure 6.5 it may be seen
that an almost constant voltage drop and a rising trend in the current
value characterize region (IV) during a good weld.
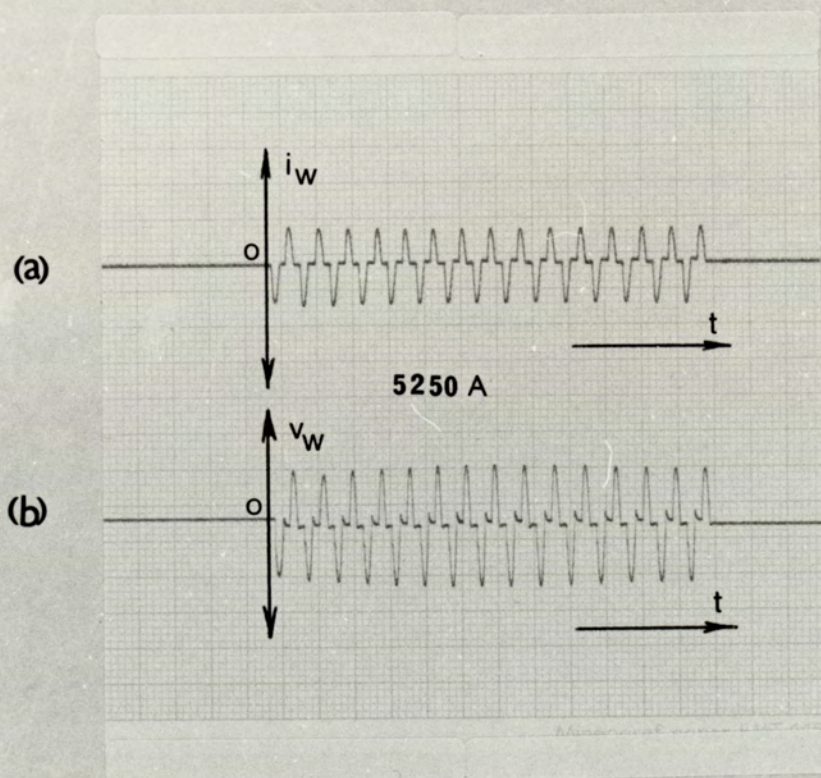
FIG. 6.1 Typical Recorded Traces of Weld Voltage and
Welding Current.

(a) Current Trace, 2V/cm.

(b) Voltage Trace, 2V/cm.
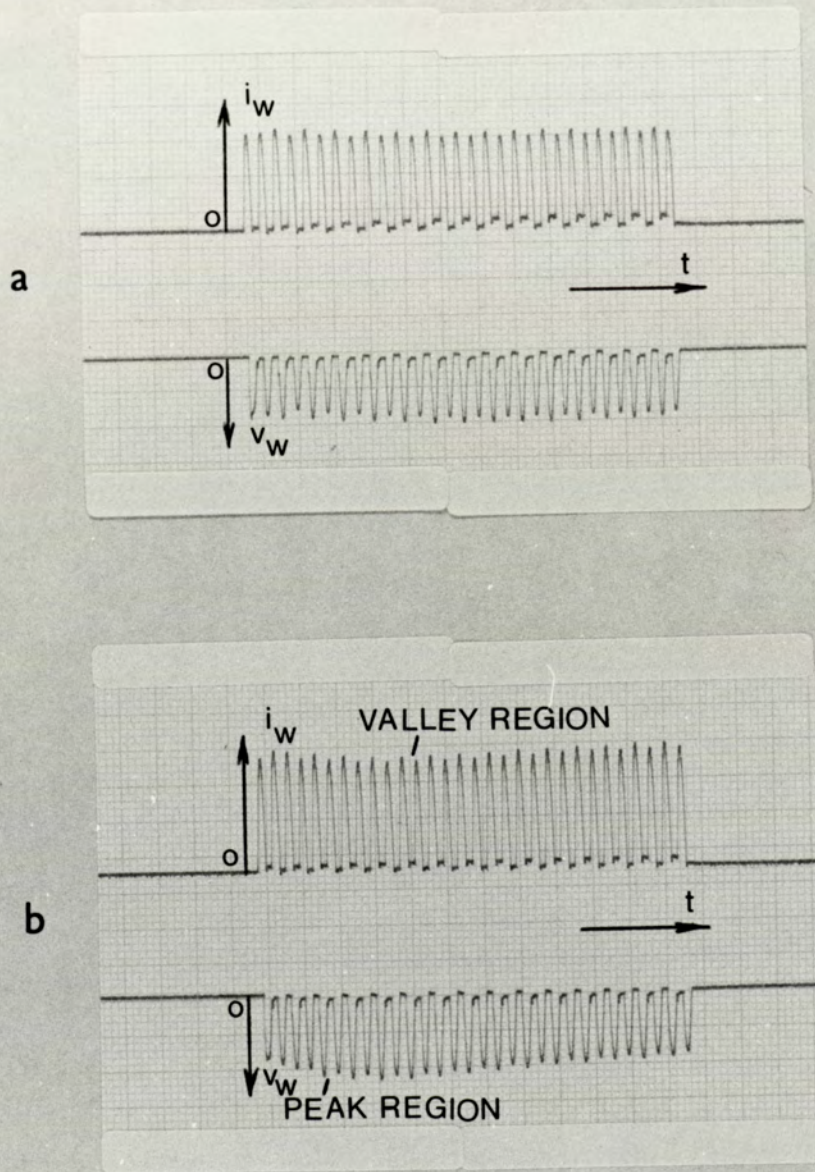
FIG. 6.2.   Current and Voltage Traces after Full-wave
            Rectification.

            Upper Trace: Current, 4V/cm;

            Lower Trace: Voltage, 4V/cm.

            (a) Low Current, 5300A;
            (b) High Current, 6800A.
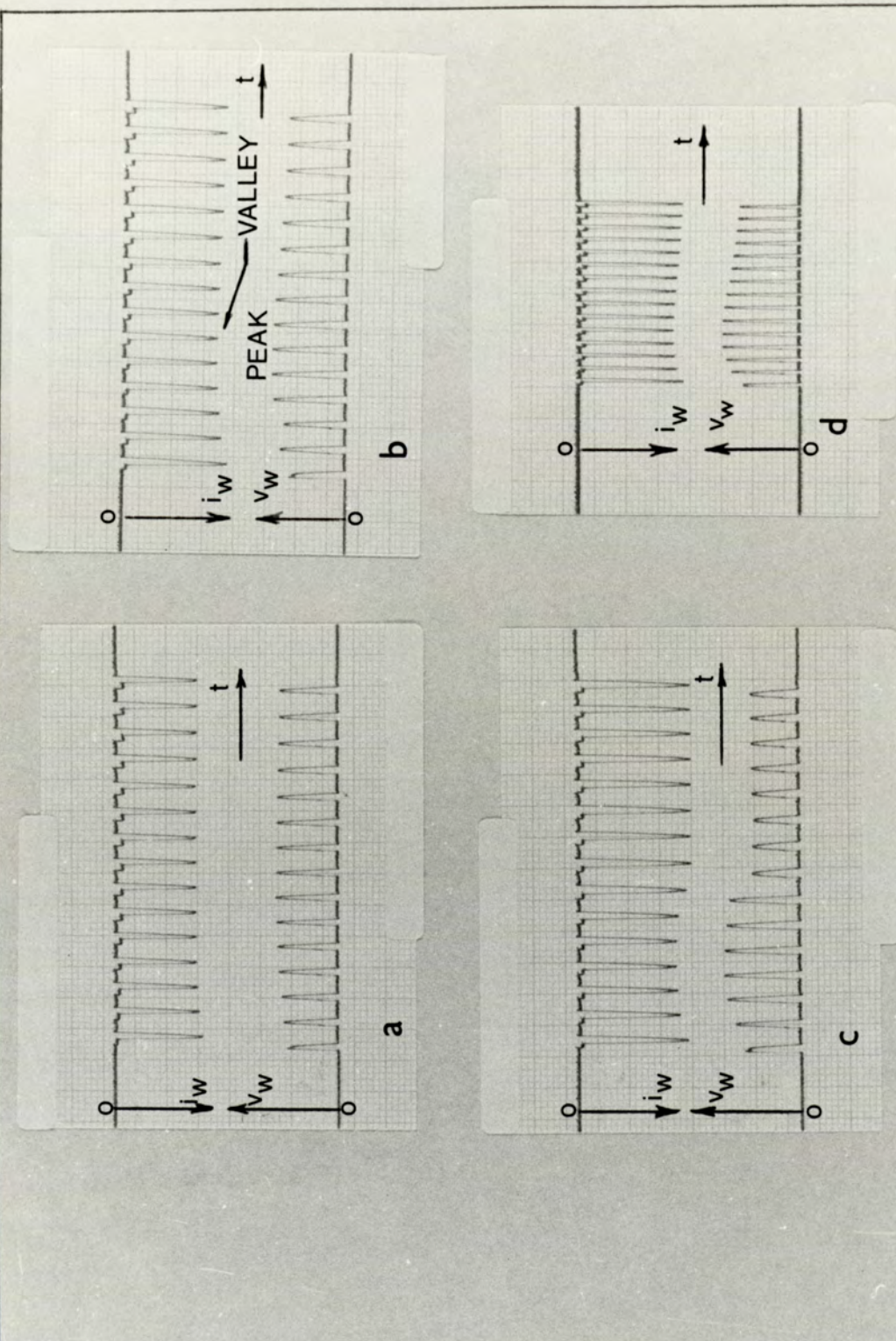
FIG.6.3. Current and Voltage Traces after Half-wave
Rectification.

Upper Trace: Current, 4V/cm.   Lower Trace: Voltage, 4V/cm.

(a) No Weld, 5300A;   (b) Weld, 6800A;

(c) Splash Weld, 7800A; (d) Same as (b) recorded at
                                  10 cm/sec.
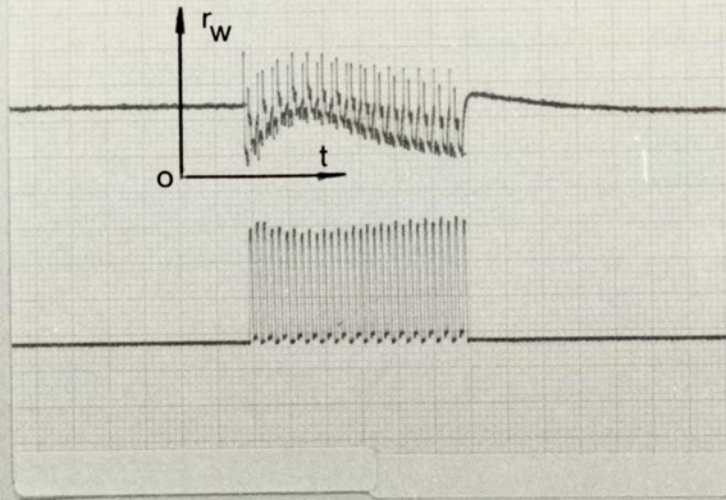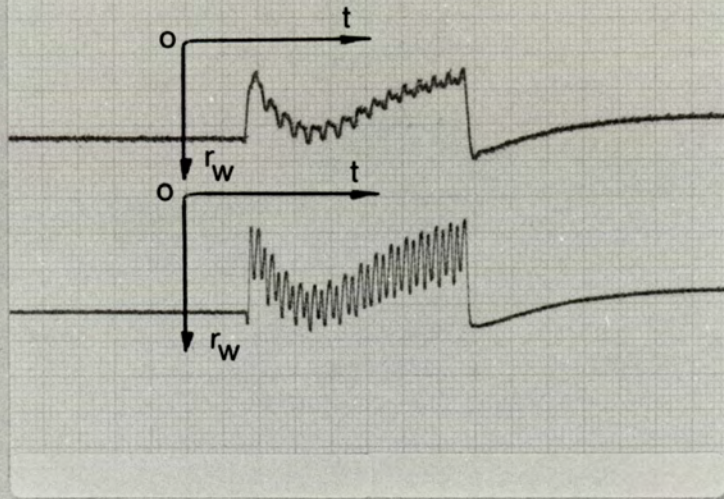
FIG.6.4. Typical Dynamic Resistance Traces.

(a) Upper Trace: Dynamic Resistance Recorded as
   Direct Divider Output, 4V/cm;
   Lower Trace: Current, 4V/cm.

(b) Upper Trace: Dynamic Resistance, after Passage through
   50 Hz. Low-pass Active Filter, 2V/cm.
   Lower Trace: Dynamic Resistance, after Passage through
   100 Hz. Low-pass Active Filter, 2V/cm.
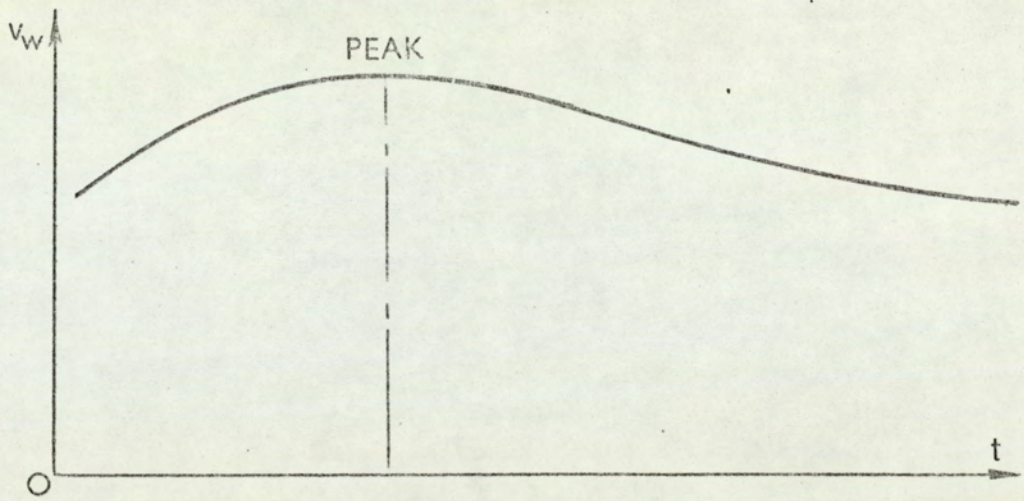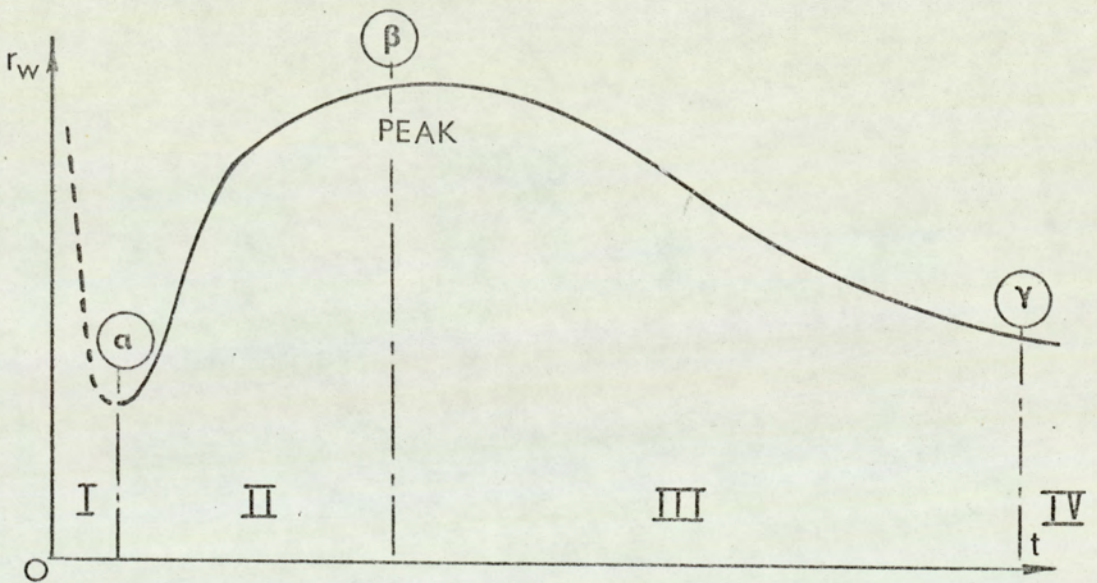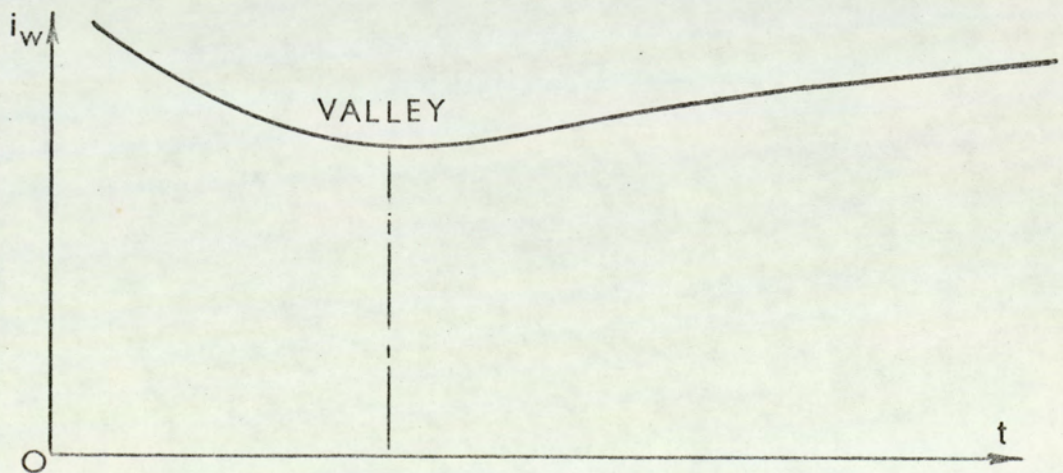
FIG. 6.5 Voltage, Resistance and Current Variation for a
Good Weld in Mild Steel.

(a) Voltage; (b) Dynamic Resistance; (c) Current.

7. DISCUSSION OF DYNAMIC RESISTANCE TRACES AND CONCLUSIONS

7.1 General Discussion of the Experimental Recordings of Dynamic Resistance

Using the electronic instrumentation system described in Section 5, oscillomink recordings of dynamic resistance were obtained for spot welds in low-carbon mild steel for various experimental conditions. In most cases, single spot welds were made in two overlapping specimen coupons using Sciaky tiptrodes;for reasons explained in Part II, no water-cooling was used for the electrodes. The instrumentation system shown in the block diagram of Figure 5.1 was slightly modified by inserting a zener nulling network between the divider stage and the low-pass filter. A photograph of the dynamic resistance measurement system in operation is shown in Figure 7.1.

The general objective in analysis and interpretation of the experimental recordings is to relate the pattern of dynamic resistance variation to the formation of weld nugget so that the influence of the various factors governing nugget growth can be determined from inspection of the recorded characteristics. For this purpose, it has not been necessary to calculate and compare the absolute values of dynamic resistance; the shape of the dynamic resistance trace, character-ized by the relative position and magnitude of the peak, has been found an adequate basis for qualitative comparison of the experimental recordings.

For a fuller appreciation of the dynamic resistance recordings presented in this Section, the following points may be noted.

(a) General Appearance of the Dynamic Resistance Traces

The inverted appearance of the dynamic resistance characteristics presented in this Section is due to phase reversal* caused by the low-pass active filter; this is evident from a comparison of the dynamic resistance traces shown in (a) and (b) of Figure 6.4.

Immediately after the welding current is initiated, the electrical resistance across the electrodes changes from an almost infinite value to a very low value. With the oscillomink recorder set up to respond to resistance of much smaller magnitude, the large change in resistance value during the initial part of the dynamic resistance characteristic cannot be conveniently recorded using the same scale of sensitivity. On the recorded traces, however, the initial part of the character-istics is extrapolated and shown as a broken line.

(b) Axes of Reference

The zero or base line of the recorded trace, in this context, is of no great significance; for a qualitative analysis, the pattern of variation exhibited by the resistance traces is all that is needed. However, to make the recorded traces more meaningful, a set of reference axes has been drawn in each case. The instantaneous resistance or dynamic resistance is denoted by r_w on such recordings; the zero of the r_w-axis has been chosen arbitrarily for this purpose, the arrow indicating the direction of increasing resistance.

Strictly speaking, the resistance trace should be expressed in units of ohms; however, for the sake of simplicity, the volt/centimetre scale of the oscillomink recorder has been retained without conversion

---

* The phase inversion of the dynamic resistance trace occurs in all cases except in the upper traces of Figure 7.9.

to the more appropriate mΩ or $\mu\Omega$ units. For a qualitative analysis this has been found adequate; if, however, it is necessary to determine the change in resistance between two instants in time, equations (5.7) and (5.8) derived in Section 5 can be used for such calculation.

The weld time on the recorded traces has been denoted by t, the arrow indicating the direction of increasing weld time. Weld time may be calculated in units of seconds from the recorder speed. Otherwise, a count of the number of half-cycles of the current or voltage trace is adequate for most practical purposes.

(c) Use of Voltage Trace or Current Trace as a Reference Trace

The pattern of resistance variation, in most cases, has been set against the voltage or current trace; the voltage or current trace, in this respect, has been used as a reference trace to indicate the start and finish of weld time. Both voltage and current traces were obtained as full-wave rectified outputs from the precision rectifier stages described in Section 5; the recorded voltage trace is of negative polarity, and the current trace is of positive polarity.

(d) Running Parameters and other Machine and Instrumentation Settings
for the Dynamic Resistance Traces

Since only a single factor affecting weld formation was varied in any particular set of experimental conditions, the specific running parameter is indicated in each case along with the peak r.m.s. current.

For the recorded traces illustrated in Figures 7.2 through 7.9, the oscillomink recorder and the electronic instrumentation system were set as overleaf.

Oscillomink Recorder Settings

Recording Head Position - 20 millimetre

Recorder speed   - 10 centimetre per second

Recorder sensitivity   - Set to maximum

Electronic Instrumentation Settings

Voltage Branch Gain Setting   - 2

Current Branch Gain Setting   - 5

Attenuation Ratio of Toroid Output - 1/5

It may also be added that the 5.IV zener nulling network was included in the circuit for all such recordings except for those of Figure 7.9. Again, the 50 Hz low-pass filter was used in all cases except in recording the upper trace of dynamic resistance in the illustrations of Figure 7.9.

The machine settings or welding variables corresponding to each set of illustrations are included in the appropriate sub-section in each case.

(e) Tests for Weld Quality

Although macrosection tests and tension-shear tests were performed to determine the state of nugget growth and to define the optimum values of welding variables, the details of such tests have been excluded from the analysis presented in this Section.

(f) D.C. Shift of the Zero or Base Line

The recorded traces of dynamic resistance were obtained over a period of experimentation lasting a few weeks; after the initial setting for zero offset, no further resetting of the individual stages was undertaken. Thus, a slight shift in the base line of the recorded

traces may be noticed in some cases, because of the cumulative off-set error due to operational amplifier drift over a long period of time. Such d.c. shift of the base line of the recorded traces, although introduces some error in the absolute value of dynamic resistance, does not affect the relative pattern of resistance variation. Thus, the interpretation of the recorded characteristics and the inferences drawn from the inspection of such characteristics are not invalid because of the referred shift in the base line of the resistance trace.

7.2 Influence of Welding Variables

7.2.1 Effects of Varying Welding Current

The welding current can be varied, either (A) by changing the secondary open-circuit voltage, or (B) by altering the phase-shift heat-control setting on the electronic control panel. For (A), the transformer turns-ratio was changed by means of the rotary tap switch; for (B), the phase-shift heat-control knob was set to various values marked on the dial. The recorded traces of dynamic resistance obtained for both (A) and (B) are similar in nature, and are shown in Figures 7.2 and 7.3 respectively. The machine settings corresponding to the illustrations of Figures 7.2 and 7.3 were as below:

A. Machine Settings for Figure 7.2

    Electrode Force - 1.55 kN (350 lbf) corresponding to
                    $0.5 N/mm^2$ or 70 lb/in^2 on the Pressure Gauge.

    Weld Heat Control - 60

    Weld Time   - 15 cycles.

B. Machine Settings for Figure 7.3

    Electrode Force   - 1.55 kN (350 lbf)

    Transformer Tapping - Number 6.

    Weld Time   - 15 cycles.

The following observations are made from an inspection of the
recorded traces illustrated in Figures 7.2 and 7.3.

  (i) With low current values, the resistance trace does not show a
prominent peak (see resistance traces lebelled (a) in Figures
7.2 and 7.3); with increased welding current, however, a well-
defined peak appears in the recorded trace (see resistance
traces in (b) and (c) of Figure 7.3).

 (ii) With higher current values, the position of the peak in the
resistance trace is shifted towards the left; in other words,
the maximum or peak resistance of the weld is reached earlier.

(iii) The resistance trace indicates a lower value of resistance
after completion of a weld, for welds produced with high
currents.

 (iv) A splash weld, caused by excessive welding current, is character-
ized by a sudden step in the resistance trace. Thus, an abrupt
reduction in resistance value can be seen immediately after the
splash, and no significant change in resistance can be noticed
during the remainder of weld time (see Resistance trace in (c)
of Figure 7.3).

7.2.2 Effects of Varying Weld Time

The weld time can be preset on the control panel as the desired
number of cycles of welding current, and the recorded traces shown in
Figure 7.4 were obtained for various values of weld time. The machine
settings corresponding to Figure 7.4 were as below.

Electrode Force - 1.55 kN (350 lbf) corresponding to

70 lb/in^2 on the Pressure Gauge.

Transformer Tapping - Number 6.

Weld Heat Control   - 65.

The following observations are made from an inspection of the recorded traces of Figure 7.4.

(i) When weld time is increased above a minimum value, the magnitude and position of the peak in the dynamic resistance trace remain unaltered (compare the resistance traces in (b), (c) and (d) of Figure 7.4).

(ii) The resistance after completion of a weld decreases for increased values of weld time. With very long weld times, however, the gradual reduction in resistance value towards the end of weld time is not noticeable (see resistance trace in (d) of Figure 7.4).

(iii) With the chosen values of welding variables, no splash weld occurred even for very long weld times.

7.2.3 Effects of Varying Electrode Force

The recorded traces shown in Figure 7.5 were obtained for various values of electrode force, the following machine settings being used for the recordings:

Transformer Tapping - Number 6

Weld Heat Control - 65

Weld Time   - 15 cycles

Inspection of the recorded traces shows the following characteristics.

(i) Very low electrode force almost inevitably results in a splash weld; occurrence of multiple splash is characterized by two or more steps in the dynamic resistance trace (see (a) of Figure 7.5). With low electrode force, the values of peak r.m.s. current registered on the current meter vary over wide limits for welds made under otherwise identical conditions; with the electrode force set to a moderately high value, however, little change occurs in the registered current values.

(ii) As the electrode force is increased, the dynamic resistance
trace becomes flatter, the peak value of resistance being
smaller for higher electrode force (see resistance trace in (d)
of Figure 7.5)

(iii) The peak in the resistance trace occurs later as the electrode
force is increased; the resistance value at the end of a weld,
however, does not alter appreciably due to variation in electrode
force.

7.3 Effects of Variation in Electrode Tip Diameter

The gradual 'mushrooming' of the electrode tips, resulting in an
increase in the current-conducting area of the tips, is a serious
problem under production conditons. In the absence of an adequate
maintenance schedule for the electrodes, such increase in tip diameter
may result in bad welds. The pattern of dynamic resistance variation
monitored at different stages of deformation of the electrode tips may
indicate the stage when increase in tip diameter causes deterioration
in weld quality.

Recorded traces of dynamic resistance shown in Figure 7.6 were
obtained using electrodes of various tip diameters, the machine
settings being as below:

Transformer Tapping -	Number 6
Weld Heat Control -	60
Electrode Force -	1.55 kN (350 lbf), corresponding to 70 lb/in^2 on the Pressure Gauge.
Weld time -	15 cycles

The following observations are made from an inspection of the recorded traces of Figure 7.6.

(i) As the diameter of the electrode tips is increased, the dynamic resistance trace becomes flatter and the magnitude of the peak resistance also diminishes; with very large tip diameters a defined peak ceases to exist (see resistance trace in (c) of Figure 7.6).

Although the electrode force was set to a specific value and maintained at the set value throughout the experiment, variation in tip diameter effectively alters the pressure per unit area of the specimen coupons held together between the electrode tips. Thus, welds made with small diameter tips show excessive indentation. Large diameter tips, on the other hand, produce areas of non-uniform contact at the electrode-to-sheet interfaces; this is evident from the incomplete 'heat rings' on the surface of spot welds made with large diameter electrode tips. The irregular shape of the partially fused zone at the inter-facial contact, when shear failure occurs during tension-shear tests, indicates that large areas of uniform contact between the sheets cannot be established, simply by using large diameter tips.

(ii) The peak r.m.s. current registered by the current meter increases when welds are made with large diameter tips. For this set of experiments, the current was set to a low value to avoid any splash weld; thus, the conditions for the production of a good weld were met only when 3.18 mm (0.125 in) diameter electrode tips were used.

7.4 Influence of Surface Conditions

It is known that the existence of insulating films of various oxides and other chemicals, dirt, and grease influences the contact resistance effective at the interface of two contacting members. Consequently, any variation in the surface conditions of the contacting surfaces modifies the initial static resistance of the weldment, and hence the build-up of current through the constriction. In this instance, an attempt has been made to determine how the formation of weld nugget is influenced by the presence of insulating films of oxides and other chemicals at the sheet-to-sheet interface, and whether extreme variations in the surface condition of the specimen coupons can be detected from inspection of the dynamic resistance characteristics. The following machine settings were used for this investigation:

Transformer Tapping   - Number 6

Electrode Force   - 1.55 kN (350 lbf) corresponding to
                         70 lb/in^2 on the Pressure Gauge

Weld Time   - 15 cycles

Weld Heat Control   - 65 and 70

The recorded traces of Figure 7.7 were obtained using 1.22 mm (0.048 in) thick specimen coupons and tiptrodes with 4.76 mm (0.1875 in) diameter tips. In one batch, both surfaces of the specimen coupons were cleaned with emery paper and degreased; these coupons formed a 'clean' contact at the sheet-to-sheet interface when offered to the electrodes. For the other batch, only one side of the specimen coupons was cleaned and degreased; these specimens were offered to the electrodes such that the sheet-to-sheet interface was formed by the 'unclean' surfaces, thus creating an 'unclean' contact at the interface. The following observations are made from a comparison of the recorded traces and the corresponding current values.

(i) Values of peak r.m.s. current registered by the current meter show that, for identical machine settings, larger current flows through the specimens making 'clean' contacts. Thus, in spite of identical machine settings, exact correspondence of current values could not be achieved in this set of experiments.

(ii) The patterns of resistance and voltage variation, immediately after initiating the weld, are slightly different for welds made with 'clean' and 'unclean' interfacial contacts.

In the presence of insulating films at the sheet-to-sheet interface, a higher voltage is necessary to cause breakdown of contact insulation before a conducting channel can be established across the interfacial contact; hence, for welds made with 'unclean' interfacial contacts, a higher initial value of weld voltage is recorded in the voltage trace. Since weld resistance is computed from the relationship $r_w = \dfrac{v_w}{i_w}$, a corresponding change in the pattern of dynamic resistance characteristics for 'unclean' contacts is also noticeable. The conditions of almost zero current and finite voltage across the electrodes persist longer when the specimen coupons form an 'unclean' interfacial contact, resulting in the changed pattern of the resistance trace immediately after the welding current is switched on.

(iii) The initial part of the dynamic resistance characteristic shows a 'trough' before reaching the peak; the resistance of the 'trough' is denoted by r_t on the recorded traces. It can be seen that r_t has a lower value with 'clean' interfacial contacts; furthermore, a well-defined peak appears in the dynamic resistance characteristics when the specimen coupons form a 'clean' contact at the interface (see resistance traces in (a) and (c) of Figure 7.7).

For welds made with 'unclean' interfacial contacts, on the other hand, the resistance value r_t is higher after contact insulation is broken down, and the pattern of resistance variation beyond the peak shows a slightly different trend (see resistance traces in (b) and (d) of Figure 7.7.). The peak value of resistance, however, does not seem to be significantly affected by the nature of the interfacial contact.

7.5 Effects of Current Shunting

Experimental investigation in the foregoing has mainly been concerned with single spot welds. Frequently, under production conditions, it is necessary to join two components with more than one spot weld; in such cases, each additional weld after the first weld adds a new channel for conduction of current through the work-piece. Thus, whenever a fresh weld is made, part of the total current is shunted away through spot welds made previously. This shunting effect due to one or more existing welds causes a reduction in the current flow through any fresh weld. The principal objective of the experimental investigation undertaken in this connection was to determine how the pattern of dynamic resistance variation of a second weld was modified by the shunting effect of a weld already made. For this purpose, two 20 S.W.G. specimen coupons measuring 102 mm x 25.4 mm (4 in x 1 in) were overlapped end to end and spot welded with the machine set as below:

Transformer Tapping - Number 6

Electrode Force   - 1.55 kN (350 lbf) corresponding to

                         70 lb/in^2 on the Pressure Gauge.

Weld Heat Control   - 65

Weld Time   - 15 cycles.

Two spot welds were made in each set of coupons, the spacing between two consecutive welds varying from 76.2 mm (3 in) to 12.7 mm (0.5 in). The resistance traces are shown in Figure 7.8, and the following observations are made.

(i) The peak r.m.s. current registered by the current meter does not alter appreciably when the spacing between the two welds is varied.

(ii) When the two spots are spaced a large distance apart, the dynamic resistance trace for the second weld does not differ noticeably from that for the first (compare resistance traces in (a) and (b) of Figure 7.8). However, as the spacing between two consecutive spot welds is reduced, an appreciable flattening of the resistance trace becomes apparent, and the magnitude of the resistance peak diminishes (compare resistance traces in (a) and (c) of Figure 7.8.).

Since the coupons were held by hand at one end when offered to the electrodes, any small unbalancing torque could alter the fit-up; slight difference in the pattern of resistance variation in the initial part of the resistance trace, observed in certain cases, could have resulted from change in fit-up.

7.6 Resistance Welding and Resistive Heating

The process of heat generation in the work-piece during resistance welding and resistive heating of a single thickness of material is almost identical in nature; the significant difference in resistive heating of a single thickness is the absence of the sheet-to-sheet interface. In this instance, the pattern of dynamic resistance variation is investigated for both resistance welding and resistive heating, in order to ascertain how the dynamic resistance character-istics for the two processes are influenced by the existence of an

additional interface in one case and the lack of it in the other. The recorded traces shown in Figure 7.9 demonstrate the basic differences in the nature of dynamic resistance characteristics peculiar to the two processes, the machine settings being as below:

    Transformer Tapping - Number 6
    Electrode Force   - 1.55 kN (350 lbf)
    Weld Heat Control   - 65
    Weld time   - 15 cycles

The dynamic resistance trace in (a) of Figure 7.9 was obtained when two 0.735 mm (.029 in.)thick specimen coupons were welded, and re-presents the dynamic resistance characteristic for resistance welding mild steel. The resistance traces of (b) and (c) shown in Figure 7.9, however, are for resistive heating; these traces represent the dynamic resistance characteristics of resistively heated single specimen coupons of thickness 1.55 mm (0.061 in) and 2.06 mm (0.081 in) respect-ively. The above recordings were obtained without any zener nulling. The lower trace, in each case, was recorded with a 50 Hz low-pass filter at the output of the divider stage, whereas the upper trace was recorded without any filter.

Sciaky tiptrodes with 4.76 mm (0.1875 in) diameter tips were used for all three sets of recordings, and both sides of the specimen coupons were cleaned with emery paper and degreased with Solvere III. The following observations were made from a comparison of the recorded traces and the registered current values.

(i) Although the total material thickness corresponding to two 0.735 mm

   (0.029 in) thick coupons is less than the single thickness of

   1.55 mm (0.061 in) and 2.06 mm (0.081 in) thick materials, the

   peak r.m.s. current in the case of resistance welding is less than

that for resistive heating. Thus, the presence of a sheet-to-sheet interface raises the effective electrical resistance and restricts the current in the constriction far more effectively in resistance welding than in the case of resistive heating.

(ii) The distinctive patterns of the dynamic resistance traces for resistive heating, as opposed to resistance welding, are evident from the recorded traces. The dynamic resistance traces for resistive heating are distinguished by the absence of a well defined peak;, moreover, for resistive heating, the resistance trace does not show any appreciable fall in resistance value after reaching the maximum.

7.7 Summary of Conclusions correlating Dynamic Resistance Characteristic to Weld Formation

The following conclusions relating the formation of weld nugget to the pattern of dynamic resistance variation are summarized from the observations made earlier in this Section.

(a) Typical Dynamic Resistance Characteristic for a Good Weld in Mild Steel

A good or acceptable weld in low-carbon mild steel is characterized by a well-defined peak in the dynamic resistance curve, appearing quite early during a weld. Provided that the diameter of the electrode tips and the electrode force are selected properly, the appearance of a prominent peak in the dynamic resistance trace is an indication that the welding current has been set approximately in the range of optimum values.

(b) Influence of Variation in Current

With very low welding current, the dynamic resistance trace does not show a prominent peak. As the welding current is increased above

a threshold value, a well-defined peak appears. In this instance, the threshold value was 5400 A. With excessive current, a splash weld occurs and is characterized by one or more steps in the resistance trace.

(c) Influence of Variation in Weld Time

Provided that the approximate range of welding current, appropriate to a specific situation, has been selected by suitable choice of transformer tapping and phase-shift heat control setting, any increase in weld time above a minimum threshold does not alter the position or the magnitude of the peak in the resistance trace. In this case, the minimum weld time for the appearance of the peak was 7-8 cycles. A longer weld time does not substantially affect the process of nugget formation, and a very long weld time does not necessarily produce a better weld.

(d) Influence of Variation in Electrode Force

The factor most likely to create confusion in interpreting dynamic resistance characteristics is electrode force. With low electrode force, the dynamic resistance curve shows a prominent peak and a high peak value of resistance. Thus, to safeguard against any wrong interpretation of the dynamic resistance characteristics, it is suggested that the electrode force be set to a value slightly higher than the recommended minimum in a particular situation. The probability of occurrence of splash welds is significantly reduced when welds are made with a higher electrode force.

(e) Influence of Variation in Electrode Tip Diameter

Interpretation of the dynamic resistance characteristics, when the size of the electrode tips is in accordance with the recommended practice*, is no problem. If, however, the tip size is very much different from the recommended value, the resistance traces are likely to be misinterpreted.

---

*See .B.S.1140: 1957.

Thus, with electrode tips of small diameter, the dynamic resistance trace shows a prominent peak. With tips of large diameter, on the other hand, the dynamic resistance traces show a flattened peak.

Although the total current through the weldment may be high when using tips of large diameter, the effective current density in the metallic constriction may not be high enough to produce a good weld. On the contrary, use of electrode tips of large diameter results in (i) increased heat loss by conduction, and (ii) a less uniform contact over the surface of the work-piece. To overcome (i), the current has to be increased further; to eliminate (ii), the electrode force has to be increased. Thus, use of electrode tips of large diameter does not effectively enhance the conditions for the creation of a good weld.

(f) Influence of the Sheet-to-Sheet Interface in Resistance-spot Welding

It is evident from the discussion in 7.6 that the existence of a sheet-to-sheet interface in resistance welding effectively increases the resistance and restricts the current to lower values. The pattern of dynamic resistance variation for resistance welding is also distinctly different from that for resistive heating, and this is clearly demonstrated by the recorded traces shown in Figure 7.9. Again, in 7.4 it has been shown that there is a significant difference in the registered current values for welds with 'clean' and 'unclean' interfacial contacts using identical machine settings; the distinguishing features of the pattern of resistance variation peculiar to 'clean' and 'unclean' contacts are exemplified by the recorded traces of Figure 7.7.

It may, therefore, be concluded that any modification in the nature of the sheet-to-sheet interface affects the process of nugget formation, and that dynamic resistance characteristics reflect such modifications. Thus, the pattern of dynamic resistance variation can

be a pointer to whether a sheet-to-sheet interface exists or not; or it may indicate whether layers of oxides and other chemicals offering a high initial resistance are present at the contacting surfaces of the workpiece. Experimentation has also shown that the probability of occurrence of splash welds increases when welding 'unclean' specimens. It is, therefore, recommended that (i) to ensure adequate current flow and (ii) to avoid splash welds, the work-piece should have reasonably clean surfaces.

(g) Shunting Effect

The problem of current shunting is not usually encountered in single resistance-spot welds; knowledge of the changing pattern of resistance variation due to shunting effect, however, provides some additional insight into the process of nugget formation, and may find application in monitoring nugget growth in situations where the work-piece contains a large number of spot welds.

It is noted from 7.5 that when a fresh weld is made close to an existing spot weld in a work-piece, the dynamic resistance curve of the second weld is flattened; the closer a second weld is made to an existing weld, the flatter is the dynamic resistance curve. It is interesting to note in this context that, although the total current enclosed by the toroid and indicated by the current meter may show a slight increase, the effective current through the second weld may be lower because of the shunting effect.

The results of investigations have so far been analysed with a view to relating dynamic resistance characteristics to nugget growth and no attempt has been made to analyse the physical process of spot welding in detail. On the basis of electron theory of conduction in metals it can be shown* that there is a definite relationship between

---

* See Appendix 1.

electrical and thermal properties[27] of metals, and a rigorous treatment of such topics, with special reference to electrically heated metallic contacts, is to be found in the work of Greenwood and Williamson[28]; further discussion in this respect is included in Section 16.
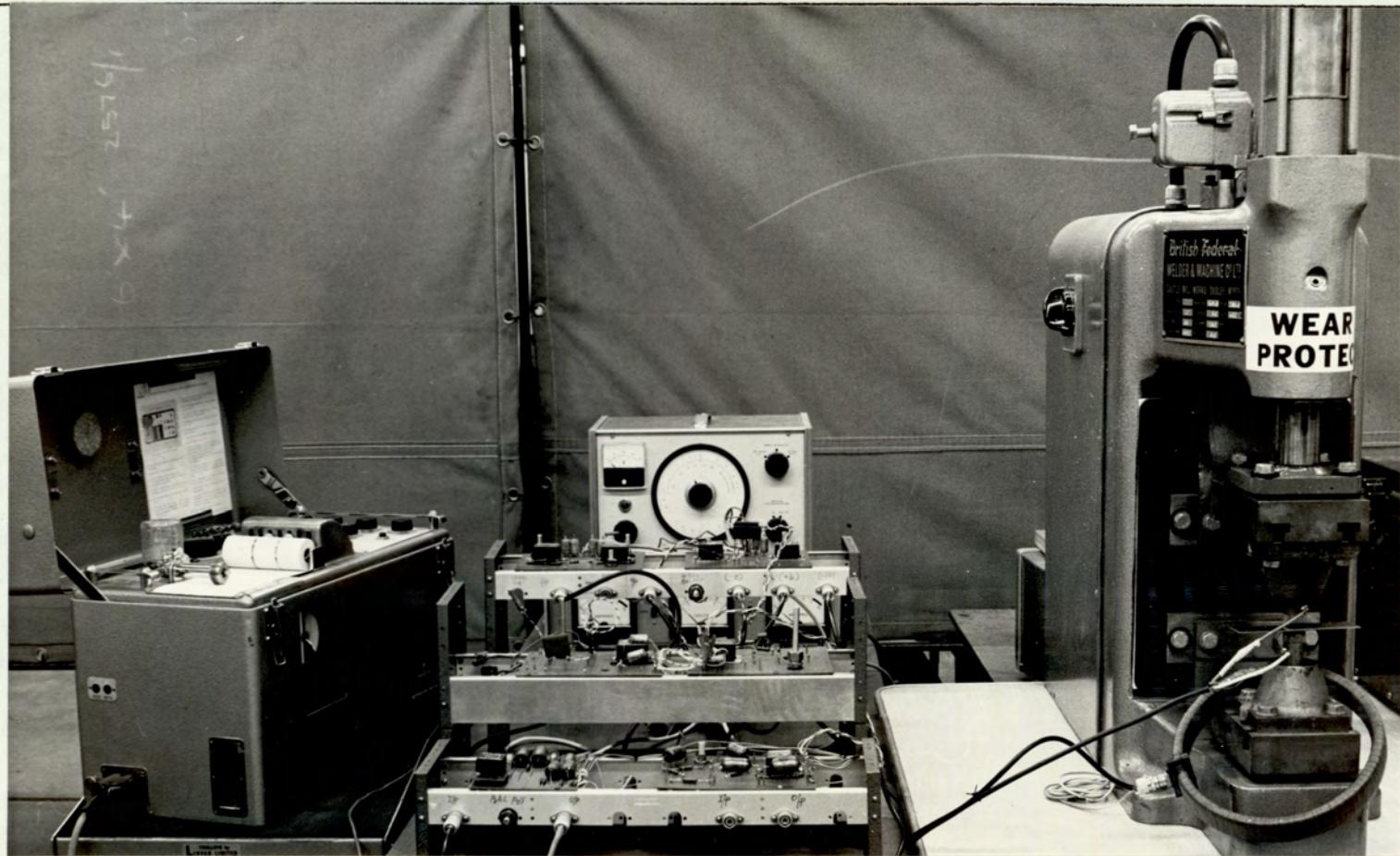
FIG. 7.1. Dynamic Resistance Measurement System in Operation.
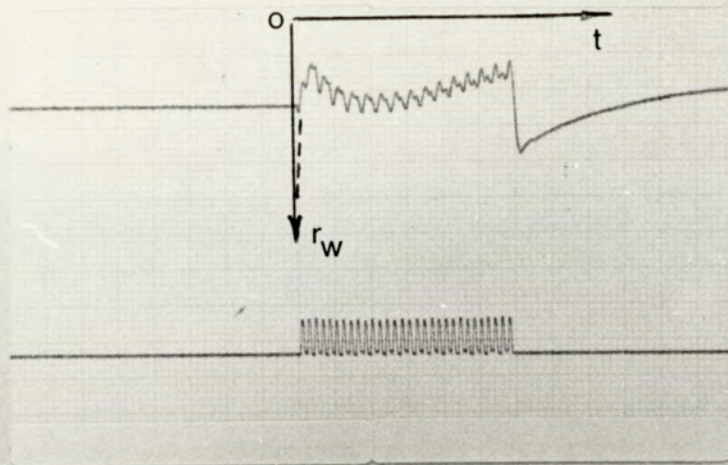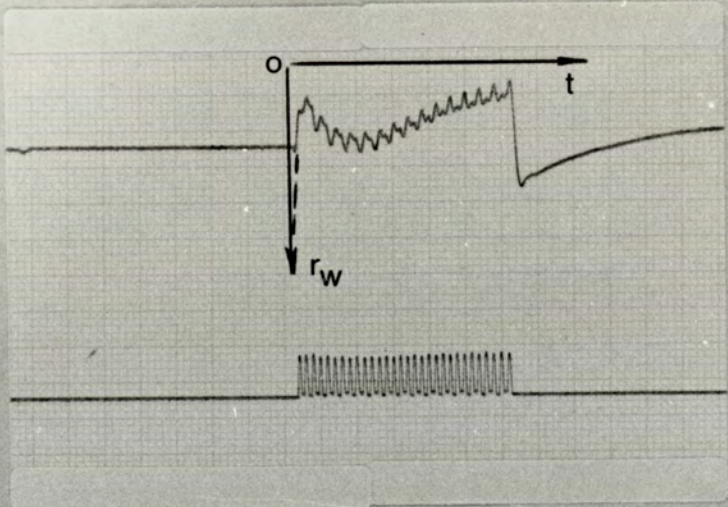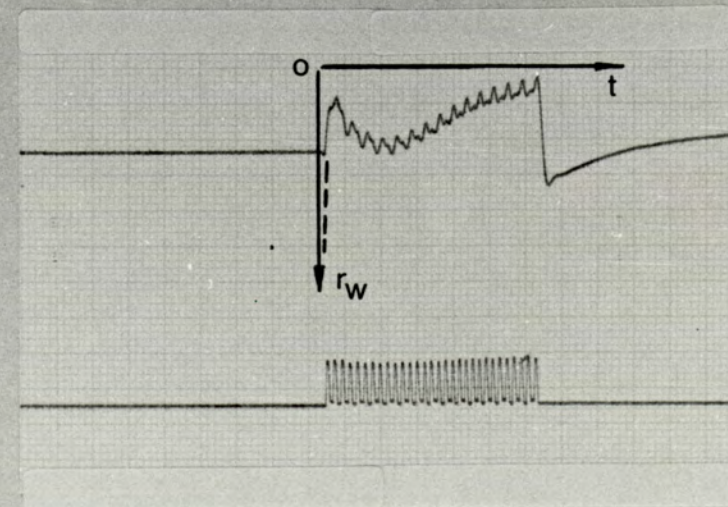
FIG.7.2. Dynamic Resistance Traces when Current was Varied by Altering Transformer Tapping.

Upper Trace: Resistance, 2V/cm; Lower Trace: Current, 10V/cm.

Transformer Tappings: (a) No.5; (b) No.6; (c) No.7.
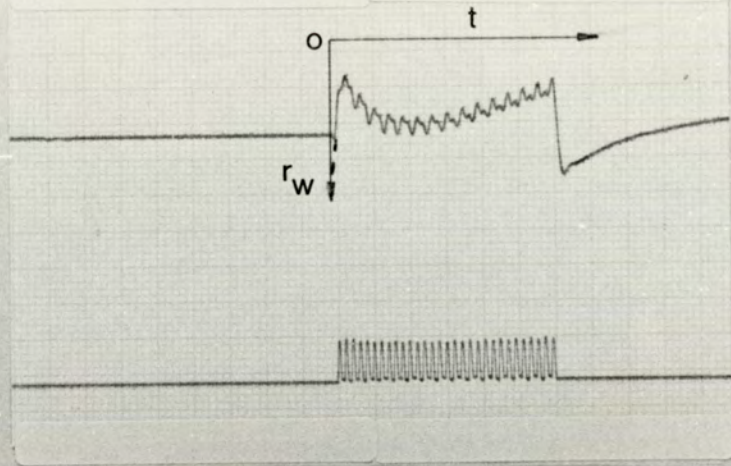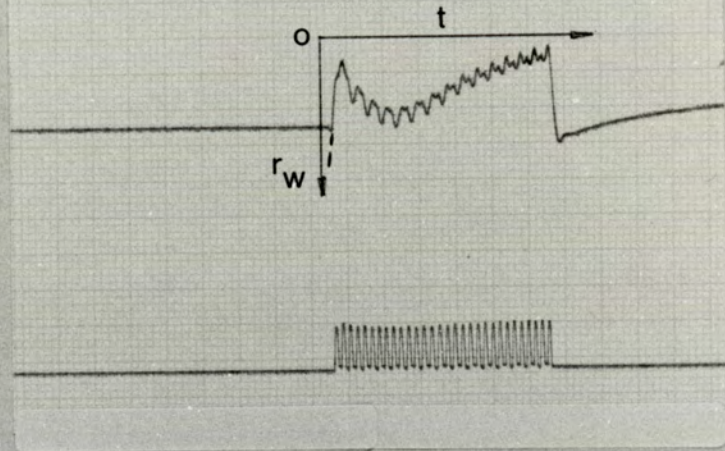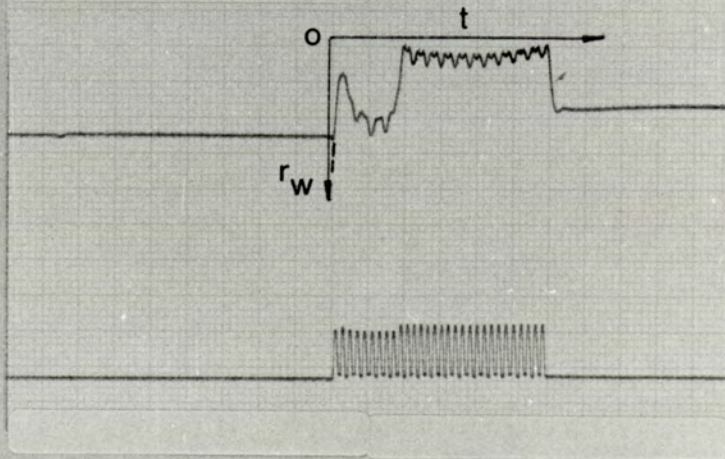
FIG.7.3. Dynamic Resistance Traces when Current was Varied by Phase-Shift Control.

Upper Trace: Resistance, 2V/cm; Lower Trace: Current, 10V/cm.

Weld Heat Settings: (a) 60; (b) 65; (c) 75, Splash Weld.
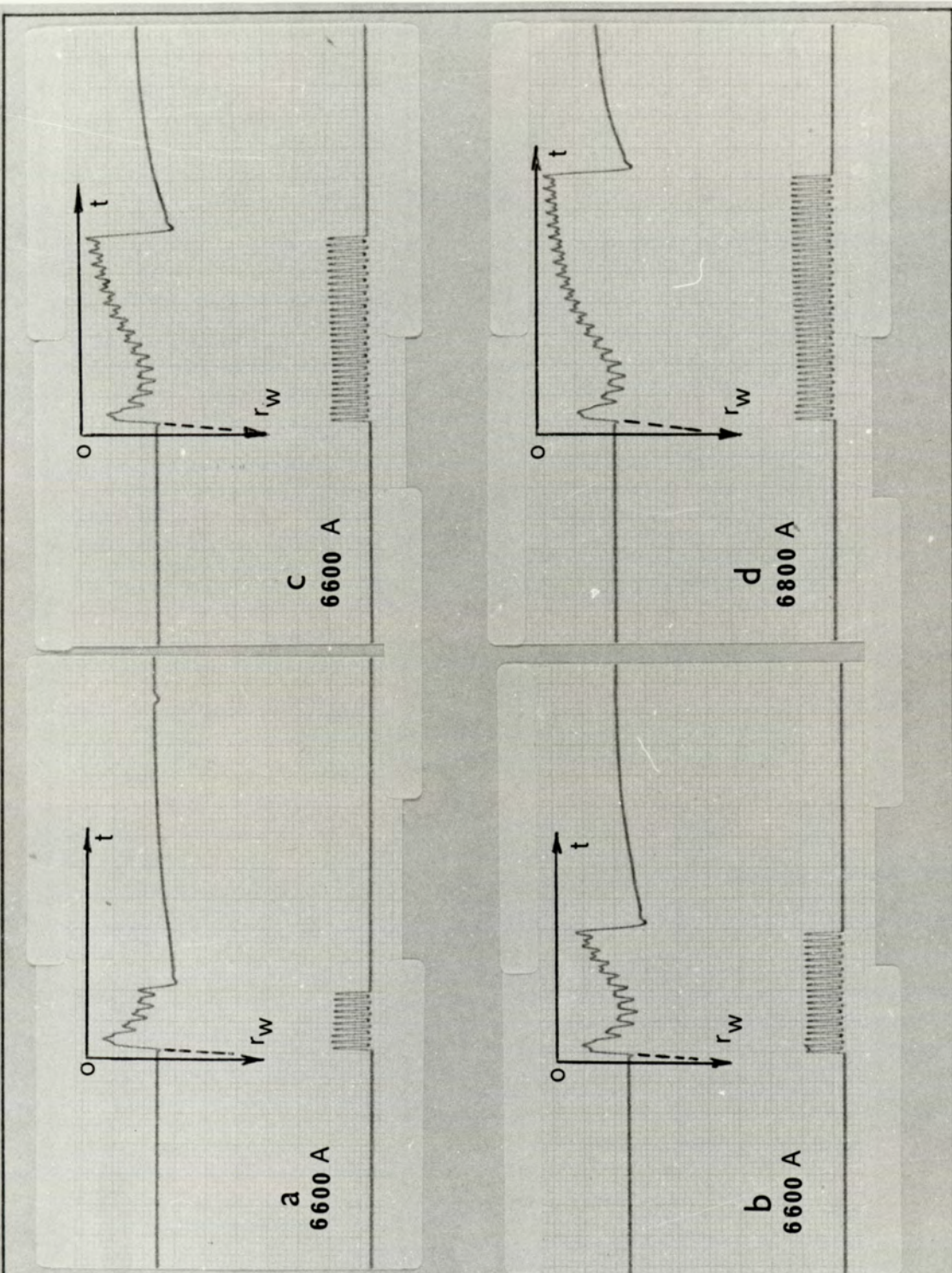
FIG.7.4. Dynamic Resistance Traces for Different Weld Times.

Upper Trace: Resistance,2V/cm; Lower Trace: Current, 10V/cm.

Weld Times: (a) 5 cycles; (b) 10 cycles; (c) 15 cycles;
(d) 20 cycles.
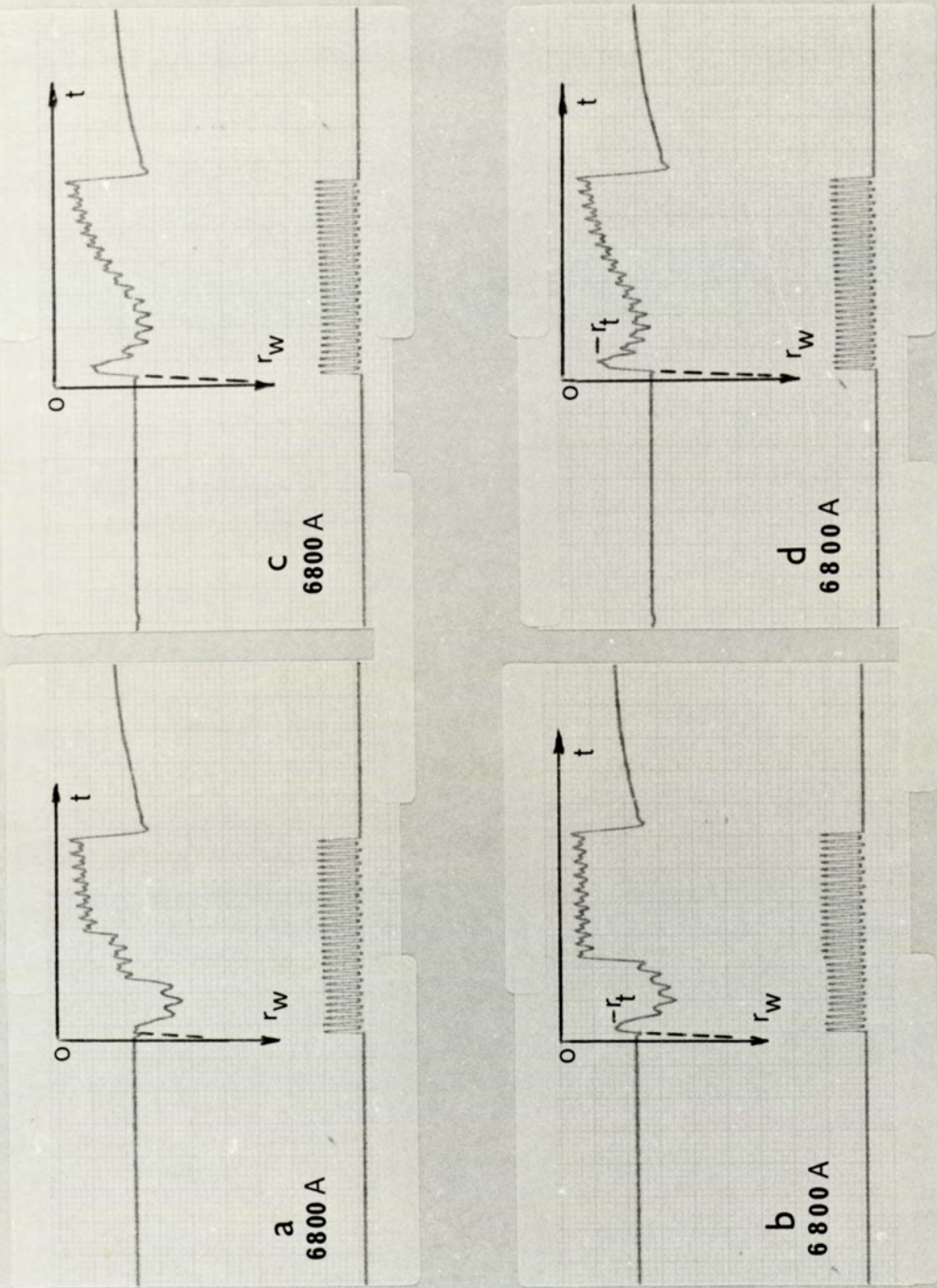
FIG.7.5.Dynamic Resistance Traces when Electrode Force was Varied

Upper Trace: Resistance, 2V/cm; Lower Trace: Current, 10V/cm.

Electrode Force: (a) 868N (195 lbf); (b) 1.07 kN (240 lbf);
(c) 1.31 kN (295 lbf); (d) 1.78 kN (400 lbf).
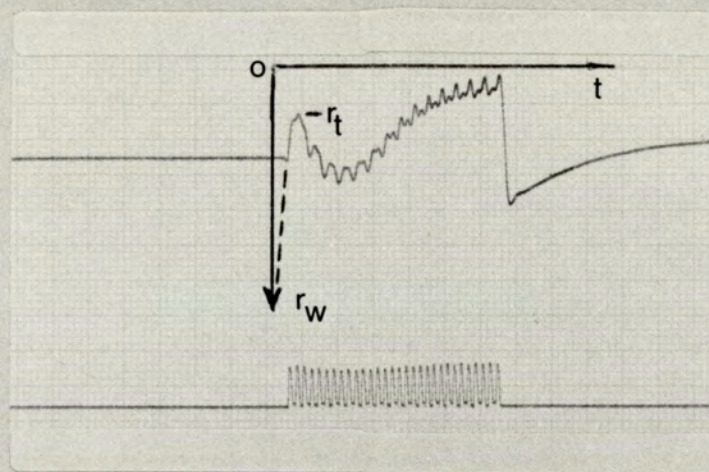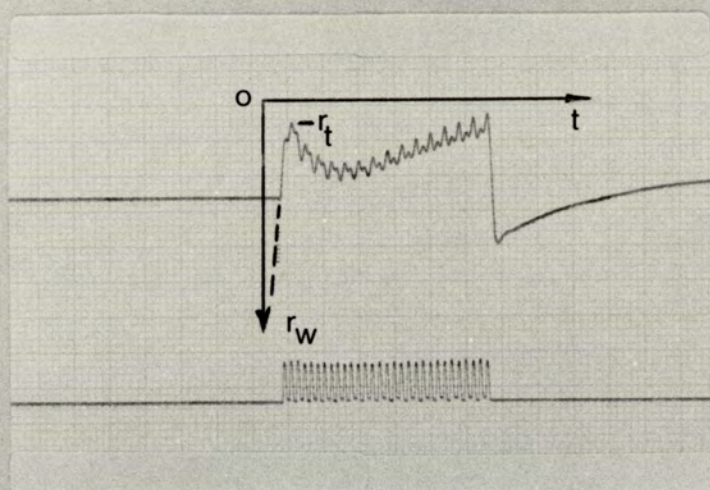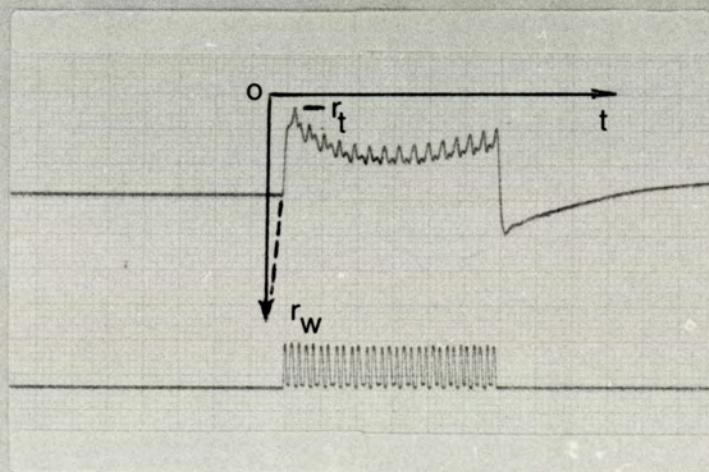
FIG.7.6. Dynamic Resistance Traces using Electrode Tips of Different Diameters.

Upper Trace:Resistance, 2V/cm; Lower Trace:Current,10V/cm.

Tip Diameters: (a) 3.18 mm; (b) 4.76 mm; (c) 6.35 mm.
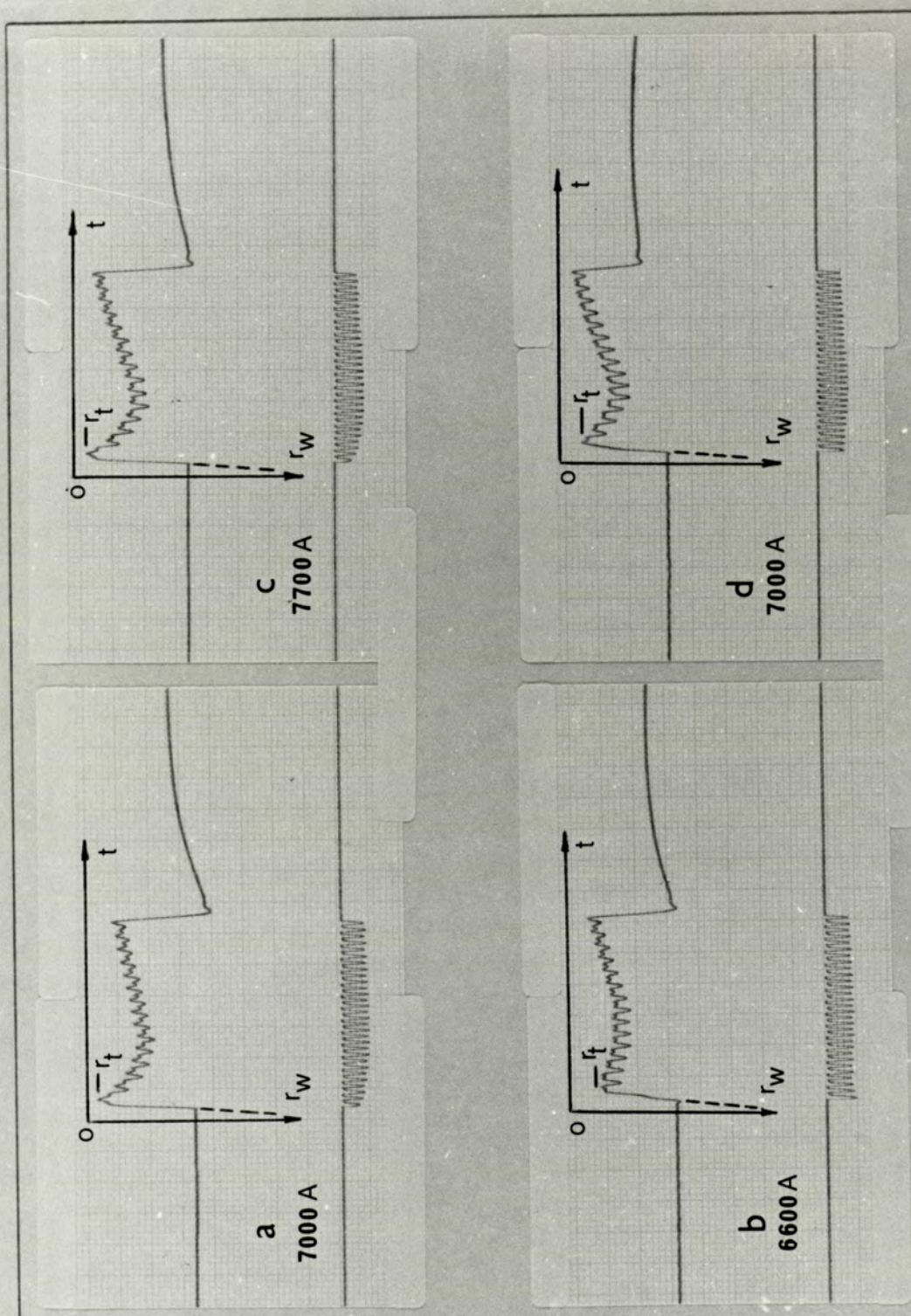
FIG.7.7. Dynamic Resistance Traces with Clean and Unclean
Sheet-to-Sheet Contact.

Upper Trace: Resistance, 2V/cm; Lower Trace: Voltage, 10V/cm.

(a) and (c) 'Clean' Contacts; (b) and (d) 'Unclean' Contacts.

a
6700 A
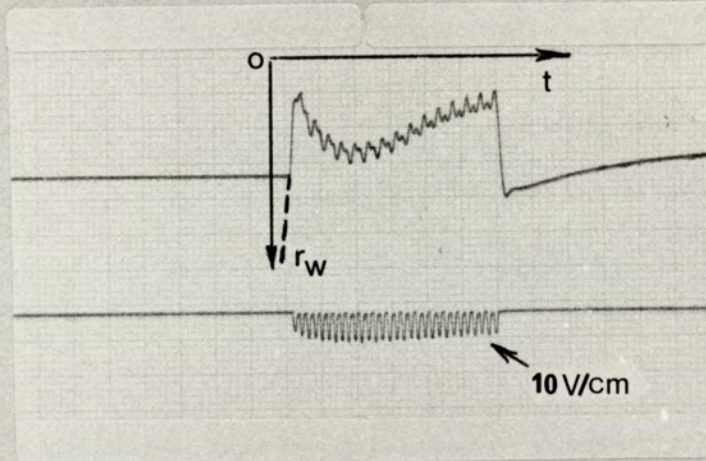
b
6800 A
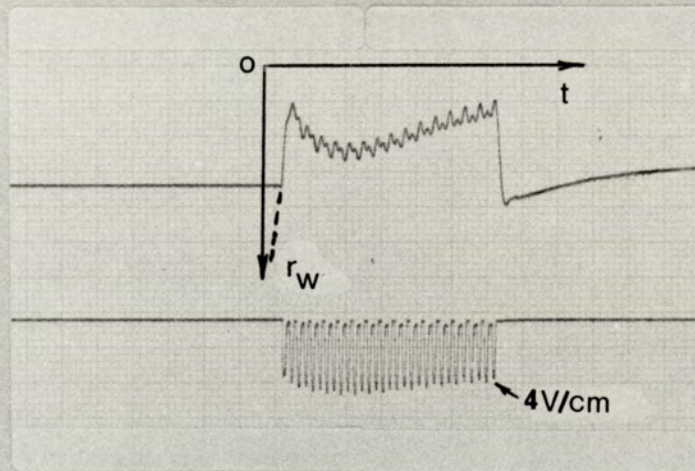
c
6850 A
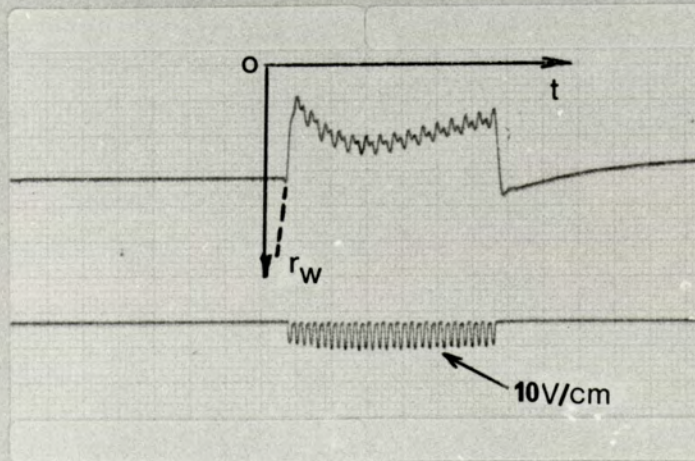
FIG.7.8. Dynamic Resistance Traces Modified by Current Shunting.

Upper Trace: Resistance, 2V/cm; Lower Trace: Voltage.

(a) Single Spot; (b) Second Spot 76.2 mm away;
(c) Second Spot 12.7 mm away.
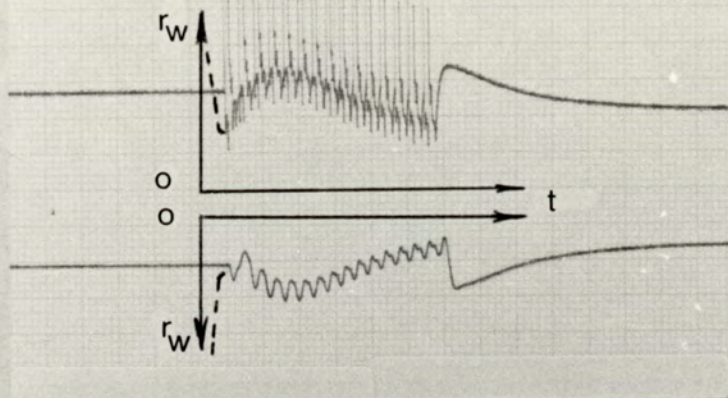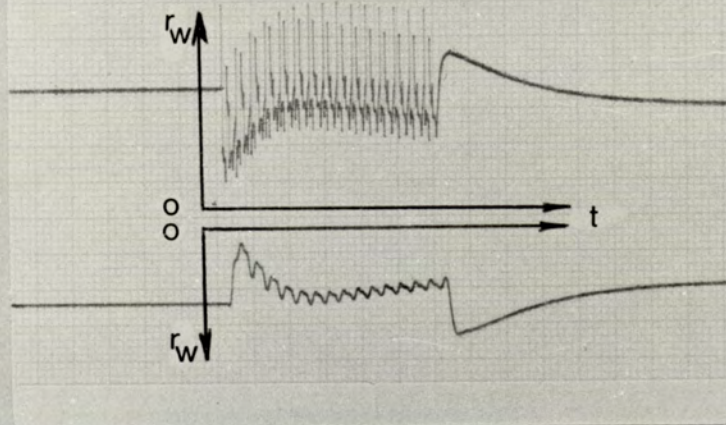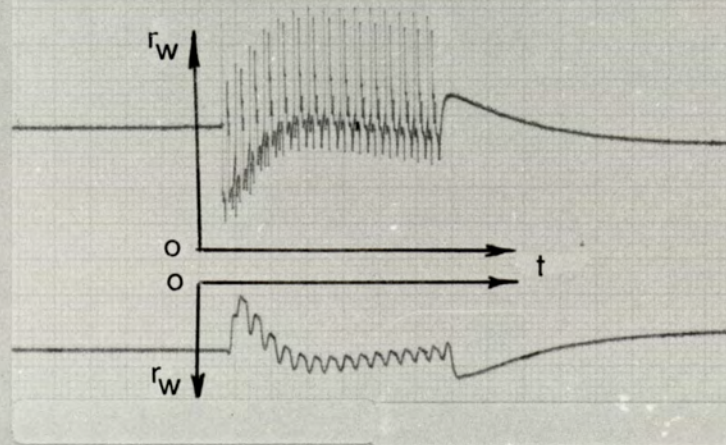
FIG.7.9. Dynamic Resistance Traces for Resistance Welding and Resistive Heating.

Upper Trace: Direct Divider Output, 2V/cm.

Lower Trace: Through a 50 Hz Low-pass Filter, 2V/cm.

(a) Resistance Welding - 2 x ·735 mm; (b) and (c) Resistive Heating - Single thickness of 1.55 mm and 2.06 mm respectively.

8.   UTILIZATION OF DYNAMIC RESISTANCE IN WELD QUALITY MONITORING

8.1 Outlines of a Modified Instrumentation System for
      Measuring Dynamic Resistance

The electronic instrumentation system of Figure 5.1, although
adequate to provide a qualitative representation of the pattern of
dynamic resistance variation, has certain drawbacks. The accuracy of
the recorded signal, using the above electronic instrumentation system,
is somewhat impaired because of the following:

(a) Unequal current conduction by the pair of ignitrons in the
primary circuit of the welding transformer.

(b) Inherent problem of divider operation when the denominator
goes through zero.

To improve accuracy of measurement and to remove the unwanted
oscillations from the dynamic resistance trace the following modifica-
tions can be incorporated in the instrumentation system.

(i) Use of Half-wave Rectifiers

Referring to the recorded traces of Figure 6.2, it may be seen
that the voltage and current waveforms after full-wave rectification
have unequal peaks in successive half-cycles. This is due to unequal
current conduction through the ignitrons in the primary circuit of the
welding transformer. Discussion with the manufacturers of the welding
machine confirmed that such inequality in the current-conducting
properties of the two ignitrons was usually noticed after a period
of use. It is also to be noted that the full-wave precision
rectifier circuit produces an unbalanced output unless the half-
cycles of the input a.c. waveform have equal amplitude.

By contrast, a more accurate representation of current and voltage variation may be obtained after half-wave rectification, and dynamic resistance computed on the basis of voltage and current values during alternate half-cycles will be equally effective in monitoring weld quality.

(ii) Use of Gated Inputs to the Divider Stage

A major problem in continuous computation of dynamic resistance is that the denominator of equation (5.1) cannot be maintained at a non -zero value during a complete half-cycle, because of the 'dead periods' in weld time. It is suggested that, to prevent positive feedback at the instants when the denominator goes through zero, the inputs to the divider stage may be gated[29] at predetermined intervals so that the divider operation is meaningful only during such intervals. To ensure elimination of harmonics from the inputs to the divider, however, the half-wave rectifiers may be followed by low-pass filters. The divider output may also be sampled[30] at definite intervals for display or recording.

A block diagram of the instrumentation system with the proposed modifications is shown in (a) of Figure 8.1; the block diagram of (b) is included to illustrate the method of generating synchronous gating signals to operate the analogue gates shown in (a).

8.2 Use of Dynamic Resistance Characteristics for Initial Selection of Welding Variables

It is evident from Sections 6 and 7 that a close inspection of the pattern of dynamic resistance variation can reveal whether the correct welding variables have been selected or not. Thus, for a mild steel work-piece, the machine settings may be varied and the

dynamic resistance trace recorded for each set of machine variables. Provided that the electrode force and the size of the electrode tips have been chosen according to the recommended practice, a well-defined peak in the resistance trace will indicate that the other welding variables have been set to approximately correct values. This suggests that the dynamic resistance characteristic can be used for initial selection of the welding variables.

8.3 Application of Dynamic Resistance Measurement in In-process Weld Quality Monitoring

The exact nature and extent of control required to maintain a desired weld quality may depend on several factors. Under certain conditions, an indication signifying completion of a good weld may be adequate. For this purpose, a suitable process parameter may be monitored and an indication, in the form of a visible or audible signal, may confirm the completion of a good weld. For single spot welds, a simple in-process monitoring system of the above nature may be all that is required in many cases and is outlined in the following.

With the instrumentation system shown in the block diagram (a) of Figure 8.1, the machine is initially set with the optimum welding variables and a test weld is made. Figure 8.2 shows the typical pattern of dynamic resistance variation, drawn in the positive quadrant, for a good weld in mild steel; the instants of sampling are marked as t_1, t_2 ....t_5. The sampled values of dynamic resistance for the test weld may be retained in electronic memory and compared with values of dynamic resistance for subsequent welds. Thus, all subsequent welds, where the resistance values at the instants t_1, t_2,.......t_5 are in agreement with those for the test weld, within an acceptance band, may be declared as good as the test weld made in the beginning.
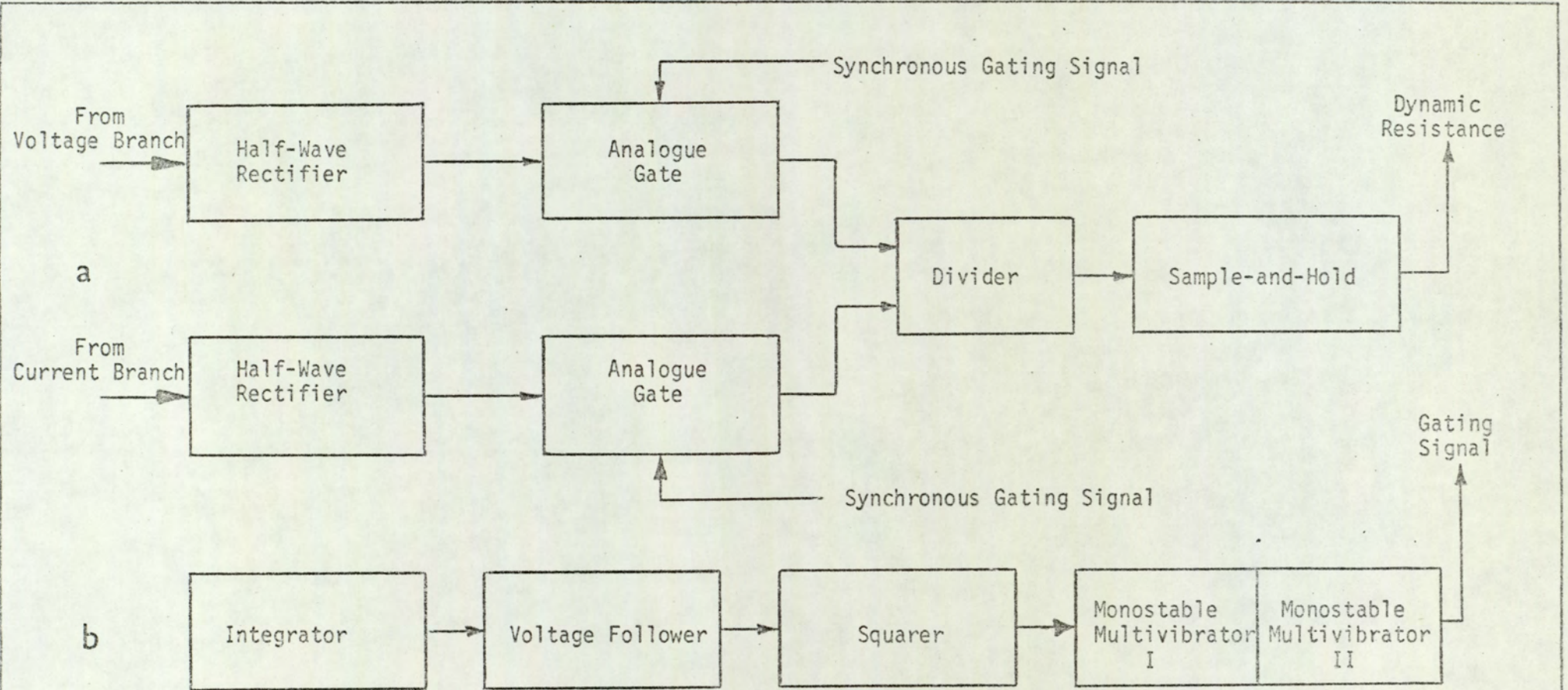
FIG. 8.1 Block Diagram of Dynamic Resistance Measurement System with the Proposed Modifications.

(a) Proposed Modifications; (b) Method of Generating Synchronous Gating Signals.
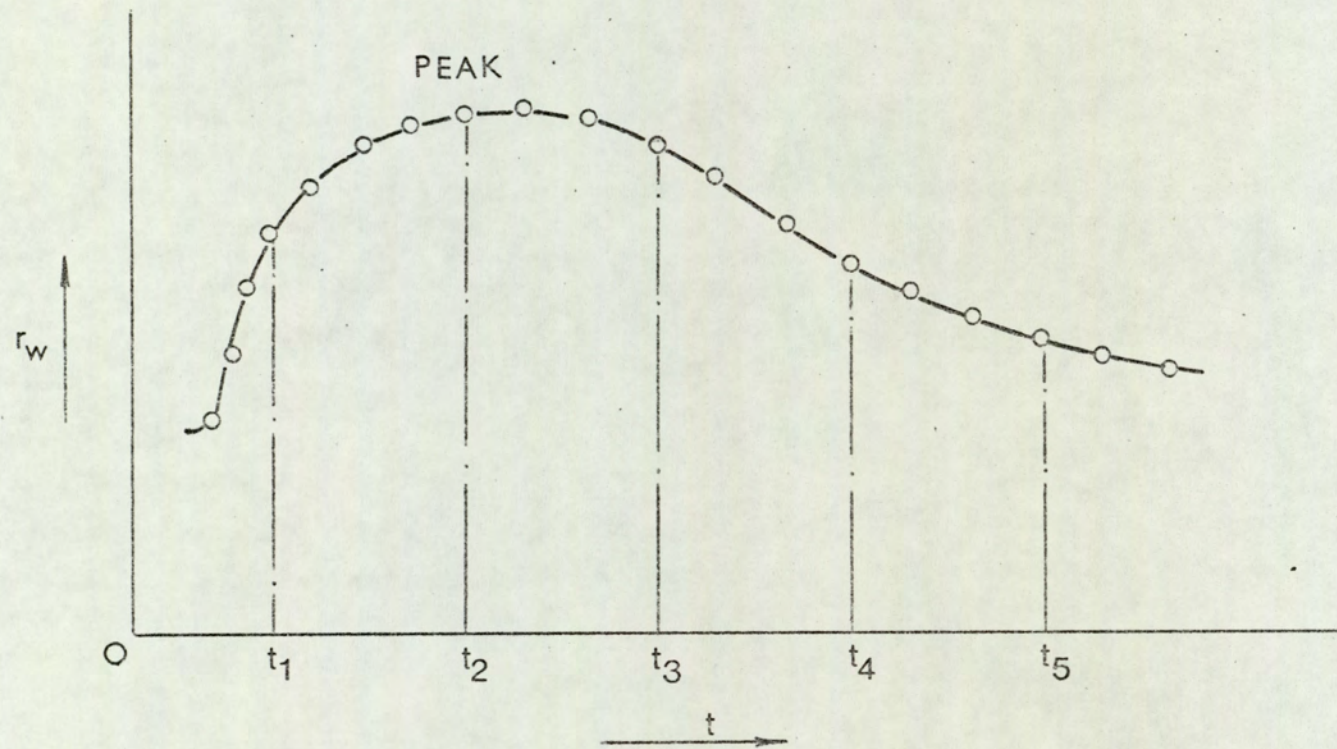
FIG. 8.2 Periodic Sampling of Dynamic Resistance for a Test Weld in Mild Steel.

PART II

WELD QUALITY MONITORING BY DETECTING THERMAL

RADIATION FROM THE WELD.

9.   INTRODUCTION AND LITERATURE SURVEY

9.1 Significance of Thermal Condition of the Weld as a
     Process Parameter

During a spot weld, Joule heating occurs in the bulk resistance
of the specimen coupons as well as in the contact resistance effective
at the electrode-to-sheet and sheet-to-sheet interfaces, and the
resulting change in thermal condition sets off the complex chain of
events leading to the characteristic variation exhibited by the dynamic
resistance curve*. Similarly, the change in volume due to thermal
expansion and change of state of the weld metal, observable as electrode
separation or electrode displacement,(9,10) is caused by temperature
rise of the welded joint. Thus, the physical phenomena, observed as
variation of electrical resistance of the weld and electrode separation,
are manifestations of the thermal changes affecting the weldment.
Furthermore, if the process of spot welding is thought of as a method of
forging an intimate metallic bond between two pieces of metal, then it
is essential that the mass of metal held between the electrode tips must
be raised to an adequately high temperature for the forging action to
be effective. It will, therefore, be appreciated from the preceding
logic that thermal changes occurring in the weldment are more fundamental
in nature, and knowledge of the thermal condition of the weld is of primary
significance in assessing the progress of nugget development.

Evaluating thermal condition of the weld implies knowledge of its
temperature in the first place. To specify thermal condition more fully,
it is necessary to know the temperature at various points of the welded
joint at any instant, since the spatial distribution of temperature
progressively changes during the formation of a weld.

---

* See Part I

9.2 Literature Survey of Temperature Measurement in Spot Welding

Experimental determination of temperature within a spot weld has proved to be extremely difficult. Knowlson[23] and Beevers[31] used specially prepared specimens and thermocouple junctions to measure the temperature at the edge of the weld. Leads from the thermocouple junction were taken through a twin-bore fused alumina tube which was located in a machined groove in one of the specimen coupons. A fresh thermocouple was used each time a weld was made. It is obvious that the technique does not lend itself to application under production conditions; moreover, it is debatable whether the region near the edge of the weld responds instantaneously to the thermal cycle to which the centre of the weld is subjected.

Using a simulation model, Greenwood[32] obtained a computer solution for temperature distribution in a spot weld. However, the computer solution suggested by Greenwood was based on the following simplifying assumptions:

(i) There is no contact resistance, and so there is no localized heat production at the contact interfaces.

(ii) Material properties such as thermal conductivity, specific heat, and electrical resistivity remain unaltered during the process.

(iii) There is no heat loss from the free surface.

Although the computer solution of Greenwood gives an approximate idea as to the pattern of temperature distribution, the above simplifying assumptions are not valid during an actual spot weld.

A more comprehensive account of temperature distribution in a spot weld was given by Bentley et al.[33]; approximate determination of temperature, in various parts of the weldment in the vicinity of the

weld, was based on metallographic techniques whereby the changes in microstructure were related to various temperature ranges. The authors[33] compared their observations made for simulated and actual welds with the theoretical predictions based on the work of Greenwood[32]. Although Bentley et al. claim a good agreement between experimental results and theoretical calculations, they point out the limitations imposed by the simplifying assumptions of Greenwood.

It is interesting to note at this juncture that the significance of temperature as a process parameter in predicting weld quality was appreciated by Archer[6]; and his "voltage-constraint" principle was an attempt to relate the weld voltage to the "ultimate temperature" attained by the weld at "heat balance". The close connection between nugget dimensions and the temperature of metal in the nugget prompted Chuloshinkov et al.[7] to suggest the use of temperature as a process parameter. However, because of practical difficulties in evaluating the temperature of the weld, the indirect method proposed by Archer[6] was seen as the solution by Chuloshinkov et al. It is shown in 16.2 that Archer's equation relating weld voltage and weld temperature lacks the rigour of classical theories and cannot be supported by experimental results.

10. DETECTION OF THERMAL RADIATION FROM THE WELD

10.1 Weld Temperature and Thermal Radiation

It is a common experience in resistance-spot welding that, with adequate heat input, the weldment in the vicinity of the electrodes is heated to incandescence; the visible radiation emitted by the incandescent metallic mass may be observed as a glow from a distance, without the aid of any special apparatus. Since the emitted radiant intensity of an incandescent body can be related to its temperature, attempts were made in the past to relate the radiation from the weld zone to the thermal condition of the weld. Thus, a method of controlling the 'level of heating' during a seam weld was devised by Truschenko and Sukhova[34]; in this method, a photoelectric detector was located externally and focused on to the weld. A similar attempt was made by Gubenko et al.[35] in the case of spot welds; in this case, infra-red detectors were located around the top electrode holder to receive radiation from an annular zone of the weldment surrounding the electrodes. In their treatment, Gubenko et al. do not explain the reasons for detecting the radiant emission from a zone outside the actual weld spot; perhaps the practical difficulty of gaining access to the weld spot was the deciding factor in their selection of a zone outside the weld. Results due to Bentley et al.[33] indicate that the highest temperature is attained at the centre of the nugget and gradually falls off at regions remote from the axis of the constriction. This is illustrated in Figure 10.1., which shows the theoretical distribution of temperature due to Greenwood and Williamson[28]. T_s, the temperature of the weld surface is determined by the maximum temperature T_i at the centre of the nugget; therefore, the existence of an isothermal T_s at the weld surface is an

indirect confirmation of the attainment of a much higher temperature T_i at the centre of the weld nugget.

Again, the theoretical curves of heating and cooling obtained by Greenwood[32] show that temperature variation with time is maximum near the centre of the weld spot, and is less at points further away from the centre. Thus it seems more appropriate to detect thermal radiation emitted from the centre of the weld spot, provided that a suitable detection technique can be adapted in practice. Accordingly, a method has been developed by Bhattacharya and Andrews[36]; in this method, thermal radiation from the centre of the weld surface can be collected through a minute aperture at the tip of the bottom electrode. The underlying principle of collecting thermal radiation from the weld surface is shown in Figure 10.2. The spectral radiant intensity over a specific waveband will, of course, be influenced by the radiating properties of the metal surface, and the spectral emittance ϵ_λ of the surface will have to be taken into account for correlating radiant intensity and temperature. For monitoring weld quality, however, an exact measurement of temperature is not necessary as long as an indication, representative of the thermal condition of the weld, can be obtained and related to weld quality. Initial experimentation, in this context, was carried out using a simple apparatus for visual observation of the glow from the centre of the weld spot; for more objective investigation, methods of photoelectric detection have been developed.

It may be noted in this context that the present series of investigations was conducted without any water-cooling of the electrodes; it is suggested that future developments, using electrodes with an aperture at the tip, could incorporate a suitable cooling system. In fact, at the time of writing this dissertation, an M.Sc. project*,

---

* See M.Sc. project of John Edgely, Department of Production Engineering (Welding Technology), 1971.

based on detection of thermal radiation from the weld spot, has been in progress in the Department.

10.2 Visual Observation of Glow from the Weld Surface

10.2.1. Description of the Apparatus used for Visual Observation

A photograph of the apparatus used for visual observation of the glowing weld spot is shown in Figure 10.3. The electrode holder was bored from one side, at a suitable angle, for smooth insertion of the light-guide. Nominal length of the light-guide was 0.914 m (36 in), the diameter of the fibre bundle being 1.5 mm (0.059 in.). One end of the light-guide was securely placed within the electrode and centrally located by means of an electrode-insert. The other end of the light-guide was used for viewing, and was held inside a black polythene tube; an ordinary retort stand was used to hold the polythene tube in position by means of clamps. An outer tube with an ordinary magnifying eye-piece mounted at the free end could slide along the length of the inner tube and facilitate easy focusing.

Initially, electrodes of one-piece construction as well as Sciaky tiptrodes, with a 0.685 mm (0.027 in.) diameter aperture at the electrode tip, were used. However, preparation of the tiptrodes was found comparatively simpler. Details of a specially prepared tiptrode are shown in Figure 10.4. Components used in the construction of the viewing apparatus are shown in the photograph of Figure 10.5. The receiving end of the light-guide was protected with a thin piece of mica to prevent any hot metal damaging the polished end face of the light-guide. The complete viewing apparatus in operation is shown in the photograph of Figure 10.6.

10.2.2. Results of Visual Observation

Visible radiation from the centre of the weld could be seen as a diffused glow, when viewed through the eye-piece of the apparatus described in 10.2.1. Using the colour temperature charts[27], an approximate estimation can be made of the surface temperature of the weld from the observed glow. Thus, with insufficient welding current, the base metal between the electrode tips did not reach incandescence, and no glow could be observed; in the absence of any visible glow, the temperature was estimated to be below 773 K (500°C). With adequate welding current, the weld spot could be seen to glow, the intensity and colour of the glow changing as the weld nugget was formed. During a satisfactory weld, the glow changed from dull red to a sustained bright red towards the end of weld time; on the colour charts, bright red denotes a temperature in the range 1073 K - 1173 K (800°C - 900°C). Excessive current resulted in a splash weld indicated by a bright, orange flash; a bright, orange colour indicates a surface temperature in the region of 1173K - 1373 K (900°C - 1100°C).

The weld times for the above observations were about 10 - 15 cycles or 200 - 300 ms. Such short periods of observation do not permit anything more than a subjective impression of the varying intensity and colour of the glow. It is, therefore, suggested that a cine camera, used in conjunction with colour films, may yield more objective results under these conditions.

10.3. Photoelectric Detection of Radiation from the Weld

10.3.1. Selection of Radiation Detectors

Because of the small dimension of the aperture at the tip,

the radiant power collected through the aperture is very small. Again, the variation in radiant power through the aperture is to be interpreted as temperature variation of the weld surface. Thus, a reasonably high sensitivity and a fast response time are desirable in a detection system to operate under these conditions. In this respect, photoelectric detectors with high normalized detectivity D_λ^* and short time constant are preferable to thermal detectors. Since the response of the detector is dependent upon the spectral distribution of radiant power emitted by the source, it is necessary to have knowledge of the approximate temper- ature range of the source. From the experimental results of Bentley et al.[33], the maximum temperature at the centre of the weld nugget is about 1723 K (1450°C) when a weld is made using two 6.35 mm (0.25 in) thick mild steel specimens; the corresponding temperature of the weld surface immediately above (or below) the electrode tip is about 1023 K (750°C). With some approximation, therefore, the maximum and minimum temperature in the weld region may be taken as 1800 K and 1000 K res- pectively. Let λ_{1800} and λ_{1000} be the wavelengths of maximum radiant intensity corresponding to 1800 K and 1000 K. By Wien's displacement law, the values of λ_{1800} and λ_{1000} can be calculated. Thus λ_{1800} = 1.6 μm, and λ_{1000} = 2.9 μm. Since both the wavelengths are in the near infra-red region, a considerable proportion of the radiant power emitted by the weld is in the near infra-red region of the spectrum. It may appear, therefore, that a photodetector should be selected to respond to wavelengths between 1.6 μm and 2.9 μm; in fact, it may be argued that for sensing temperatures around 1000 K, detection at the longer wavelength of 2.9 μm is more desirable. However, an important factor in the present context is the temperature variation of the weld surface, and the dynamic range of operation of the detector is to be considered as well.

Let λ_{max} denote the wavelength of maximum radiant intensity from a source at temperature T. It may be shown[37] that the radiant intensity $W(\lambda,T)$ in the neighbourhood of λ_{max} varies as the fifth power of temperature. Thus, a very small change in temperature will result in a large change in radiant intensity, if radiant intensity is measured at wavelengths near λ_{max}. This, in turn, requires a large dynamic range for detection and signal processing. Therefore, although the selection of a waveband in the neighbourhood of λ_{max} makes available a larger amount of radiant power for detection, the signal processing system must have a large dynamic range as well. Inclusion of an absorbing glass, similar to that used in optical pyrometers, in the path of the radiant beam, is one solution under such circumstances. If, on the other hand, the effective wavelength is further removed from λ_{max}, then $\frac{d}{dT}\{W(\lambda,T)\}$ is less, and the detection system can operate over a wider temperature range. A fuller theoretical treatment of the above aspects is given by Franson et al.[37].

Commercially available silicon detectors with peak responses at 0.9 μm were used in conjunction with red glass filters, for the major part of the present investigation, thus eliminating the problem of small dynamic range of detection. In order to detect longer wavelengths around 2 μm, a detection system employing a lead sulphide photoconductive cell was used.

Finally, most methods of photoelectric detection usually require some means of modulating or 'chopping' the radiation signal. In this instance, however, the intensity of thermal radiation from the weld goes through a maximum at the instant of peak welding current during each half-cycle of weld time. This is equivalent to chopping the radiation signal at 100 Hz, and the detector output is an amplitude modulated

waveform with 100 Hz as its carrier frequency. Thus, by taking the output of the detector through a tuned amplifier, an amplitude modulated signal representing the thermal condition of the weld surface can be recorded.

10.3.2. Direct-Incidence Mode Detection

In the 'direct-incidence mode', the detector is located inside the electrode or in the hollow of the electrode holder; thermal radiation from the centre of the weld spot is directly incident upon the active surface of the detector, through the aperture at the tip of the bottom electrode (see (a) in Figure 10.2.). The photodetector transforms the radiation signal into an electrical signal, which is then processed to derive the relevant information.

10.3.3. Remote-Transmission Mode Detection

In the 'remote-transmission mode', the radiation detector is located remote from the machine; a light-guide or fibre optic component, one end of which is located inside the electrode, transmits the radiation on to the detector (see (b) in Figure 10.2.). Thus, conversion of radiant power to an electrical signal as well as further processing of the signal are carried out away from the welding machine.
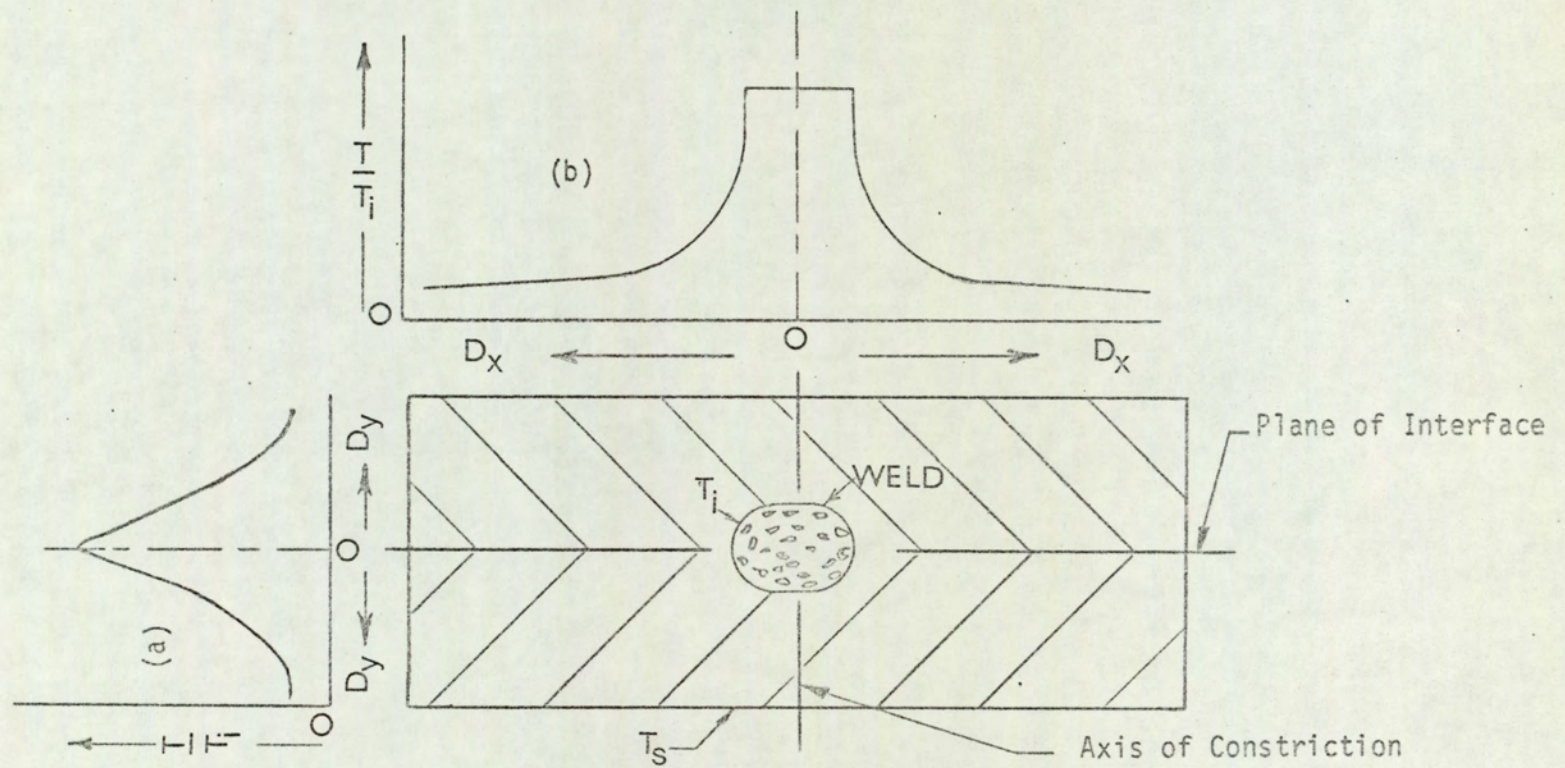
FIG. 10.1 Temperature Distribution in Spot Weld Related to Maximum Temperature at the Centre.

(a) Variation along the Axis of Constriction; D_y is the distance away from the Plane of Interface.

(b) Variation in the Plane of the Interface; D_x is the distance from the Axis of Constriction.

A - Protuberance

B - Aperture

Detector

Light-guide
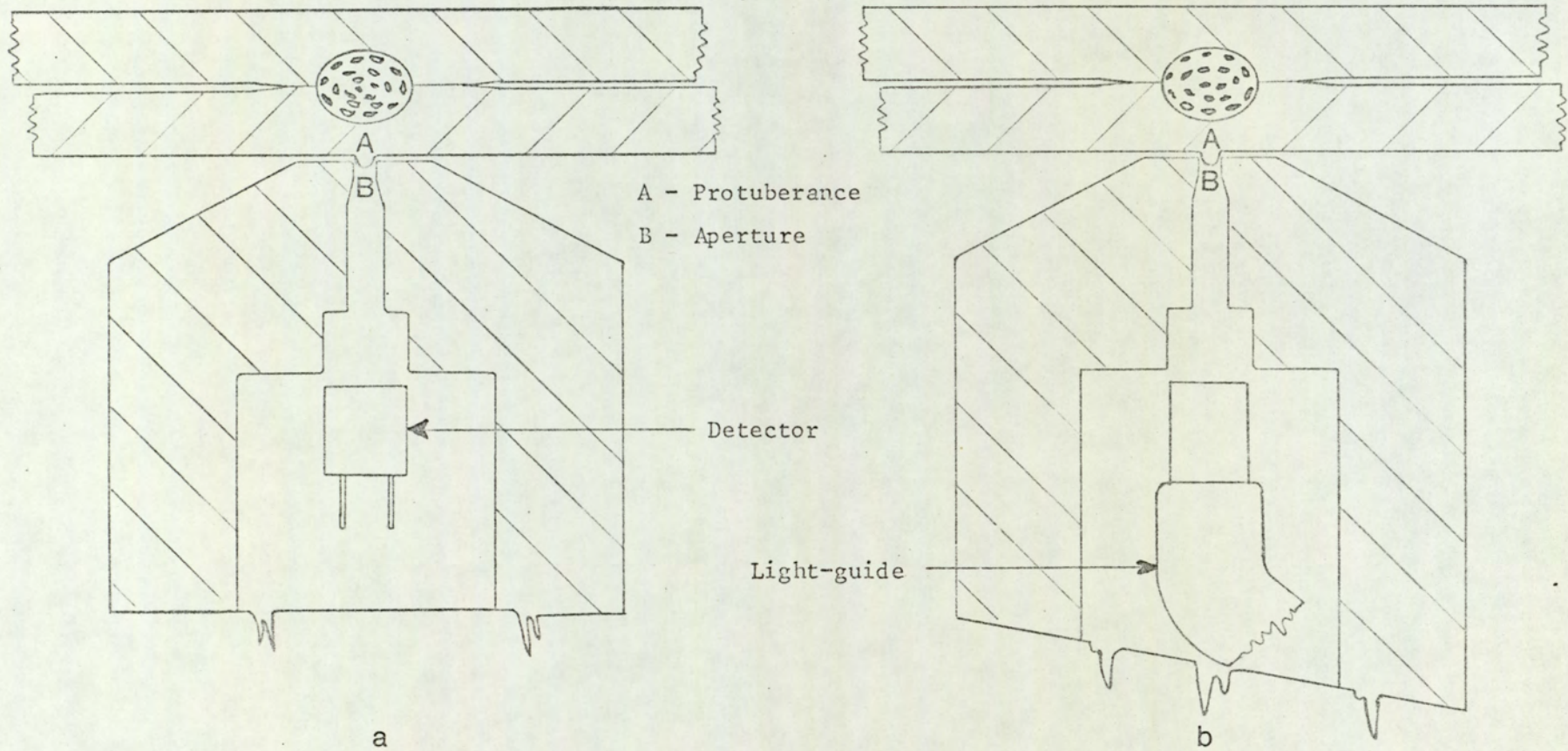
FIG. 10.2 Principle of Collecting Thermal Radiation from the Weld through a Minute Aperture at the Electrode Tip.
(a) Direct Incidence Mode Detection; (b) Remote Transmission Mode Detection

FIG. 10.3. Apparatus for Visual Observation of Weld Glow
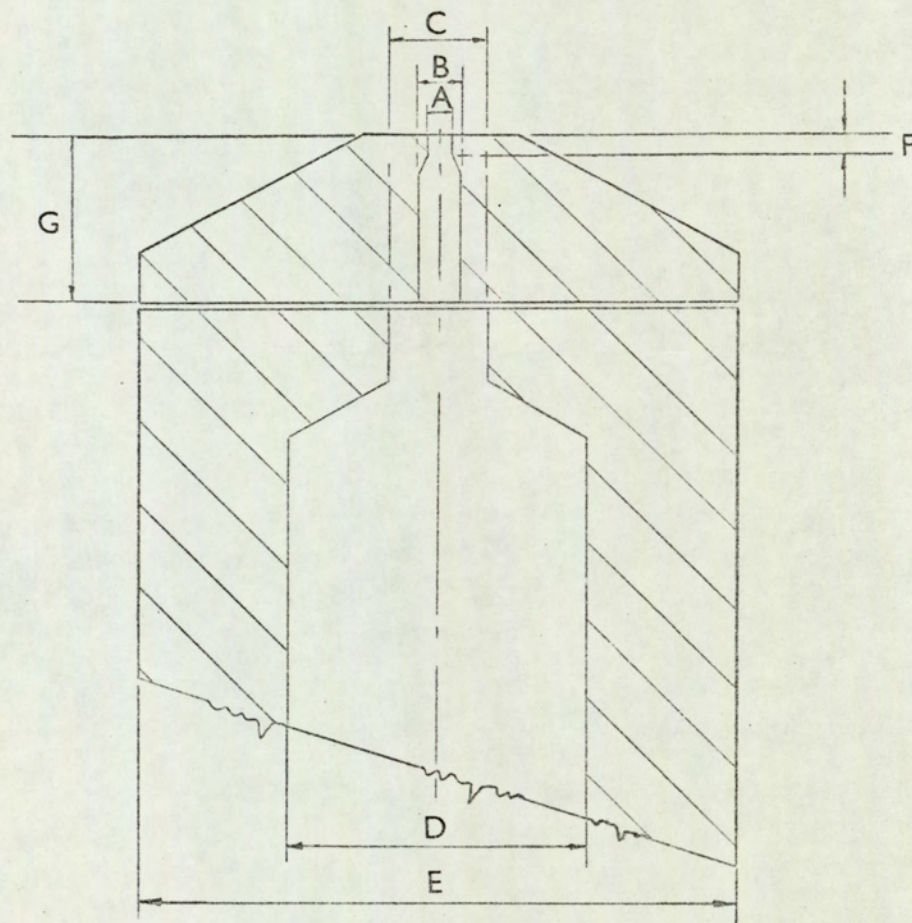
Diameters

A = .685 mm (.027 in).

B = 1.6 mm (.0625 in).

C = 3.2 mm (.125 in).

D = 9.5 mm (.375 in).

E = 19 mm (.750 in).

F = .8 mm (.03125 in).

G = 5.6 mm (.219 in).

FIG. 10.4 Tiptrode with Aperture.   Scale: Twice Full Size.
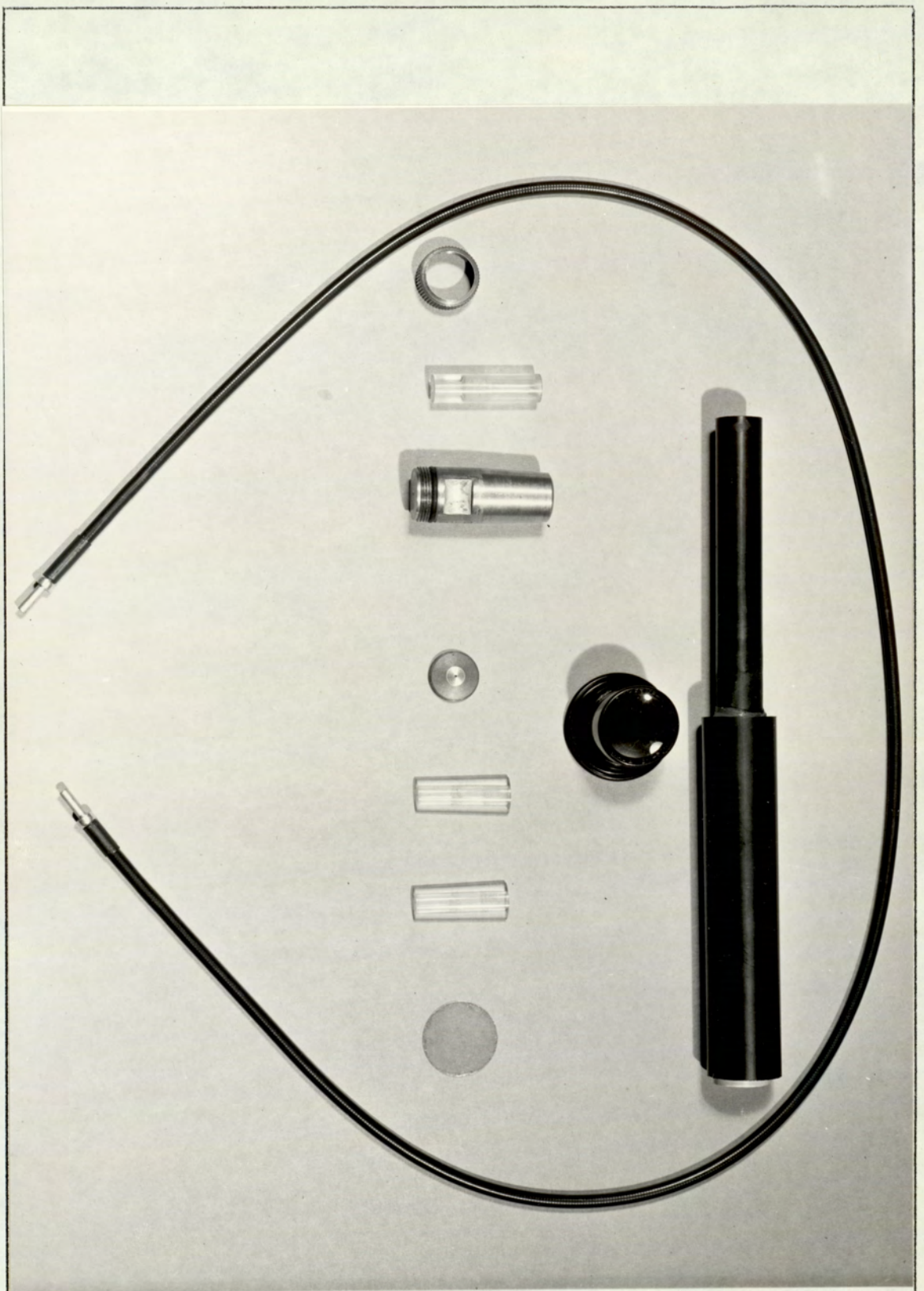
FIG. 10.5. Components used in Constructing the Viewing Apparatus
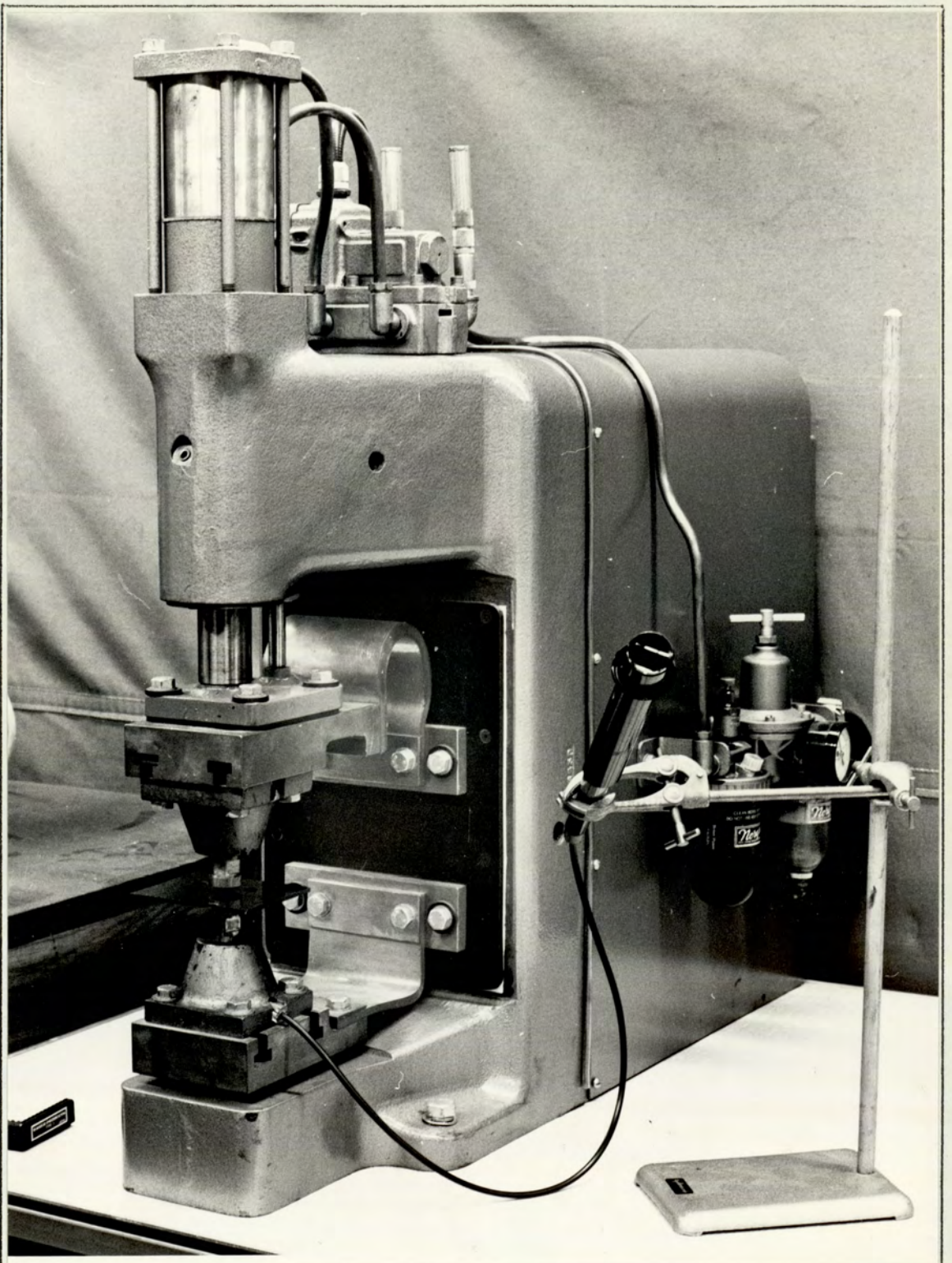
FIG. 10.6. Viewing Apparatus in Operation

11. MONOCHROMATIC EMISSION RELATED TO NUGGET GROWTH

11.1 Detection of Monochromatic Emission from the Weld

11.1.1 Radiant Flux from the Weld

Spectral radiant power over a finite wavelength interval is usually derived from a finite area of the source and is received upon a finite area of the detector surface. Therefore, a more useful form of the equation relating spectral radiant power and temperature is given by

$$\delta E = \varepsilon_\lambda . A. W(\lambda, T) \delta\lambda \qquad (11.1),$$

where δE = emitted power in the wavelength interval

between λ and $\lambda + \delta\lambda$,

ε_λ = spectral emittance at wavelength λ,

and A = area of the real body from which emission

takes place.

$W(\lambda, T)$ is defined as the hemispherical spectral radiant intensity measured over 2π steradians, per unit area of the source.

In most practical situations, the radiant flux received on the detector surface is within a limited solid angle less than 2π steradians. The radiant flux emerging from the weld spot is limited by the aperture in the body of the electrode. Referring to Figure 11.1, if the semi-angle of the cone of radiation reaching the detector (or the light-guide) is θ, then the actual radiant power intercepted by the detector may be written as

$$\delta E = k_\theta . \varepsilon_\lambda . A. W(\lambda, T).\delta\lambda \qquad (11.2),$$

where k_θ is the fraction of total flux determined by the angle θ.

11.1.2. Detector Response due to Monochromatic Radiant Flux

The general scheme of radiation transfer from the weld to the radiation detector is shown in Figure 11.1. Radiation emanating from the minute aperture of the tip is derived from the protuberance A; the protuberance is caused by the plastic flow of metal into the aperture, and may also be referred to as the weld 'pip'. The radiation traverses a medium B of transmissivity t_λ and an optical filter C of transmittance F_λ, before impinging on the detector D of responsivity S_λ. If the detector responsivity is given in $A.W^{-1}$, then the detector output current is given by

$$i_D = \int_0^\infty k_\theta \cdot \varepsilon_\lambda \cdot A \cdot W(\lambda,T) \cdot F_\lambda \cdot t_\lambda \cdot S_\lambda \cdot d\lambda \qquad (11.3),$$

where the integration is performed over the wavelength interval between $\lambda = 0$, and $\lambda = \infty$. Let R_D be the response indicated by the signal processing system. Then R_D may be expressed as

$$R_D = k_D \cdot i_D \qquad (11.4),$$

where k_D is a constant for the signal processing system following the detector. Further simplification of equation (11.3) can be achieved if certain assumptions are made regarding the bandwidth of the detected radiation. Let the optical filter and the detector be so selected that the complete system responds to a very narrow waveband L centred around λ_o, such that $\lambda_o - \frac{L}{2}$ and $\lambda_o + \frac{L}{2}$ represent the limits of the effective pass-band. The pass-band can be defined by equations (11.5) and (11.6).

$$\varepsilon_\lambda \cdot F_\lambda \cdot t_\lambda \cdot S_\lambda = 0 \qquad (11.5),$$

for $\lambda < \lambda_o - \frac{L}{2}$, and for $\lambda > \lambda_o + \frac{L}{2}$

$$\varepsilon_\lambda . \ F_\lambda . \ t_\lambda . \ S_\lambda \ = \ a_m \qquad\qquad (11.6),$$

for $\lambda_o \ - \frac{L}{2} < \lambda < \lambda_o + \frac{L}{2}$.

Using equations (11.5) and (11.6), equation (11.3) can be simplified and rewritten as

$$i_D \ = \ \int_{\lambda_o - \frac{L}{2}}^{\lambda_o + \frac{L}{2}} a_m . \ k_\theta . \ A. \ W(\lambda,T)d\lambda \qquad\qquad (11.7).$$

The final output R_D of the detection system can therefore be written as

$$R_D \ = \ k_D \ \int_{\lambda_o - \frac{L}{2}}^{\lambda_o + \frac{L}{2}} a_m . \ k_\theta . \ A. \ W(\lambda,T)d\lambda \qquad\qquad (11.8).$$

Let $\quad k_m \ = \ k_D . \ a_m . \ k_\theta . \ A \qquad\qquad (11.9),$

where k_m is a constant dependent upon the pass-band of the detector.

Combining equations (11.8) and (11.9)

$$R_D \ = \ k_m \ \int_{\lambda_o - \frac{L}{2}}^{\lambda_o + \frac{L}{2}} W(\lambda,T)d\lambda \qquad\qquad (11.10).$$

$W(\lambda,T)$ in equation (11.10) can be expressed according to Planck's radiation law and written as

$$W(\lambda,T) \ = \ c_1 . \ \lambda^{-5} . \ (\exp. \ \frac{c_2}{\lambda T} - 1)^{-1} \qquad\qquad (11.11).$$

Therefore, $\int_{\lambda_o - \frac{L}{2}}^{\lambda_o + \frac{L}{2}} W(\lambda,T)d\lambda$ in equation (11.10) can be evaluated by

standard techniques* and can be written as

---

* See Appendix 4.

$$\int_{\lambda_0 - \frac{L}{2}}^{\lambda_0 + \frac{L}{2}} W(\lambda,T)d\lambda = F(L).\ \sigma T^4 \qquad\qquad (11.12),$$

where $F(L)$ is the fraction of radiant power determined by the pass-band width, within the limits $\lambda_0 - \frac{L}{2}$ and $\lambda_0 + \frac{L}{2}$, and σ is the Stefan-Boltzmann radiation constant. From equations (11.10) and (11.12), R_D can be written as

$$R_D = k_m.\ F(L).\ \sigma T^4 \qquad\qquad (11.13).$$

The right-hand side of equation (11.13) is seen to be proportional to the fourth power of temperature. If an instrumentation system is designed so that it indicates R_D, the indication is a function of the temperature of the radiating source. In practice, the exact relationship of equation (11.13), between temperature and the spectral response of the detection system, is not achieved; the indicated value of R_D, however, still remains a function of temperature, and can be taken as an indication of relative thermal condition of the source.

11.2 Monochromatic Emission from Weld as Indication of Nugget Growth

11.2.1. Simplifying Assumptions

Referring to Figure 11.1, the following simplifying assumptions are made, so that the monochromatic emission from the protuberance A can be interpreted as being indicative of the thermal condition of the weld surface.

(a) The dimension of the aperture, and hence the dimension of the protuberance A is assumed to be very small in comparison with its distance from the surface receiving radiation; thus, it may be assumed

that the radiant beam reaching the light-guide or detector originates from a point source. With 0.685 mm (0.027 in) diameter aperture at the tip, and with the detector located at about 9.53 mm (0.375 in) away from the aperture, the conditions for point source approximation are virtually satisfied.

(b) Because of the comparatively large distance of the detector from the virtual point source, any small variation in the dimension of the source will have negligible effect on the radiant power collected by the detector. Similarly, any small variation in the distance between the protuberance and the detector surface will be assumed to have no effect on the radiant power detected.

(c) The protuberance or 'pip' is assumed to be an integral part of the radiating surface of the weld spot, and is therefore subject to the same thermal cycle as the weld surface.

11.2.2. Temperature Distribution in the Weld and
Nugget Growth

The pattern of typical temperature distribution at the end of a weld, shown in Figure 11.2, is based on the results of Greenwood[32], and Greenwood and Williamson[28]; the isotherms are such that $T_1 > T_2 > T_3 > T_4$, and so on. If, due to increased heat input to the weld, the central region reaches a temperature T_1', where $T_1' > T_1$, then the isotherms receding from the centre take up values such that $T_2' > T_2$, $T_3' > T_3$, and so on. If, on the other hand, the temperature attained at the centre of the nugget is less than T_1, then a corresponding reduction in temperature occurs for the isotherms away from the centre. The temperature distribution curves due to Bentley et al.[33] indicate a 773 K (500°C) isothermal at the surface corresponding to a temperature of 1173 K (900°C) at the centre; the

surface temperature is 1273 K (1000°C) when a large pool of molten metal exists at the centre, the approximate temperature at the centre being about 1723 K (1450°C). It may, therefore, be assumed that the temperature of the weld surface is an indication of the state of affairs existing at the centre of the weld, and the existence of a molten pool of adequate size may be confirmed or negated by the attainment of a specific surface temperature.

The diagrams of Figure 11.3 have been included to illustrate the principle of correlating nugget growth to monochromatic emission from the weld surface. The progressive stages of development in the formation of a weld nugget are shown as (a), (b) and (c) in Figure 11.3. In (a), a small core of high temperature is present at the centre of the nugget; a small fraction of the central core may be in the molten state, depending on the temperature T_A. The isothermal T_{S1} in (a) represents the temperature of the outermost layer of weld surface in contact with the electrode tip. In (b) of Figure 11.3, the central core of high temperature T_B extends further on either side of the sheet-to-sheet interface; the isothermal T_{S2} now represents the surface temperature, and $T_{S2} > T_{S1}$. Finally, in (c), the central core of temperature T_C extends to an even larger volume of metal, and the surface temperature is represented by T_{S3}, where $T_{S3} > T_{S2}$.

Let W_1, W_2 and W_3 be the spectral radiant intensities corresponding to surface temperatures T_{S1}, T_{S2} and T_{S3}. Therefore, radiant intensities W_1, W_2 and W_3 can be expressed as,

$$\left. \begin{array}{l} W_1 = W(\lambda, T_{S1}) \\ W_2 = W(\lambda, T_{S2}) \\ W_3 = W(\lambda, T_{S3}) \end{array} \right] - \tag{11.14}$$

Since $T_{S3} > T_{S2} > T_{S1}$, therefore $W_3 > W_2 > W_1$.

Thus, the monochromatic radiant power emitted by the weld surface increases, as the central core of high temperature extends further to either side of the interface with the development of the weld nugget. Consequently, the output signal of the detection system, proportional to radiant intensity, also increases with the dimension of the weld nugget.

It has been assumed here that the growth of a nugget is influenced by the maximum temperature at the centre, and that the existence of a large central core of metal at a high temperature is an essential condition for a large-size nugget. The validity of such assumptions can be verified from the results of Bentley et al.[33].

11.3 Spectral Emittance and Radiant Emission from the Weld Spot

Although the radiation reaching the surface from the inner depths of a radiating body is a bulk phenomenon, the radiation finally emerging through the surface is modified by the surface properties. Thus, in correlating the thermal condition of the weld surface to the radiant emission from the surface, the radiating properties of the weld surface have to be taken into account. The most important radiating property in this respect is the spectral emittance ε_λ of the weld surface. The two most important factors which influence ε_λ are (i) surface condition, and (ii) temperature.

For most metals, the values of ε_λ given in handbooks[27] are those for smooth polished surfaces, and even with apparently similar surface finish the spectral emittance may vary over wide limits because of the existence of surface films of oxides and other chemicals. In general, however, ε_λ is greater for surfaces covered with oxide layers

and tarnish films, and is less when such surfaces are cleaned. The indication of the detection system will, therefore, be less for cleaned emitting surfaces. Hence, a slight variation in the indicated output of the detection system will result because of non-uniform surface conditions of the different sets of specimen coupons.

Variations of spectral emissivity with temperature is dependent on the wavelength; for many metals the spectral emissivity decreases[27] with temperature in the visible and near infra-red regions of the spectrum. Thus, some inaccuracy in the indicated output of the detection system may result from the temperature coefficient of emissivity.
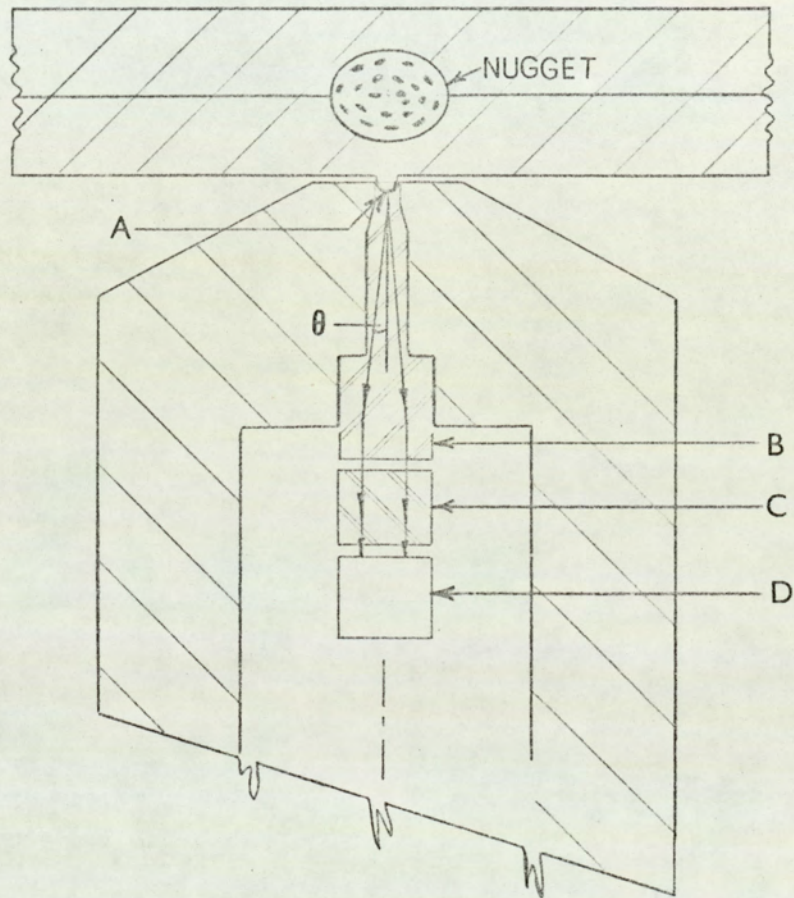
A - Protuberance or Pip.

B - Optical Medium.

C - Optical Filter.

D - Optical Detector.

θ - Semi-angle of Cone of Radiation.

FIG.11.1 General Scheme of Radiation Transfer from the Weld.

Specimen Coupons

Axis of Constriction

T_1 T_2 T_3 T_4

Plane of
sheet-to-sheet
Interface.
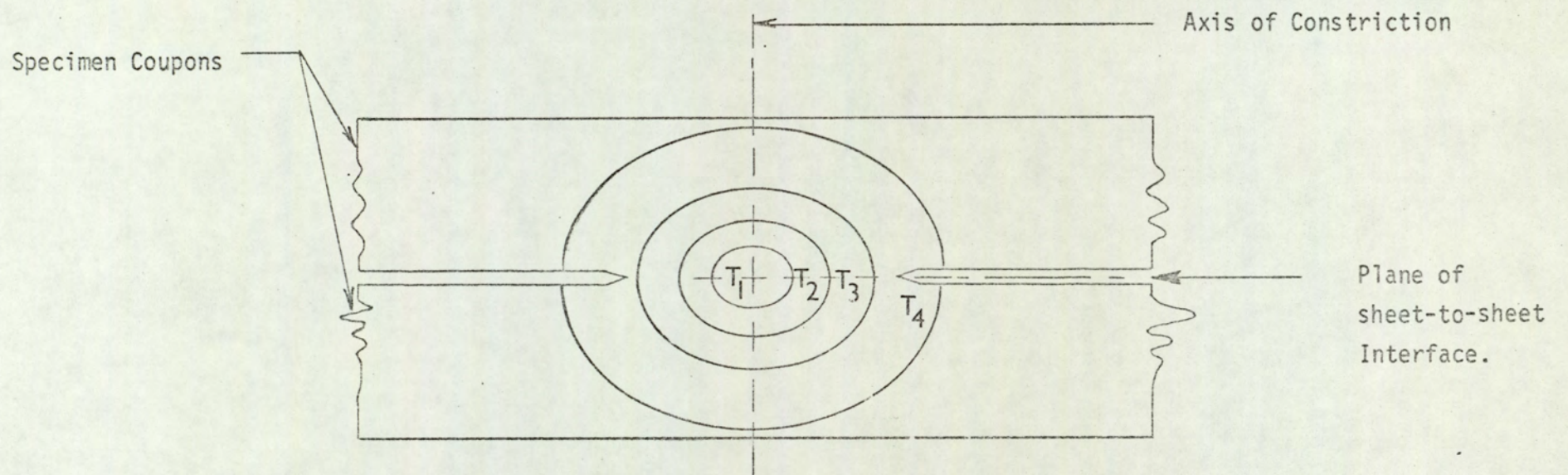
FIG. 11.2.   Pattern of Isothermals in a Spot Weld.
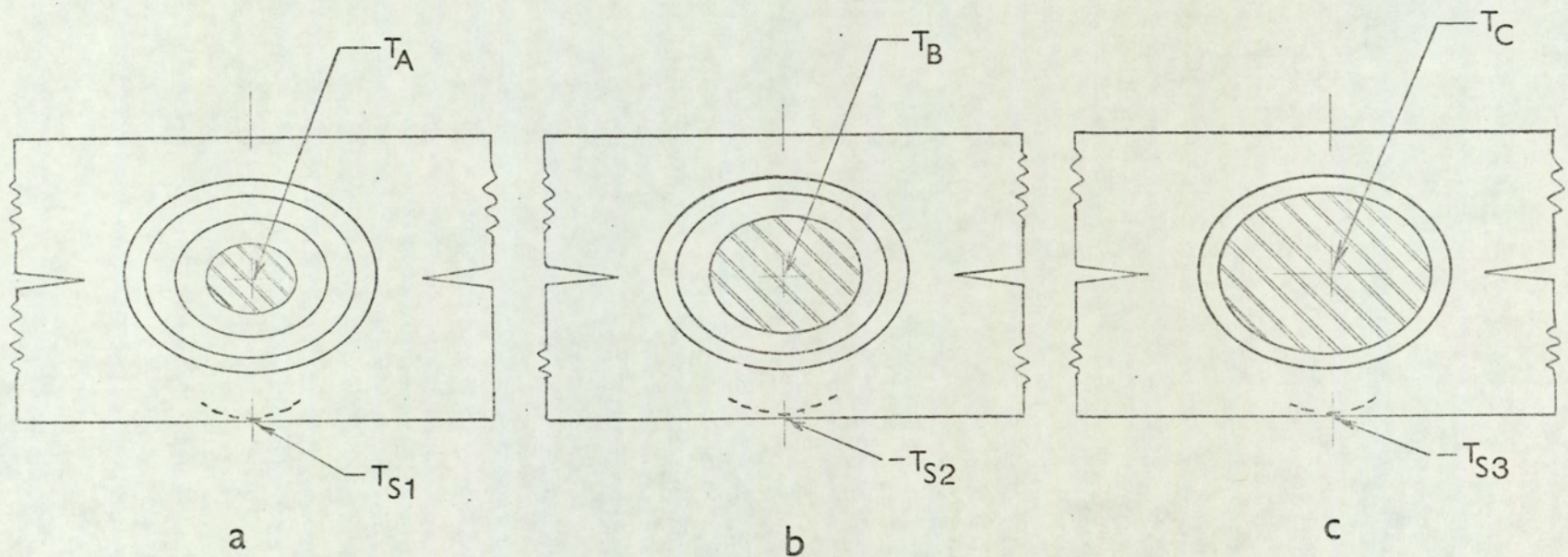
FIG. 11.3. Progressive Stages of Nugget Formation.

    (a) Maximum Temperature at the Centre = T_A, Surface Temperature = T_{s1};

    (b) Maximum Temperature at the Centre = T_B, Surface Temperature = T_{s2};

    (c) Maximum Temperature at the Centre = T_C, Surface Temperature = T_{s3}.

12. DIRECT INCIDENCE MODE DETECTION SYSTEMS

12.1 General Principle of Detection

In the direct-incidence mode, the detector is located inside the electrode or in the hollow of the electrode holder. Thermal radiation from the weld spot is collected through the aperture at the tip of the bottom electrode and is incident upon the detector. The amplitude modulated output of the detector is taken through a tuned amplifier and recorded. The amplitude of the recorded signal is proportional to the monochromatic radiant power emitted by the weld surface and is a function of the temperature of the weld surface.

In the present investigation, a silicon photovoltaic cell was used for detection in the visible region of the spectrum; detection in the near infra-red was attempted by employing a lead sulphide photo-conductive cell.

12.2 Detection System using a Silicon Photovoltaic Cell

12.2.1. System Description and Principle of Operation

A block diagram of the direct-incidence mode detection system using a silicon photovoltaic cell is shown in Figure 12.1. The photo-voltaic cell, Ferranti type MS9BE, was chosen for its small size. For concentric alignment with the aperture at the electrode tip, the photocell was placed within an electrode-insert. The electrode-insert was made from tufnol, an insulating material; thus the photocell was electrically insulated from the current carrying electrode. A red glass filter, located in a slot at the top of the electrode insert, provided spectral isolation of the detected waveband. The electrode-insert shown in the photograph of Figure 12.2 contains the photocell; the minute aperture at the tip and the larger opening in the body of

the tiptrode can also be seen in this photograph.

The photovoltaic cell was operated in the unbiased mode[38] so that the current output of the cell was proportional to the intensity of incident radiation. The output photocurrent was converted into a voltage by a current-to-voltage transduction stage, the final output being taken through a tuned amplifier.

12.2.2. Electronic Circuits

In order to reduce any stray pick-up from the machine and other sources, the output of the photocell was taken outside the machine by means of a pair of twisted leads, through a slot at the base of the electrode holder. The circuit configuration of Figure 12.3 shows the current-to-voltage transduction stage along with the photocell. An Analog Devices type 40JV operational amplifier was used in the design of the current-to-voltage transduction stage; the 100 kΩ potentiometer in the feedback loop of this circuit is for adjusting the output voltage level.

The tuned amplifier, shown in Figure 12.4 was designed to operate with a centre frequency of 100 Hz; the gain at the centre frequency could be adjusted by the 500 kΩ potentiometer in the feedback loop. The tuned amplifier was built using a Computing Techniques type F1-4 operational amplifier, frequency selection being achieved with a twin-T resistance-capacitance network in the feedback loop.

12.3. Detection System using a Lead Sulphide Detector

12.3.1. System Description and Principle of Operation

In this instance, the lead sulphide detector, along with its associated biasing circuitry and a preamplifier, was placed in the hollow of the electrode holder; a suitable slot was machined in the

base of the electrode holder for housing the package containing the
detector and the relevant circuitry for biasing and preamplification.
The resistance variation[39] of the photoconductive cell was converted
into a voltage variation and amplified by means of a preamplifier stage.
Further amplification was provided by a tuned amplifier.

12.3.2. Electronic Circuits

A Mullard type 139-1CPY lead sulphide detector was chosen
for detection in the near infra-red region around 2 μm. The lead
sulphide detector was connected in series with a 200 kΩ resistor
between the +15V supply rail and ground. The quiescent bias current
through the cell was about 12 μA. The voltage drop across the 200 kΩ
resistor was a.c. coupled to the preamplifier. The circuit diagram of
the preamplifier, along with the detector bias circuit, is shown in
Figure 12.5. The detector-preamplifier package of Fig. 12.5 was en-
capsulated in silicone rubber so that the package was electrically
isolated from the machine body when placed in the slot. The detector-
preamplifier package, before and after encapsulation, is shown in
Figure 12.6. The gain of the preamplifier circuit, measured at 1 kHz
was 23. The tuned amplifier used in this instance was the same as
that shown in Figure 12.4.
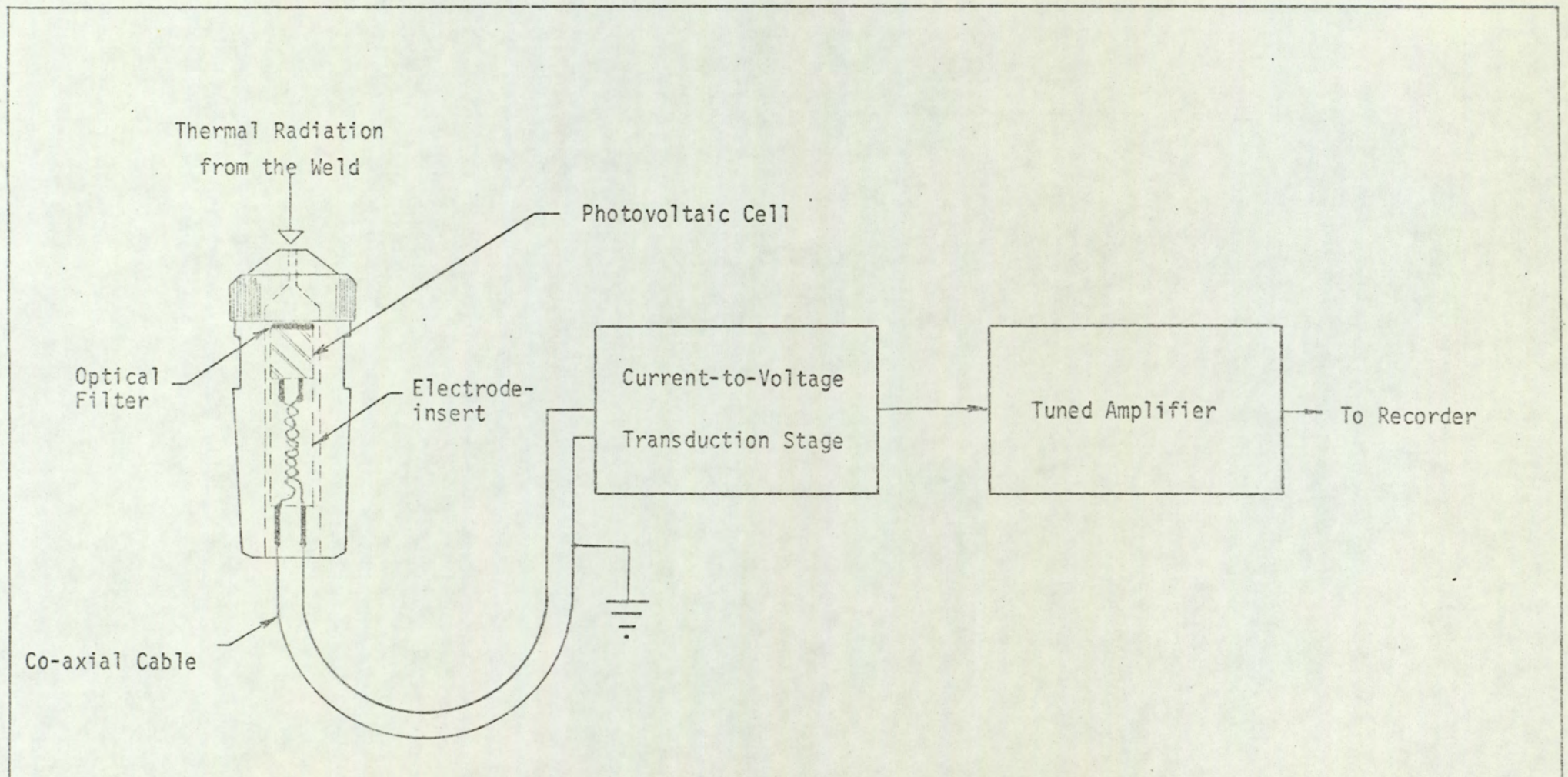
FIG. 12.1 Block Diagram of Detection System employing a Photovoltaic Cell.
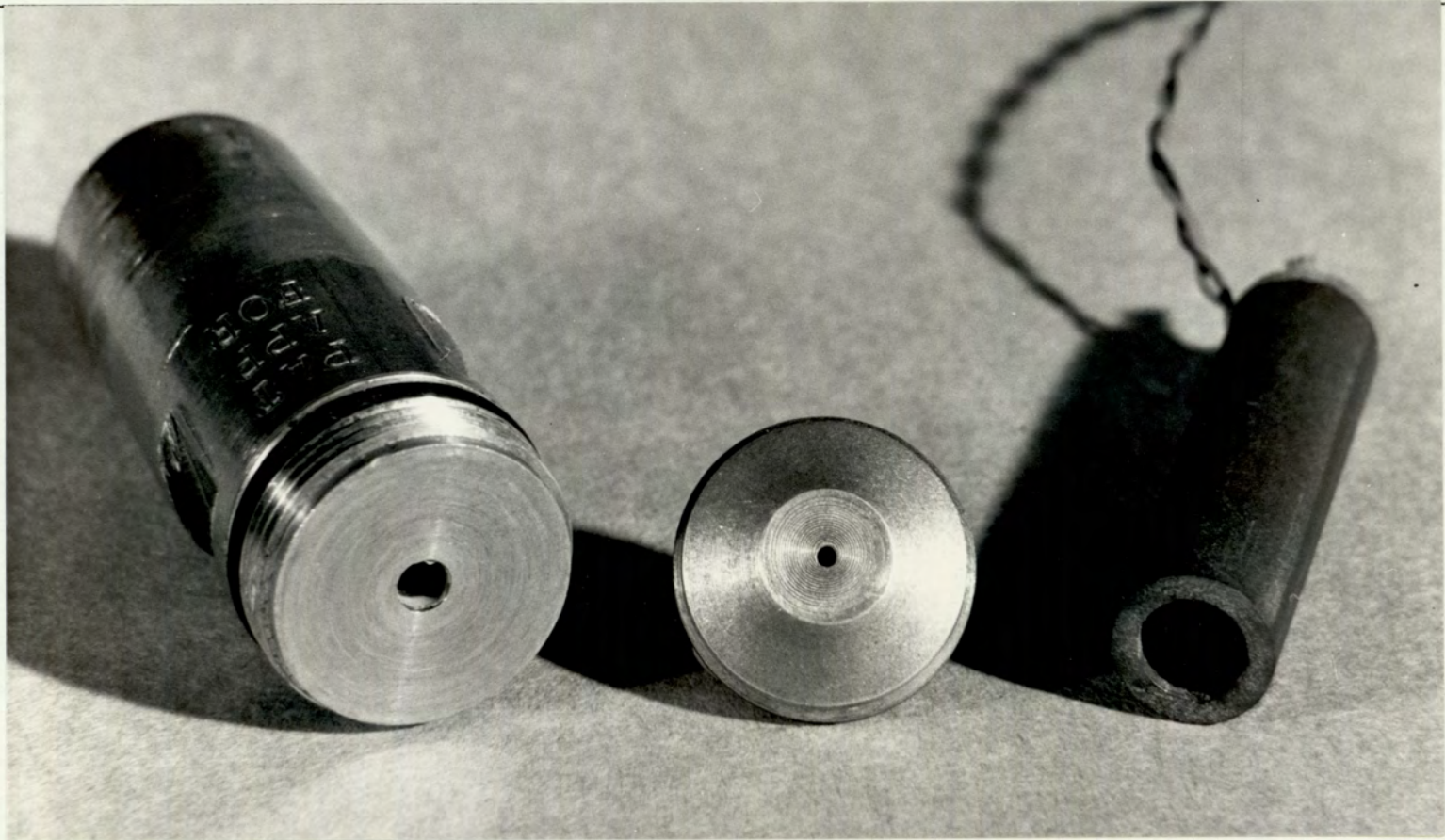
FIG. 12.2. Constituent Parts of Tiptrode with Aperture and Electrode-insert containing Photocell.

Left: Tiptrode Body with Large Aperture;
Centre: Tiptrode Tip with Aperture;
Right: Electrode-insert containing Photocell.
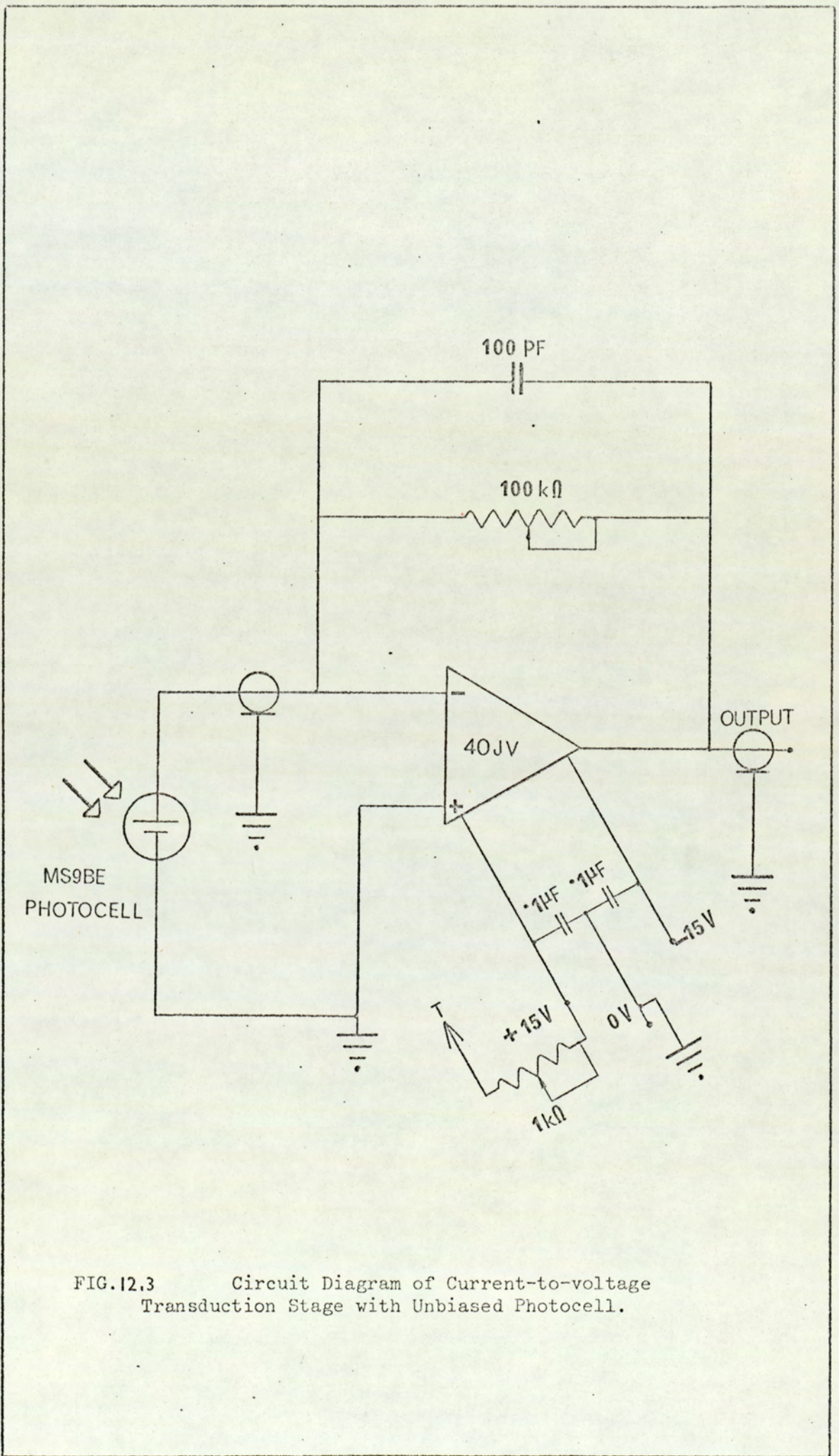
FIG. 12.3   Circuit Diagram of Current-to-voltage
Transduction Stage with Unbiased Photocell.
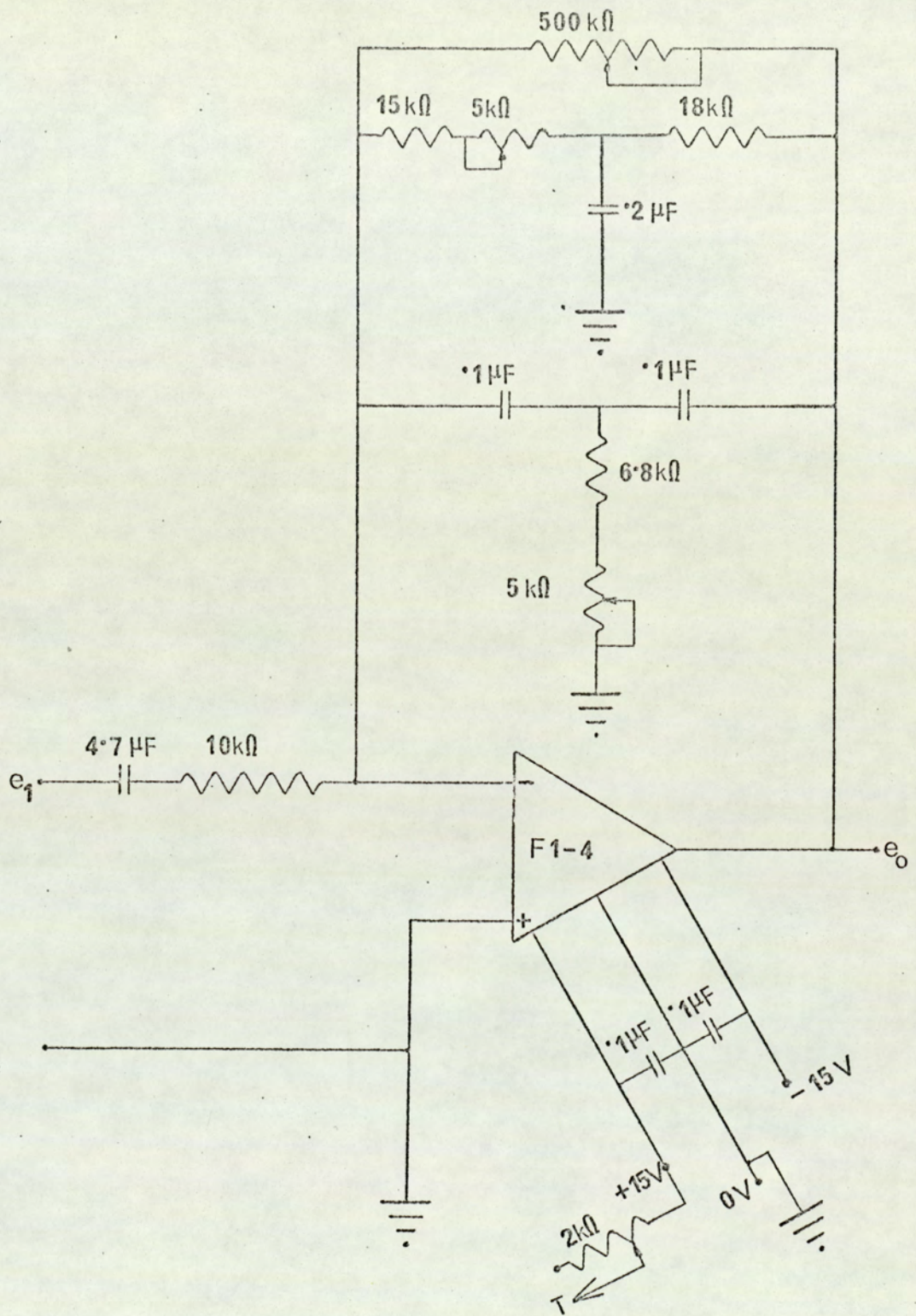
FIG. 12.4   Circuit Diagram of Tuned Amplifier with 100 Hz
Centre Frequency - used with Detection System employing
MS9BE Photocell.
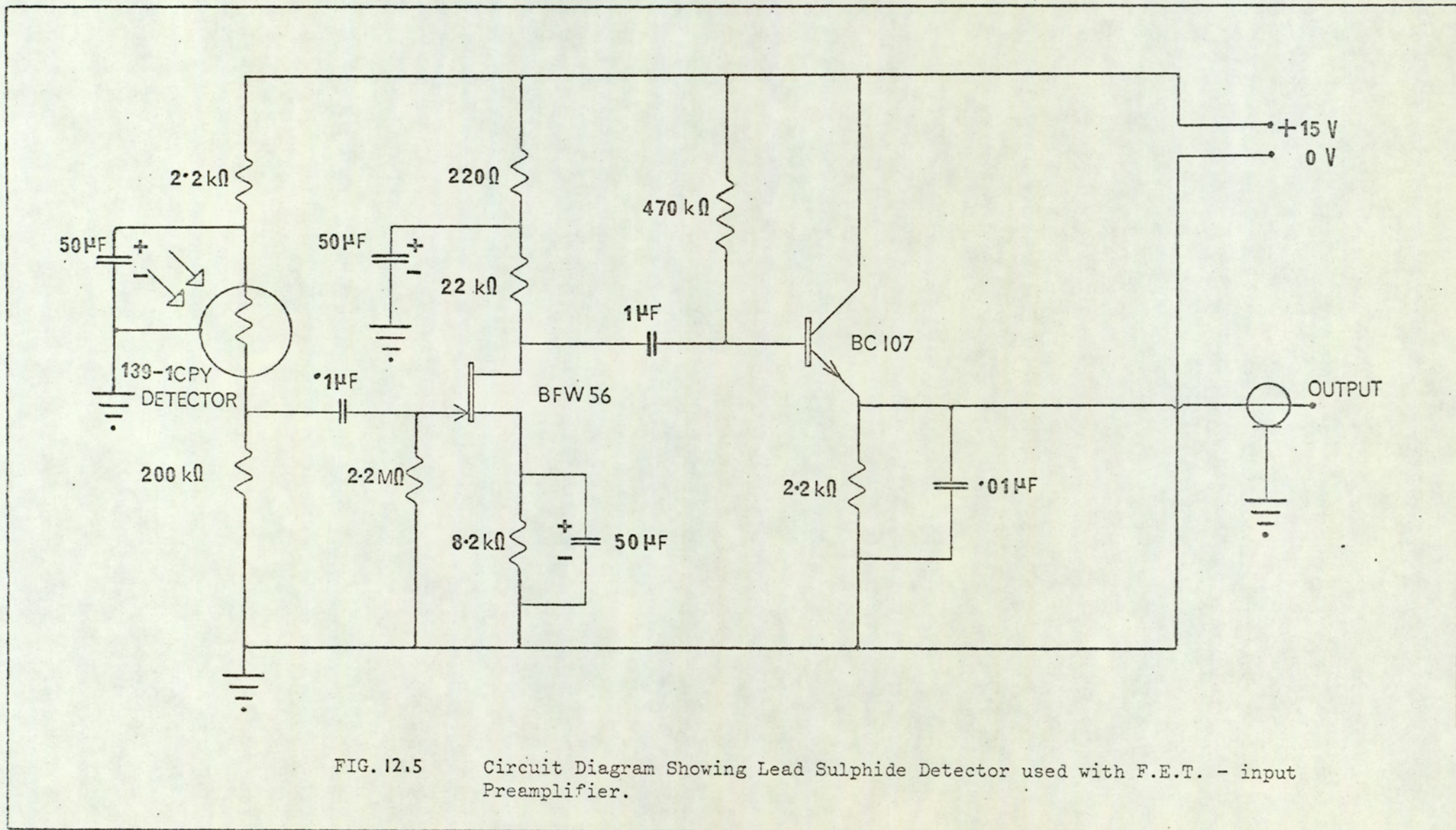
FIG. 12.5   Circuit Diagram Showing Lead Sulphide Detector used with F.E.T. – input
Preamplifier.
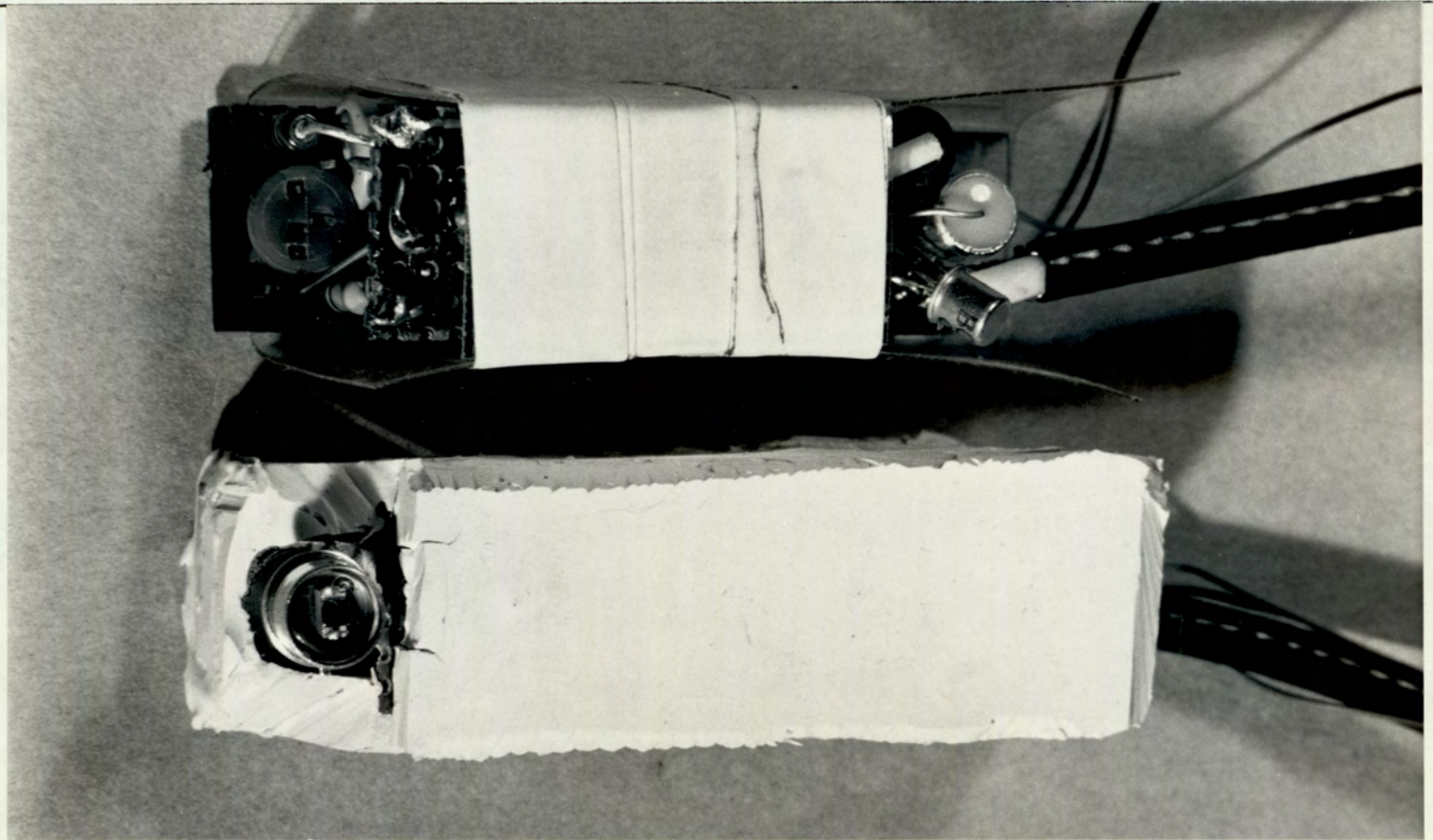
FIG. 12.6. Detector-Preamplifier Package before and after Encapsulation.

Top: Circuit Package before Encapsulation
Bottom: Circuit Package after Encapsulation

13. REMOTE TRANSMISSION MODE DETECTION SYSTEMS

13.1 General Principle of Detection

In the remote-transmission mode, one end of the light-guide is inserted within the bottom electrode; thermal radiation from the weld spot, emerging through the aperture at the tip of the bottom electrode, is incident upon the receiving end of the light-guide. The receiving end of the light-guide was held in position by means of an electrode-insert; the transmitting end of the light-guide was taken outside, through a slot in the base of the electrode holder, and located in front of the radiation detector within a light-proof enclosure.

For the present investigation, silicon detectors with peak spectral response at about 0.9 μm were used in conjunction with Fibrox light-guides[40]. Two different types of silicon detector were used, the detector output in each case being fed into a tuned amplifier for further amplification. The recorded output of the detector is an indication of the thermal condition of the weld surface and can be correlated to nugget growth.

13.2 Detection System using a P-I-N- Photodiode

13.2.1. System Description and Principle Operation

A Monsanto type MD2 P-I-N photodiode[41] was employed for detection, and was mounted vertically inside a light-proof box. The transmitting end of the light-guide was held in position, concentrically aligned with respect to the detector, within a cylindrical housing. The cylindrical housing was fixed on the light-proof box, and is shown in Fig. 13.1. The light-guide assembly comprising of the tiptrode and the cylindrical adaptor is shown in the photograph of Figure 13.2. along with the cylindrical housing for the detector. The red glass

filter, cut from Schott type RG715 optical filter glass, was located
in a slot at one end of the cylindrical adaptor for the light-guide,
and provided spectral isolation of the radiant power received by the
photodiode. The photodiode was operated in the reverse-biased mode[42].
A current-to-voltage transduction stage mounted inside the light-proof
box produced a voltage output proportional to the photocurrent, the
output of the current-to-voltage transduction stage being taken through
a tuned amplifier for further amplification.

13.2.2. Electronic Circuits

Figure 13.3 shows the current-to-voltage transduction stage,
a 9V dry battery being used to provide the reverse bias for the P-I-N
photodiode. An Analog Devices type 40JV operational amplifier was
used in the circuit.

The tuned amplifier used in this instance was the same as that
shown in Figure 12.4.

13.3. Detection System employing an Integrating Light Detector

13.3.1. System Description and Principle of Operation

An integrating light detector[43], Plessey type OPT1, was
used in the detection system shown in the block diagram of Figure 13.4.
The detector was mounted horizontally on a circuit board containing
part of the associated circuitry. A cylindrical housing, which fitted
around the detector socket is shown in Figure 13.5; the red glass filter
was mounted on the adaptor for the transmitting end of the light-guide.

The integrating light detector,OPT1,was used in the constant
frequency mode, the constant frequency pulses being derived from a
pulse generator. The sawtooth output waveform from OPT1 was amplitude
modulated at 100 Hz because of the inherent 100 Hz modulation of the

radiation signal. Amplification of OPT1 output was provided by an a.c.
amplifier and a 100 Hz tuned amplifier connected in tandem.

The complete electronic circuitry, along with the detector, was
placed within a large metal box. The metal box served as a light-proof
enclosure and 'shielded' the enclosed circuitry from spurious pick-ups.

13.3.2. Electronic Circuits

The integrating light detector, OPT1, is encapsulated in an
8-lead TO-5 can, and model 'A' of the device was chosen because of its
smaller dark current specification.

Figure 13.6 shows the circuit diagram of the pulse generator
used to activate the integrating light detector. The pulse repetition
frequency could be altered by the 500 kΩ potentiometer in the emitter
circuit of the unijunction transistor; the pulse width could be
adjusted by means of the 100 kΩ potentiometer in the base bias circuit
of the 'ON'-transistor of the monostable multivibrator. The output
from the integrating light detector was taken through an a.c. amplifier
which had a high input impedance and provided a voltage gain of 10.
The a.c. amplifier was designed with a Computing Techniques type F1-4
operational amplifier and was operated in the non-inverting mode with
a capacitor-coupled input. Further amplification was provided by the
tuned amplifier circuit of Figure 13.7. The 100 Hz tuned amplifier,
in this instance, was designed with a Computing Techniques type F1-4
operational amplifier, frequency selection being provided with a twin-T
resistance-capacitance network in the feedback loop.

FIG. 13.1. Cylindrical Housing for P-I-N Photodiode.   Scale: Full Size.
    (a) Complete Housing Assembly; (b) Adaptor for Light-guide.

Legend:

① — P-I-N Photodiode

② — Light-guide

③ — Optical Filter

④ — Adaptor for Light-guide

⑤ — Three clear holes for ⅛ in. B.S.W.

⑥ & ⑦ — Tapped Holes ⅛ in. B.S.W.

⑧ — Coarse Thread for Mating.
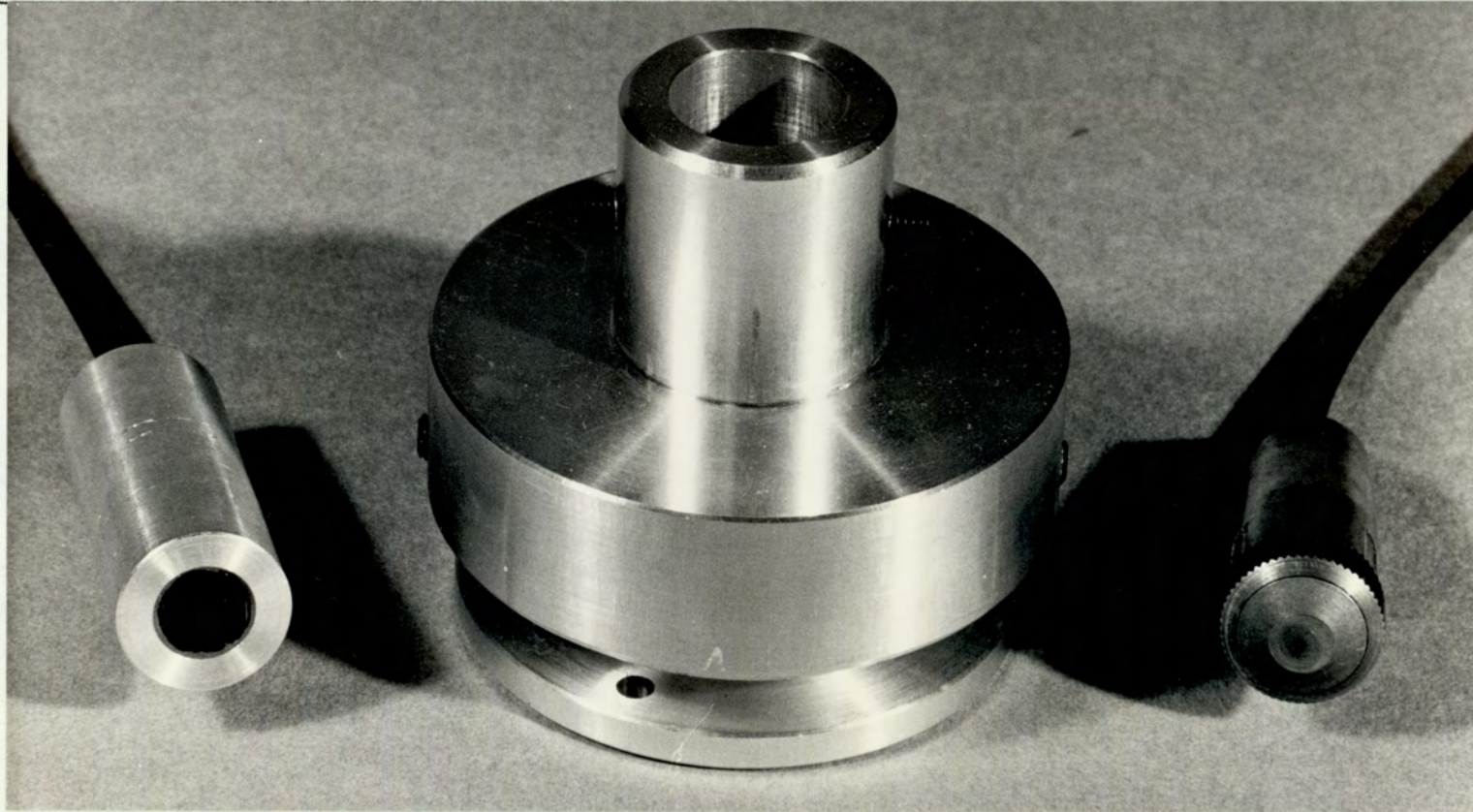
FIG. 13.2. Light-guide Assembly and Cylindrical Housing used in Detection System employing P-I-N Photodiode.

Left: Cylindrical Adaptor fitted with Optical Filter for the Transmitting End of the Light-guide;
Centre: Cylindrical Housing;
Right: Tiptrode at the Receiving End of the Light-guide.
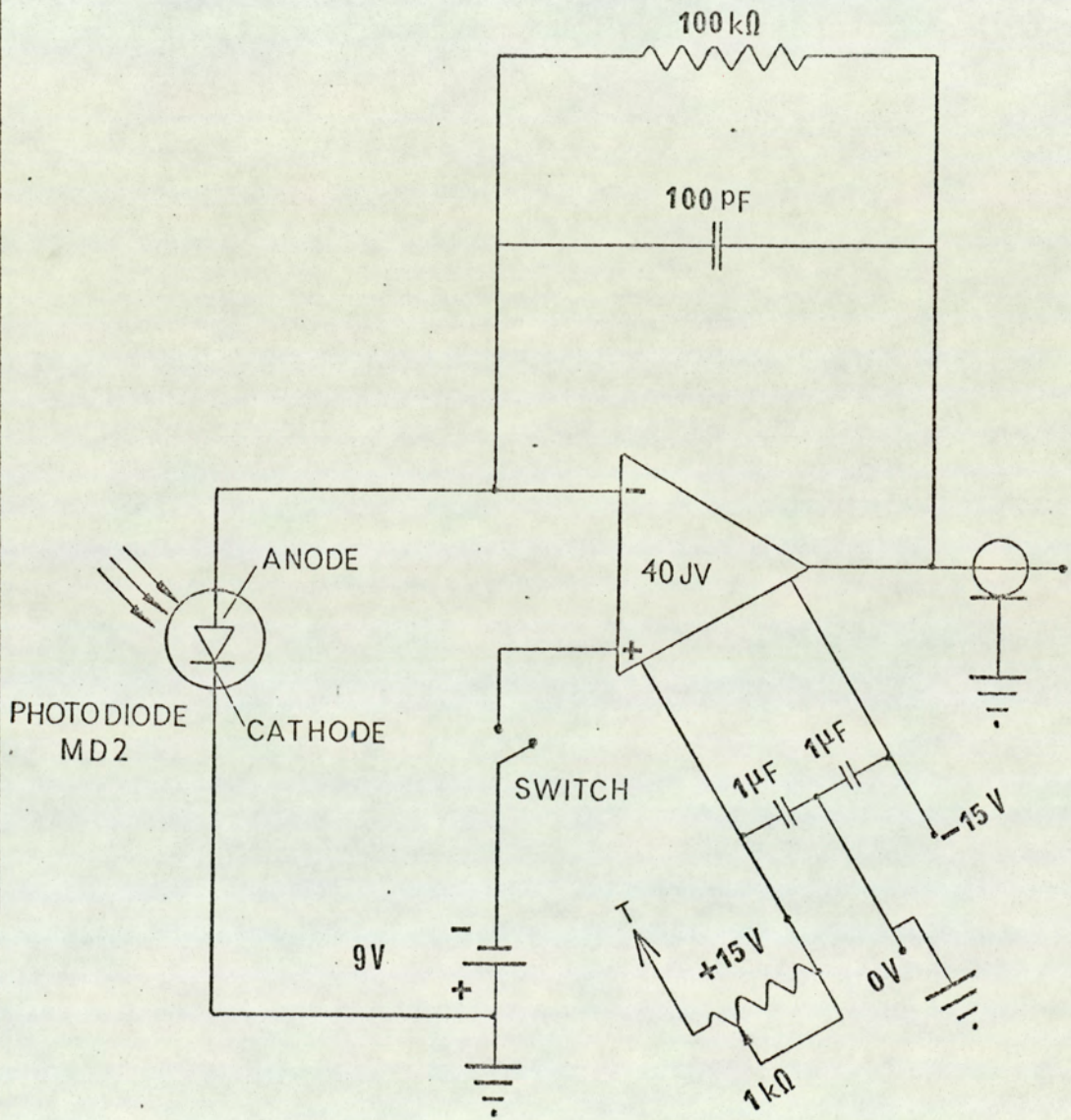
FIG. 13.3   Circuit Diagram of Current-to-voltage
Transduction Stage with Reverse-biased P-I-N
Photodiode.
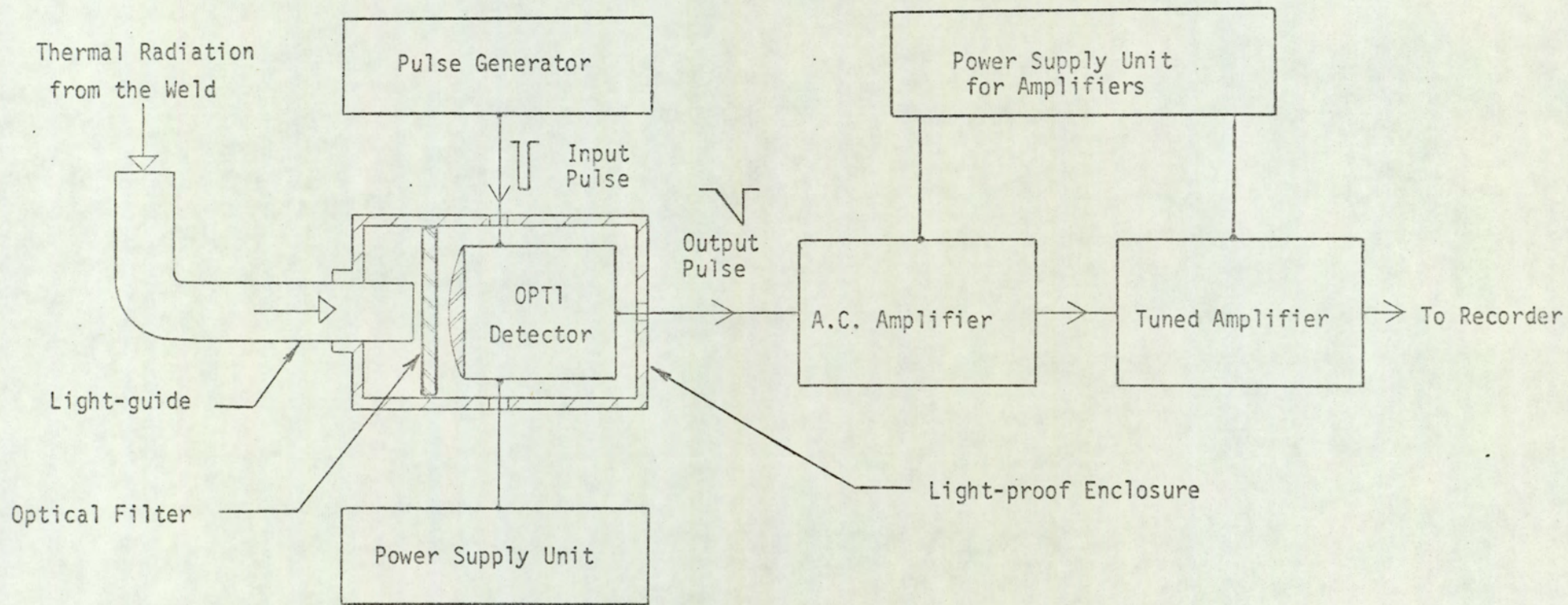
FIG. 13.4 Block Diagram of Detection System employing Integrating Light Detector OPT1.

(Please note that the Output Pulse Characterizes OPT1 Output with Constant Illumination Level).

Diameters

A = 15.9 mm.

B = 27 mm.

C = 44.5 mm.

D = 47,6 mm.

E = 9.5 mm.

F = 12.7 mm.
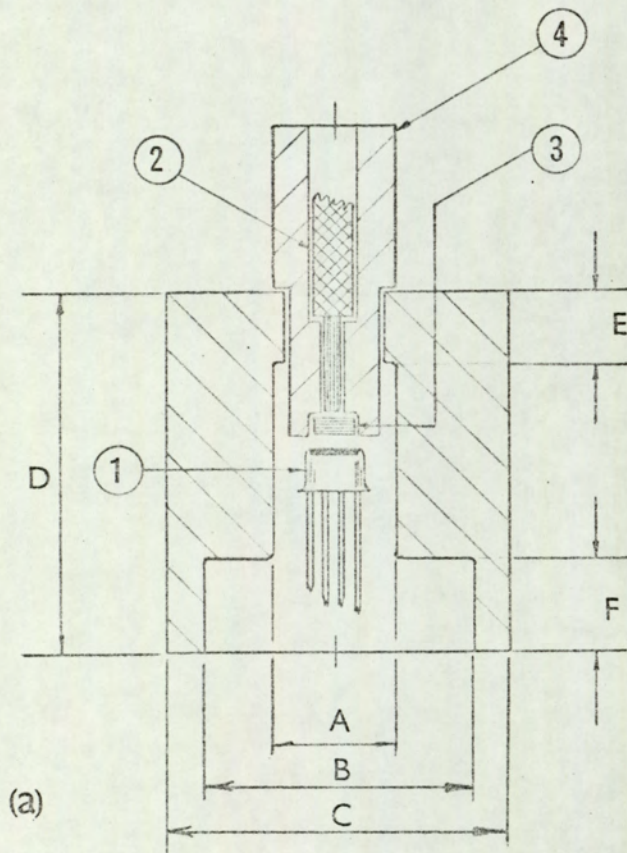
(1)— Detector, OPT1.

(2)— Light-guide.

(3)— Optical Filter.

(4)— Adaptor for Light-guide.
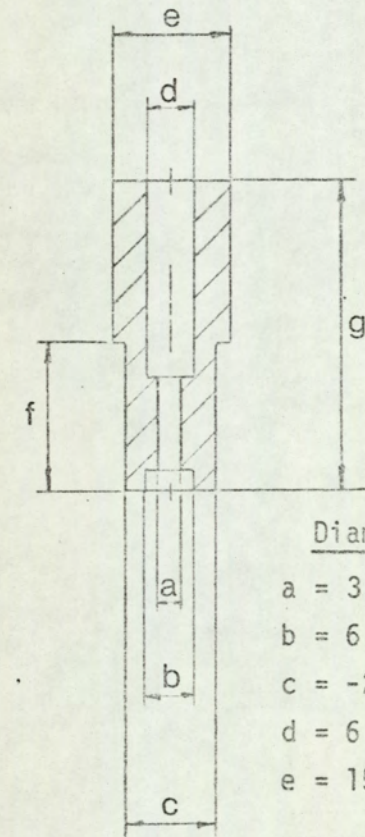
Diameters

a = 3.18 mm.

b = 6.35 mm.

c = -2½7 mm.

d = 6.35 mm.

e = 15.9 mm.

f = 10.3 mm

g = 32.5 mm.

FIG. 13.5. Cylindrical Housing for OPT1.   Scale: Full Size
(a) Complete Housing Assembly;   (b) Adaptor for Light-guide.
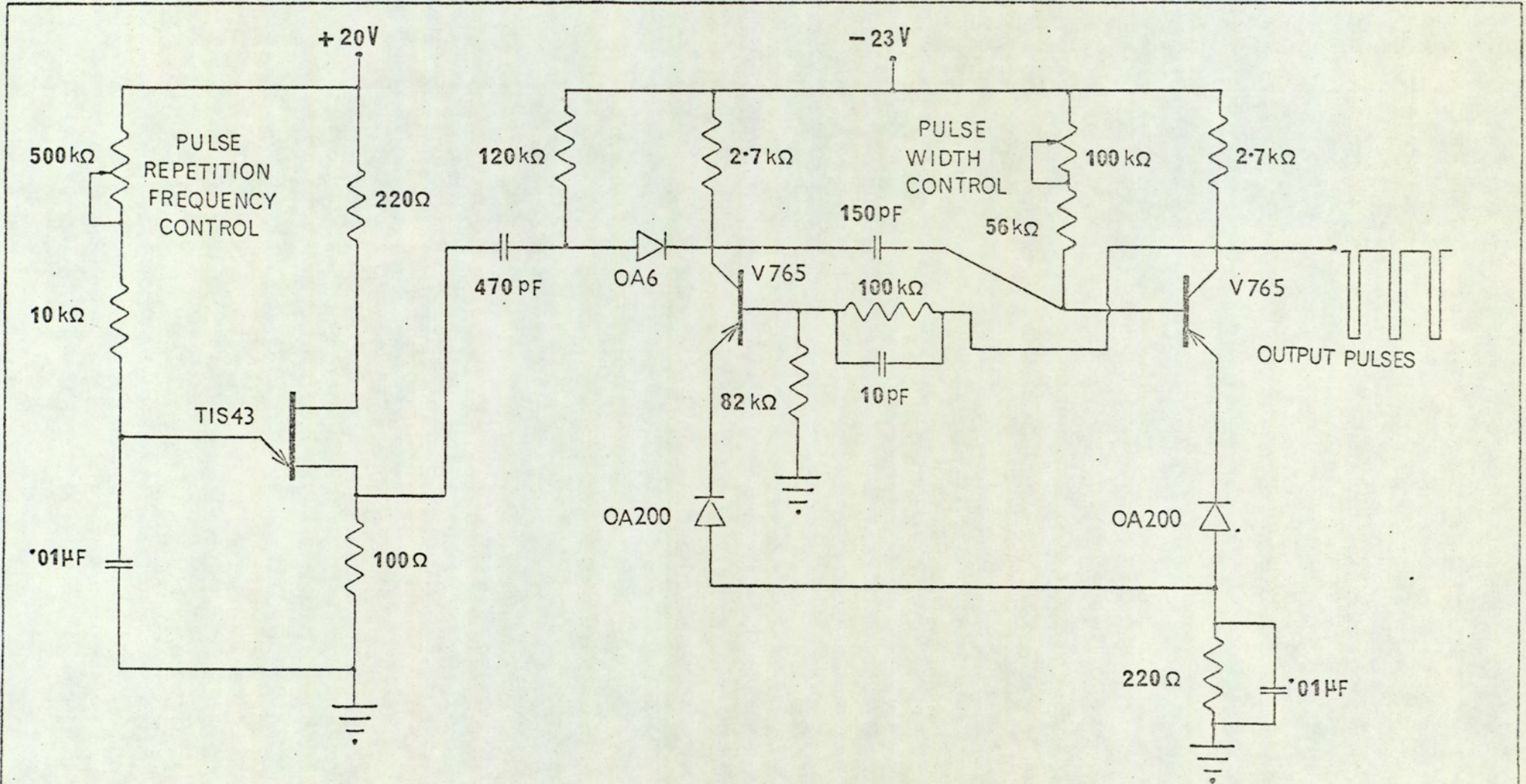
FIG.13.6   Circuit Diagram of Pulse Generator used with OPT1
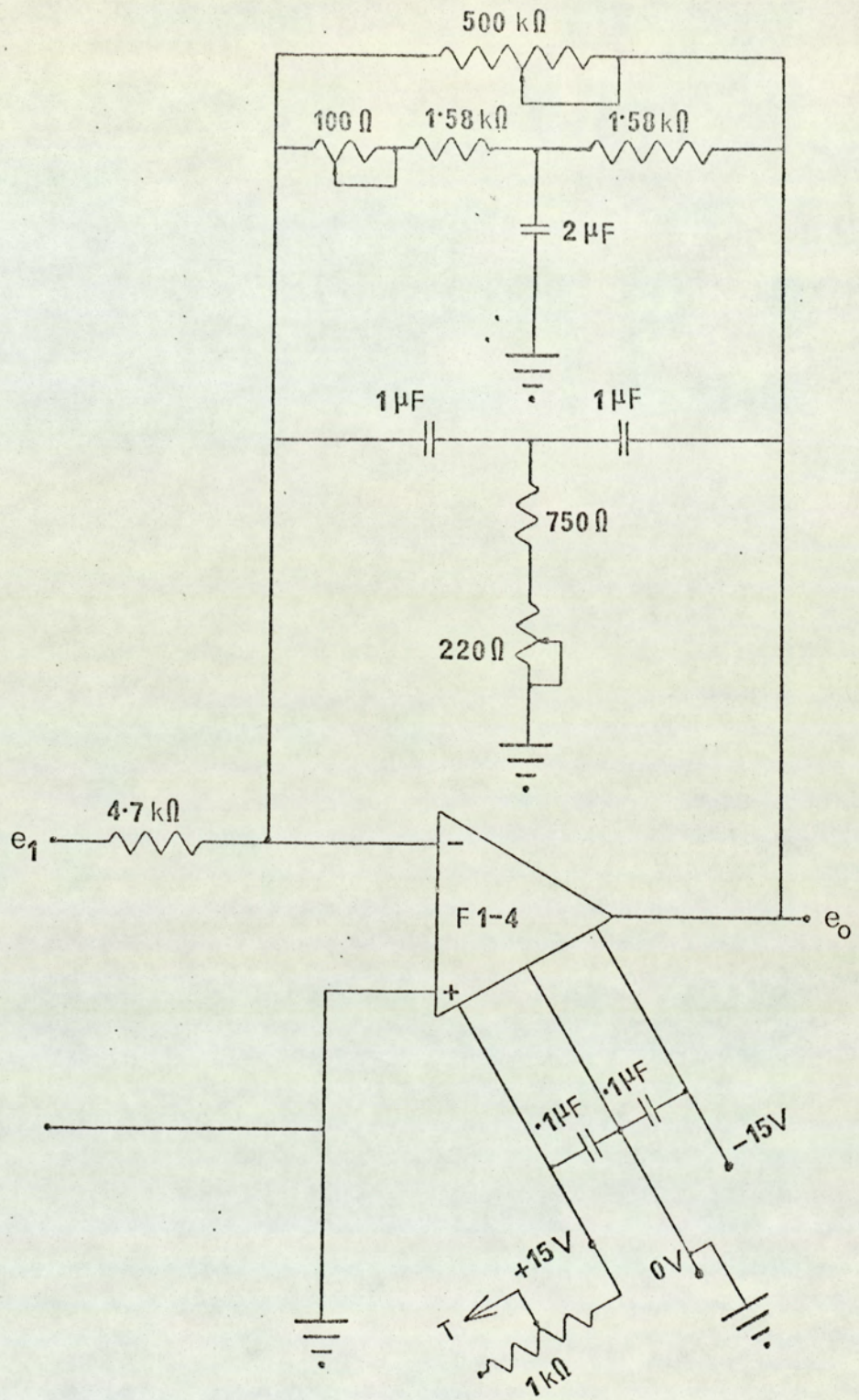
FIG. 13.7   Circuit Diagram of Tuned Amplifier with 100 Hz
Centre Frequency – for Detection System employing OPT 1.

14. DISCUSSION OF THE MONOCHROMATIC RADIANT INTENSITY TRACES AND CONCLUSIONS

14.1 Monochromatic Waveband of Maximum Response

Thermal radiation from the weld surface was detected by employing the various photoelectric detection systems described in Sections 12 and 13, and the recorded traces are presented in Figures 14.2 through 14.10. The recorded trace, in all such cases, is called the 'monochromatic radiant intensity' trace or the 'monochromatic emission characteristic', the former being abbreviated as the M.R.I. trace. Strictly speaking, the term monochromatic is used in the context of a very narrow waveband centred around a single wavelength. In the present context, although the detected waveband is fairly wide, the term monochromatic will be retained.

Thermal radiation from the weld was collected through a 0.685 mm (0.027 in.) diameter aperture at the tip of the bottom electrode. Operating principles of the detection systems employing various detectors have been discussed in Sections 12 and 13, and a photograph of the remote-transmission mode detection system employing a silicon P-I-N photodiode is shown in Figure 14.1.

For all silicon detectors, the detected waveband was spectrally isolated by means of optical filters cut out of RG 715 red filter glass. The spectral response of the silicon detectors is such that the long-wave limit of response is at about 1 μm; again, the maximum transmittance of the red glass filter occurs in the waveband between 0.75 μm and 2.4 μm. A further restriction is imposed on the transmitted waveband in the remote-transmission mode, since the light-guide virtually cuts off all radiation of wavelengths above 1.3 μm. Thus,

the waveband of maximum response, when using silicon detectors in conjunction with red glass filters, lies approximately between 0.75 μm and 1 μm.

In the case of the lead sulphide cell, type 139-1CPY, a germanium optical filter is incorporated as an integral part of the detector, and cuts off radiation below 1.5 μm. The long-wave limit of spectral response of the device is at about 3 μm, and the waveband of maximum response lies between 1.5 μm and 2.5 μm.

Finally, it may be added that, for maximum response from the detection systems, the radiating source must be optically aligned with respect to the receiver of radiation. Optical alignment, in this instance, was achieved by correct positioning and orientation of the detector with respect to an external light source shone through the aperture. A miniature incandescent lamp, run from a battery or from the mains through a 6.3 V transformer, was used as the external light source for optical alignment.

14.2 General Discussion of the Monochromatic Radiant Intensity Traces

The major part of analysis and interpretation of the monochromatic radiant intensity traces is based on the recordings obtained by employing a photovoltaic cell and a P-I-N photodiode as detectors. M.R.I. traces were also recorded using an integrating light detector and a lead sulphide cell. The recordings obtained with the lead sulphide detector, however, suffered from excessive signal distortion and could not easily be interpreted in terms of the thermal condition of the weld.

The principal aim of the analysis of experimental results presented in this Section is to relate the pattern of M.R.I. variation to the

thermal condition of the weld surface, and hence to the progress of nugget growth. For this purpose, a qualitative analysis of the M.R.I. traces has been found to be adequate. It is shown here that the M.R.I. traces can be interpreted in terms of nugget growth, so that these traces may indicate whether the correct welding variables have been selected or not in a specific situation.

For a fuller appreciation of the M.R.I. traces discussed in this Section, the following features of the recorded traces may be noted.

(a) Amplitude Modulation of the Recorded Output

The 100 Hz carrier frequency generated by resistive heating of the work-piece is modulated by the varying radiant intensity, and the resultant output is recorded as an amplitude modulated signal in each case. The 100 Hz carrier frequency, in the present context, may also be referred to as the 'chopping' frequency of the radiation signal. The amplitude of the recorded trace is proportional to the mono-chromatic radiant intensity of the weld surface and is denoted by M.R.I. on the vertical axis. For the sake of comparison, the amplitude of the M.R.I. trace can be taken as an approximate indication of temper-ature of the weld surface. Weld time is denoted by t on the horizontal axis.

(b) Reference Trace

The current trace, obtained as the output of the integrator, is used as a reference trace to indicate the 'start' and 'finish' of weld time. In using the current trace as a reference trace, it is to be noted that while the M.R.I. trace is a 100 Hz amplitude modulated signal, the current trace is a 50 Hz chopped sine wave.

(c) Ringing due to Tuned Amplifiers

Since the detector output was taken through a high-Q tuned amplifier in each case, some 'ringing' is always present in the M.R.I. trace.

(d) M.R.I. Trace during Start and Finish of Weld Time

The outer surface of the weld does not attain a very high temperature immediately after the welding current is switched on, and very little radiation is emitted in the visible region of the spectrum. Since the optical passband of the detection system is mainly in the visible and near infra-red, no significant output was recorded until the radiant intensity in the passband reached a certain threshold level. Similarly, when the current is switched off the incandescence of the weld persists for some time; in the absence of the 100 Hz chopping frequency the decaying output was recorded as a d.c. signal.

(e) Spurious Pick-ups and Electrical Interference

Some spurious pick-ups and extraneous noise are almost always present in the recorded traces of M.R.I. Theoretically[39], no detection system can be made absolutely free from such noise and interfering signals; thus, until a reasonably high signal-to-noise ratio was attained the detection system did not produce a recognizable pattern in the recorded output. In the direct-incidence mode as well as in the remote-transmission mode, the interfering signal from the machine could not altogether be avoided without proper shielding and 'grounding'[44] of the enclosures housing the electronic detection systems. The electrical interference from the machine was more serious because of the use of high-gain tuned amplifiers in the signal-processing circuitry.

(f) Nature of the M.R.I. Traces recorded with Different Detection
Systems

The M.R.I. traces, in general, were obtained with detection
systems employing a photovoltaic cell and a P-I-N photodiode. The
detection system employing the integrating light detector, shown in
Figure 13.4, however, was found to be more sensitive than that employing
a P-I-N photodiode. Although the M.R.I. traces were slightly different
for the various detection systems, the general pattern of the recorded
traces conveyed the same information regarding temperature variation
of the weld surface.

(g) Running Parameters and Machine and Instrumentation Settings for
the M.R.I. Traces

The M.R.I. traces for any particular set of experiments, were
obtained by varying a single factor affecting weld formation; on the
recorded traces, therefore, only the specific running parameter is
shown, along with the peak r.m.s. current in each case. For the
recorded traces shown in Figures 14.2 through 14.10, the oscillomink
recorder was set as below

Oscillomink Recorder Settings

Recording Head Position - 20 millimetre.

Recorder Sensitivity   - Set to maximum.

Recorder Speed   - 20 centimetre per second,

except in the case of Figure 14.8.

The electronic instrumentation systems for recording monochromatic
radiant intensity and welding current were set as below.

For the Direct-Incidence Mode Detection System employing MS9BE
Photovoltaic Cell:

Attenuation Ratio of Toroid Output   - $\frac{1}{5}$

Tuned Amplifier Gain at 100 Hz   - 500.

The 100 kΩ potentiometer in the feedback loop of the current-to-voltage transduction stage of Figure 12.3 was adjusted to give maximum output voltage from this stage.

For the Remote-Transmission Mode Detection System employing MD2 P-I-N Photodiode:

      Attenuation Ratio of Toroid Output   - $\frac{1}{5}$

      Tuned Amplifier Gain at 100 Hz   - 500

For the Remote-Transmission Mode Detection System employing OPT1 Integrating Light Detector:

      Attenuation Ratio of Toroid Output - $\frac{1}{10}$

The pulse train activating OPT1 had the following characteristics:

      Pulse Repetition Frequency = 5 kHz

      Pulse Width   ≃ 5 μs

The total gain of 400 at 100 Hz for the detection system was made up as follows:

      A.C. Amplifier Gain   - 10

      Tuned Amplifier Gain at 100 Hz - 40

The machine settings corresponding to each set of recordings are given in the appropriate sub-Section in each case.

(h) Tests for Weld Quality

The welding variables for a good or acceptable weld were previously determined by macrosection tests and tension-shear tests in the context of monitoring by dynamic resistance measurement (see Part I). In the analysis presented in this Section, details of such tests are not included.

14.3 Influence of Welding Variables

14.3.1. Effects of Varying Welding Current

The recorded traces of Figure 14.2 and Figure 14.3 were obtained for various values of welding current, the current values being set on the control panel by means of phase-shift heat control. For the recorded traces of Figure 14.2, the direct-incidence mode detection system employing a silicon photocell was used. The recorded traces of Figure 14.3 were obtained with the remote-transmission mode detection system employing a silicon P-I-N photodiode. In both cases the following machine settings were used.

> Transformer Tapping - Number 6.
>
> Electrode Force   - 1.55 kN (350 lbf), corresponding to $0.5N/mm^2$ or 70 lb/in^2 on the Pressure Gauge.
>
> Weld Time   - 15 Cycles.

The following observations are made from an inspection of the M.R.I. traces shown in Figures 14.2 and 14.3.

(i) With low current, the temperature attained by the weld surface is such that only a small proportion of the emitted radiation is within the optical passband of the detection system; therefore, the amplitude of the recorded trace is small (see radiant intensity trace (a) in Figures 14.2 and 14.3).

As the current is increased, the monochromatic radiant intensity increases and is recorded as a signal of higher amplitude (see radiant intensity traces in (b) and (c) of Figure 14.2, and (b) of Figure 14.3).

(ii) With a high current, a high temperature is attained by the weld surface earlier during a weld; the peak in the M.R.I. trace, however, does not shift noticeably to demonstrate this effect clearly.

14.3.2. Effects of Varying Weld Time

The pattern of the monochromatic radiant intensity traces when
the weld time is varied is shown in Figures 14.4 and 14.5. The M.R.I.
traces shown in Figure 14.4 were obtained as output of the direct-
incidence mode detection system employing a silicon photocell. Recorded
traces shown in Figure 14.5 were obtained with the remote-transmission
mode detection system employing an integrating light detector. The
welding machine in both cases was set as below.

Transformer Tapping   - Number 6.

Electrode Force   - 1.55 kN (350 lbf)

Weld Heat Control   - 65.

The following observations are made from an inspection of the recorded
characteristics.

(i) For spot welds made with very short weld times, the total amount
of generated heat is small; moreover, the generated heat cannot diffuse
through the metallic mass instantaneously. Thus, with a short weld
time, the weld surface cannot attain a high temperature; the small
amplitude of the recorded trace, under such conditions, indicates a
lower temperature of the weld surface (see M.R.I. trace in (a) of
Figure 14.4.).

(ii) As the weld time is increased to 10 cycles, a peak appears in
the M.R.I. trace; when the weld time is increased to 15 cycles or more,
the change in the amplitude of the recorded trace is not very signifi-
cant (see M.R.I. traces in (b), (c) and (d) of Figure 14.4).

(iii) Closer inspection of the recorded traces of Figure 14.5 shows
that, when a very long weld time is used, the amplitude of the recorded
trace diminishes even before the welding current ceases to flow. Thus,
comparing the monochromatic radiant intensity traces for 16 cycles and
22 cycles, it is evident that there is no increase in amplitude of the

M.R.I. trace with the longer weld time; on the contrary, with 22 cycles of weld time, the amplitude of the M.R.I. trace decreases after the 18th cycle, indicating a reduction in temperature of the weld surface (see M.R.I. traces in (a) and (b) of Figure 14.5). Two factors may be responsible for the observed reduction in the temperature of the weld surface, when a very long weld time is used. Firstly, the electrical resistance of the metallic constriction at the sheet-to-sheet interface is less when a substantial nugget development has taken place, and therefore Joule heat generated is less. Secondly, with a long weld time, the plastic deformation of the work-piece produces larger areas of contact at the electrode-to-sheet interfaces; also, an enlarged nugget provides a larger area for conducting the heat away from the centre. Thus a reduced rate of heat production and the increased heat loss tend to counteract any rise in temperature of the weld surface.

14.3.3 Effects of Varying Electrode Force

The monochromatic radiant intensity traces of Figures 14.6 and 14.7 were obtained for various values of electrode force. The M.R.I. traces of Figure 14.6 were obtained with the direct-incidence mode detection system employing a silicon photocell; the recordings shown in Figure 14.7, however, were obtained with the remote-transmission mode detection system employing a P-I-N photodiode. The following machine settings were used in both cases.

> Transformer Tapping - Number 6.
>
> Weld Heat Control - 65.
>
> Weld Time - 15 cycles.

An examination of the recorded traces reveals the following character-istics.

(i) With low electrode force, the amplitude of the peak in the monochromatic radiant intensity trace is high. The occurrence of a splash weld is characterized by the pattern of M.R.I. traces labelled (a) in Figures 14.6 and 14.7; the M.R.I. traces during splash welds indicate that, in the absence of adequate electrode force, a sudden increase in the temperature of the weld surface may occur very soon after initiating the weld.

(ii) As the electrode force is increased, the peak r.m.s. current registered by the current meter is slightly higher.

Use of higher electrode force also permits more efficient conduction of heat away from the electrode-to-sheet and sheet-to-sheet contacts. Thus, in spite of slightly higher current flow through the weldment, the diminished amplitude of the M.R.I. traces indicates attainment of a lower temperature by the weld surface (see M.R.I. traces in (c) of Figure 14.6 and (d) of Figure 14.7).

14.4 Effects of Current Shunting

When a fresh weld is made in a work-piece which has already been spot welded in several places, the current flow through the fresh weld is reduced because of the shunting effect of the existing welds (also see Section 7). The experimental investigation, in this instance, was conducted to ascertain whether the phenomenon of current shunting would be evident from the monochromatic radiant intensity traces. For this purpose, the direct-incidence mode detection system employing a silicon photocell was used; the following machine settings were used to produce the spot welds.

Transformer Tapping   -   Number 6.

Electrode Force   -   1.55 kN (350 lbf).

Weld Heat Control   -   65.

Weld Time   -   15 cycles.

Two 20 S.W.G. specimen coupons measuring 102 mm (4 in.) x 25.4 mm (1 in.) were overlapped end to end and spot welded at five different points along the entire length; the welds were numbered 1, 2, 3, 4 and 5 according to the sequential order in which the work-piece was welded. The sequential number of each spot weld is shown on the left of each recorded trace in Figure 14.8. It may also be noted that the recordings of Figure 14.8 were obtained with a recorder speed of 10 centimetre/second. The following observations are based on examination of the recorded traces and the peak r.m.s. values of welding current.

(i) The peak r.m.s. current registered by the current meter increases with the number of spot welds.

(ii) The amplitude of the monochromatic radiant intensity trace diminishes as more spot welds are created on the same work-piece (compare the M.R.I. traces in (b) and (c) of Figure 14.8.).

The shunting effect of the existing welds is such that, although the total current indicated by the current meter may be higher than that registered for a single spot weld, the effective current through a fresh weld is very much reduced due to current sharing amongst the welds already made. Consequently, the rate of heat generation in a fresh weld is less, and the resultant temperature of the weld surface is lower. It may also be added that any existing spot weld enhances the heat loss by providing an additional parallel path for heat conduction, and counteracts any rise in temperature.

14.5   Influence of Surface Conditions

The influence of the surface condition of the work-piece on the weld has already been discussed in Section 7 of Part I. In 14.5, it is shown that the monochromatic emission characteristics are modified by the conditions of the emitting surface of the work-piece. The M.R.I. traces of Figure 14.9 were obtained with the aid of the direct-incidence mode detection system employing a silicon photocell, the machine settings being as below.

Transformer Tapping	-	Number 6
Electrode Force	-	1.55 kN (350 lbf).
Weld Heat Control	-	65.
Weld Time	-	15 cycles.

The underside of the bottom coupon acts as the emitting surface; from theory, the monochromatic radiant intensity is dependent upon the spectral emittance ε_λ and varies with the conditions of the emitting surface. The M.R.I. trace in (a) of Figure 14.9 was obtained when the underside of the bottom coupon was not cleaned; the M.R.I. trace in (b) corresponds to the situation when the underside of the bottom coupon was cleaned with emery paper and degreased. The diagram on the right of each set of recorded traces depicts the arrangement of the specimen coupons in each case. The following observations are made from the current values registered on the current meter and the recorded M.R.I. traces.

(i) The peak r.m.s. current value does not alter appreciably due to modifications of the electrode-to-sheet interface.

(ii) The amplitude of the M.R.I. trace diminishes when the underside of the bottom specimen is cleaned, thus confirming the theoretical supposition that ε_λ is less for polished surfaces (compare the amplitude

of M.R.I. traces in (a) and (b) of Figure 14.9).

14.6 Detection of Radiant Emission employing a Lead Sulphide Photoconductive Cell.

In view of the fact that a considerable amount of radiant power emitted by the weld surface lies in the infra-red region around 2 μm, detection of radiant emission between 1.5 μm and 2.5 μm was attempted by employing the direct-incidence mode detection system of Figure 12.5 where a lead sulphide photoconductive cell was used as the radiation detector. The following machine settings were used in obtaining the recordings of Figure 14.10.

Transformer Tapping	-	Number 6.
Electrode Force	-	1.55 kN (350 lbf)
Weld Heat Control	-	65.
Weld Time	-	25 cycles.

Traces (a) and (b) of Figure 14.10 were obtained without the tuned amplifier stage. Trace (a) was recorded using a solid tip without any aperture, so that no thermal radiation was incident upon the detector; thus, only the spurious pick-up from the machine can be seen in (a). Trace (b) was obtained by employing an electrode with an aperture, and therefore represents the radiant emission characteristic of the weld surface; the spurious pick-ups are recognizable in trace (b).

Trace (c) represents the infra-red emission characteristic when the output was taken through the tuned amplifier stage, and the reversal of signal polarity relative to trace (b) is due to the inclusion of the tuned amplifier.

Since it has not been possible to obtain consistent recordings of radiant intensity variation employing the detection system of Figure 12.5, the M.R.I. traces of Figure 14.10 do not truly represent the thermal changes occurring at the weld surface. The poor quality of the recorded traces can be attributed to two major factors. Firstly, the spurious pick-ups from the machine are further amplified when taken through the tuned amplifier stage; secondly, as explained earlier in 10.3.1, a large change in radiant intensity tends to saturate the output of the preamplifier stage, thus causing signal distortion.

It is, therefore, suggested that, (i) the preamplifier stage be redesigned with a larger dynamic range of operation, and (ii) appropriate measures be taken to provide 'shielding' of the circuit package for a more consistent and meaningful recording of infra-red emission.

14.7 Interpretation of a Typical Monochromatic Radiant Intensity Trace

Provided that an adequate electrode force is maintained, the radiant intensity trace in (a) of Figure 14.5 represents the typical temperature cycle of a spot weld in mild steel. The redrawn curve of Figure 14.11 is the envelope of the trace obtained by joining the positive-going peaks of the M.R.I. trace in (a) of Figure 14.5. The redrawn curve is termed the 'heating-and-cooling' curve of a spot weld, the 'heating' and 'cooling' portions of the curve being labelled separately.

The 'heating curve' consists of two regions. The steadily increasing amplitude of the 'heating curve' in region (I) indicates that there is a steady rise in temperature during this period. The 'heating curve' attains a stable maximum towards the end of region (I) and forms region (II). Region (II) of the 'heating curve' however, may not exist

unless the weld time exceeds a minimum threshold value (see M.R.I.
traces in Fig. 14.4.)

The part of the M.R.I. trace after the welding current has been
switched off constitutes the 'cooling curve'. The gradual decay of the
cooling curve depicts the pattern of cooling of the weld surface after
completion of a spot weld, in the absence of any water-cooling.

14.8 Conclusions and Comments

14.8.1. Summary of Conclusions

The M.R.I. traces were checked for consistency and repeata-
bility under identical experimental conditions, and the following is a
summary of the observations made earlier in this section.

(i) Typical Monochromatic Radiant Intensity Trace

The recorded traces of M.R.I. shown in Figure 14.5 can be taken as
examples of the pattern of radiant intensity variation during a typical
spot weld in mild steel. The welding current, in this instance, was
slightly lower than that recommended.

The characteristic shape of the 'heating-and-cooling' curve of
Figure 14.11, redrawn from the M.R.I. trace, is also similar to that of
the theoretically derived temperature cycles of Greenwood[32].

(ii) Influence of Current Variation

With low welding current, the amplitude of the peak in the M.R.I.
trace is small, indicating thereby a comparatively low temperature of
the weld surface. As the current is increased, a higher temperature is
attained by the weld surface, and a higher peak is observed in the M.R.I.
trace, the general shape of the various traces remaining the same.

(iii) Influence of Variation in Weld Time

When weld time is increased above a certain threshold, no significant increase is observed in the amplitude of the M.R.I. peak value, indicating that the temperature of the weld surface does not increase indefinitely with time. Since the heat losses increase with weld time, a slight reduction in the amplitude of the M.R.I. trace occurs when a very long weld time is used. A better weld does not necessarily result from the use of a longer weld time, although the heat input to the weld is sustained for a longer period.

(iv) Influence of Electrode Force Variation

With low electrode force, the probability of occurrence of splash welds increases. The larger amplitude of the M.R.I. peak for low electrode force indicates that the temperature at the electrode-to-sheet interface tends to be higher when a low electrode force is used; also, the shape of the M.R.I. trace for a splash weld differs from that for a weld made with adequate electrode force.

When the electrode force is increased, the amplitude of the peak in the M.R.I. trace diminishes, although the welding current registered by the current meter is higher. This apparent anomaly can be resolved by taking into account the reduced rate of heat generation at the electrode-to-sheet interfaces and the increased heat loss across these interfaces under higher electrode force. Thus, to avoid any misinterpretation of the M.R.I. trace, it is suggested that the electrode force be set to a value slightly higher than the recommended minimum (also see Section 7 of Part I).

(v) Shunting Effect

When several spot welds are made very close to one another on the same work-piece, a large proportion of the total current registered by the current meter is shunted away through the existing welds. The effective reduction in the current flow through a fresh weld, therefore, results in a reduced heat input to any fresh weld. Again, the existing welds provide additional paths of heat conduction across the thickness of the work-piece. Consequently, temperature attained by the weld surface is lower, and the M.R.I. trace shows a lower peak.

(vi) Influence of Surface Conditions

The radiant power detected by the various detection systems originates at the surface of the work-piece in contact with the bottom electrode. Any variation in the spectral emittance ε_λ of this surface affects the monochromatic radiant emission from the surface. Since ε_λ is less for a cleaned surface. the M.R.I. trace shows a peak of smaller amplitude when the emitting surface was cleaned. Therefore, care must be taken in interpreting the M.R.I. traces so that the low peak exhibited by a cleaned emitting surface is not misunderstood to be due to low current or some other factor.

14.8.2 Comments on the Use of Electrodes with Aperture

The following comments are relevant to the use of electrodes with an aperture at the tip.

(a) Location of the Electrode

Thermal radiation from the weld can be collected with almost equal efficacy by introducing an aperture at the top or the bottom electrode. However, the bottom electrode holder being stationary for most spot or projection welders, any light-guide or radiation detector located inside

the bottom electrode is not disturbed during operation of the machine. Hence, the electrode with an aperture was located in the bottom electrode holder.

(b) Selection of Aperture Diameter

The diameter of the aperture at the electrode tip was so selected that there was a minimum loss of contact area at the electrode-to-sheet interface. An aperture of large diameter will result in a severe reduction in the current-conducting area at the bottom electrode and may affect the current distribution in the electrode-to-sheet contact; also, lack of adequate pressure at the centre of the weld spot may give rise to insufficient fusion at the centre of the nugget. Too small an aperture, on the other hand, may easily be blocked by dust particles from a dirty work-piece. The 0.685 mm (0.027 in.) diameter aperture was opened out to a larger diameter at the underside of the tip to allow a larger cone of incident radiation; it was also easier to drill a small hole in the tip after some metal had been removed from the underside.

(c) Cooling of Electrodes

Since the inclusion of an aperture at the electrode tip demands certain modifications of the conventional water-cooling system, the present series of investigations was conducted without any water-cooling of the electrodes. Any undesirable rise in the temperature of the electrode tips was avoided by allowing a sufficient cooling time between two consecutive welds. Further development work* has since been carried

---

* M.Sc. thesis of J. S. Edgley,

"Further Development Work on a Resistance Welding Monitoring System" Department of Production Engineering, University of Aston in Birmingham, October 1971.

out with the specific objective of providing a suitable cooling system
for electrodes with aperture; the photograph of Figure 14.12 shows the
compact detection system developed for this purpose. It is, however,
felt that there is room for further improvements, and additional work
should be undertaken in respect of electrode-cooling.

(d) Appearance of Weld Surface

A small protuberance or 'pip' usually appears on that surface
of the work-piece which rests on the bottom electrode. This protuber-
ance is created by the plastic flow of weld metal into the aperture
at the tip of the electrode. In Figure 14.13 two sets of specimen welds
are shown. Spot welds made with a pair of ordinary or standard elec-
trodes without any aperture are shown in (a); appearance of the weld
surface when the bottom electrode had an aperture at the tip is shown
in (b).

(e) Effects on Weld Quality

Investigation into the effects of the aperture on weld quality
was undertaken in a separate research project* within the Department.
The results of the referred investigation indicate that the weld defects,
which normally occurred when using standard electrodes without any
aperture, were not in any way worsened due to the inclusion of a minute
aperture;also, no noticeable reduction in the mechanical strength of
the welded joint occurred due to the aperture. This has been confirmed
by the results of the tension-shear tests and macro-etch tests per-
formed for the present investigation.

* M.Sc. Project of P.R. Ellis,

"A Study of the Effects arising out of a Change in Electrode Geometry upon
Weld Quality and Welding Schedules, in Resistance Spot Welding",
Department of Production Engineering, University of Aston in Birmingham,
October 1970.

Macrosections of two spot welds are shown in Figure 14.14; the macrosection in (a) shows a spot weld made with a pair of standard electrodes without any aperture; the macrosection in (b) is for a weld when the bottom electrode had a 0.685 mm (0.027 in.) diameter aperture at the tip.

————————————
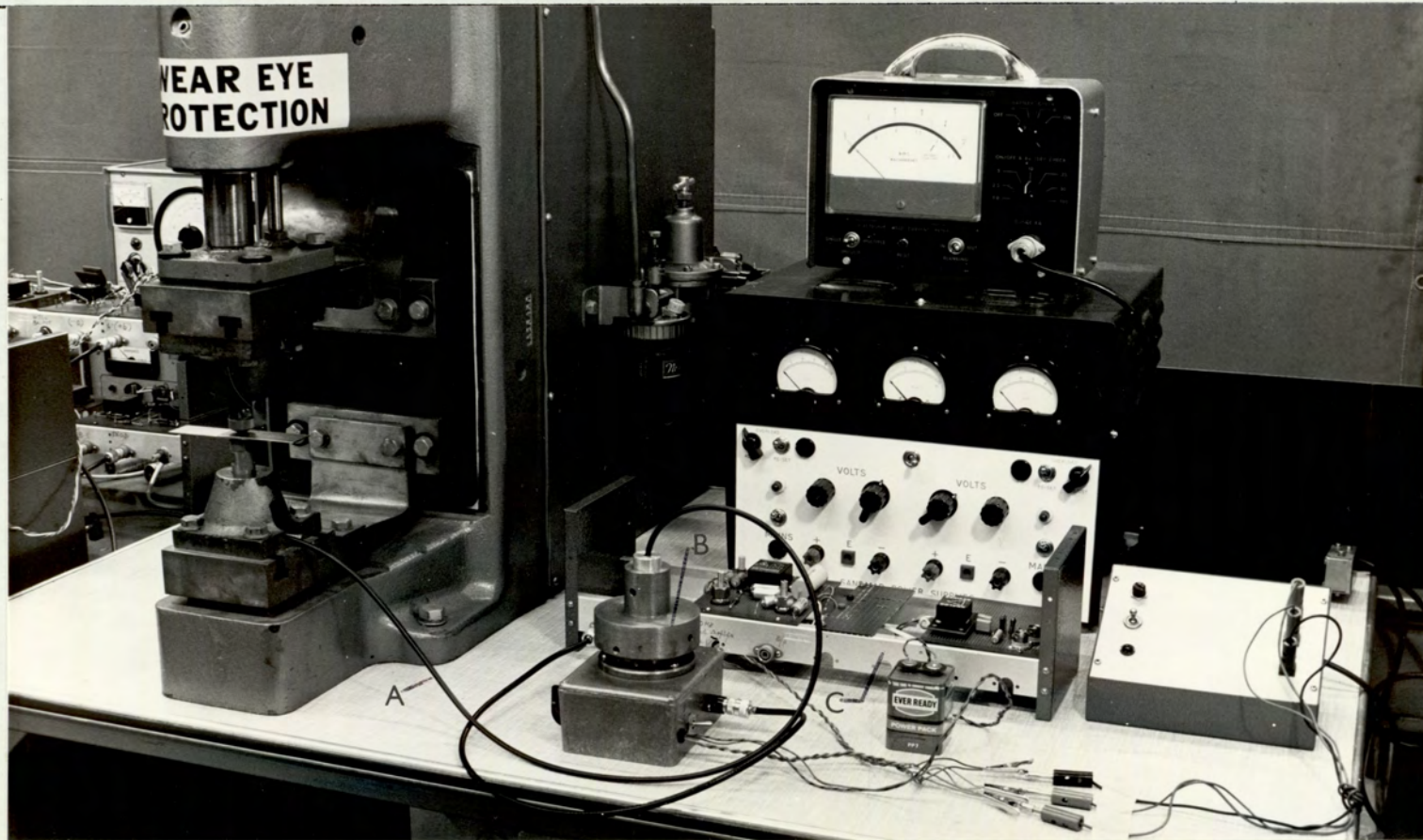
FIG. 14.1. Remote-Transmission Mode Detection System employing P-I-N Photodiode.

(A) - Light-guide;   (B) - Detector Housing;   (C) - Further Signal Processing Circuitry.
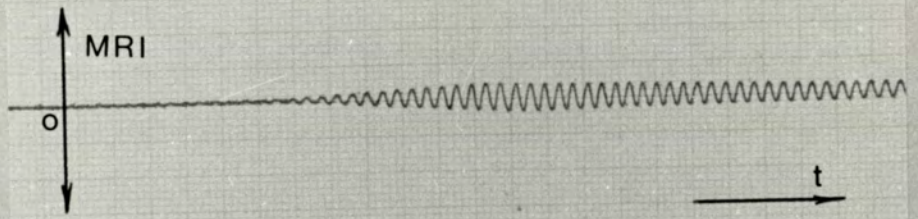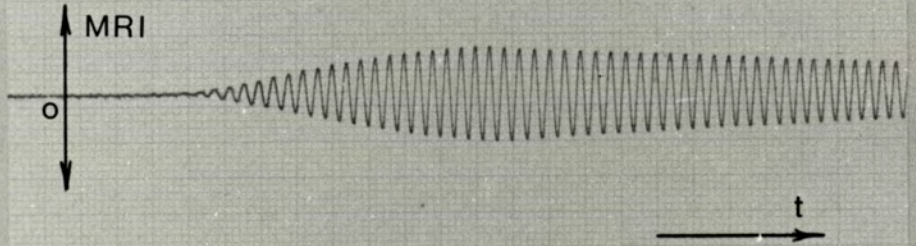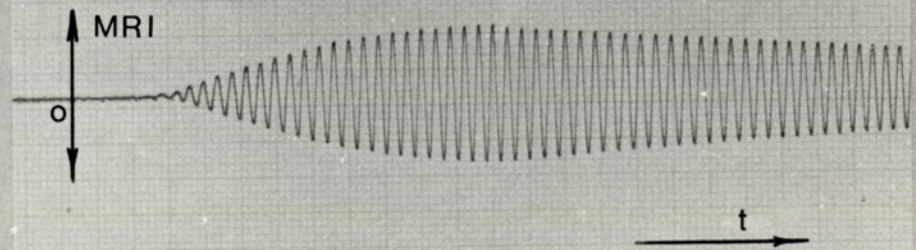
FIG. 14.2. M.R.I. Traces for Different Current Values -
Direct Incidence Mode.

Upper Trace: M.R.I., 1V/cm; Lower Trace: Current, 4V/cm.

Weld Heat Setting: (a) 50; (b) 60; (c) 65.
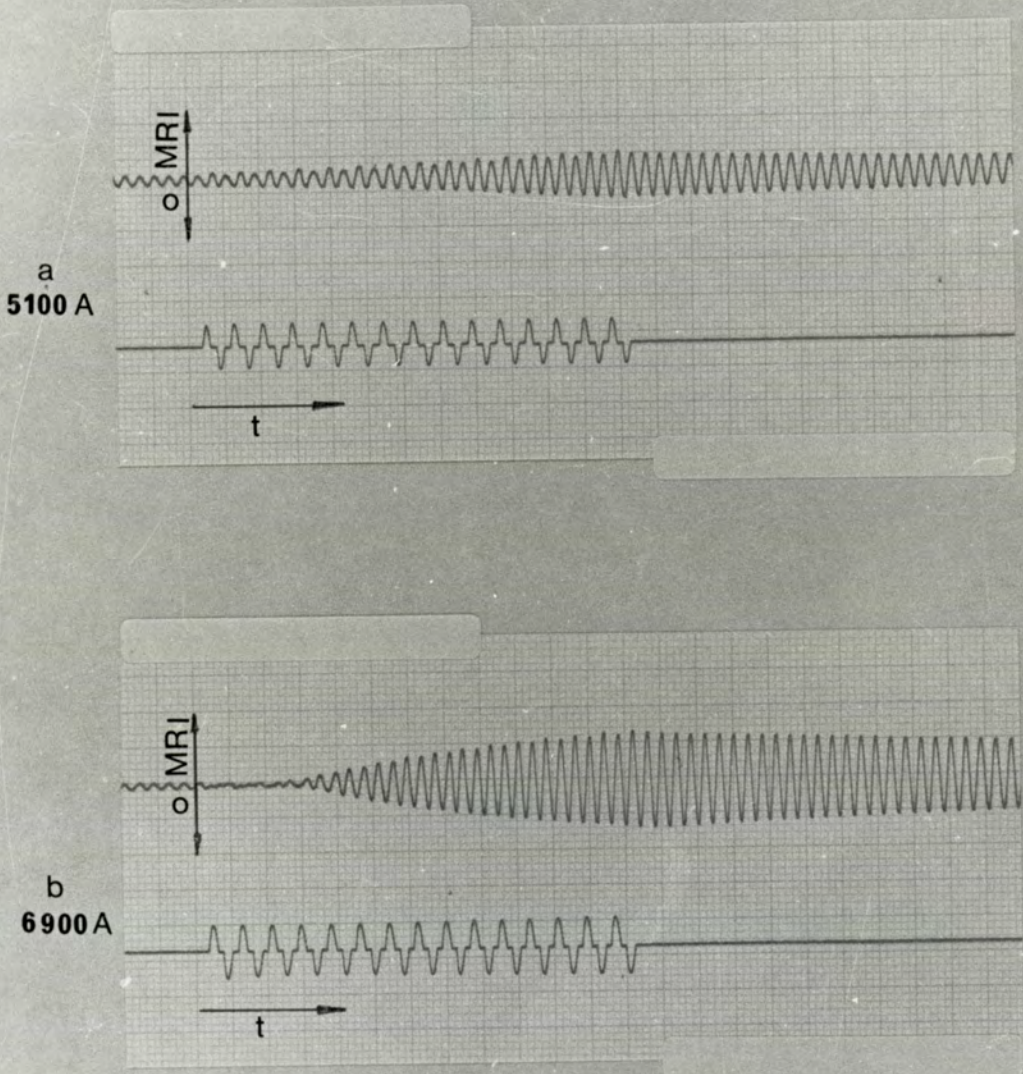
FIG. 14.3. M.R.I. Traces for Different Current Values -
Remote Transmission Mode.

Upper Trace: M.R.I.,0.1V/cm; Lower Trace: Current, 4V/cm.

Weld Heat Setting: (a) 50; (b) 70.
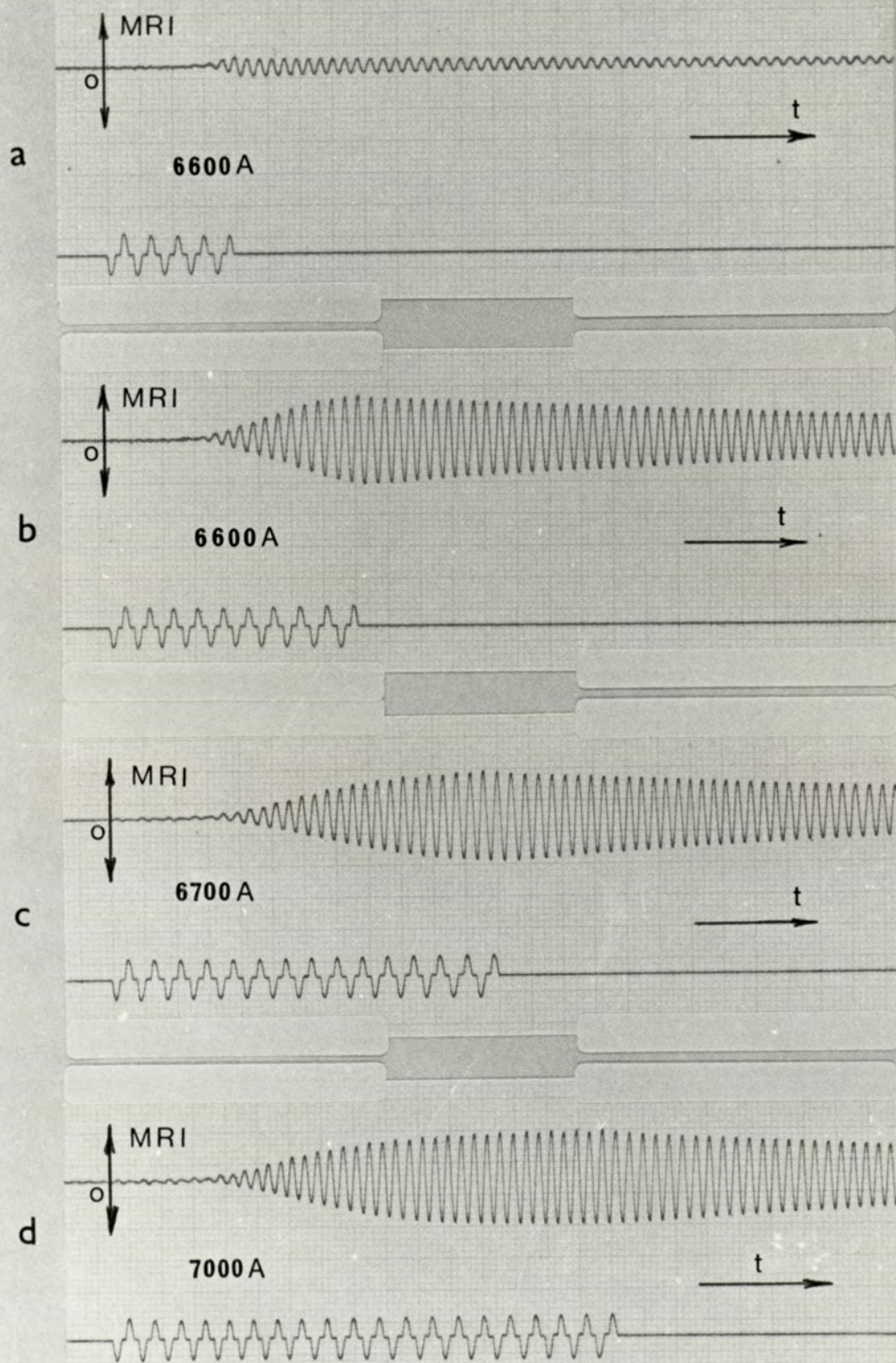
FIG.14.4. M.R.I. Traces for Different Weld Times -
Direct Incidence Mode.

Upper Trace: M.R.I., 1V/cm; Lower Trace: Current, 4V/cm.

Weld Time: (a) 5 Cycles; (b) 10 Cycles;
(c)15 Cycles; (d) 20 Cycles.
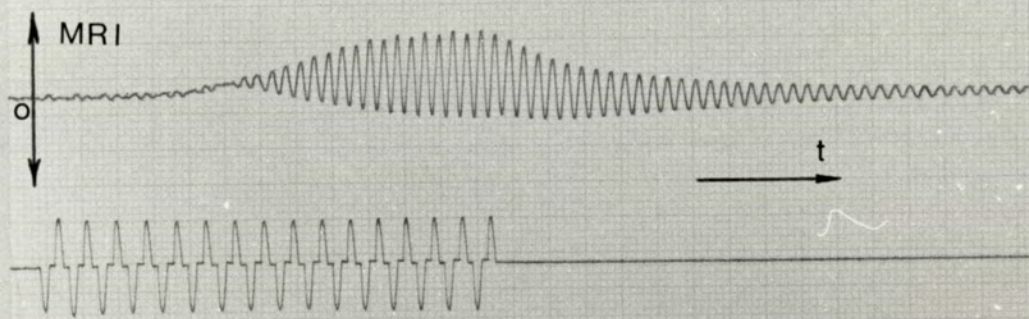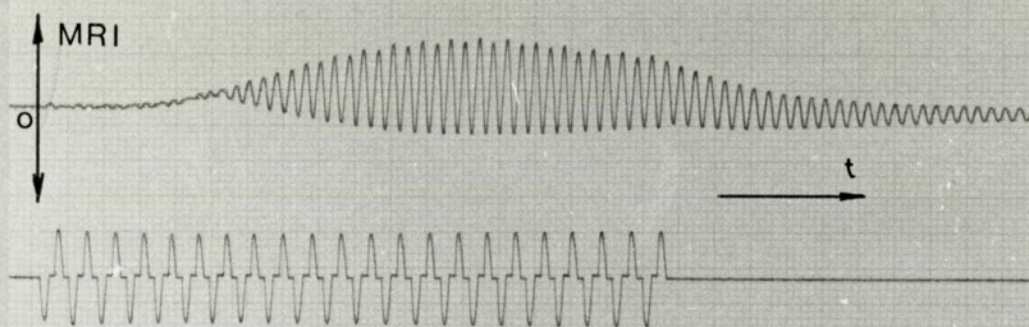
FIG. 14.5. M.R.I. Traces for Different Weld Times -
Remote Transmission Mode employing OPT1 Detector.

Upper Trace: M.R.I.,0.4V/cm; Lower Trace: Current,1V/cm.

Weld Time: (a) 16 cycles; (b) 22 cycles.
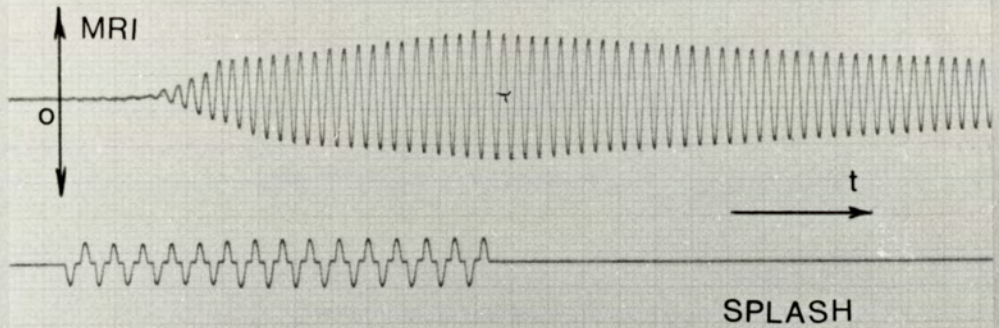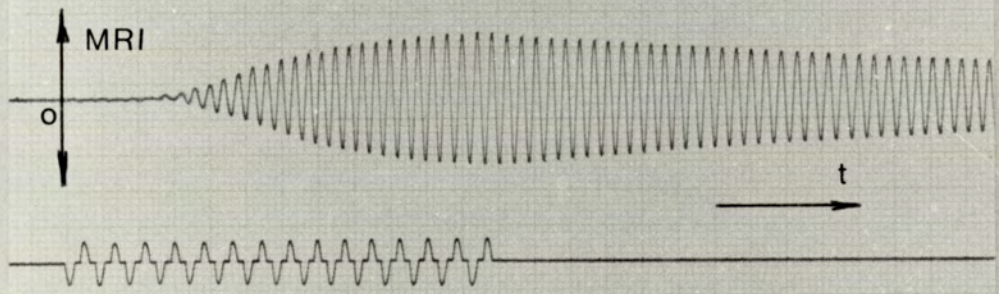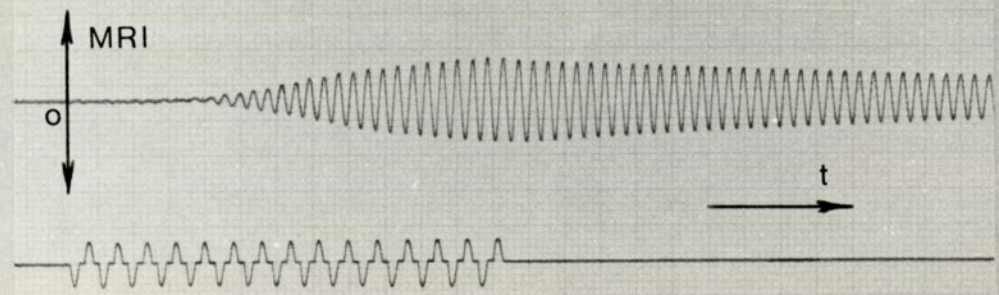
FIG. 14.6. M.R.I. Traces when Electrode Force was Varied -
Direct Incidence Mode.

Upper Trace: M.R.I., 1V/cm; Lower Trace: Current, 4V/cm.

Electrode Force: (a) 1.07 kN; (b) 1.31 kN; (c) 1.78 kN.
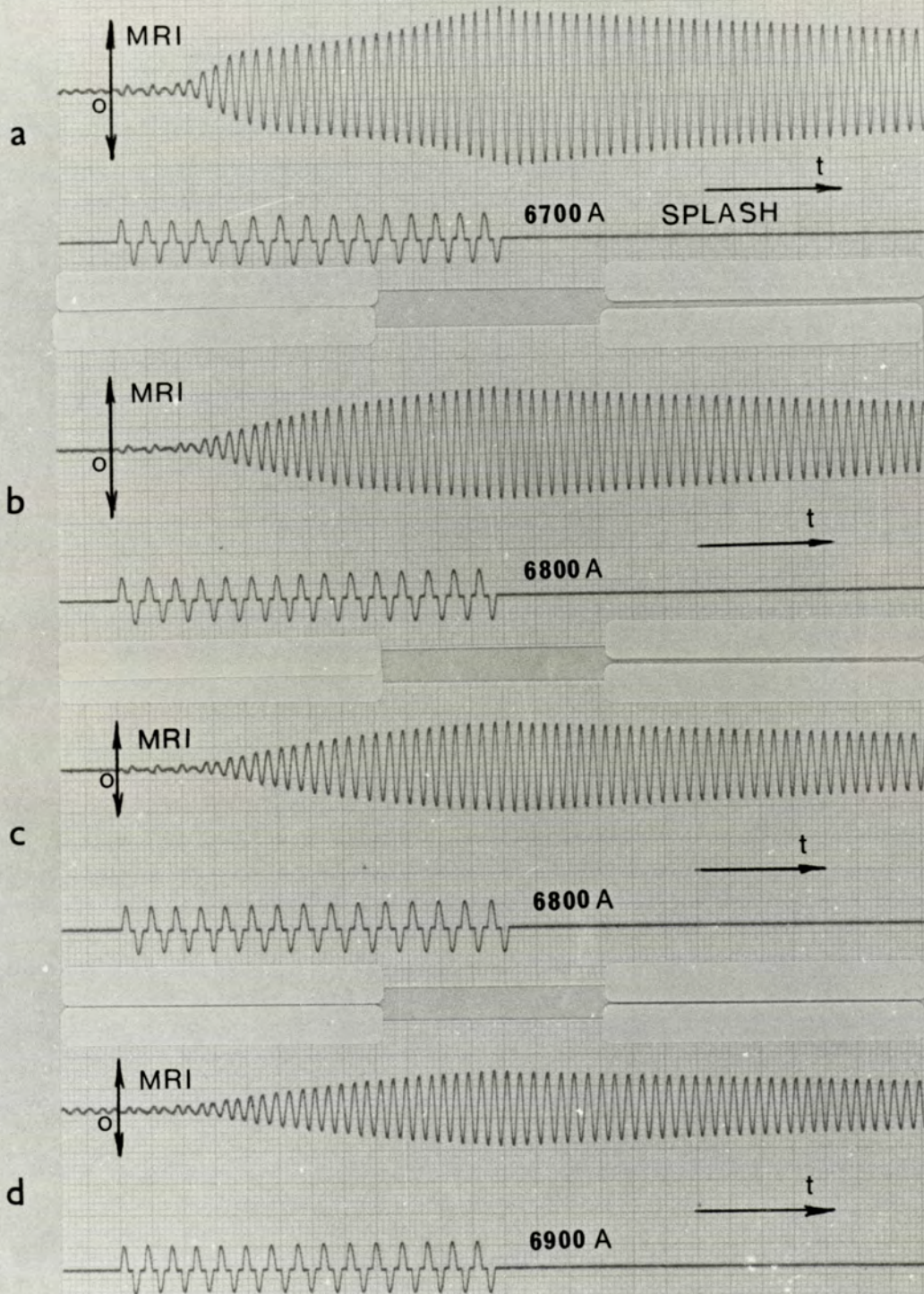
FIG.14.7.M.R.I. Traces when Electrode Force was Varied -
Remote Transmission Mode.

Upper Trace: M.R.I.,0.1 V/cm; Lower Trace:Current, 4V/cm.

Electrode Force: (a) 1.07 kN; (b) 1.31 kN;
                 (c) 1.55 kN; (d) 1.78 kN.
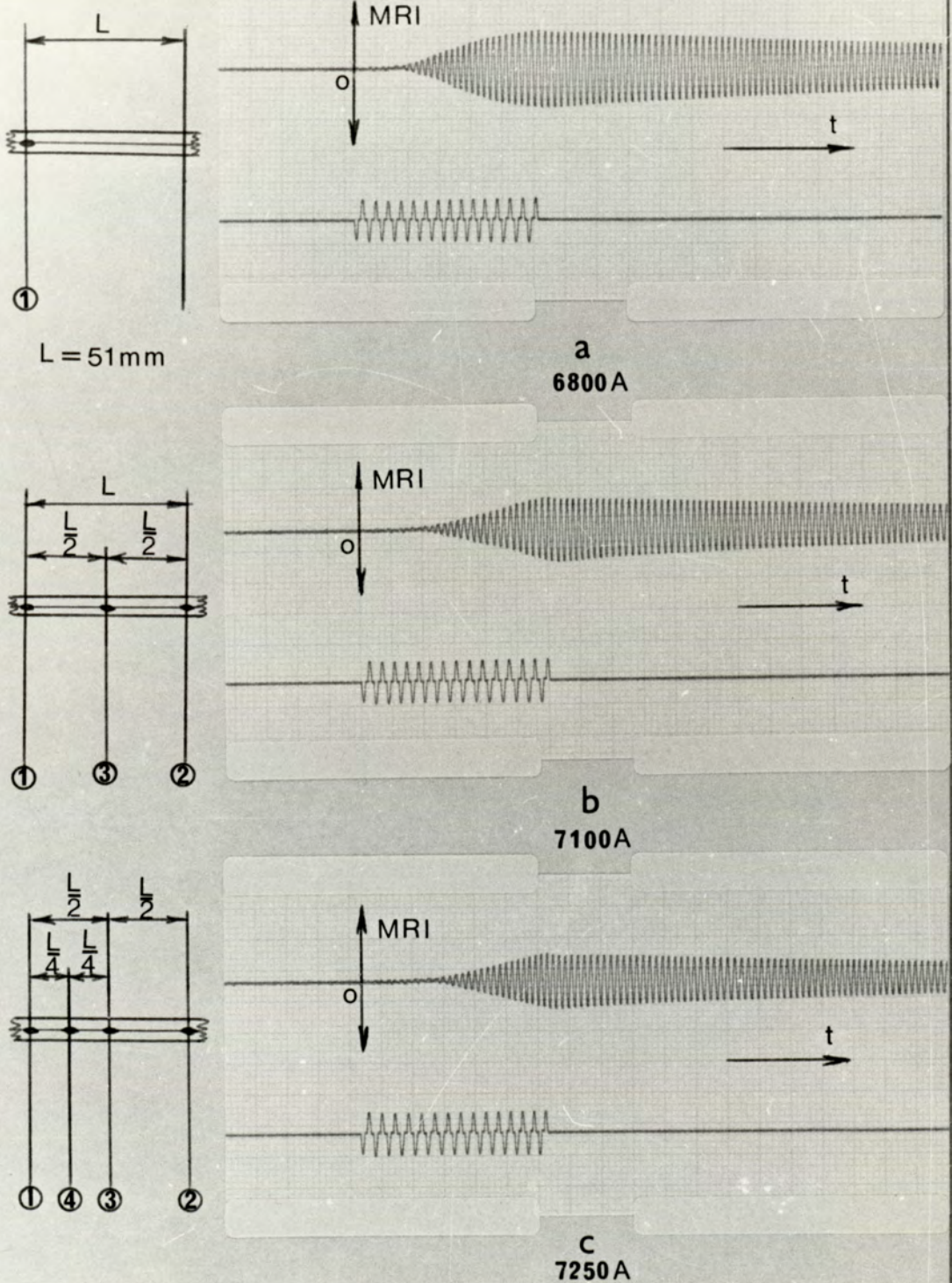
FIG. 14.8. M.R.I. Traces Modified by Current Shunting -
Direct Incidence Mode.

Upper Trace: M.R.I., 1V/cm; Lower Trace: Current, 4V/cm.

(a) Single Spot; (b) Spot No.3; (c) Spot No.4.
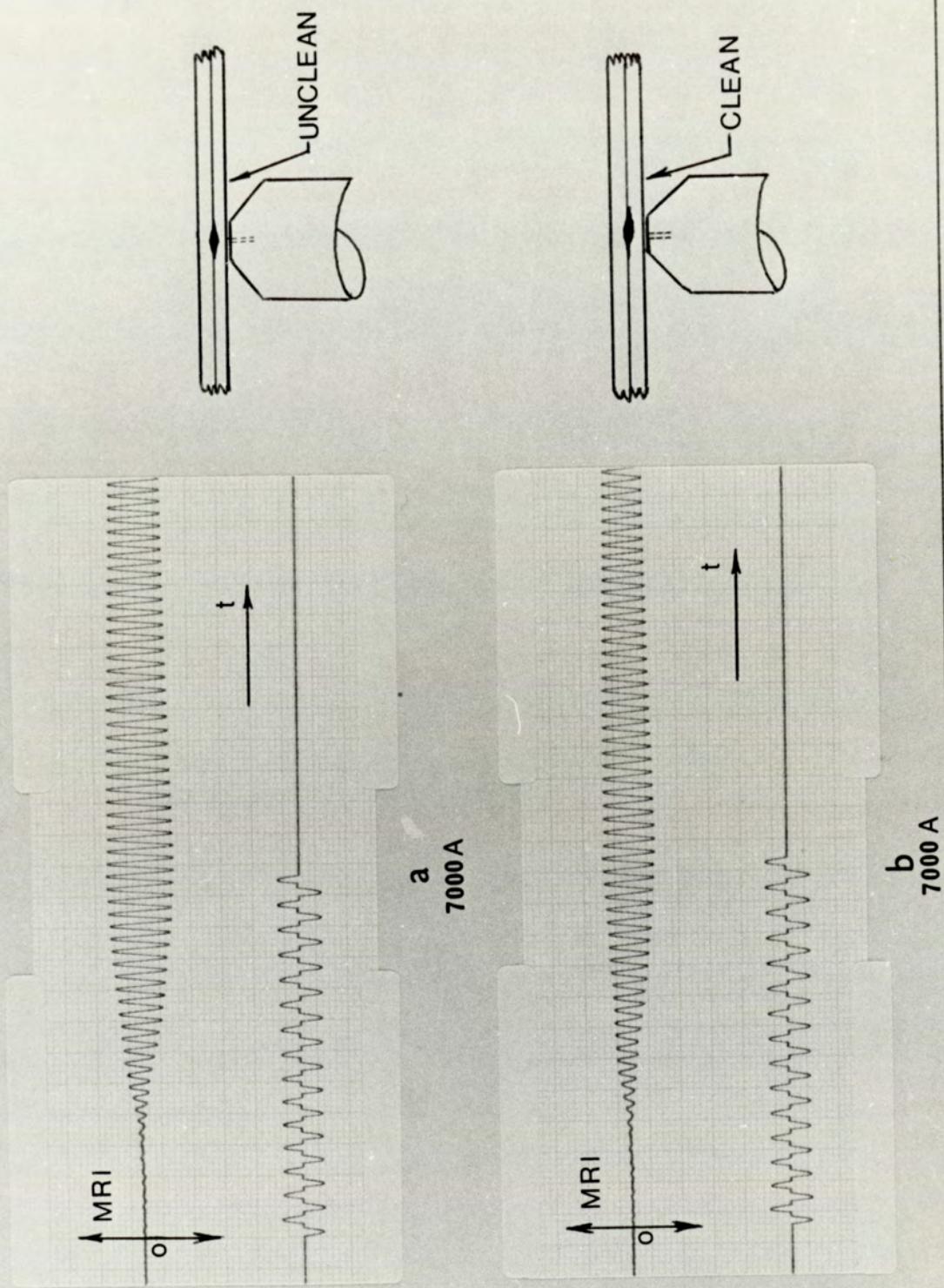
FIG. 14.9. M.R.I. Traces for Clean and Unclean Emitting Surface -
Direct Incidence Mode.

Upper Trace:M.R.I., 1V/cm; Lower Trace: Current, 4V/cm.

(a) 'Unclean' Emitting Surface;

(b) 'Clean' Emitting Surface.
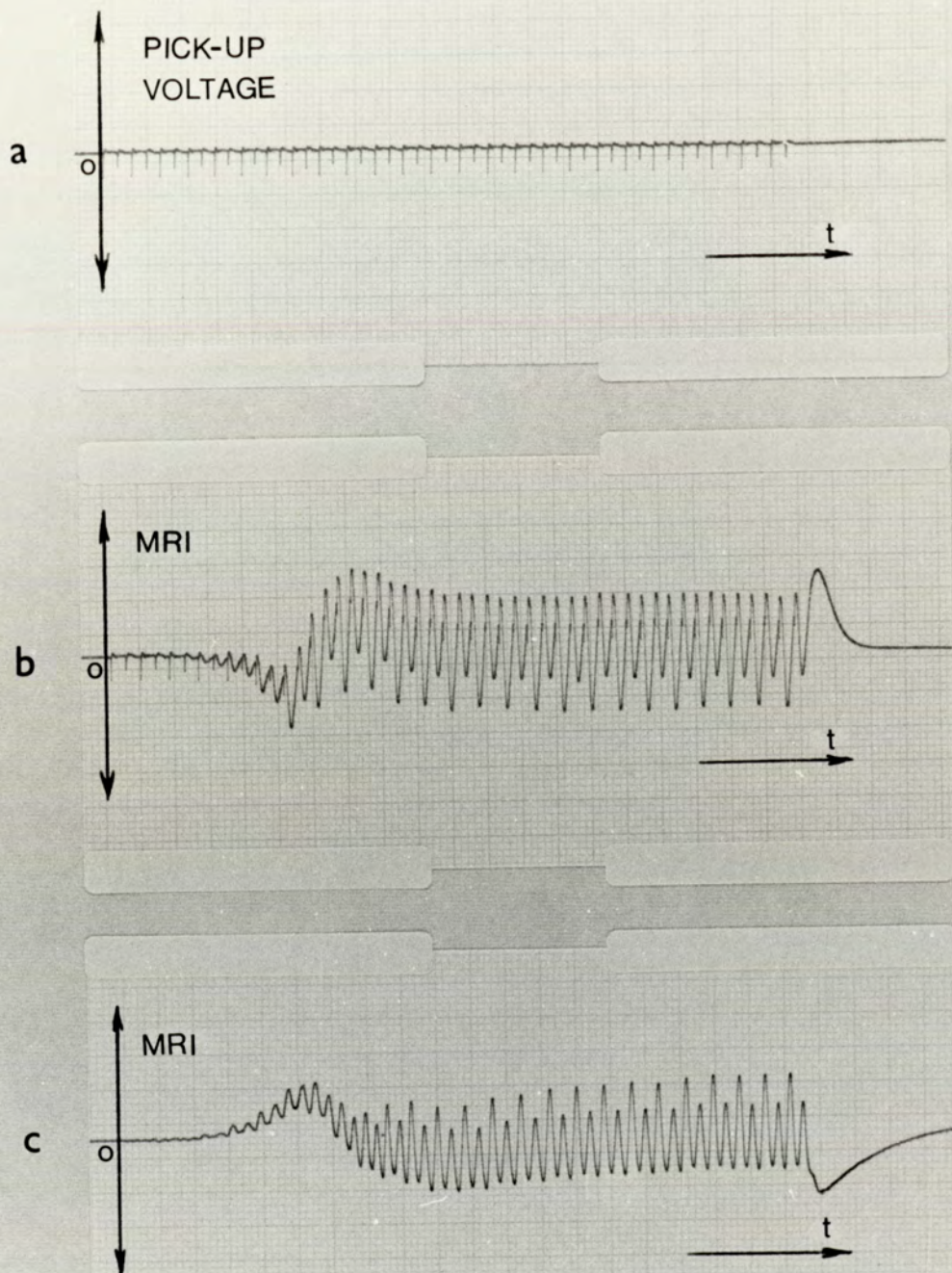
FIG. 14.10 Radiant Intensity Traces using Lead Sulphide Detector.

(a) Spurious Pick-up, 1V/cm;
(b) Output without Tuned Amplifier, 1V/cm;
(c) Output with Tuned Amplifier, 5V/cm.
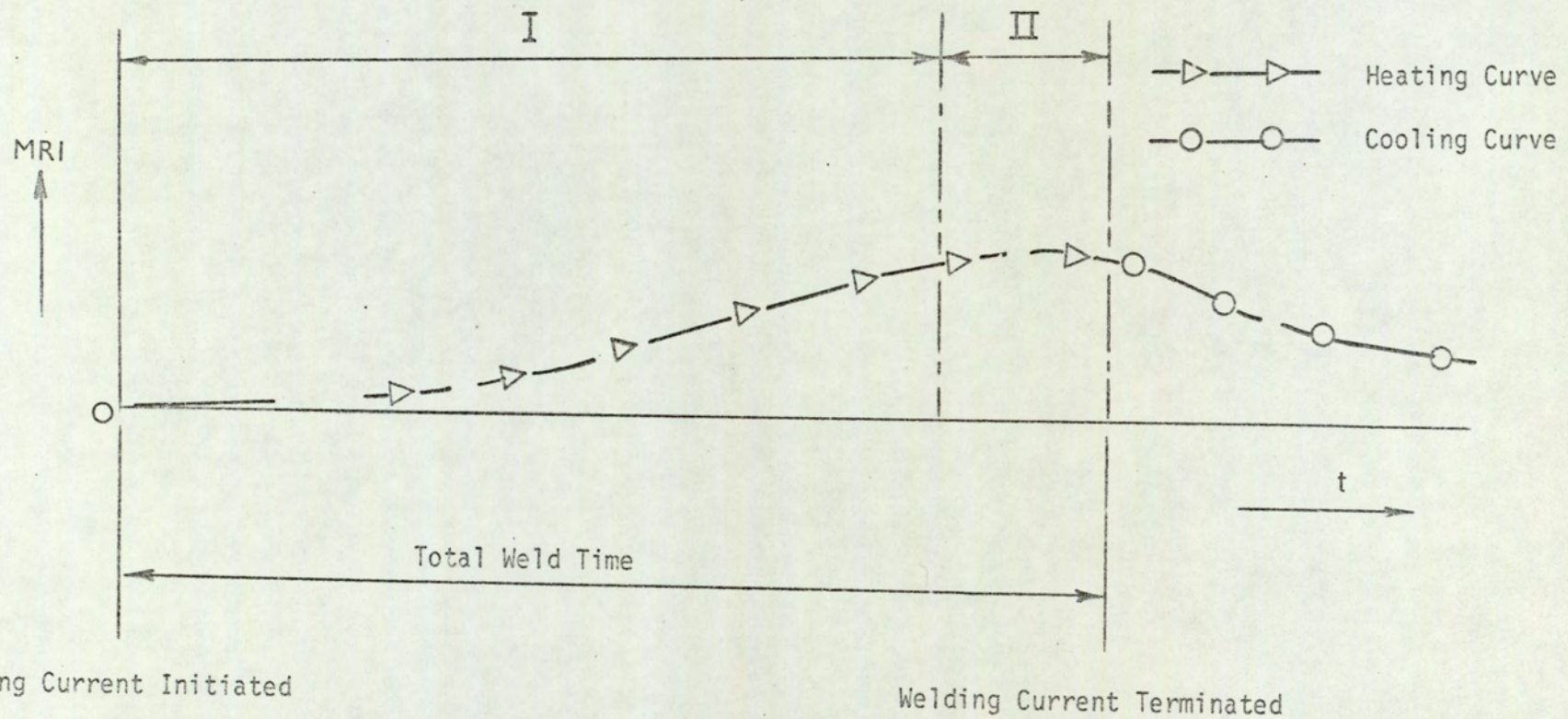
FIG. 14.11. Temperature Cycle or Heating-and-Cooling Curve for a Spot Weld.

(Please note that the curve has been redrawn after magnification of the original M.R.I. trace).
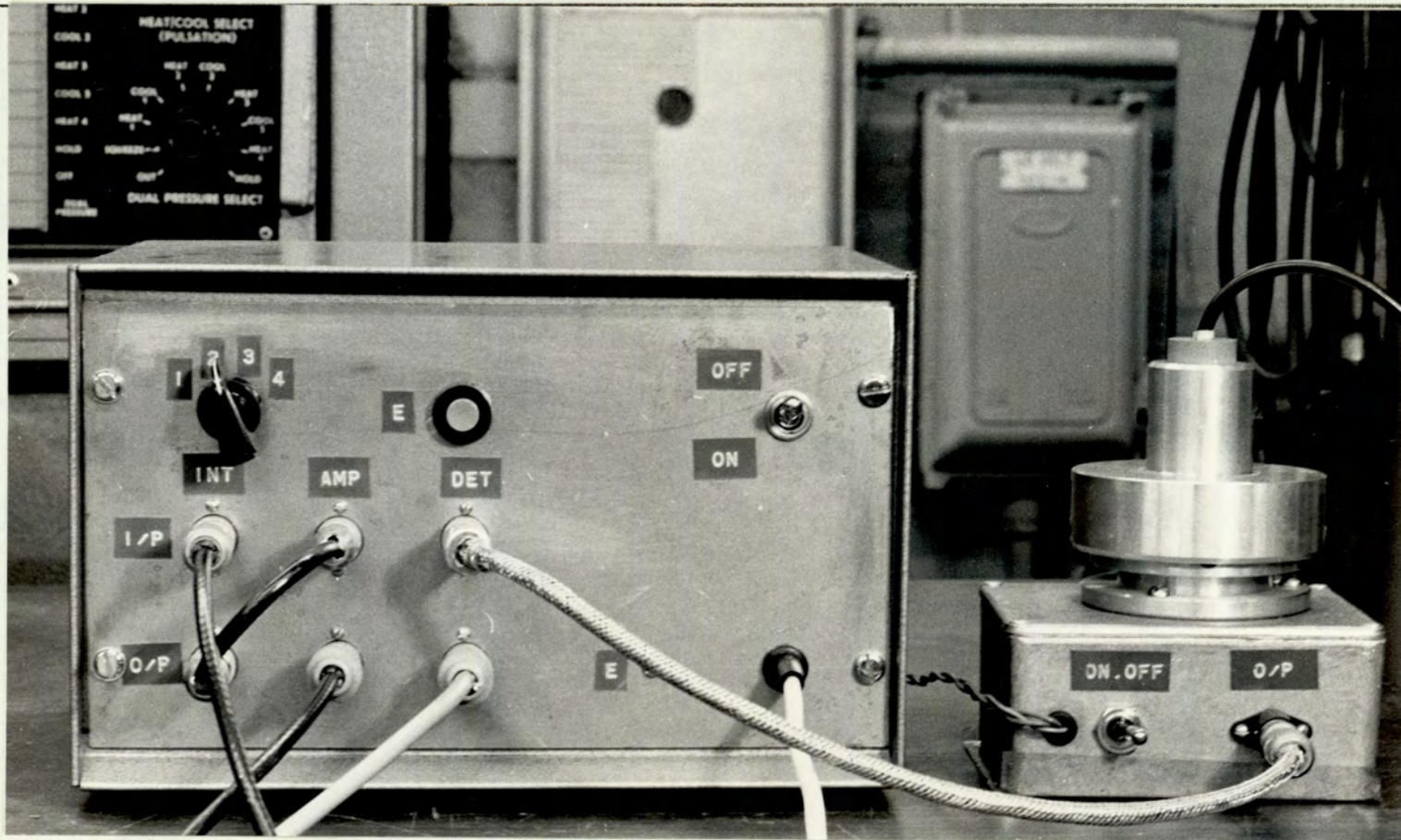
FIG. 14.12. Compact Electronic Instrumentation System for Remote-Transmission Mode Detection.

Left: Metal Cabinet housing Signal-processing Circuitry;

Right: Detector Housing.
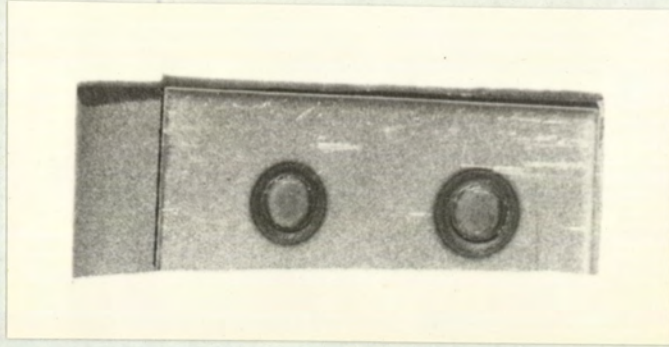
a
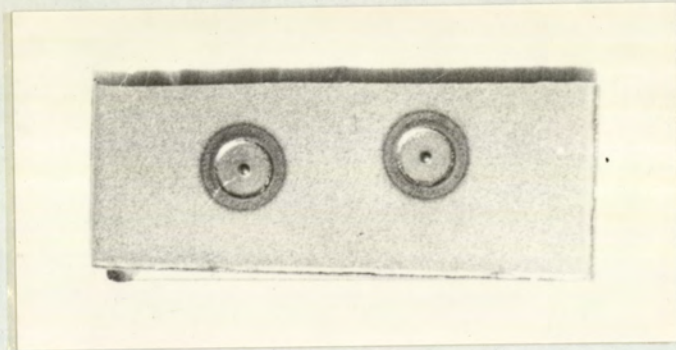
b

FIG. 14.13. Appearance of Weld Surface.

     (a) Spot Welds made with Ordinary or Standard Tiptrodes
        without any Aperture;

     (b) Spot Welds when the Bottom Tiptrode had an Aperture
        at the Tip.
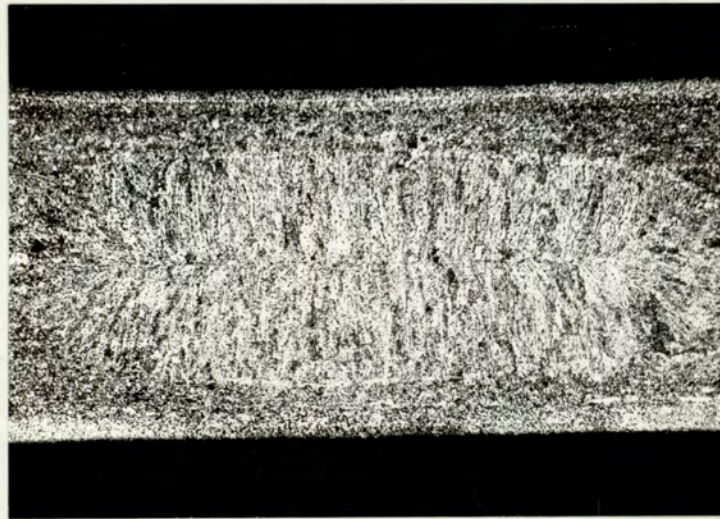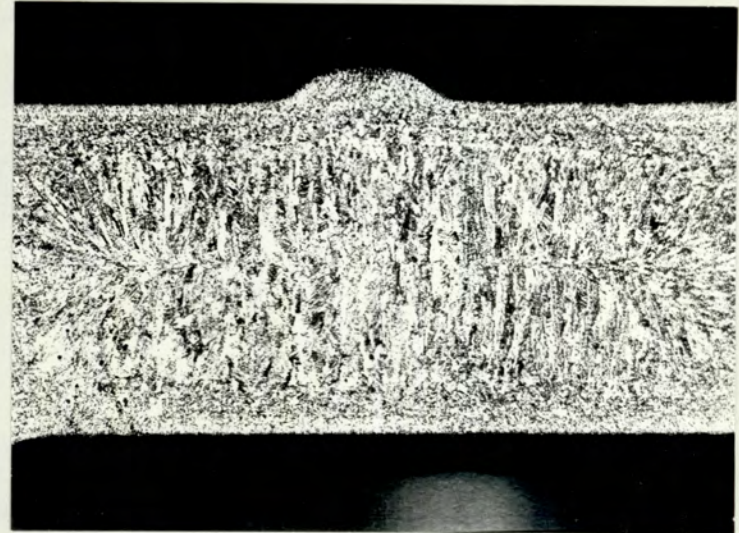
FIG. 14.14. Macrosection of Spot Welds.

(a) Spot Weld using Standard Tiptrodes without any Aperture;

(b) Spot Weld when the Bottom Tiptrode had an Aperture at the tip.

Material: 2 x 18 S.W.G Mild Steel.   Magnification: Approximately 17.5.

15. REVIEW OF CERTAIN THEORETICAL ASPECTS IN SPOT WELDING

15.1 Significance of Initial Static Resistance in the Theory of Spot Welding

The distinction between the dynamic resistance of the weld and the static resistance of the work-piece has been briefly covered in Section 3. Since the static resistance of the work-piece has little or no significance for the purpose of monitoring, the main emphasis throughout Part I of the dissertation has been on measurement and utilization of dynamic resistance as a process parameter. It will, however, be appreciated that the static resistance of the work-piece, although of little significance in respect of in-process monitoring techniques, exerts a great deal of influence on the welding process. For example, the current through the weldment is initially restricted to a finite value by the static resistance of the workpiece.

In the following sub-Sections an attempt has been made to develop a mathematical equation relating static resistance of the work-piece to the various factors which govern it. Such factors include electrode geometry, electrode force, and thickness and material properties of the work-piece among others. Theoretical work of this nature can be justified for two main reasons. Firstly, because no systematic development of this nature exists in the field of spot welding, except for that due to Gelman[45]. Secondly, the eventual development of a mathematical expression connecting dynamic resistance and the welding variables may become easier, when the nature and behaviour of static resistance are more clearly understood.

15.2 Derivation of the General Equation for Static Resistance

15.2.1 Contact Phenomenon and Microcontacts

Whenever two metallic members are brought into contact, their surfaces touch first at those points where the tips of asperities on one meet those on the other; a model representing the contact phenomenon is shown in Figure 15.1. Even with small loads, the local pressure at the contact tips is so high that metal in the microcontacts yield plastically; the resultant intimate metallic contacts are, however, established at a very few points on the surface. Each contact point or microcontact may, in the context of electrical conduction, be assumed to form a conducting path between the metallic members, and the effective contact area is due to an assemblage of such microcontacts over the entire area of apparent contact.

15.2.2 Macroscopic Area of Contact

Following the exposition due to Bowden and Tabor[46], the effective macroscopic contact area due to the aggregate of such micro-contacts is dependent on (i) the number of microcontacts, and (ii) the area of such microcontacts. Assuming each microcontact to be of the same area, let

$$a_c = \text{radius of a microcontact,}$$

and $$n_c = \text{total number of such microcontacts.}$$

Thus, M_a, the effective macroscopic area of contact, expressed as a function of both a_c and n_c, can be written as

$$M_a = f(a_c, n_c) \tag{15.1}$$

Both a_c and n_c in equation (15.1) are dependent[46] on the load acting

on the contact members and the yield pressure of the metal or metals at the contact. Determination of the exact nature of the function relating a_c and n_c to M_a will not be attempted here; theoretical analysis of the contact phenomenon and experimental methods for determining the actual macroscopic contact area, are to be found in a collection of papers by Dyachenko et al.[47].

15.2.3 Constriction Resistance of the Interfaces and
Bulk Resistance

From definition, the constriction or contact resistance at an interface appears as a resistance in excess of the bulk resistance offered by the contacting members. To evaluate the total electrical resistance effective between the electrode tips, the bulk resistance of sheet steel as well as the constriction resistance at the various inter- faces have to be taken into account. Thus, referring to Figure 15.2, R_x, R_y and R_z represent constriction resistance at the interfaces marked X, Y and Z respectively. Also, let R_B represent the total bulk resistance of the steel sheets. Therefore, R_T, the total electrical resistance effective between the electrode tips, can be expressed as

$$R_T = R_x + R_y + R_z + R_B \qquad (15.2).$$

Assuming that A_x, A_y and A_z represent the radius of effective macro- scopic area of contact at the interfaces X, Y and Z respectively, the resistances R_x, R_y and R_z can be expressed in terms of the electrode geometry and resistivity of the materials used for the electrodes and the work-piece. In deriving the mathematical expressions for R_x, R_y ..... R_B, the following symbols have been used:

d_t = electrode tip diameter,

t_s = thickness of each steel sheet,

ρ_s = resistivity of steel,

and ρ_c = resistivity of the copper alloy

for the electrodes.

(a) Expression for R_x and R_z

From symmetry, $A_x = A_z$, and $R_x = R_z$.

$$\therefore \quad R_x = R_z = R_{cc} + R_{cs} \tag{15.3},$$

where R_{cc} = constriction resistance in the copper side

of the electrode-to-sheet contact,

and R_{cs} = constriction resistance in the steel side

of the electrode-to-sheet contact.

From equation (A2.1) of Appendix 2,

$$R_{cc} = \frac{\rho_c}{4A_x} \tag{15.4}.$$

Similarly, $\quad R_{cs} = \frac{\rho_s}{4A_x} \tag{15.5}.$

Combining equations (15.4) and (15.5), equation (15.3) becomes

$$R_x = R_z = \frac{\rho_c}{4A_x} + \frac{\rho_s}{4A_x} \tag{15.6}.$$

(b) Expression for R_y

At the interface Y, both members being mild steel,

$$R_y = 2 \cdot \frac{\rho_s}{4A_y} = \frac{\rho_s}{2A_y} \qquad (15.7).$$

(c) Expression for R_B

R_B, the bulk resistance of steel is equivalent to that of a solid cylinder, the length and diameter of the cylindrical body being $2t_s$ and d_t respectively. R_B can be written as

$$R_B = \frac{\rho_s \cdot 2t_s}{\pi \cdot \frac{d_t^2}{4}} = \frac{8 \cdot \rho_s \cdot t_s}{\pi \cdot d_t^2} \qquad (15.8).$$

15.2.4 Expression for Total Static Resistance

Since $R_x = R_z$, the total static resistance of work-piece given by equation (15.2) can be expressed as

$$R_T = 2R_x + R_y + R_B \qquad (15.9).$$

Substituting for R_x, R_y and R_B, equation (15.9) becomes

$$R_T = 2\left(\frac{\rho_c}{4A_x} + \frac{\rho_s}{4A_x}\right) + \frac{\rho_s}{2A_y} + \frac{8 \cdot \rho_s \cdot t_s}{\pi \cdot d_t^2} \qquad (15.10).$$

The term for R_B in equation (15.10) can be further simplified as below

$$\frac{8 . \rho_s . t_s}{\pi . d_t^2} = \frac{8 . \rho_s . t_s}{3.14 \times d_t^2} \simeq \frac{2.5 \times \rho_s . t_s}{d_t^2} \qquad (15.11).$$

Equation (15.10) can therefore be rewritten as,

$$R_T = 2 \left(\frac{\rho_c}{4A_x} + \frac{\rho_s}{4A_x} \right) + \frac{\rho_s}{2A_y} + \frac{2.5 \times \rho_s . t_s}{d_t^2}$$

$$= \frac{1}{2} \left(\frac{\rho_c}{A_x} + \frac{\rho_s}{A_x} + \frac{\rho_s}{A_y} \right) + \frac{2.5 \times \rho_s . t_s}{d_t^2} \qquad (15.12).$$

Equation (15.12) is the general equation for initial static resistance of the weldment.

15.3 Discussion of the Equation for Static Resistance

15.3.1 Relative Significance of the various Terms and the resulting Simplification.

In order to recognize and appreciate fully the contribution of each term in the expression for R_T, realistic values of ρ_c and ρ_s have to be taken into account, along with the relative magnitudes of A_x and A_y.

(i) Relative values of ρ_c and ρ_s

For pure copper, the numerical value of resistivity given by Smithells[27] is 1.67×10^{-8} Ωm; for copper alloys, however, the resistivity is higher. The resistivity of copper-berylium alloy, for example, may lie in the range $(6.8 - 7.4) \times 10^{-8}$ Ωm. In comparison, the resistivity of mild steel containing 1% carbon and 1.8% silicon is given as 12×10^{-8} Ωm. It may therefore be stated that ρ_s is about twice the value of ρ_c in equation (15.12).

(ii) Relative magnitudes of A_x and A_y

In their treatment Bowden and Tabor[46] have shown that the macroscopic area of contact is inversely proportional to the yield pressure of the contacting metallic members. Copper is softer than mild steel and has a lower yield pressure. At the electrode-to-sheet contact, it is more appropriate to consider that the contact area is predominantly controlled by the plastic flow of the softer metal; consequently, the area of macroscopic contact formed at the electrode-to-sheet interface is larger than that at the sheet-to-sheet interface. It may, therefore, be stated quite justifiably that $A_x > A_y$.

Combining the effects of relative magnitudes of resistivity and macroscopic contact area, it is apparent that the term $\dfrac{\rho_c}{A_x}$ is smaller in comparison with $\left(\dfrac{\rho_s}{A_x} + \dfrac{\rho_s}{A_y}\right)$, and equation (15.12) may be simplified with little error to

$$R_T = \frac{1}{2}\left(\frac{\rho_s}{A_x} + \frac{\rho_s}{A_y}\right) + \frac{2.5 \times \rho_s \cdot t_s}{d_t^2} \qquad (15.13).$$

Since numerical values cannot be attributed to A_x and A_y, equation (15.13) does not lend itself to immediate application in determining the exact value of initial static resistance under a given set of conditions. It will, however, be shown that the more significant aspects regarding the nature and behaviour of initial static resistance can be analysed on the basis of this equation, even without any knowledge of the exact relationship connecting the various factors which govern the effective area of macrocontact.

In deriving an expression for the bulk resistance R_B, it has been assumed that the cylindrical body of material enclosed between the

electrode tips has the same diameter as the electrode tips. It is suggested that further experimental investigation be undertaken to establish such logic more conclusively. In the meantime, it is noted in Taz'ba's[48] analysis that the nugget diameter usually lies between $0.9 \times d_t$ and $1.2 \times d_t$; it may therefore be justified to assume that the lines of current flow within the material of the work-piece are initially confined within a region of approximately the same diameter as the electrode tip.

Finally, the subtle distinction between constriction resistance and contact resistance has been ignored for the above derivation, for the sake of simplicity. In most practical situations, the term 'constriction resistance' should more appropriately be replaced by the term 'contact resistance' because of the presence of tarnish films and layers of oxides and other chemicals at the contact interfaces.

15.3.2 Influence of Electrode Tip Diameter

At first sight, it may seem that the effective macroscopic area of contact at the interfaces is significantly affected by the apparent area of contact; the experimental evidence due to Bowden and Tabor[46], however, contradicts such assumption. The results obtained by Bowden and Tabor indicate that the contact resistance between two flat surfaces is not significantly affected when the apparent area of contact is made 25 times larger. Gelman[45], from his experimental investigation, also confirms that there is no distinct relationship between the apparent area of contact determined by the size of the electrode tips and the effective contact resistance.

Thus, the first two terms containing A_x and A_y in the expression for R_T will not alter a great deal due to changes in the electrode tip diameter. The last term in the right-hand side of equation (15.13) representing bulk resistance of the work-piece, however, is

inversely proportional to the square of the electrode tip diameter, and therefore alters very significantly with tip size. With electrode tips of small diameter, the bulk resistance term is large and the total static resistance is expected to be high; as the diameter of the electrode tips is increased, the bulk resistance term becomes smaller, resulting in a low value of total initial static resistance. Although no experimental verification of the above hypothesis has been made by separate measurements of static resistance, it is appropriate to assume that the initial 'trough' in the dynamic resistance characteristics is an approximate indication of the resistance value immediately after the welding current is switched on. It is evident from the dynamic resistance traces of Figure 7.6 that the finite value of r_t in the region of the initial 'trough' is higher for electrode tips of small diameter. The theoretical speculations and the supporting evidence from the dynamic resistance traces are also in agreement with the observations of Gelman[45].

15.3.3 Influence of Electrode Force

Investigation into the effect of load on the contact area was conducted by several researchers including Holm[24], Bowden and Tabor[46], and D'yachenko et al.[47]. Although opinions differ as to the exact relationship between load and effective area of contact, the common observation was that the effective macroscopic area of contact increased with load. In the specific case of spot welding, the effects of varying the electrode force can be determined from an examination of equation (15.13).

Thus, with a small electrode force, both A_x and A_y are small, the terms $\dfrac{\rho_s}{A_x}$ and $\dfrac{\rho_s}{A_y}$ are, therefore, comparatively large and make significant contribution to the total static resistance of the work-piece.

As the electrode force is increased, A_x and A_y become larger and the

terms $\dfrac{\rho_s}{A_x}$ and $\dfrac{\rho_s}{A_y}$ become smaller and the importance of these two

terms diminishes with a resulting reduction in the value of R_T. Again,

assuming that the value of r_t in the region of the initial 'trough'

in the dynamic resistance characteristic is, to a degree, indicative

of the electrical resistance at the early stages of welding, r_t is

found to be higher for low electrode force (see recorded traces in

Figure 7.5).

15.3.4 Influence of Surface Conditions

Although the experimental investigation discussed in 7.4

shows that the surface condition of the constituent parts of the work-

piece is of significance in governing the progress nugget growth, the

exact role of surface conditions in modifying the initial static

resistance cannot be defined very precisely, mainly because of the

practical difficulty in describing surface conditions in a quantitative

manner. Metallic contacts formed by 'clean' as well as 'unclean'

surfaces offer contact resistance. During the cleaning process,

however, surface films are disrupted in several places; thus, when

the constituent components of the work-piece form a 'clean' contact

at the sheet-to-sheet interface, a large number of intimate micro-

contacts are established through disrupted regions of the surface films.

The surface films referred to in the present context are 'thick' surface

films[24,29] and act as layers of insulation; by contrast, electrical

conduction can take place across 'thin' surface films* due to the

quantum-mechanical tunnel effect[24].

---

* 'Thin' surface films on cleaned metallic surfaces can only exist in an
  ultra-clean environment and may be of the order of 10 μm in thickness;
  surface films of this nature are rarely met in practice under ordinary
  industrial conditions.

The comparatively high value of 'trough' resistance r_t in the case
of 'unclean' contacts, demonstrated by the dynamic resistance traces of
Figure 7.7, is a pointer to increased static resistance for such
contacts.

15.3.5. Influence of Thickness and Electrical Resistivity
of the Material

R_B, the bulk resistance term in equation (15.13) is directly
proportional to t_s and ρ_s. The bulk resistance term represents higher
resistance when the thickness of the sheets is increased, or when the
material of the work-piece has higher resistivity. It may also be noted
that the thickness of the material constituting the work-piece also
changes the pattern of current distribution in the work-piece and thus
modifies the contact resistance terms as well. The 'screen' represent-
-ation of the macrocontacts, suggested by Gelman[45], although adequate
in explaining the effect of sheet thickness on the pattern of current
distribution in the work-piece, needs further development to establish
its theoretical rigour.

15.4 Joule Heat in the Weldment and Resultant Changes in
Resistance and Voltage Characteristics

15.4.1 Softening and Melting Voltages

Let V_{oc} be the secondary open circuit voltage applied across
the electrodes. Providing that this voltage is adequate to cause initial
breakdown of surface films, conducting channels will be established
across the electrode-to-sheet and sheet-to-sheet contacts. Since the
total static resistance may range from a few hundred microhms to a
few milliohms, a comparatively small voltage will force an appreciably
high current through the electrodes. The resulting current density

through the microcontacts at the interfaces is therefore sufficient
to provide Joule heating, thereby causing partial or complete collapse
of such microcontacts   very soon after the welding current has been
switched on.

'Softening' Voltage

The partial or complete collapse of the microcontacts is accompanied
by a decrease in contact resistance effective at the interface, since a
larger number of intimate metallic bonds are established across the
contact. The drop in the 'resistance-voltage' characteristics for mono-
metallic contacts has been termed a 'softening drop' by Holm[24]; the
voltage corresponding to the resistance drop has been termed the
'softening voltage'. Experimentally determined values of 'softening
voltage' for various metals are given by Holm. Thus, the 'softening
voltage' for a copper contact is 0.12 V and corresponds to a contact
temperature of 463 K (190°C) on the basis of the $\psi - \theta$ theorem;
similarly, for iron the corresponding values are 0.21 V and 773 K
(500°C).

Thus, the initial 'trough' in the dynamic resistance trace is to
be regarded as the region where softening of the electrode-to-sheet
and sheet-to-sheet contacts has occurred. Furthermore, the 'softening-
voltage' of copper being less than that of iron, it may be concluded
that the final area of macrocontact is almost complete at the electrode-
to-sheet interfaces as the dynamic resistance trace goes through the
'trough'. The sheet-to-sheet contact requires a comparatively larger
voltage for softening and the final area of macrocontact at the sheet-
to-sheet interface is formed later during the process.

'Melting' Voltage

'Melting voltage', for a monometallic contact, according to Holm[24], is a limiting voltage and is restricted to a maximum value across a contact; any attempt to increase the applied voltage across the contact above this limiting value results in the contact members sinking together and forming a fused metallic bond. The resultant area of current conduction increases rapidly when the 'melting' voltage is reached, and the increased area of intimate metallic bond is capable[28] of carrying a much larger current. The 'melting voltage' of copper, given by Holm, is about 0.43 V and corresponds to a maximum contact temperature of 1356 K (1083°C); for iron the corresponding values are 0.6 V and 1812 K (1539°C).

It may be concluded that the peak in the dynamic resistance characteristic denotes the instant when the voltage developed across the sheet-to-sheet contact approaches the 'melting voltage' appropriate to the contact; the tendency of the welding current to increase beyond the instant of peak resistance is demonstrated by the recorded traces shown in Section 6.

15.4.2 Change of State of the Weld Metal and its Influence on the Shape of the Dynamic Resistance Curve

The region of the dynamic resistance curve from the initial 'trough' to the 'peak' shows a steady increase in resistance; this almost linear change in resistance can be attributed to the temperature rise of the weldment. However, without further investigation it cannot be confirmed whether the slope of this part of the curve is similar to the relationship proposed by Holm[24] for a simple monometallic contact.

The prominent 'peak' in the dynamic resistance characteristic suggests that the large change in resistance may be due to change of

state, when temperature at the sheet-to-sheet interface reaches the melting point, rather than due to temperature coefficient slone. A clearer explanation of such changes in the resistivity of metals due to change of state requires a more thorough understanding of the physical processes of thermal and electrical conduction in metals. Following the detailed discussions of Powell[26], and Mott and Jones[25] in this respect, it appears that, for pure metals such as copper, silver, gold, aluminium, tin, lead and many others, the electrical resistivity changes abruptly on melting. Experimental results[25,26] suggest that, for a number of common metals, the resistivity ρ changes on melting such that the ratio $\dfrac{\rho_{Liquid}}{\rho_{Solid}}$ approximates to 2. Although iron is not included in the list of metals for which results are available, it is realistic to suppose that ratios of the order of 2 or more may be effective for iron and low-carbon mild steel. Thus, the 'peak' in the dynamic resistance curve corresponds to the instant in time when a substantial amount of metal in the sheet-to-sheet interface reaches the melting temperature. However, because of the 'melting voltage' phenomenon, any increase in resistance is arrested beyond the 'peak' and the enlarged conducting area of the fused zone permits larger current flow without any subsequent rise in temperature. The Joule heat generated is less because of the reduced current density in the enlarged metallic bond, and no further increase in resistance occurs. The welded joint tends to reach a thermal equilibrium, with almost all the generated heat being lost to the electrodes and the surrounding metal; the gradual decrease in the resistance of the weld beyond the 'peak' supports the above explanation.

15.5 Heat Generation, Heat Transfer and Temperature Distribution
in Spot Welds

Some contradiction exists as to the significance of the various
zones of the weld region in respect of heat generation. Alov and
Bulgachev[50] concluded that the contribution of the interfacial
contact resistance towards the heating of the work-piece was negligible.
Dix[51] lends support to this idea. However, since the contact resist-
ance at the interfaces accounts for a substantial part of the total
static resistance of the work-piece, the conclusions of Alov and
Bulgachev[50] and Dix[51] do not seem to be justified.

The temperature distribution suggested by Greenwood and
Williamson[28] based on the ψ-θ theorem remains the most rigorous
treatment of its kind in spot welding. According to these authors, most
of the heat is liberated around the periphery of the contact circle
formed at each interface; rate of heat production at the centre of the
contact area is less in comparison. The steady-state temperature,
however, falls off comparatively slowly with distance in the plane of the
interface, but rather sharply away from this plane. Following Greenwood
and Williamson, it may therefore be concluded that the bulk of the metal
in a spot weld is indirectly heated by conduction from the peripheral
regions of the contact areas, and not by Joule heat generated within
the bulk. Also, the heat generated at the interfaces cannot be conducted
throughout the medium very quickly in the absence of intimate metallic con-
tact all-round. This is demonstrated by the sharp rise in temperature
of the electrode-to-sheet interface in the beginning of a weld, when the
components of the work-piece are held together with low electrode force
(see M.R.I. traces in Figures 14.6 and 14.7).

The pattern of heat transfer during cooling can usually be deter-
mined from the preferential orientation of the grain structure of the
nugget, and is usually radially outwards from the centre of the nugget.

15.6 Probable Forms of Mathematical Equations relating Dynamic Resistance and Weld Time

15.6.1 Mathematical Equation of the Resistance-Time curve for Mild Steel

The ideal shape of the dynamic resistance curve for a good
weld in mild steel is as shown in (a) of Figure 15.3. The initial part
of the curve over the region 0-A does not provide any useful information
as to the progress of nugget development; the remaining part A-B, however,
can be correlated to nugget growth. The A-B part of the curve is redrawn
in (b) of Figure 15.3. It can be shown that an equation of the form

$$Y = \frac{X}{P + QX^2}$$ fits the curve (b) of Figure 15.3, where X and Y are the

variables, and P and Q are the coefficients. The corresponding equation
for the redrawn resistance-time curve can be written as

$$r'_w = \frac{t'}{P + Qt'^2} \tag{15.14},$$

where r'_w and t' represent resistance and time respectively, referred to
the new set of reference axes; the coefficients P and Q have to be
evaluated by further analysis of numerical values.

Although equation (15.14) is of no great significance in itself,
it enables one to generate the useful part of the resistance-time curve
electronically. Thus, in utilizing dynamic resistance as a process
parameter, the sampled values of dynamic resistance of production welds
can be compared with those of the ideal resistance-time curve generated
electronically, without the need for long electronic memory (see Section 8
of Part I).

15.6.2 Probable Form of General Equation of Resistance-Time
Curves for Spot Welds in various Metals and Alloys

The dynamic resistance curves for spot welds in mild steel, stainless steel and some aluminium alloy are shown in (a) of Figure 15.4; the curves in (b) of Figure 15.4 represent the p-v characteristics[53] of real gases over a wide temperature range. It is interesting to note that a common pattern emerges when the dynamic resistance curves are compared with the p-v characteristics shown in (b). The p-v character-istics can be described by Van der Waal's equation[53] of state for real gases which can be written as

$$(p + \frac{a}{v^2})\ (v - b) = R'\ T \qquad (15.15),$$

where p = pressure,

v = volume,

T = temperature

R' = modified universal gas constant,

and a and b are correction terms. By analogy, it is suggested that the resistance-time curves for various metals and alloys can be described by an equation similar to that of Van der Waal. Thus, the corresponding equation for the resistance-time curve can be written as

$$(r_w + \frac{\alpha}{t^2}).\ (t - \beta) = \gamma.\ \mu_\theta \qquad (15.16),$$

where r_w = resistance,

t = time,

μ_θ = some critical property of the material of the work-piece,

and α, β and γ are constants replacing a, b and R' of equation (15.15).

The symbol $(\mu_\theta)_k$ in (a) of Figure 15.4 is similar to the critical temp-
erature T_k of the p-v characteristics in (b); the changing pattern of
the resistance-time characteristics above and below $(\mu_\theta)_k$ is analogous
to the pattern above and below T_k. Without further experimental investi-
gation with various other metals, it is not possible to define the exact
nature of μ_θ, the specific material property which influences the
change of pattern above and below $(\mu_\theta)_k$. However, since both aluminium
and stainless steel are non-magnetic, some correlation between μ_θ and
the magnetic properties of metals cannot be ruled out.
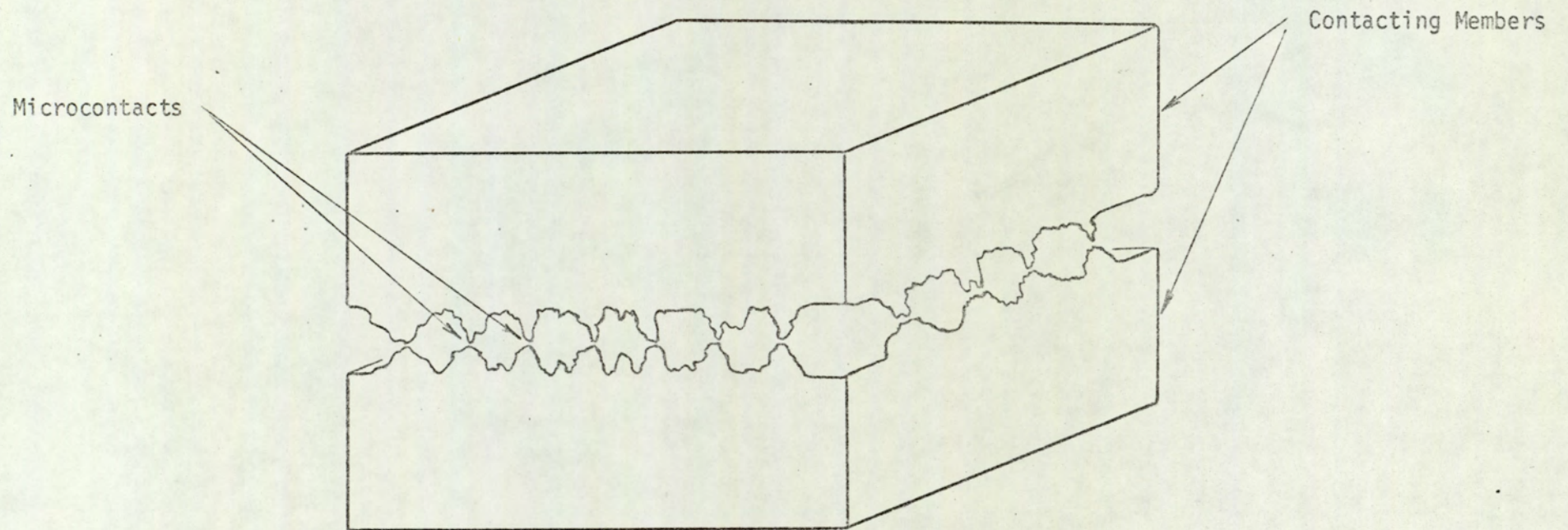
FIG. 15.1 Model Representation of the Phenomenon of Microcontacts in Contacting Members.
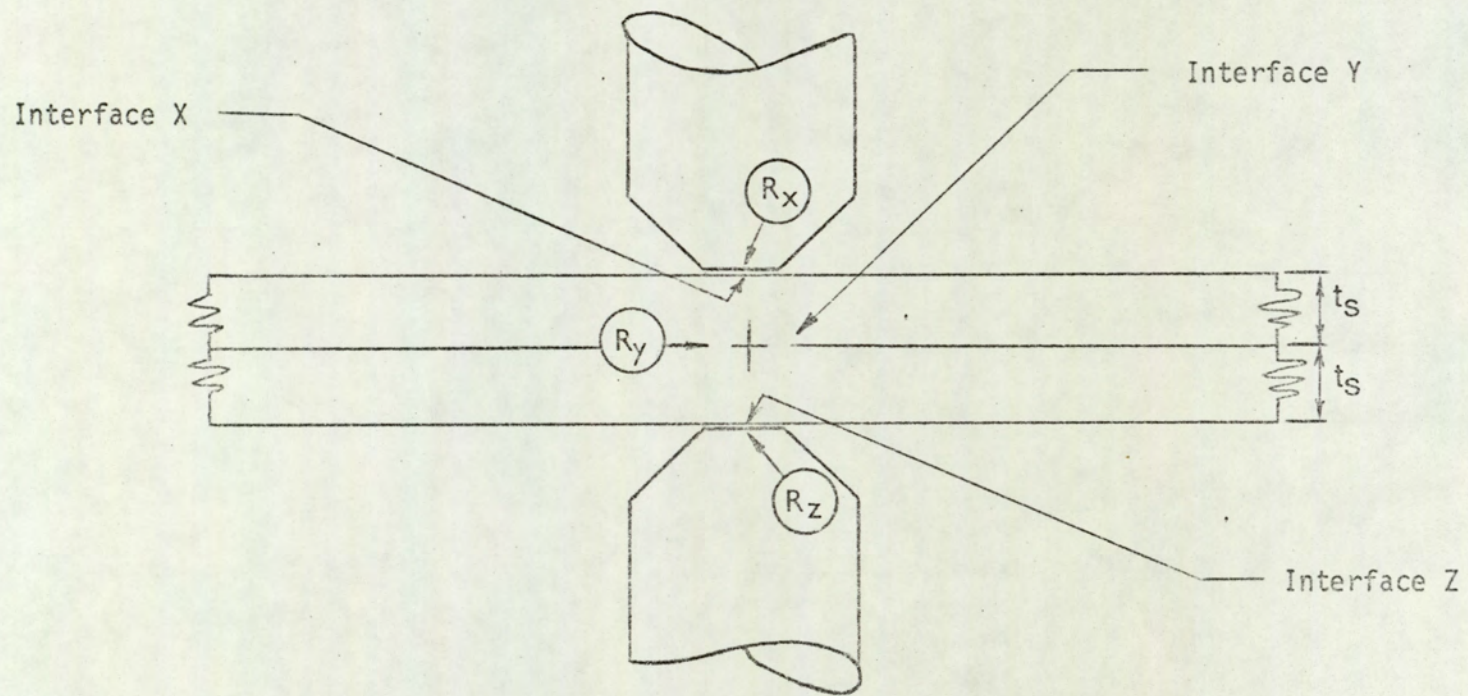
FIG. 15.2 Interfaces and Contact Resistances in the Weldment.
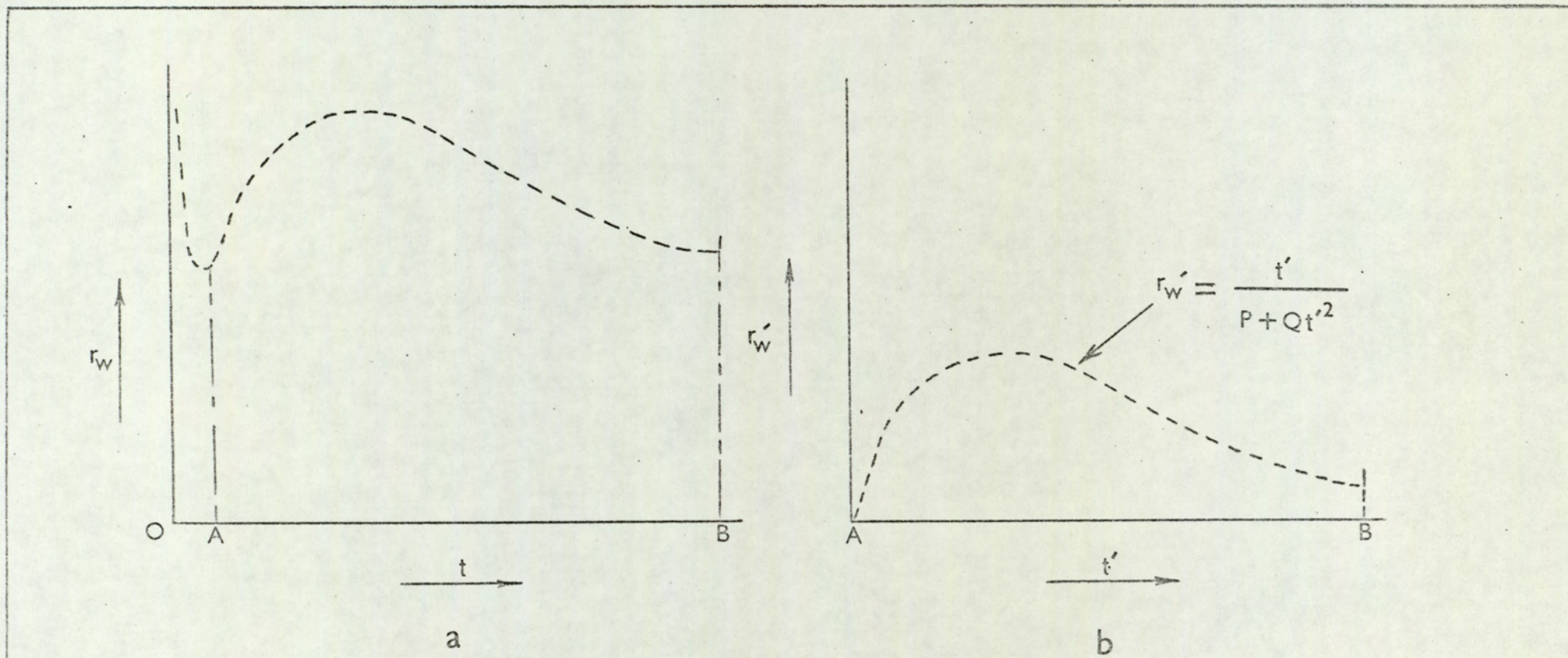
FIG. 15.3 Useful Portion of the Dynamic Resistance Characteristic for Spot Welds in Mild Steel.

(a) Full Curve; (b) Useful Portion of the Curve Redrawn.
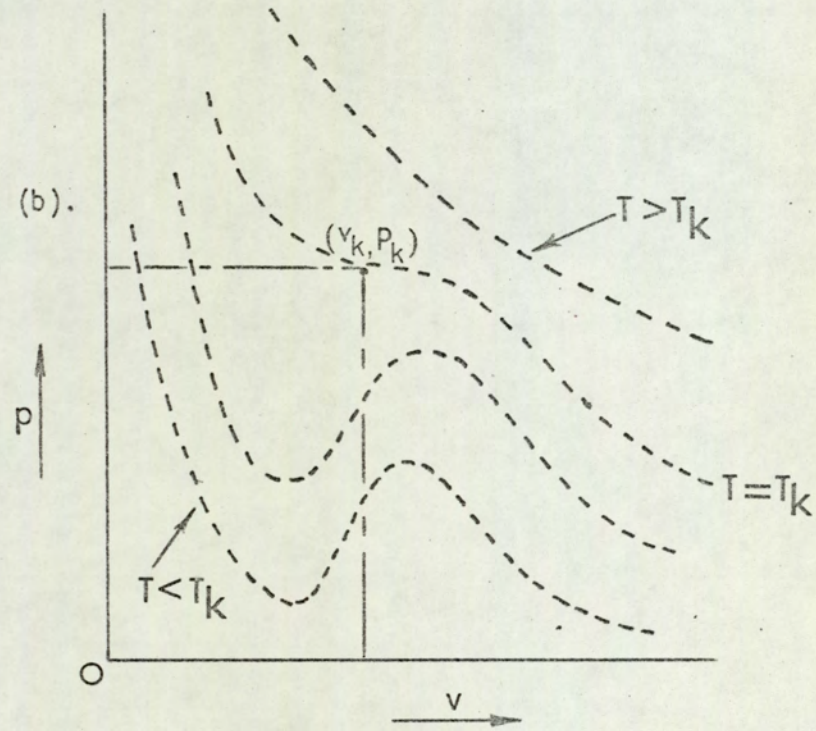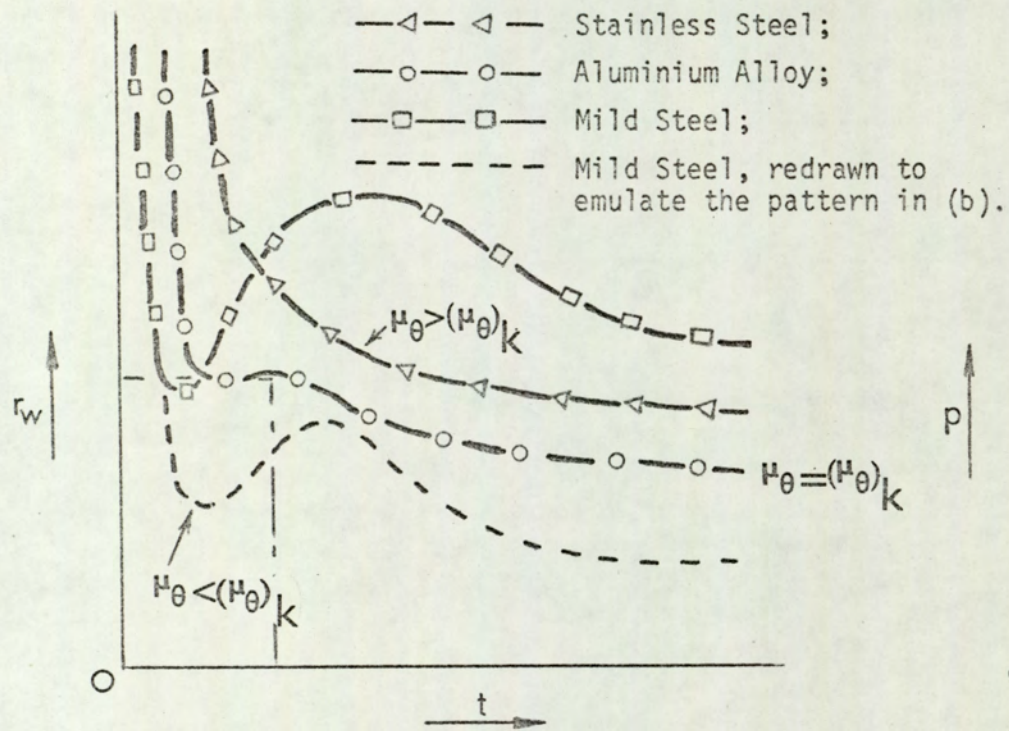
FIG. 15.4   Dynamic Resistance or r_w-t Curves for Various Metals and Alloys set against p-v Characteristics of Real Gases.

(a) r_w-t Curves for Stainless Steel, Aluminium Alloy and Mild Steel;

(b) p-v Characteristics of Real Gases.

16. GENERAL CONCLUSIONS AND SUGGESTIONS FOR FURTHER WORK

16.1 Welding Current, Weld Voltage and Dynamic Resistance as Process Parameters

The welding current is possibly the most important of all the welding variables governing the progress of nugget development, and may be considered as a process parameter of considerable significance. The concentration of Joule heat in the weldment is, however, dependent upon the current density in the regions of constricted current flow rather than the total current through the weldment. The current value registered by the current meter serves only as an indication of the maximum current used in the process, and cannot in itself be an indication of weld quality. Thus, when electrode tips of large diameter are used, the resulting high current does not produce a sound weld (see 7.3 in Part I). It has, however, been shown in Section 6 that the pattern of the current traces may reveal more about the growth of the nugget. Thus, a well-formed 'valley' in the current trace signifies a good weld; provided that the other welding variables have been properly chosen, a prominent 'valley' indicates an adequately high current (see current traces in Figure 6.3). The pattern of current variation during a weld should, therefore, be taken into account in conjunction with the peak r.m.s. current, for a more meaningful assessment of nugget growth.

There are certain similarities between the patterns of resistance and voltage variation as can be seen from the recorded traces of Figures 6.3 and 6.4. Thus a prominent 'peak' signifying a good weld appears in the voltage trace as well as in the resistance trace; again, an abrupt step in each case indicates a splash weld. The logic supporting the use of dynamic resistance as a process parameter in preference to weld

voltage can be summed up in the following:

(i) In computing dynamic resistance, both weld voltage and welding current are taken into account, and therefore dynamic resistance is more meaningful than either voltage or current taken singly as a process parameter.

(ii) Although weld voltage can be utilized as an indication of weld quality, the claims regarding its successful application in controlling weld quality on the basis of Archer's 'voltage-constraint' principle cannot be substantiated. It will be shown in 16.2 that the weld temperatures predicted by Archer's equation[6] are far in excess of experimental results supported by the classical $\psi - \theta$ theorem.

16.2 Review of Archer's Voltage Constraint Principle

The underlying theory of Archer's 'voltage-constraint' principle[6] is that "for each ultimate temperature attained by resistively heated metal, a certain voltage must appear across the metal". This also happens to be the central theme of the $\psi - \theta$ theorem outlined in Appendix 3. In its application, the voltage-constraint principle aims at constraining the weld voltage within predetermined limits,and thus claims to ensure a uniform weld quality. It is claimed that variations in supply voltage, electrode force and surface conditions of the work-piece are taken care of, when weld quality is controlled by techniques based on this principle; in addition, the voltage-constraint principle is also supposed to take into account the effects of electrode wear and shunting effect of existing welds in the work-piece. Conclusive proofs for or against such claims cannot be made available, since no commercial control system based on the voltage-constraint principle has been tried out in the present investigation. An attempt has, however, been made in the following to verify such claims by examining Archer's equation which forms the basis of the voltage-constraint principle.

'Heat balance' is defined by Archer as the physical condition when the heat generated in the weldment does not cause the temperature to rise any further, but is used up entirely as heat loss to the electrodes. It may be added in this context that, in Archer's analysis, the temperature of the weld is not specifically referred to any particular point or zone of the weld; neither does he specify the temperature scale used in the analysis. It may be assumed that the temperature at the centre of the nugget has been referred to as the 'weld temperature'; again, from the units of resistivity used in his analysis, it is apparent that the referred temperature is in the Celsius scale.

Referring to diagram (a) in Figure 16.1, Archer's equation relating weld voltage and temperature at the sheet-to-sheet interface can be written in the form,

$$T_u - T_a = 3.5 \times 10^4 . V_w^2 \tag{16.1}$$

where T_u = ultimate temperature at the sheet-to-sheet interface
          at thermal balance,

         T_a = ambient temperature,

and V_w = r.m.s. value* of weld voltage.

Since $T_u \gg T_a$, equation (16.1) can be written as

$$T_u = 3.5 \times 10^4 . V_w^2 \tag{16.2}$$

Again referring to diagram (b) in Figure 16.1, the relationship between

---

* R.M.S. value in the case of alternating current.

contact voltage* and contact temperature* may be given by

$$T_c = 3200. V_c.$$ (16.3),

where T_c = maximum temperature at the contact

expressed in the kelvin scale,

and V_c = r.m.s. value of the contact voltage.

The validity of equation (16.3) has been verified for several pure metals. Experimental results due to Holm[24] show that, in contacts of pure iron, melting occurs at V_c = 0.6 V. Substituting V_c = 0.6 V in equation (16.3) T_c becomes 1920 K.

Again, assuming that $V_c \simeq V_w$ and substituting V_w = 0.6 V, equation (16.2) yields,

$$T_u = 3.5 \times 10^4 \times (0.6)^2 = 12600^o C.$$

In the kelvin scale T_u is 12873 K. Thus, for the same voltage drop across the contact, the temperature at the centre of the nugget on the basis of the ψ - θ theorem is only 1920 K, whereas that evaluated by Archer's equation is nearly 13000 K. The melting temperature of pure iron being 1810 K ($1537^o C$), the former value is more realistic and is in line with the results of Bentley et al.[33]; a temperature of the order of 13000 K, on the other hand, is far in excess of any realistic estimation in the present context. Therefore, although some correlation exists between weld quality and weld voltage, Archer's equation for the 'voltage-constraint' principle is not tenable in its present form.

---

* See Appendix 3

16.3 Dynamic Resistance and Thermal Condition of the Weld as Process Parameters in Monitoring Weld Quality

(a) Monitoring by assessment of thermal condition is a first-order technique

As explained earlier, the changes in the thermal condition of the weldment due to Joule heating are primary or first-order changes. By contrast, the variation in electrical resistance and thermal expansion are second-order effects brought about by thermal changes in the metal held between the electrode tips. Therefore, monitoring techniques based on assessment of thermal condition of the weld can be classified as first-order techniques. The monitoring techniques dependent upon the second-order changes may then be termed second-order techniques, and are comparatively less effective in indicating the more fundamental changes which can be correlated to nugget formation. The terms first-order and second-order are used in a sense similar to that in defining the 'order' of differential equations in mathematics.

(b) Thermal condition of the weld is preferred as a process parameter when spot welding stainless steel and aluminium alloys

Dynamic resistance characteristics of stainless steel and certain aluminium alloys do not show[4,22] any consistent pattern which can be related to the progress of nugget formation. Thus, the thermal condition of the weld may be a more reliable process parameter when welding stainless steel and some aluminium alloys.

16.4 Comparison between Direct-Incidence and Remote-Transmission Modes of Detection

Various techniques of detecting thermal radiation from the weld, in the direct-incidence mode as well as in the remote-transmission mode, have been discussed earlier in Part II. The following comments are

based on a comparison of these two modes of detection.

(a) When carefully laid out, the light-guide or the output leads from the radiation detector cannot interfere with the working space of the machine. In this respect, therefore, the two modes of detection offer almost equal advantages.

(b) The radiation detector in the direct-incidence mode and the light-guide in the remote-transmission mode are both subjected to similar mechanical shocks and vibrations when the welding machine is in operation. Again, repair and maintenance of the detection systems in the two modes may need almost equal care and attention. However, the ease with which the damaged end of a light-guide can be repolished and the light-guide refitted seems to offer certain advantages in favour of the remote-transmission mode.

(c) The electronic signal-processing system may be less demanding in respect of spurious pick-ups when detecting in the remote-transmission mode because of its remoteness from the machine. Provided that the receiving end of the light-guide is electrically insulated from the machine body, no conducted interference can affect the performance of the detection system.

(d) The available space inside the electrode or in the hollow of the electrode holder restricts the size of the radiation detectors which can be inserted within the electrode, in the direct-incidence mode. Such restrictions, however, do not exist in the case of the remote-transmission mode.

(e) The transmission loss of commercially available fibre-optic components increases very sharply beyond 1.3 μm; the passband of useful radiation is therefore restricted in the remote-transmission mode. No such restriction in respect of the useful waveband exists in the direct-incidence mode.

16.5 <u>Application of Bichromatic Response Ratio Technique in Monitoring Weld Quality</u>

The spectral emittance ε_λ of a thermal source varies[54,55] considerably with the material properties and surface finish of the source; ε_λ also varies[54] with temperature. Therefore, any variation in the surface conditions of the work-piece will alter the radiant emission from the weld surface; also, any relationship between monochromatic radiant intensity and temperature will be subject to variation as ε_λ changes with temperature. Since the radiation detection systems described in Sections 12 and 13 respond to monochromatic radiant intensity, the monitored indication will be subject to the above inaccuracies. To overcome such inaccuracies, it is suggested that the thermal condition of the weld be related to the bichromatic intensity ratio[56]. The design of a weld quality monitor, responding to bichromatic intensity ratio and operating in the remote-transmission mode, is outlined in the following.

It may be seen from Figure 16.2 that the total radiation received by the Y-shaped light-guide is split up and transmitted along the two branches; two identical silicon detectors are used to receive the radiation transmitted by each branch of the light-guide. The spectral isolation of two narrow wavebands centred around λ_1 and λ_2 is achieved by means of a suitable optical filter in each case. A silicon P-I-N photodiode can be used in conjunction with a current-to-voltage transduction stage, for each branch of the light-guide.

Referring to Appendix 4, the bichromatic response ratio $\frac{R_2}{R_1}$ is proportional to the ratio $\frac{I_2}{I_1}$, where I_1 and I_2 represent photocurrent output corresponding to filtered wavebands centred around λ_1 and λ_2; in this instance, it will be assumed that $\lambda_1 > \lambda_2$. Following the treatment

in Section 11, it may be shown that

$$\frac{R_2}{R_1} = \frac{W_2}{W_1} = \frac{b_2 \int_{\lambda_2 - L/2}^{\lambda_2 + L/2} W(\lambda,T)d\lambda}{b_1 \int_{\lambda_1 - L/2}^{\lambda_1 + L/2} W(\lambda,T)d\lambda} \qquad (16.4),$$

where the optical passbands centred around λ_1 and λ_2 are of equal width L, and b_1 and b_2 are constants defined in the same way as k_m in equation (11.12). It has been shown by Herne[57] that equation (16.4) can be written in the form,

$$\frac{R_2}{R_1} = \frac{b_2}{b_1} \cdot f(\lambda_1, \lambda_2, L, T) \qquad (16.5),$$

and that when λ_1, λ_2 and L are suitably selected, the function $f(\lambda_1, \lambda_2, L, T)$ varies almost linearly with temperature over a wide temperature range.

In bichromatic response ratio measurement, the wavelength λ_1 and λ_2 are chosen in accordance with the desired temperature range of operation; the width L of the passband can vary from 0.01 μm or 100^oA to about 0.5 μm. With a very narrow bandwidth, however, the detectable radiant power is also very small, and may present some problems in detection; again, the interference filters usually required for isolating very narrow passbands are more expensive in comparison to ordinary filter glass. Thus, use of larger values of bandwidth L is preferred.

Herne[57] has shown that with $\lambda_1 = 0.8$μm, $\lambda_2 = 0.65$μm, and L = 0.3μm, the function $f(\lambda_1, \lambda_2, L, T)$ is linear over a temperature range between 1123K (850^oC) and 2073 K(1800^oC). Hence the proposed monitoring system

illustrated in the block diagram of Figure 16.2 can be designed with silicon detectors and colour filter glasses and may prove to be commercially feasible.

16.6 Choice between In-process Monitoring and Closed-loop Quality Control

The simple in-process monitoring technique outlined in 8.3 can only indicate whether a weld of acceptable quality has been produced or not; no corrective action can, however, be taken by the welding machine and the associated electronic controls to counteract any deviation from the limits of acceptable quality. In this respect, the complete system comprising of the machine, its electronic control equipment and the weld-quality monitor behaves as an open-loop system. In terms of control theory, a closed-loop quality control system can be defined as a self-adjusting system which ensures continued production of satisfactory welds without the operator's intervention. Ideally, in a closed-loop system, any departure from the agreed quality will be detected, and the necessary corrective action will be taken by the system itself during the process of operation; such corrective actions may mean automatic adjustment of one or more welding variables.

Realization of a closed-loop system for controlling weld quality requires that the supply voltage and air pressure be maintained at set values. It is also required that a regular maintenance schedule for the electrodes be undertaken, and, to ensure uniformity of surface conditions of the various batches of material, a systematic inspection of the work-piece be introduced. Provided that the measures cited above are undertaken, automatic control of weld quality, by detecting either the pattern of dynamic resistance variation or the pattern of thermal

cycle of the weld surface, can be a practical proposition. At present, however, opinions are divided amongst the users as well as manufacturers of welding machines regarding the desirability of a closed-loop system. Thus, although a closed-loop system may seem to be the ideal solution to the problem of quality control in spot welding, the open-loop operation of a welding machine in conjunction with a simple in-process monitoring system is deemed to be the best compromise at the present moment.

16.7 Suggestions for Further Work

16.7.1. Further Work in Developing a Weld Quality Monitor based on Dynamic Resistance Measurement

It is suggested that an electronic instrumentation system incorporating the modifications proposed in 8.1 be developed. The referred modifications will enable the user to record dynamic resistance characteristics with greater precision and accuracy. Thus, further investigation can be carried out into the dynamic resistance characteristics of various other metals and alloys.

16.7.2. Further Work in Monitoring by Detection of Thermal Radiation from the Weld

(a) Radiation Detection using a Phase-sensitive Detector

The detection of very weak radiation signals from the weld is difficult because of the presence of noise and spurious pick-ups from the machine. This is demonstrated by the pick-ups on the recorded traces of M.R.I. at very low levels of radiant intensity. In order to eliminate such extraneous signals, it is suggested that a lock-in amplifier or a phase-sensitive detector[44] be used to detect low-level

monochromatic radiation. With a phase-sensitive detector, it is possible to detect signals coherent in frequency and phase with an a.c. reference signal, rejecting essentially all other frequency components and even noise many times larger than the signal.

(b) Development of the Bichromatic Response Ratio Technique

The method of correlating thermal radiation from the weld surface to the bichromatic response ratio and its subsequent use in monitoring weld quality has been outlined in 16.5. It is suggested that a weld-quality monitor be developed along the proposed outlines and its performance evaluated for various metals and alloys.

(c) Use of Optical Windows in conjunction with Electrode Tips made of other Metals and Alloys

Experience in the use of electrodes with aperture has shown that the aperture tends to close up when spot welds are executed at a high repetition rate. Moreover, the electrode tips cannot be adequately cooled by conventional means because of the aperture, thus enhancing the process of tip deformation and eventual closure of the aperture. To facilitate efficient cooling of the electrodes and to prevent early closure of the aperture, further research can be conducted along the outlines suggested below.

(i) Use of Optical Windows.

The possibility of incorporating an optical window on the underside of the aperture may be investigated; a water-tight optical window will allow more efficient cooling of the electrode. Thus, a small slab of suitable optical material may be cemented on to the underside of the aperture. Alternatively, the piece of optical material may be mounted at one end of a small metal cylinder, which in turn may be screwed into position within the electrode. A fine wire mesh may also be positioned above the optical window to prevent any damage of the optical system

through accidental splash of hot metal during welding.

(ii) Use of other Metals and Alloys for Electrode Tips.

The ideal electrode material should have high electrical conduct-
ivity, and should be able to withstand severe mechanical stress at
elevated temperatures. The electrical and mechanical properties of
pure metals are, however, dependent on their atomic structure, and
good conductors of electricity also offer less resistance to mechanical
deformation. Hard metals, such as tungsten and molybdenum, have lower
electrical conductivity in comparison with copper, but offer more
resistance to mechanical deformation at high temperatures. It is,
therefore, suggested that research work be undertaken to investigate
the possible use of metals such as tungsten and molybdenum in
designing[58] electrode tips with aperture. Thus, electrode tips
machined from tungsten or molybdenum may be fitted on the main body
of the electrode.

It seems, therefore, that the use of optical windows in con-
junction with tungsten (or molybdenum) electrode tips may ensure more
efficient cooling and a longer life for the electrode.

(d) Research into Radiation Detection Techniques using Plain
Electrodes without any Aperture

Although the introduction of a minute aperture at the electrode
tip enables one to detect thermal radiation from the centre of the
weld surface, the main criticism of the inclusion of an aperture at
the tip stems from the need for modifications in the normal cooling
system for the electrode and the possibility of eventual closure of the
aperture. It is, therefore, suggested that research work be under-
taken to investigate alternative methods of detecting thermal radiation
from the weld, when using plain electrodes without any aperture. The

techniques suggested below are based on bichromatic response ratio measurement, and since plain electrodes are used, the conventional method of cooling the electrodes can be retained.

(i) Detecting Thermal Radiation from the Edge of the Weld.

Thermal radiation from the edge of the spot weld can be received upon the end faces of a cluster of light-guides suitably located around the bottom electrode. The transmitted radiation is incident upon two groups of radiation detectors, each group responding to a specified waveband. The photocurrent from each detector can be converted into a voltage, the resultant output of each group of detectors being obtained by summing the voltages thus derived. The bichromatic response ratio $\frac{R_2}{R_1}$, in this instance, will be proportional to the ratio of resultant photocurrents of the two groups of detectors. With λ_1 = 0.8 μm, λ_2 = 0.65 μm, and L = 0.3 μm, a detection system can be designed employing inexpensive silicon detectors in conjunction with commercial light-guides and coloured glass optical filters.

(ii) Detecting Thermal Radiation from an Annular Zone surrounding the Weld.

Since the temperature of the weldment away from the weld zone is very much lower, radiation emitted from an annular zone surrounding the weld is mainly in the infra-red. In the absence of suitable fibre-optic components transmitting in the infra-region beyond 1.3 μm, the radiation in this instance must be received directly on detectors responding to infra-red. Thus, two groups of radiation detectors may be located around the bottom electrode, the radiant power being received at normal incidence in each case. With suitable optical filters, wavebands centred around λ_1 and λ_2 can be isolated, and the principle of bichromatic response ratio measurement can be applied.

Theoretical calculations due to Herne[57] on bichromatic response ratio measurement suggest that, with $\lambda_1 = 2.5 \mu m$, $\lambda_2 = 1.5 \mu m$ and $L = 0.5 \mu m$, a reasonably linear relationship exists between bichromatic response ratio $\frac{R_2}{R_1}$ and the temperature of the radiating source, over a temperature range between 673 K (400^oC) and 1073 K (800^oC). Therefore, provided that the annular zone is not too far from the weld, commercial lead sulphide detectors can be used for this investigation.

16.7.3 Further Theoretical Work in Spot Welding

(a) Measurement of Static Resistance of Weldment and
    Verification of the Equation for Static Resistance

Although an equation for static resistance of the weldment has been developed in Section 15, experimental determination of static resistance has not been attempted. Reliable methods of measuring static resistance should, therefore, be investigated, so that equation (15.13) can be verified.

Standard techniques[21,24] of measuring static resistance, where the work-piece conducts current of the order of 10A, may not produce consistent and accurate results; current values of this order of magnitude, although small in comparison with the current used in spot welding, cause appreciable Joule heating of the microcontacts during measurement. Joule heating of the microcontacts can be minimized by using current values of the order of a few millamperes; measurement of static voltage drop across the work-piece can be made using a precision nanovolt preamplifier in conjunction with a digital voltmeter, or by applying the principle of phase-sensitive detection.

(b) <u>Determination of the Form of Equation of the Resistance -
Time curve for Mild Steel</u>

Further analysis of the experimental resistance-time curves for
mild steel may be undertaken so that numerical values of the coefficients
P and Q in equation (15.14) can be determined; the form of equation
relating dynamic resistance to weld time can thus be found by further
quantitative analysis.

(c) <u>Further Work on the General Form of the Mathematical Function
describing the Resistance-Time Curves for various Metals and
Alloys</u>.

The probable form of a mathematical equation for the family of
resistance-time curves for various metals and alloys has been suggested
in Section 15. It is, however, felt that further experimental and
analytical work be carried out in this respect. Thus, resistance-time
curves for various metals and alloys including stainless steel and
aluminium alloys can be determined experimentally, so that equation
(15.16) can be verified and a plausible explanation found for the
difference in the characteristic shape of the resistance-time curves for
various metals.
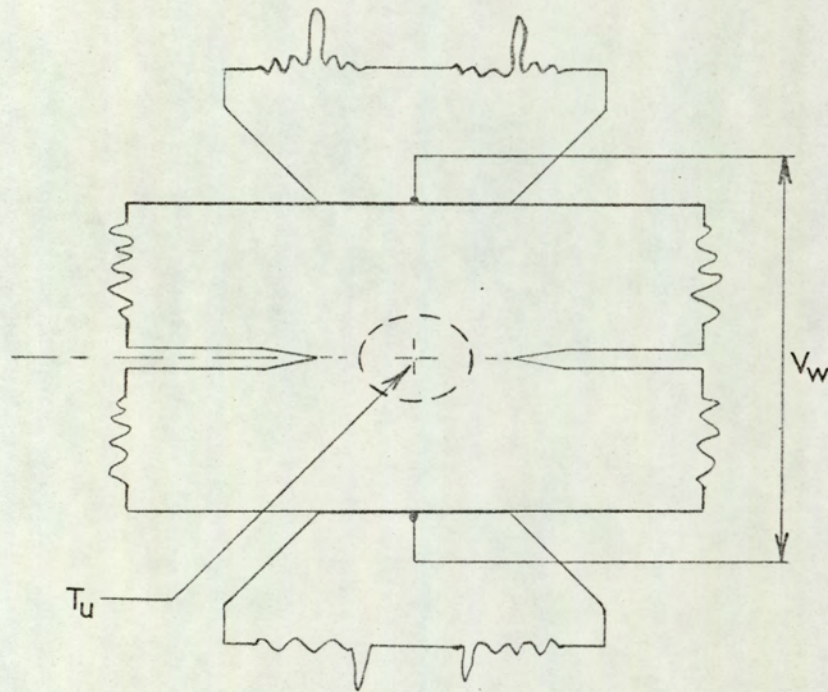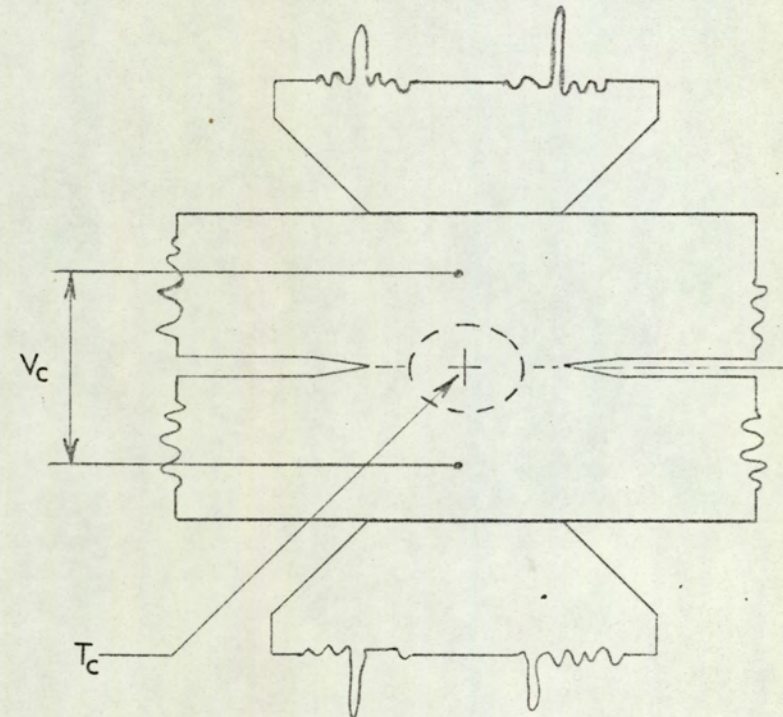
FIG. 16.1. Relationship between Voltage and Temperature in Spot Welds.

(a) Voltage and Temperature as in Archer's Equation; (b) Voltage and Temperature as in the ψ-θ Theorem.

λ_1 & λ_2 – Monochromatic Waveband

F_1 & F_2 – Optical Filter

S_1 & S_2 – Detector

A_1 & A_2 – Current-to-voltage Transduction Stage

B_1 & B_2 – Tuned Amplifier

C_1 & C_2 – Full-or half-wave Rectifier.

D – Divider

E – Low-pass Filter

Light-proof enclosure

Y-shaped Light-guide

Monitor Output
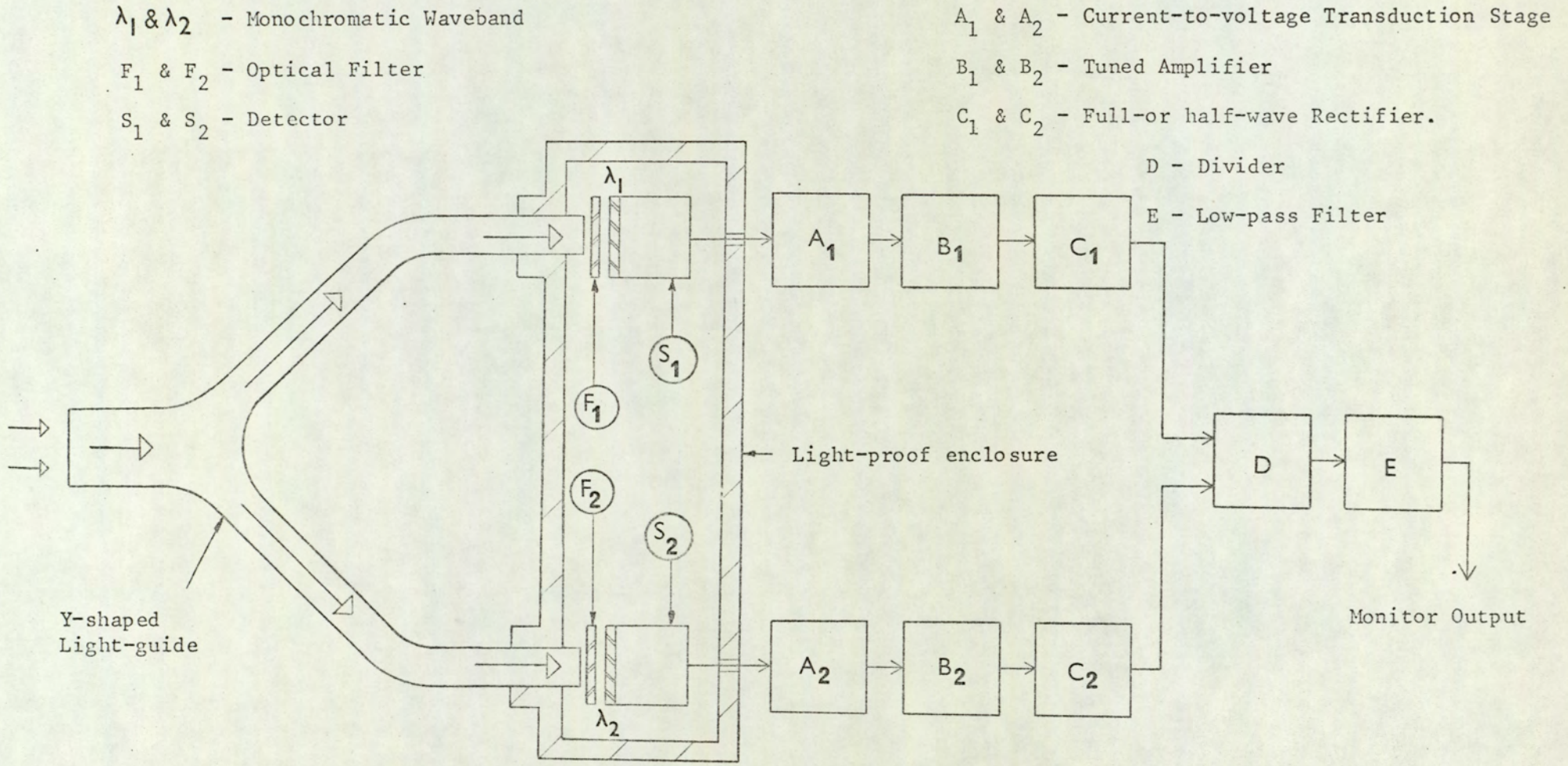
FIG. 16.2 Block Diagram of Proposed Monitoring System based on Bichromatic Response Ratio Measurement.

ACKNOWLEDGEMENTS

APPENDIX 1

WIEDEMANN-FRANZ LAW AND LORENZ NUMBER

On the basis of free-electron theory of metals, the electrical conductivity σ and thermal conductivity K can be expressed as a ratio in the form

$$\frac{K}{\sigma} = \frac{\pi^2}{3} \cdot \left(\frac{k}{e}\right)^2 \cdot T \tag{A1.1},$$

where k = Boltzmann's constant.

e = electronic charge,

and T = temperature of the electrons.

Equation (A1.1) is often referred to as the Wiedemann-Franz law. According to the Wiedemann-Franz law the ratio $\frac{K}{\sigma}$ is proportional to the absolute temperature for a given metal, and should be the same for all metals at a given temperature. This is evident when equation (A1.1) is rearranged as

$$\frac{K}{\sigma T} = L \tag{A1.2},$$

where $L = \frac{\pi^2}{3} \cdot \left(\frac{k}{e}\right)^2 \cdot$ (A1.3).

L is known as the Lorenz number, Lorenz function or Lorenz ratio, and may be calculated from equation (A1.3). Thus, substituting for π, k (Boltzmann's constant) and e (electronic charge), the numerical value of L is given by 2.45×10^{-8} watt.ohm. $(\text{kelvin})^{-2}$. Since dimensionally watt. ohm = $(\text{volt})^2$, L may also be written as

$$L = 2.45 \times 10^{-8} \left(\frac{V}{K}\right)^2 \tag{A1.4}.$$

APPENDIX 2

CONSTRICTION RESISTANCE OF A CIRCULAR AREA OF CONTACT

Equation of Constriction Resistance

Derivation of constriction resistance from first principles is rigorous, and the references cited by Holm[24] and Jones[49] should be consulted for such details. In this instance, only the resultant equation of constriction resistance for a circular conducting spot will be given. Thus, when two plane surfaces make contact over a circular area of radius a, the constriction resistance R' for one contact member is given by

$$R' = \frac{\rho}{4a} \qquad (A2.1),$$

where ρ = resistivity of the material in the particular contact member.

If both contact members are made of the same material of resistivity ρ , the total constriction resistance including both members is given by

$$R = 2R' = \frac{\rho}{2a} \qquad (A2.2).$$

Equation (A2.2) has been found[24] to be in agreement with experimental results within error limits of observation of ± 1.5%. In deriving the equations for constriction resistance, it has been assumed that ρ is constant; therefore, the expressions for constriction resistance are valid for small currents, such that any temperature gradient in the vicinity of the constriction may be neglected. The main part of the resistance is concentrated in the neighbourhood of the elementary contact area. In an actual contact there may be more than one such elementary area. In such cases mutual influence of the individual areas may in general be neglected and the complete contact resistance may then be regarded as the parallel connection of a number of individual resistances.

Lines of Current Flow and Equipotential Surfaces of a Current
Constriction

Figure A2.1 shows the system of equipotential surfaces and lines
of current flow when both members are of the same metal, and A_c re-
presents a single circular conducting spot of radius a. In practice,
the constriction may be regarded to be limited in the bulk of the
members by certain surfaces, as for example, A_e in Figure A2.1. Those
regions within the contact members C_1 and C_2, where lines of current
flow noticeably deviate from the straight course, are called constriction
regions or simply constrictions.
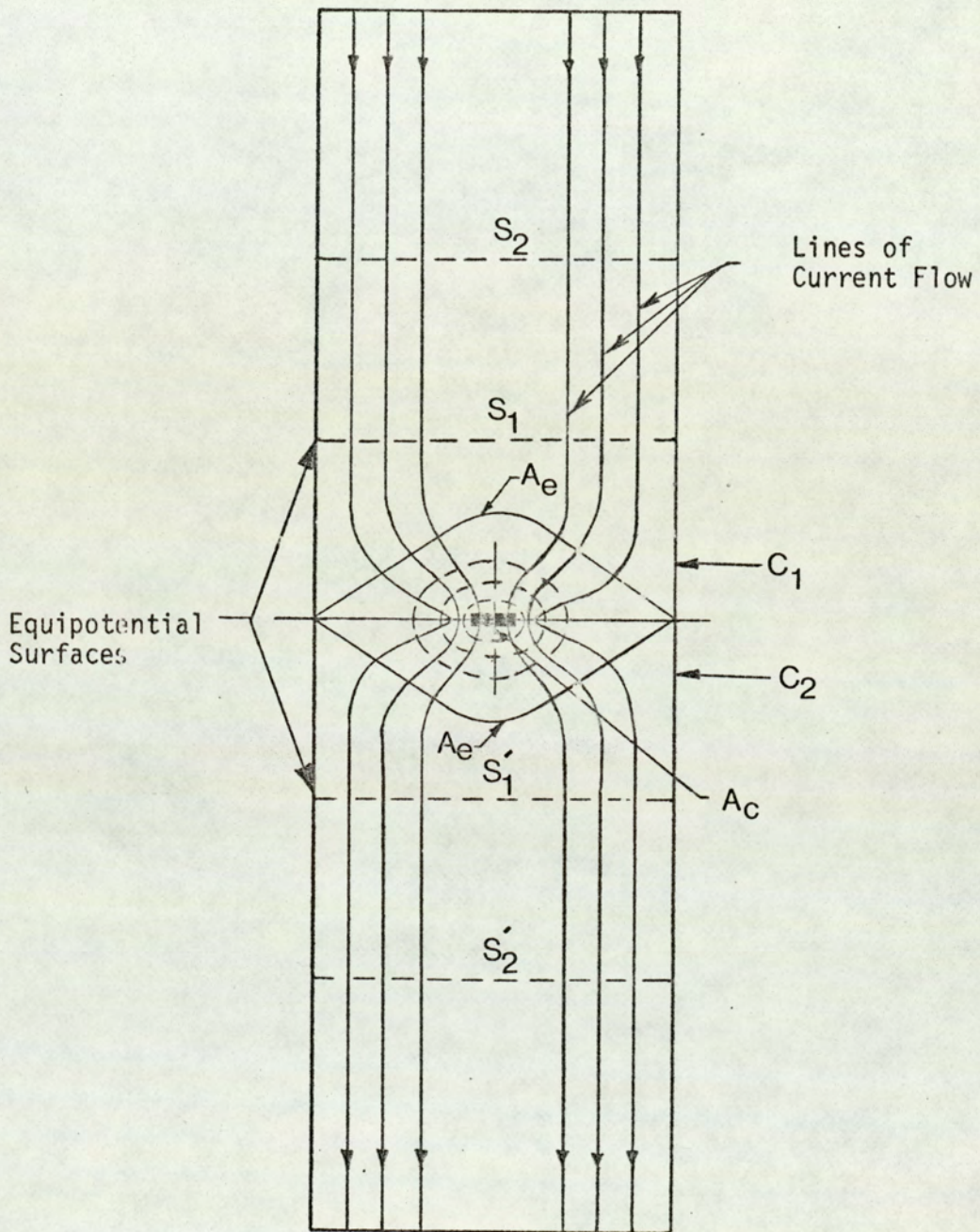
FIG. A2.1. Lines of Current Flow and Equipotential
Surfaces of a Current Constriction.

APPENDIX 3

THE $\psi - \theta$ THEOREM

General $\psi - \theta$ Relation for a Solid Conductor

Thermal and electrical conduction through metallic conductors have many features in common. Heat energy flows by virtue of temperature difference which corresponds to potential difference in the case of electric current. The general $\psi - \theta$ relation provides an equation connecting temperature difference (denoted by θ) and potential difference (denoted by ψ)in the case of an electrically heated metallic conductor, assuming that the conductor is bounded by a surface perfectly impervious to both heat and electricity. A rigorous method of derivation of the general $\psi - \theta$ relation is given by Greenwood and Williamson.[28] The $\psi - \theta$ relation has also been derived by Holm[24] and Jones[49], the former giving a slightly different method of derivation.

The general $\psi - \theta$ equation, for a solid one-piece conductor, relating electrical potential ψ to the maximum temperature θ_m can be written as

$$\psi^2 = 2 \int_{\theta}^{\theta_m} \frac{K}{\sigma} \, . \, d\theta \qquad (A3.1),$$

where   K = thermal conductivity of the material,

and σ = electrical conductivity.

Equation (A3.1), often referred to as the general $\psi - \theta$ theorem, is a steady-state equation which holds only if the conditions are such that the vector flow of energy is everywhere zero. This means that there must be no flow of energy across the bounding surface of the conductor. There is no flow of electricity across this bounding surface; so the conditions of validity of the theorem require that there should also be no flow of heat across it.

The $\psi - \theta$ relation expressed in the form of equation (A3.1) needs some modification before it can be applied to any practical situation. A more useful form of the equation is derived in the following.

Figure A3.1 shows a short cylindrical conductor joining two large masses of the same metal; the conductor is electrically heated, the direction of current flow being along the vertical axis of symmetry. The potential is defined to be zero at the surface S_0 where the temperature is θ_m. S_1 and S_2 are two surfaces in the conductor at the same temperature θ_0 and at uniform potentials with respect to the surface S_0.

If the temperature is practically uniform at S_1 and S_2, the difference in the values of ψ at these surfaces is the same as the difference between ordinary electrical potentials.

Thus, if V is the total voltage measured across the surfaces S_1 and S_2 then, S_1 and S_2 may be assumed to be at $+ \frac{V}{2}$ and $- \frac{V}{2}$ respectively. From equation (A3.1),

$$\left(\pm \frac{V}{2}\right)^2 = 2 \int_{\theta_0}^{\theta_m} \frac{K}{\sigma} \, d\theta \qquad (A3.2).$$

Equation (A3.2) can also be written as

$$\frac{V^2}{8} = \int_{\theta_0}^{\theta_m} \frac{K}{\sigma} \, d\theta \qquad (A3.3).$$

Equation (A3.3) shows that the maximum temperature in an electrically heated conductor is completely determined by the potential difference across it, and by the properties of the material, provided that the conditions are such that the loss of heat from the bounding surfaces may be neglected. It may also be noted that in deriving the

ψ - θ relation, and in the relevant discussion, the thermo-electric effects have been ignored. The influence of Thomson effect has, however, been discussed by Jones.[49]

The ψ - θ Theorem for a Symmetrical Metallic Constriction

In the case of a symmetrical mono-metallic constriction formed by two contacting members, the same logic, as in the case of a single conductor, can be followed and the resultant equation relating voltage and temperature becomes

$$\frac{V_c^2}{8} = \int_{\theta_o}^{\theta_m} \frac{K}{\sigma} d\theta \qquad (A3.4),$$

where V_c = total voltage across the contact, and θ_o and θ_m are defined in the same way as in equation (A3.3). Thus θ_m, the maximum temperature, in this case occurs at the contact interface. The integral in equation (A3.4) cannot be evaluated exactly, because K and σ are not known as functions of θ over the relevant temperature range. According to the Wiedemann-Franz law (see Appendix 1), however, the ratio $\frac{K}{\sigma}$ is proportional to the absolute temperature and can be written as

$$\frac{K}{\sigma} = L\theta \qquad (A3.5),$$

where L, the Lorenz ratio, has a numerical value of $2.45 \times 10^{-8} \left(\frac{V}{K}\right)^2$

Assuming that the contact metals obey the Wiedemann-Franz law, and substituting for $\frac{K}{\sigma}$, equation (A3.4) becomes

$$\frac{V_c^2}{8} = \int_{\theta_o}^{\theta_m} L\theta.d\theta \qquad (A3.6).$$

Integrating and simplifying, equation (A3.6) can be written as

$$\frac{V_c^2}{4} = L(\theta_m^2 - \theta_o^2) \qquad (A3.7).$$

When V_c is measured in volts, and θ_o can be neglected in comparison to θ_m, then from equation (A3.7)

$$\theta_m = \frac{V_c}{2\sqrt{L}} \qquad (A3.8).$$

Substituting for L, equation (A3.8) becomes

$$\theta_m \simeq 3200. \, V_c \, K \qquad (A3.9).$$

Equation (A3.9) applies to any practical contact, provided the following conditions are satisfied.

(a) There is negligible loss of heat from the surface
     of hot constriction .

(b) Thermal conductivity K and electrical conductivity σ
     are functions of temperature only, obeying the
     Wiedemann-Franz law.

(c) The steady state is reached very quickly.
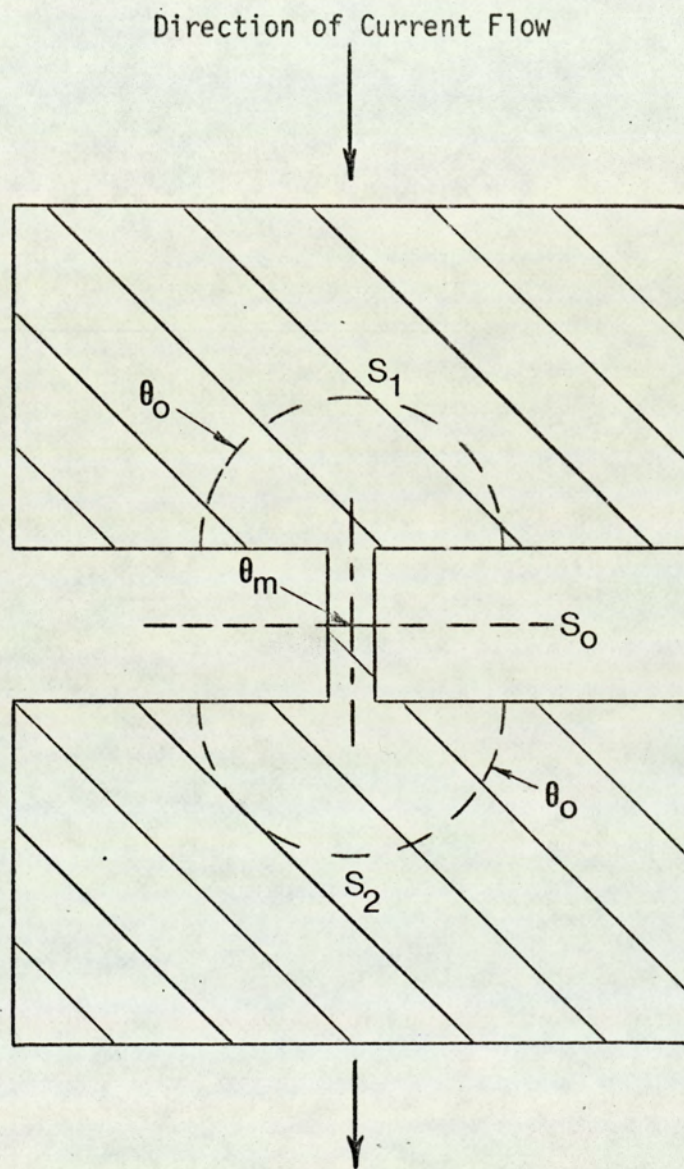
FIG. A3.1. Isothermal and Equipotential Surfaces in an
Electrically Heated Conductor.

APPENDIX 4

RADIATION LAWS AND TEMPERATURE MEASUREMENT

Planck's Radiation Law

Planck's radiation law gives the distribution of energy in the emission spectrum of a blackbody in terms of wavelength and temperature. It can be written in the form of the mathematical equation,

$$W(\lambda, T) = c_1 \cdot \lambda^{-5} \cdot \left(\exp \cdot \frac{c_2}{\lambda T} - 1\right)^{-1} \tag{A4.1},$$

where $W(\lambda, T)$, the hemispherical spectral radiant intensity is defined as the time rate of emission of radiant energy, per unit interval of wavelength centred at the wavelength λ, throughout 2π steradians, per unit area of a blackbody source at absolute temperature T.

From the definition, $W(\lambda, T)$, being the time rate of energy flow, is expressed in watts. In equation (A4.1), c_1 is known as the first radiation constant and c_2 the second radiation constant; $\exp \cdot \frac{c_2}{\lambda T}$ represents $e^{\frac{c_2}{\lambda T}}$ where e is the base of the natural logarithms, the term 'exp' being the abbreviation for 'exponential'. Numerical values of constants c_1 and c_2 are dependent on the units chosen for the wavelength and the area. Thus, when the wavelength λ is given in centimetres, area in square centimetres, and the temperature T in kelvin,

$$\text{then } c_1 = 3.7415 \times 10^{-12} \text{ W cm}^2,$$

$$\text{and } c_2 = 1.43879 \text{ cm K}$$

Expressed in SI units, $c_1 = 3.7415 \times 10^{-16} \text{ W m}^2,$

$$c_2 = 1.43879 \times 10^{-2} \text{ m K}.$$

Wien's Radiation Law

Although spectral distribution of radiant energy is most rigorously expressed by Planck's radiation law at all wavelengths and temperatures, a somewhat simpler and less accurate relationship due to Wien is given below

$$W(\lambda,T) = c_1 . \lambda^{-5} . \exp\left(\frac{-c_2}{\lambda T}\right) \qquad (A4.2),$$

where $W(\lambda,T)$ represents the hemispherical spectral radiant intensity as in equation (A4.1), and the constants c_1 and c_2 have exactly the same numerical values as before.

Wien's Displacement Law

Wien's displacement law describes the relationship between the true temperature of a blackbody and the wavelength at which maximum radiant energy occurs in its emission spectrum. Wien's displacement law states that as the temperature of a blackbody is increased, the position of maximum emission moves in the direction of shorter wavelengths in such a way that the product of the wavelength of maximum emission and the corresponding absolute temperature of the source remains constant.

In its mathematical form, Wien's displacement law can be expressed as

$$\lambda_m T = b \qquad (A4.3),$$

where λ_m = the wavelength at which maximum radiant energy occurs,

T = the absolute temperature of the source in kelvin,

and b = a constant whose numerical value depends on the unit chosen for the wavelength.

In SI units, $b = 2.8978 \times 10^{-3}$ m K.

The Stefan-Boltzmann Law

The Stefan-Boltzmann law gives the total radiant energy emitted per unit time by a blackbody as a function of its absolute temperature. The Stefan-Boltzmann law states that the total energy radiated, per unit time, per unit area of a blackbody, is proportional to the fourth power of its absolute temperature. Stated mathematically, the Stefan-Boltzmann law is

$$W = \sigma T^4 \qquad\qquad (A4.4),$$

where W = energy radiated per unit time or radiant power, from unit area of blackbody surface at absolute temperature T, including radiation of all wavelengths from 0 to ∞, throughout the solid angle 2π steradians, and σ = the Stefan-Boltzmann radiation constant. In SI units, when the area is in square metre and the temperature in kelvin, the numerical value of σ is given as $\sigma = 5.6697 \times 10^{-8}$ W m^{-2} K^{-4}.

Monochromatic Radiant Intensity and Temperature Measurement

Planck's radiation law is valid for ideal blackbody sources; for a non-blackbody or real body, however, the radiant energy emitted is less than that for a blackbody of the same temperature. Thus W(λ, T) in equation (A4.1) is the hemispherical spectral radiant intensity for an ideal blackbody; for a real body at the same temperature the hemispherical spectral radiant intensity will be given by ε_λ.W(λ,T), where ε_λ is the spectral emittance at wavelength λ.

Radiant power within a specific waveband, for a real body may be expressed as

$$E = \varepsilon_\lambda.A.W(\lambda,T)\ \delta\lambda$$

$$= \varepsilon_\lambda.A.c_1.\lambda^{-5}.(\exp\frac{c_2}{\lambda T} - 1)^{-1}\ \delta\lambda \qquad (A4.5),$$

where E = radiant energy per unit time or radiant power

in the waveband λ to $\lambda + \delta\lambda$,

ε_λ = spectral emittance, and

A = area of the source.

For a real body, if ε_λ, A, λ and $\delta\lambda$ are kept constant then E becomes a function of temperature alone. If it were possible to obtain an accurate indication of E by means of an instrument then the indication of the instrument will be dependent on the temperature of the real body.

Bichromatic Intensity Ratio and Temperature Measurement

Bichromatic or two-colour intensity ratio for a non-blackbody also gives a temperature-dependent function.

Let W_1 represent the hemispherical spectral radiant intensity at wavelength λ_1 for a non-blackbody at temperature T. Then from Wien's radiation law, W_1 becomes

$$W_1 = \varepsilon_{\lambda 1} \cdot W(\lambda_1, T) = \varepsilon_{\lambda 1} \cdot c_1 \cdot \lambda_1^{-5} \cdot \exp\left(\frac{-c_2}{\lambda_1 T}\right) \qquad (A4.6),$$

where $\varepsilon_{\lambda 1}$ = spectral emittance of the non-blackbody at wavelength λ_1. Similarly, the hemispherical spectral radiant intensity W_2 at wavelength λ_2 and temperature T will be given by,

$$W_2 = \varepsilon_{\lambda 2} \cdot W(\lambda_2, T) = \varepsilon_{\lambda 2} \cdot c_1 \cdot \lambda_2^{-5} \cdot \exp\left(\frac{-c_2}{\lambda_2 T}\right) \qquad (A4.7),$$

where $\varepsilon_{\lambda 2}$ = spectral emittance at wavelength λ_2.

From equations (A4.6) and (A4.7)

$$\frac{W_2}{W_1} = \frac{\varepsilon_{\lambda 2}}{\varepsilon_{\lambda 1}} \cdot \left(\frac{\lambda_2}{\lambda_1}\right)^{-5} \cdot \exp\left[\frac{c_2}{T}\left(\frac{1}{\lambda_1} - \frac{1}{\lambda_2}\right)\right] \qquad (A4.8).$$

If the wavelengths λ_1 and λ_2 are so chosen that $\frac{\varepsilon_{\lambda 2}}{\varepsilon_{\lambda 1}}$ remains constant over the desired temperature range, then equation (A4.8) can be written as

$$\frac{W_2}{W_1} = K_1 \cdot K_2 \cdot \exp\left(\frac{K_3}{T}\right) \tag{A4.9},$$

where the constants K_1, K_2 and K_3 are defined such that,

$$K_1 = \frac{\varepsilon_{\lambda 2}}{\varepsilon_{\lambda 1}} \tag{A4.10},$$

$$K_2 = \left(\frac{\lambda_2}{\lambda_1}\right)^{-5} \tag{A4.11},$$

$$K_3 = c_2\left(\frac{1}{\lambda_1} - \frac{1}{\lambda_2}\right) \tag{A4.12}.$$

The ratio $\frac{W_2}{W_1}$ is defined as the bichromatic or two-colour intensity ratio, and from equation (A4.9) it is seen to be a function of temperature. An instrument can be designed such that its response indicates the ratio $\frac{W_2}{W_1}$, and the method of temperature measurement based on this principle is known as the bichromatic intensity ratio method. Pyrometers designed to operate on this principle are known as bichromatic pyrometers.

For an ideal graybody, the constant K_1 in equation (A4.10) equals unity, since from definition of graybody $\varepsilon_{\lambda 1} = \varepsilon_{\lambda 2}$. In practical situations, however, an ideal graybody having the same spectral emittance at all wavelengths and temperatures is rarely encountered. Accordingly, equation (A4.9) is applicable to non-ideal graybodies with reduced accuracy.

Blackbody Radiant Intensity within a Finite Wavelength Interval

The hemispherical spectral radiant intensity $W_{o-\lambda}$, of a blackbody at temperature T, within the wavelength interval between 0 and λ, can be expressed as

$$W_{o-\lambda} = F . \sigma T^4 \tag{A4.13},$$

where σ = Stefan-Boltzmann radiation constant,

and

$$F = \frac{15}{\pi^4} \int_{\frac{c_2}{\lambda T}}^{\infty} \left(\frac{c_2}{\lambda T}\right)^3 . \left(\exp \frac{c_2}{\lambda T} - 1\right)^{-1} d\left(\frac{c_2}{\lambda T}\right). \tag{A4.14}.$$

F can be calculated for various values of the product λT, in accordance with equation (A4.14). Therefore, in the wavelength interval defined between the limits λ_a and λ_b, the hemispherical band radiant intensity can be written as

$$W_{(\lambda_a - \lambda_b)} = \int_{\lambda_a}^{\lambda_b} c_1 . \lambda^{-5} . \left(\exp \frac{c_2}{\lambda T} - 1\right)^{-1} d\lambda$$

$$= (F_b - F_a) . \sigma T^4 \tag{A4.15},$$

where the fractions F_a and F_b denote the function F corresponding to the products $\lambda_a . T$ and $\lambda_b . T$ respectively. Values of F computed for various values of λT can be found in the tables compiled by Harrison[54].

APPENDIX 5

PHOTODETECTORS, LIGHT-GUIDE, AND OPTICAL FILTER

I.   Photodetectors

Photovoltaic Cell MS9BE

Ferranti type MS9BE photovoltaic cell, when operated without any
bias behaves like a current generator whose output current is proportional
to the intensity of incident radiation. For loads below the optimum, the
short-circuit current increases linearly with increasing radiant intensity.
In pulse operation, rise and fall times can be less than 1 µs; peak
spectral response occurs around 0.85 µm.

Silicon P-I-N Photodiode MD2

Monsanto type MD2 P-I-N photodiode has a maximum dark current of
about 10nA with a reverse voltage of 20 V; its responsivity corresponding
to 0.9 µm radiation is about 0.68 µA per µW of incident radiant power;
peak spectral response time may be 3 ns.

Integrating Light Detector - OPT1

The device OPT1 is called an 'integrating light detector' by its
manufacturers*, and is designed as a combination of silicon planar
photodiodes and metal-oxide-silicon or MOS transistors fabricated on
a single chip.

Due to its virtually infinite input impedance, an MOS transistor
can be used to examine the state of electrical charge on a capacitor
without affecting the charge, and this facility of MOS construction is
made use of in OPT1. The effects of dark current and temperature
variations are reduced in this instance by using two identical photo-

---

* The Plessey Company Limited.

diodes, one of which is shielded from the incident radiation. The amplitude of the output sawtooth waveform, when the device is operated in the constant frequency mode,[43] is proportional to the intensity of incident radiation. By using a low pulse repitition frequency, this device permits detection beyond the limits of resolution of the photo-detectors mentioned earlier.

Infra-red Detector type 139-1CPY
_____

Mullard developmental type 139-1CPY is a lead sulphide photoconductive element, and is prepared by chemical deposition. It incorporates a germanium filter to restrict the spectral response, such that radiation of wavelengths below 1.5 μm is cut off. Peak spectral response with 139-1CPY occurs at about 2 μm; maximum time constant of the device is 400 μs. Its typical D_λ^* (2 μm, 800,1) value is 2×10^{10} cm $(Hz)^{\frac{1}{2}}$ W^{-1}. Typical dark resistance is 1 MΩ; when irradiated, the resistance value may fall to about 200 KΩ.

II. Light-guides or Fibre Optic Components
_____

General Features of Fibrox Light-guide
_____

The Fibrox§ light-guide is a multitude of optical fibres packed in a bundle. It is flexible and is usually designed with a metal ferrule at each end; an outer sheathing of P.V.C. provides protection against mechanical damage. The two ends of a light-guide are polished to ensure maximum transmission of radiation, the polished ends being referred to as 'end faces' of a light-guide. The cross-sectional area of the fibre bundle, measured at either end of a light-guide, is known as the area of the light-guide.

---

§ Fibrox is the trade name of a certain type of light-guides manufactured by Rank Taylor Hobson.

When a light-guide is used to transmit radiation from one point to another, the end receiving radiation from the source is often referred to as the 'receiving' end; the other end is then referred to as the 'transmitting' end of the light-guide.

Spectral Transmission in Light-guide

The spectral transmission characteristics of a light-guide are dependent on the optical glass used in the manufacture of the optical fibres. The Fibrox light-guide has a relatively high transmission factor for wavelengths between 0.5µm and 0.9µm; transmission above 1.3 µm is, however, drastically reduced.

III Optical Filter type RG715

Schott* RG715 colour filter glass has a maximum transmittance of 99% around 0.76 µm, the wavelength corresponding to 50% transmittance occurring at about 0.711 µm for a 2 mm thick specimen; in the long-wave region transmittance can be as high as 99% up to 1.8 µm. Thus, the colour filter glass RG 715 can be used for selective transmission in the red end of the visible spectrum, and may be referred to as a red glass filter.

---

* Schott refers to Jena $\underline{er}$ Glaswerk Schott and Gen., Mainz, West Germany.

REFERENCES

1. Hess, W.F. and Ringer, R.L., Welding Journal, 1939, 18, 113-115.

2. Hess, W.F. and Wyant, R.A., Welding Journal, 1939, 18,
   329S-335S and 348S-354S.

3. Tylecote, R.F., Welding Journal, 1941, Part 12, 591S-602S.

4. Roberts, W.L., Welding Journal, 1951, 30, 1004-1019.

5. Van Sciver, H.D., "Spot Weld Monitoring by Resistance Change"
   presented at A.I.E.E. 3rd Congress, Detroit, 1952.

6. Archer, G.R., Welding Journal, 1959, 38, 987-993.

7. Chuloshinkov, P.L. and Verdenskii, V.B., Automatic Welding,
   (Avt.Svarka), 1963, No.5, 9-13.

8. Johnson, K.I., "Evaluation of Resistance Spot Weld Quality
   Monitors", Welding Institute Research Report,
   Ref. P/46/70, September 1970.

9. Waller, D.N., British Welding Journal, 1964, 11, 118-122.

10. Prevost, R., Welding and Metal Fabrication, 1967, 35, 209-212.

11. Murray, E.E., Materials Evaluation, 1967, 25, 225-230.

12. Pittaway, R.G., Welding and Metal Fabrication, 1967, 35, 443-447.

13. Crecraft, D.I. and Warner, G., "Non-destructive Evaluation of
    Spot Welds using a New Technique", presented at the 6th
    Annual Conference and Exhibition organized by Ultrasonics,
    October 1970, London.

14. Welding Handbook, "Fundamentals of Welding", Section 1,
    American Welding Society, 5th Edition, 1963.

15. Resistance Welding Manual, Resistance Welder Manufacturers'
    Association, Philadelphia, Revised Edition, 1948.

16. Teece, C.J., Electrical Times, in three parts:
    (i) 1954, 126, 655-658; (ii) 1955, 127, 523-527;
    (iii) 1956, 130, 227-231.

17. Paxton, C.F. and Zeller, R., Welding Journal, 1962, 41, 556-562.

18. Grant, W.A., Welding Journal, 1962, 41, 563-567.

19. Lankin, Yu. N., Automatic Welding, 1963, No.5, 13-16.

20. Savage, W.F., Wassel, F.A. and Lundin, C.D., "The Static and
         Dynamic Resistance of Series Spot Welds", Research Report,
         Rensselaer Polytechnic Institute, New York, 1963.

21. Hayward, B.P., British Welding Journal, 1967, 14, 582-591.

22. Towey, M. and Andrews, D.R., Welding and Metal Fabrication,
         1968, 36, 383-392.

23. Knowlson, P.M., British Welding Journal, 1965, 12, 167-190.

24. Holm, R., Electric Contacts - Theory and Application,
         Springer-Verlag, Berlin/Heidelberg/New York,
         4th Edition, 1967.

25. Mott, N.F. and Jones, H., The Theory of the Properties of
         Metals and Alloys, Oxford University Press, 1936.

26. Powell, R.W., Journal of the Iron and Steel Institute,
         1949, 162, 320-324.

27. Smithells, C.J., Metals Reference Book, Volume II,
         Butterworths, London, 3rd Edition, 1962.

28. Greenwood, J.A. and Williamson, J.B.P., Proceedings of the
         Royal Society, 1958, 246A, 13-31.

29. Malmstadt, H.V. and Enke, C.G., Digital Electronics for
         Scientists, W.A. Benjamin, Inc., New York, 1969.

30. "High Performance Sample and Hold Circuit", Application
         Report B45, Texas Instruments Limited, 1968.

31. Beevers, A., British Welding Journal, 1963, 10, 173-183.

32. Greenwood, J.A., British Welding Journal, 1961, 8, 316-322.

33. Bently, K.P., Greenwood, J.A., Knowlson, P.M. and Baker, R.G.,
         British Welding Journal, 1963, 10, 613-619.

34. Truschenko, A.A. and Sukhova, O.V., Avt.Svarka (U.S.S.R.)
    1958, No.7, 44-47.

35. Gubenko, T.P. et al., Welding Production (Svar.Proiz),
    1963, No.2, 42-45.

36. Bhattacharya, S. and Andrews, D.R., Welding and Metal
    Fabrication, 1969, 37, 448-449.

37. Franson, K., Katz, S., and Raisen, E., "Some Radiation
    Characteristics of Blackbody Sources", Temperature,
    Its Measurement and Control in Science and Industry,
    3, Part 1, 529-535, Reinhold Publishing Corporation,
    New York, 1962.

38. "Silicon Photocell Applications", Application Report No.9,
    Ferranti Limited.

39. Smith, R.A., Jones, F.E. and Chasmar, R.P., "The Detection
    and Measurement of Infra-red Radiation", Oxford
    University Press, 2nd Edition, 1968.

40. Technical Bulletins and Data Sheets on "Fibrox" Light-guides,
    Rank Taylor Hobson.

41. Hyde, F.J., "Semiconductors", Macdonald & Company Limited,
    London, 1965.

42. Hewlett-Packard Application Notes 915 and 917, Hewlett-Packard,
    California, 1967.

43. Walker, J.A., "The Use and Applications of OPT1",
    Allen Clark Research Centre, The Plessey Co. Ltd., 1968.

44. Klein, G. and Van Zelst, J.J.Z., Precision Electronics,
    Philips Technical Library, Eindhoven, 1966.

45. Gel'man, A.S., Automatic Welding, 1961, No.7, 21-28.

46. Bowden, F.P. and Tabor, D., The Friction and Lubrication of
    Solids, Oxford University Press, 1954.

47. D'yachenko, P.E., Tolkacheva, N.N., Andreev, G.A. and
       Karpova, T.M., The Actual Contact Area Between Touching
       Surfaces, Authorized translation from the Russian,
       Consultants Bureau, New York, 1964.

48. Taz'ba, S.M., Automatic Welding, December 1959, 33-41.

49. Jones, F.L., The Physics of Electrical Contacts,
       Oxford University Press, 1957.

50. Alov, A.A. and Bulgachev, E.A., Automatic Welding, 1960, No.12,
       33-41.

51. Dix, A.F.J., British Welding Journal, 1968, 15, 7-15.

52. Hoerl, A.E. Jr., "Fitting Curves to Data" 20-55 - 20-77,
       Chemical Business Handbook edited by J.H. Perry,
       McGraw-Hill Book Company, 1954.

53. Joos, G., Theoretical Physics, Blackie and Son Ltd, London,
       3rd Edition, 1958.

54. Harrison, T.R., Radiation Pyrometry and its underlying
       Principles of Heat Transfer, John Wiley and Sons Inc.,
       New York, 1960.

55. Forsythe, W.E., Measurement of Radiant Energy, McGraw-Hill
       Book Company Inc., New York, 1937.

56. Nutter, G.D., "General Considerations Influencing the Design
       of High-accuracy Pyrometers", Temperature, Its Measurement
       and Control in Science and Industry, 3, Part 1, 537-549,
       Reinhold Publishing Corporation, New York, 1962.

57. Herne, H., British Journal of Applied Physics, 1953, 4, 374-377.

58. Ganowski, F.J. and Williams, N.T., "Advances in Resistance Spot
       and Seam Welding of Zinc Coated Steel Strip", presented
       at the Conference on Steel Sheet and Strip Welding,
       Kenilworth, 1972.

TEMPERATURE MEASUREMENT OF
RESISTANCE SPOT WELDS

S. BHATTACHARYA* and Dr. D. R. ANDREWS*

MEASUREMENT of temperature of the weld nugget in resistance spot welds has been investigated in various ways in the past, and even now with large scale application of resistance welding techniques it poses many problems. Nevertheless, its importance in analysing the thermal conditions at the weld spot can hardly be over-emphasized. The forging action occurring during the "Hold" or "Forge" period of the operation cycle can proceed to the best advantage when a substantial amount of metal at the sheet-to-sheet interface is in a semi-molten or plastic state. The semi-molten condition of metal at the weld is in turn dependent upon the temperature attained at the weld spot during the process of heat generation due to the passage of electric current.

The main problems facing previous workers[1,2,3] attempting measurement of temperature at the weld spot can be appreciated when one comprehends the general inaccessibility of the location and the brevity of operation time.

The method, outlined by Beevers[1] for measuring the temperature at the edge of the weld spot by using thermocouples in conjunction with specially prepared specimens, is a direct and standard method widely used in temperature measurement. However, the disadvantages in this method are:

1. The actual conditions at the weld spot are modified by the inclusion of the thermocouple itself.
2. The response of the thermocouple is slow compared to the process time of, say, 200—300 ms (milliseconds) using 50 c/s supply.
3. The technique does not lend itself to easy application under industrial conditions.
4. The thermocouple is usually destroyed after each weld.

Attempts by Bentley[2] and his co-workers are based on metallographic techniques, and in this method the actual weld specimen is simulated by using a spigot and ring combination. Macrosection of the spigot is analysed for specific microstructural changes, and isothermal contours and zones plotted. These authors claim good agreement between theory and experimental results. However, the limitation in this technique is because the simulated set-up excludes the sheet-to-sheet contact resistance and, therefore, does not take into account one of the most important factors affecting the process.

J. A. Greenwood[3] in his computer solution of the weld temperature distribution finds good agreement between the known experimental data and the computer solution. In spite of some simplifying assumptions this technique is very useful. Its principal drawbacks are that it does not take into account (a) the contact resistance at the sheet-to-sheet interface, and (b) the varying material properties at the weld junction.

A method which shows promise in experimental determination of temperature at the weld spot has been pursued through the initial stages and brief outlines of the technique are given in the following sections.

It is evident from the foregoing that conventional methods of temperature measurement which necessitate sampling of the thermal condition by direct conduction between the sensing element and the weld spot are bound to modify the physical process itself to some degree. This particular problem can be overcome if the temperature sensing element samples the thermal condition by radiative energy transfer.

Radiation pyrometry offers certain advantages under these circumstances (1) in not requiring any direct contact with the object of which the temperature is to be measured, and (2) the response time of a suitable detector element can be made very short, and, therefore, the brief process time presents no limitation.

The method of collecting thermal radiation from the weld spot, favoured in this instance, is by introducing a minute aperture at the tip of one of the electrodes. A typical electrode with the aperture is shown in Fig. 1.

Thermal radiation emanating from this aperture may be
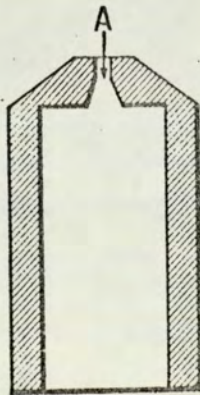
Fig. 1 (left). General appearance of electrode with aperture (sectional view). A: Minute aperture at the electrode tip for collecting thermal radiation from the weld-spot.

Fig. 2 (right). Optical radiation detector, inserted within the electrode. A: Optical radiation detector. B: Weld nugget. C: Active face of the optical radiation detector. D: Leads to the electronic processing system.

Fig. 3 (far right). Optical radiation transmitted to points remote from the machine. E: Active end-face of the fibre optic component. F: Fibre optic component.
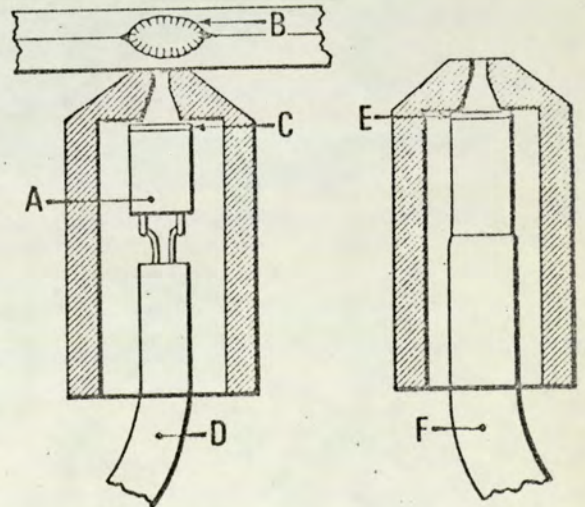
* S. Bhattacharya is a research student and Dr. Andrews a member of the staff at the University of Aston, Birmingham.

448

(a) received on the active surface of an optical radiation detector inserted within the electrode, or (b) transmitted by means of a fibre optic component to points remote from the machine for further processing and analysis. Methods (a) and (b) are depicted in Figs. 2 and 3 respectively.

The intensity of thermal radiation in a defined wavelength interval is a function of the temperature at the weld spot, according to Planck's radiation law[4,5]. Principles of radiation pyrometry[6,7,8,9,10,11] can be suitably adapted for measuring the temperature at the weld spot by analysing the thermal radiation collected through the aperture at the electrode tip.

The laws of radiation are accurate only for ideal black-body radiators, and since the conditions at the weld spot are not identical with those of an ideal black-body there would be some discrepancy in the results. However, considering that there is no suitable method for measuring experimentally the temperature of the weld spot, this technique promises some definite advantages.

Initial experimentation was carried out using a specially prepared electrode (Fig. 1) in the lower arm and a plain electrode in the upper arm. And no water-cooling was used for either electrode. The arrangement is shown in Fig. 4. The following observations were made:

1. Intensity of thermal radiation received on the active surface of a typical detector located as shown in Fig. 2 is appreciable during a normal spot weld and the electrical signal output of the detector element gives a reasonable indication of the thermal conditions of the weld spot.

2. The glow observed through a fibre optic component (Fig. 3) is a realistic visual indication of the thermal conditions at the weld spot. For example, increase of weld time or effective weld current is indicated by a change in the colour and brightness of the glow.

Investigation as to the quality of welds produced by using such specially prepared electrodes was carried out by tension-shear tests and macrosection tests in the following way:

Specimen welds, specified "a", were produced by using two plain electrodes; and specimen welds, specified "b", were produced by using the set-up of Fig. 4, where a specially prepared was used in the lower arm.

Tension-shear tests: Specimens "a" and "b" were tested for mechanical strength by tension-shear tests. Results of such tests indicate minimal reduction in failing load in the case of specimens "b". However, such reduction in mechanical strength was overcome by slightly increasing the electrode force.

Macrosection tests: Macrosection tests carried out using specimen types "a" and "b" indicate slight macrostructural change at the sheet-to-sheet interface immediately above the aperture in the case of specimen types "b".

It is hoped at this stage that (i) increased electrode force and (ii) water-cooling of both electrodes may eliminate the adverse effects observed in tension-shear tests and macrosection tests.

Although the idea was initially inspired by the need for a method of measuring temperature at the weld spot it will be evident from the foregoing that this method can also be applied in weld quality monitoring.

Thus the electrical signal output from the detector (visible radiation detector or infra-red detector) can be related to the temperature attained at the weld spot and suitable indication for overheating (splash), underheating (no weld) and optimum heating can be obtained. Since no mechanical transducer is involved, a monitoring system based on these principles would operate virtually with no time lag, that is, the physical conditions at the weld spot can be monitored with almost instantaneous response.

Fig. 4. Electrode arrangement used for producing specimen welds specified "b". A: Upper arm electrode holder. B: Plain electrode. C: Electrode with minute aperture at the tip. D: Specimen coupons to be welded. E: Lower arm electrode holder.
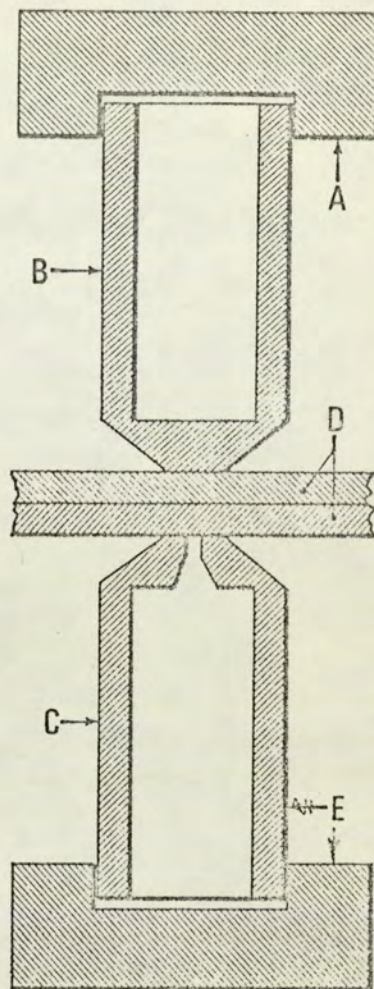
Hence an extension of this principle can be made use of in automatic control of weld quality. Thus automatic correction of weld parameters (current, time, etc.) can be carried out more easily (no interference with the working space) and with greater speed than similar systems employing mechanical transducers. In contrast to other systems it can readily be adapted for use with portable welding machines.

Details of experimental techniques and results may eventually be the subject of another paper in the near future and the authors regret the omission of such details in this article.

1. A. Beevers, Brit. Welding J., 1963, 10, 173-183.
2. K. P. Bentley, J. A. Greenwood, P. McK. Knowlson and R. G. Baker, Brit. Welding J., 1963, 10, 613-619.
3. J. A. Greenwood, Brit. Welding J., 1961, 8, 316-322.
4. E. U. Condon and H. Odishaw, Handbook of Physics (2nd Edition).
5. F. K. Richtmeyer and E. H. Kennard, Introduction to Modern Physics.
6. P. H. Dike, W. T. Gray and F. Schroyer, Leeds and Northrup Tech. Pub. A1.4000/1966.
7. M. H. Sweet, J. of the Optical Society of America, 1940, 30, 568-571.
8. H. W. Russel, C. F. Lucks and L. G. Turnbull, J. of the Optical Society of America, 1940, 30, 248-250.
9. Grover F. Hubing, J. of the Optical Society of America, 1936, 26, 260-261.
10. Thomas R. Harrison, Radiation Pyrometry and its underlying Principles of Radiant Heat Transfer (1960 Edition).
11. W. E. Forsythe (Edited by), Measurement of Radiant Energy (1937 Edition).

Resistance-weld quality monitoring

By S. BHATTACHARYA, B.Sc.(Hons.), Grad.I.E.R.E. (Department of Production Engineering, University of Aston in Birmingham) and D. R. ANDREWS, Ph.D., C. Eng., F.I.M., M.I.Prod.E. (Department of Production Engineering, University of Aston in Birmingham; director, Welding Liaison Ltd.)

The need for a suitable technique for inspection of spot welds by non-destructive means is recognized by the engineering industries in general, and, specifically, the sheet-metal-fabrication industries; the principal aim of any such technique must be to provide an 'in process' indication of the quality of the weld so that no separation inspection, at a later stage, is necessary.

The large number of inter-related variables inherent in the process itself can cause special problems. Measurement of welding current, weld time, electrode force and electrode movement is discussed along with the relative significance of such measurements in predicting weld quality. In addition, an assessment of the existing methods of monitoring weld quality is made with special reference to a method based on evaluation of the thermal condition of the weld. It has been found that an indication of the state of development of the nugget can be obtained by processing the thermal radiation from the centre of the weld.

Le besoin qui s'impose pour que soit élaborée une technique convenable pour le contrôle des soudures par points à l'aide de méthodes non-destructives est reconnu par les industries de la technogénie en général et notamment par celles dans le domaine de la fabrication de la tôlerie. Une telle technique devrait avoir pour objet principal de fournir une indication 'en cours de traitement' de la qualité de la soudure, évitant de ce fait la nécessité de procéder à un contrôle ultérieur.

Le nombre important de variables en corrélation, qui sont propres au procédé lui-même, peut poser des problèmes, particuliers. L'article passe en revue la mesure de l'intensité de soudure, de la durée de l'opération, de la force et du mouvement de l'électrode ainsi que l'importance relative de telles mesures dans la pronostication de la qualité des soudures. L'article présente en outre une appréciation des méthodes actuellement mises en oeuvre pour contrôler la qualité de la soudure, notamment la méthode basée sur une évaluation de l'état thermique de la soudure. Il a été constaté qu'une indication de l'état de développement du noyau peut être obtenue en analysant le rayonnement thermique en provenance du centre de la soudure.

Cette communication fut présentée à l'occasion d'une conférence organisée en mars 1972 sous les auspices de l'Institute of Sheet Metal Engineering du Welding Institute, et de la revue 'Sheet Metal Industries'.

Die Notwendigkeit eines geeigneten Verfahrens zur Kontrolle von Punktschweissungen durch zerstörungsfreie Prüfung wird von der Industrie im allgemeinen und den blechverarbeitenden Industriezweigen im besonderen anerkannt. Ein solches Verfahren muss als Hauptziel die Lieferung einer während des Schweissvorgangs erfolgenden Anzeige der Schweissgüte haben, die eine besondere Inspektion zu einem späteren Zeitpunkt überflüssig macht.

Die grosse Zahl der beim Schweissvorgang auftretenden und in Wechselbeziehung zueinander stehenden Veränderlichen kann besondere Probleme verursachen. Der Aufsatz behandelt die Messung von Schweissstrom, Schweisszeit, Elektrodenkraft und Elektrodenbewegung sowie die relative Bedeutung dieser Messungen für die Bestimmung der Schweissgüte. Er gibt ausserdem eine Beurteilung der bestehenden Verfahren zur Kontrolle der Qualität von Schweissungen mit besonderer Berücksichtigung einer auf Auswertung des thermischen Zustandes der Schweissstelle beruhenden Methode. Es wurde festgestellt, dass sich ein Aufschluss über den Entwicklungsstand der Linse durch Messung der Warmestrahlung aus der Mitte der Schweissstelle gewinnen lässt.

Dieser Aufsatz bildete einen Beitrag zu der von the Institute of Sheet Metal Engineering, the Welding Institute und 'Sheet Metal Industries' im März 1972 veranstalteten Konferenz über Schweissen von Stahlblech und Stahlband'.

La necesidad de disponer de una técnica adecuada para la inspección de las uniones soldadas por puntos empleando métodos no destructivos está reconocida por las industrias de ingeniería en general y, de modo particular, las industrias dedicadas a las construcciones de chapa metálica; el principal objetivo de toda técnica de esa clase ha de ser el de proporcionar una indicación de la calidad de la soldadura mientras está realizándose la misma, de manera que no haya necesidad de hacer ulteriormente una inspección aparte.

El gran número de variables interconexas inherentes al propio proceso de soldadura puede ocasionar problemas especiales. En este trabajo se explican las mediciones de la corriente de soldadura, del tiempo invertido en la misma, la fuerza y movimiento de los electrodos, así como la importancia relativa que tienen dichas medidas en la predicción de la calidad de la soldadura. Además se hace una evaluación de los actuales métodos de observación de la calidad de las uniones, con especial referencia a un método basado en la evaluación de la condición thémica de la soldadura. Se ha hallado que puede obtenerse una indicación del estado de desarrollo del punto de la soldadura analizando la radiación térmica desde el centro de la soldadura.

Este trabajo fue presentado en una conferencia sobre 'La soldadura de chapa y banda de acero', organizada por la Institute of Sheet Metal Engineering, the Welding Institute y 'Sheet Metal Industries', en marzo de 1972.

1. INTRODUCTION

1.1 Inspection and testing of spot welds

IN THE METAL fabrication industry in general, resistance-spot welding is a well-established production process; the inspection and testing of spot-welded joints is incorporated in the production line in many instances as a routine measure to ensure reliability of the welds. If the safety requirements imposed upon the motor cars manufactured and marketed in the USA are considered, then the indications are that the inspection of spot welds for 'quality' and consistent 'quality control' under production conditions will be of greater importance to all concerned in the years to come. In the context of testing or inspection of spot welds, the term 'quality' is used to mean 'suitability for service', involving as it invariably does an occasional misuse or overload. The term 'quality control', in this context, will be used to denote 'maintenance of an agreed quality'.

Spot welds can be tested for quality using destructive as well as non-destructive methods. Both macro-examination and the tension shear test, commonly employed for destructive testing, give comparatively positive indications of weld quality. The objections to the destructive methods of testing, under production conditions, stem from the following reasons:

a The tension-shear test is not always suitable unless the shape and size of the work-piece falls within certain limits; the macro-etch test can be carried out only on a small number of specimens from a production batch. Moreover, both these destructive methods of inspection are time consuming.

b No corrective action can be undertaken during the actual welding operation.

The aim of a suitable technique for inspection of spot welds by non-destructive means should be to provide an indication of the quality of the weld *during welding*, so that no separate inspection at a later stage is necessary. The term 'monitoring', in this context, is used to denote such in-process techniques of non-destructive inspection. Any consistent indication which is observable as a manifestation of the physical processes during a spot weld and is thus indicative of the state of nugget growth may be termed a 'process parameter'.

1.2 Brief survey of the various monitoring techniques

The fact that some relationship exists between the state of development of weld nugget and the pattern of variation exhibited by the electrical resistance of the weld has been known to the researchers in the field for some time. Similar
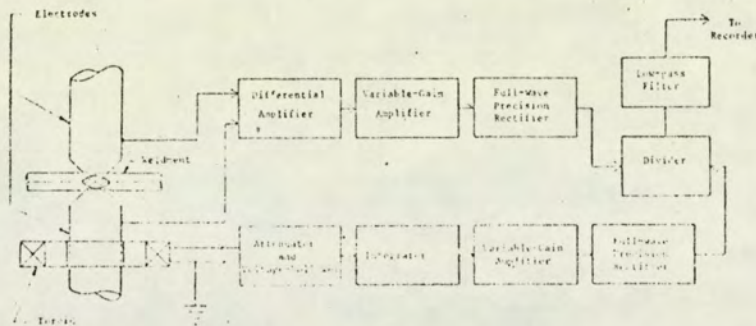
Fig 1 (above) Block diagram of electronic instrumentation system for computing dynamic resistance of weld.

Fig 2 (right) Recordings of dynamic resistance for two x 0.9mm mild-steel specimen coupons (a) 6100A; (b) 6700A; (c) 8000A splash.
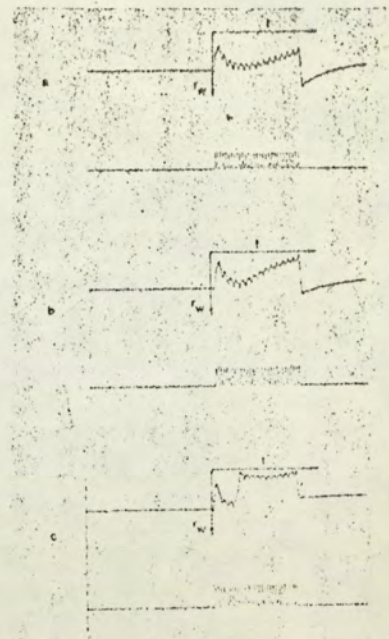
investigations have also been undertaken in attempts to relate weld voltage or electrode voltage to nugget growth. Attention has also been drawn to the fact that the thermal expansion of the weldment, detectable as a relative movement of one electrode with respect to the other, can be utilized in monitoring weld quality. Finally, in recent years, ultrasonic techniques have also been developed for monitoring weld quality.

Although various degrees of success have been claimed for the monitoring techniques cited above, some confusion still exists as to the selection of the most reliable technique under industrial conditions.

1.3 Machine, materials, and process parameters under investigation

(a) Welding machine and electrodes

A 10kVA bench spot/projection welder, in conjunction with an electronic control unit, has been used in the current investigation; both the machine and the electronic control unit were manufactured by the British Federal Welder and Machine Co Ltd. Sciaky Tiptrodes with truncated-cone tips of 4.76mm (0.1875in) diameter have been used.

b Materials

For the present investigation, low-carbon mild steel containing less than 0.1 per cent carbon has been used.

c Process parameters under investigation

Dynamic resistance and thermal condition of the weld are the two process parameters which have been monitored and correlated to weld quality. The quality of the spot welds has been tested according to the established procedures of tension-shear test and macro-etch test. In the absence of any well-defined specifications for weld quality, acceptability of a weld has been arbitrarily decided from such destructive tests and related to the monitored indications.

2. DYNAMIC RESISTANCE VARIATION AND ITS APPLICATION IN WELD QUALITY MONITORING

2.1 Dynamic resistance and static resistance

The rate of heat generation in a resistance-spot weld is in accordance with the principle of Joule heat generation in a resistive element and therefore the electrical resistance of the weld is an important parameter governing the progress of weld nugget formation.

The term 'instantaneous' or 'dynamic' resistance refers to the quotient $\dfrac{v_w}{i_w} = r_w$, where v_w and i_w represent instantaneous values of weld voltage and welding current respectively. Weld voltage, in this context, may be defined simply as the voltage drop across the weldment. The dynamic resistance of the weld is modulated by the process itself during welding. In contrast, the static resistance offered by the work-piece, held under pressure, in the absence of any welding current, is a combination of the bulk resistance of the material and the constriction or contact resistance due to the electrode-to-sheet and sheet-to-sheet contacts. Although the initial static resistance can and does influence the welding process, it can in no way indicate or characterize the physical process during welding.

2.2 Electronic instrumentation system for monitoring dynamic resistance

With the exception of Van Sciver[1] and Hayward[2], the previous workers calculated dynamic resistance from the recorded waveforms of weld voltage and welding current. To explore the potential of dynamic resistance as a parameter indicative of weld quality, it is necessary to devise methods so that the resistance may be obtained as an in-process parameter in the form of a recorded trace. Moreover, any possible application of dynamic resistance in controlling weld quality requires that an electrical signal representative of dynamic resistance be available.

A block diagram of the instrumentation system developed for this purpose is shown in Fig 1, the operation of the system being described below.

The difference of voltages appearing across the electrodes is obtained as the output of the differential amplifier and is amplified before conversion to a dc voltage e_v by the full-wave precision rectifier. Again, the output of the toroid is attenuated and integrated; the output of the integrator is amplified by means of a variable-gain amplifier and is taken through a full-wave precision rectifier to produce the dc voltage e_c. Voltage signal e_c is a unidirectional representation of the welding current.

The function of the divider stage is to operate on the inputs e_v and e_c, and produce the output E_o given by,

$$E_o = -10 \cdot \frac{e_v}{e_c} \qquad (2.1)$$

The low-pass filter eliminates spurious signals of higher frequencies so that a clearer recording of the output signal is obtained.

2.3 Typical recordings of dynamic resistance

Typical recordings of dynamic resistance when welding two 0.9mm mild steel specimen coupons are shown in Fig 2, the following machine settings being used for this purpose:

Electrode Force—1560N, corresponding to 0.5N/mm² on the pressure gauge.
Transformer Tapping—No. 6.
Weld Time—15 cycles.

The welding current was varied by adjusting the weld heat control knob, which controls the firing angle of the ignitrons.

The following observations are made from an inspection of the recorded traces shown in Fig 2.

i With low current values, the resistance trace does not show a prominent peak; with increased welding current, however, a well-defined peak appears in the recorded trace.

ii With higher current values, the position of the peak is shifted towards the left; in other words, the maximum or peak resistance occurs earlier during a weld.

iii For welds produced with high currents the resistance trace indicates a lower value of resistance towards the completion of weld time.

iv A splash weld, caused by excessive welding current, is characterised by a sudden step in the resistance trace.

Further investigation shows that the pattern of dynamic resistance variation is modified by the selection of the welding variables such as weld time, electrode force, and other external conditions.

2.4 Utilization of dynamic resistance characteristics in weld-quality monitoring

Under certain conditions, an indication signifying completion of a good weld may be all that is necessary. A simple technique outlined below may be adequate for this purpose.

The redrawn characteristics of weld voltage, welding current and dynamic resistance obtained for a good weld in mild steel are shown in Fig 3. Curve 'b' may be obtained using a slightly modified instrumentation system whereby the values of dynamic resistance for a test weld are sampled at the instants marked t_1, t_2, ... t_5 and stored in electronic memory.

The sampled values of dynamic resistance for the test weld may be compared with the resistance values sampled at the predetermined instants for subsequent welds. All subsequent welds,

where the resistance values at the instants t_1, t_2, ... t_5 are in agreement with those for the test weld within an acceptance band, may be declared as good as the test weld made initially. A green light, for example, may indicate that the welds are within the limits of agreed quality, thus ensuring the operator of a consistent production of good welds.

3 THERMAL CONDITION OF THE WELD AS A PROCESS PARAMETER IN MONITORING WELD QUALITY

3.1 Significance of thermal condition as a process parameter in spot welding

During a spot weld Joule heating occurs in the bulk resistance of the specimen coupons as well as in the contact resistance effective at the electrode-to-sheet and sheet-to-sheet interfaces. The resulting change in the thermal condition sets off the complex chain of events. The physical phenomena observable as variation in the electrical resistance of the weld and electrode separation are manifestations of the thermal changes effecting the weldment. Furthermore, if the process of spot welding is thought of as a method of forging an intimate metallic bond between two pieces of metal, then it is essential that the mass of metal held between the electrode tips must be raised to an adequately high temperature for the forging action to be effective. It will, therefore, be appreciated from the preceding logic that thermal changes occuring in the weldment are more fundamental in nature, and knowledge of thermal condition of the weld is of immense significance in assessing the progress of nugget development.

It is interesting to note at this juncture that the significance of thermal condition or temperature as a process parameter in predicting weld quality was appreciated by Archer[3] and his 'voltage-constraint' principle was an attempt to relate weld voltage to the 'ultimate temperature' attained by the weld at 'heat balance'. The close connection between nugget dimensions and the temperature of metal in the nugget prompted Chuloshinkov[4] et al to suggest the use of temperature as a process parameter. However, because of practical difficulties in measuring the temperature of the weld, the indirect method proposed by Archer was suggested by Chuloshinkov et al as the possible solution. It can, however, be shown that Archer's equation relating weld voltage and weld temperature lacks the rigour of the classical ψ–θ theorem.[5, 6]

3.2 Detection of thermal radiation from the weld surface as a means of assessing the temperature distribution within the weld

It is common experience in resistance-spot welding that, with adequate heat input, the weldment in the vicinity of the electrodes is heated to incandescence; the visible radiation thus emitted by the incandescent metallic mass may be observed from a distance without the aid of any special apparatus. Since the radiant intensity of an incandescent body can be related to its temperature according to Planck's radiation law or Wien's radiation law[7], the nature and intensity of thermal radiation emitted by the weld surface can be taken as an indication of the temperature of the weld surface. Again, the result of Greenwood and Williamson[8], based on the ψ–θ theorem indicate that the
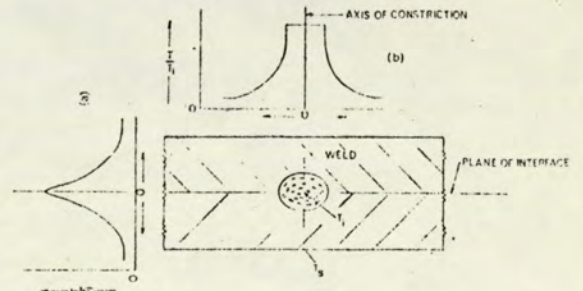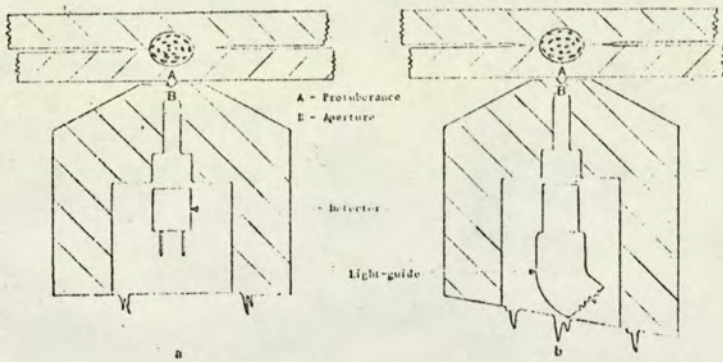
Fig 3 (left) Curves of weld voltage, current and dynamic resistance for good weld in mild steel.
Note: Resistance curve is redrawn in the positive quadrant.

Fig 4 (right) Temperature distribution in spot weld related to maximum temperature T_1 at the centre.
(a) Variation along the axis of constriction; T_s represents surface temperature.
(b) Variation in the plane of the interface.

temperature at the weld surface can be related to the maximum temperature at the centre of the nugget. This is illustrated in Fig 4; temperature T_s of the weld surface is determined by the maximum temperature T_i at the centre. It may, therefore, be assumed that the temperature of the weld surface is an indication of the state of affairs existing at the centre of the weld, and the existence of a molten pool of adequate size may be confirmed or negated by the attainment of a specific surface temperature.

It seems that various attempts[9, 10] made in the past in developing monitoring techniques along these lines have not met with such success, mainly because of the practical difficulties in gaining access to the weld spot. For the present investigation, however, a technique has been developed[11] which permits collection of thermal radiation through an aperture, located centrally at the tip of the bottom electrode. The underlying principle of this technique is illustrated in Fig 5.

3.3 Methods of visual observation and photoelectric detection of thermal radiation
3.3.1 Visual observation of weld glow
Some initial experimentation was conducted by observing the glow of the weld by means of a light-guide inserted within the bottom electrode. An approximate indication of the temperature of the weld surface can be obtained from the colour and intensity of the glow thus observed. For example, during a satisfactory weld, the dull red glow shortly after initiation changes to a bright red; on the colour charts[12], dull red denotes a temperature of the order of 600deg C–700deg C, and bright red corresponds to a temperature range 800deg C–900deg C. Excessive current resulting in a splash weld produces a bright orange flash, indicating a surface temperature in the region 900deg C–1100deg C. In view of the very brief period of observation, it is suggested that a cine camera, used in conjunction with colour films, may yield more objective results.

3.3.2 Methods of photoelectric detection
(a) *Direct incidence mode detection*
In the direct incidence mode, the detector is located inside the electrode or in the hollow of the electrode holder; thermal radiation from the centre of the weld spot is *directly incident* upon the active surface of the detector, through the aperture at the tip of the bottom electrode. The photodetector transforms the radiation signal into an electrical signal which is then processed to derive the relevant information.
(b) *Remote transmission mode detection*
In the remote transmission mode, the radiation detector is *located remote* from the machine, a light-guide or fibre-optic component, one end of which is located inside the electrode, *transmits* the radiation onto the detector. This conversion of radiant power to an electrical signal as well as further processing of the signal are carried out away from the welding machine.
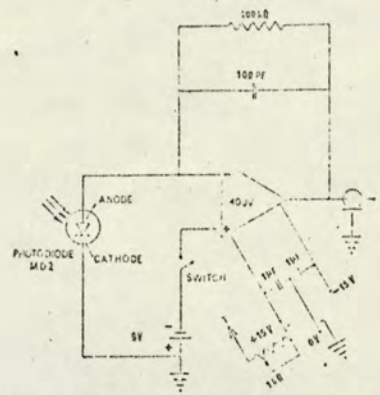
3.4 Typical recordings of monochromatic radiant emission from the weld surface and its correlation to nugget growth
3.4.1 Remote transmission mode detection system employing a silicon P-I-N photodiode
The detection system employed to obtain recordings of monochromatic radiant intensity is outlined below.

One end of a Fibrox light-guide is inserted within the bottom electrode and held in position, concentric with the aperture at the electrode tip, a Sciaky tiptrode being used in this instance. The transmitting end of the light-guide is taken outside through a slot at the base of the electrode holder. The transmitted radiation is incident upon a silicon P-I-N photodiode located within a light-proof enclosure, a red glass filter with 99 per cent transmittance in the waveband between 0.76 μm and 1.8 μm being used to provide monochromatic spectral isolation. Except for the initial current-to-voltage transduction stage the remainder of the electronic circuitry is placed within a separate enclosure.

The circuit configuration depicting the P-I-N photodiode operating in conjunction with the current-to-voltage transduction stage is shown in Fig 6. The photocurrent output of the reverse-biased P-I-N photodiode is transformed into a voltage signal, which is amplified by means of a tuned amplifier. The tuned amplifier, in this instance, has been designed for a centre frequency of 100Hz, employing an operational amplifier with a twin-T resistance-capacitance network in the feedback loop.

3.4.2 Interpretation of monochromatic radiant intensity recordings in weld quality monitoring
The intensity of thermal radiation from the weld goes through a maximum at the instant of peak welding during each half-cycle of weld time. This is equivalent to chopping the radiation signal at 100Hz, and the voltage signal appearing at the ouput of the current-to-voltage transduction stage is an amplitude modulated waveform with 100Hz as its carrier frequency. Thus, by taking the output of this stage through a tuned amplifier, an amplitude modulated signal representing the varying thermal condition of the weld surface can be recorded.

The recorded traces shown in Fig 7 are obtained when two 0.9mm low-carbon mild-steel specimen coupons are spot welded with machine settings similar to those cited in 2.3 in the context of dynamic resistance recordings. The following observations can be made from an inspection of the recorded traces, which illustrate the effect of varying the current by means of phase-shift heat control.

(i) With low welding current, the temperature attained by the weld surface is such that only a small proportion of the emitted radiation falls within the optical pass-band of the detection system; therefore, the amplitude of the recorded trace is small.

i A 'peak' appears in the voltage trace as well as in the resistance trace.

ii Corresponding to the 'peak' in the voltage trace a 'valley' occurs in the current trace.
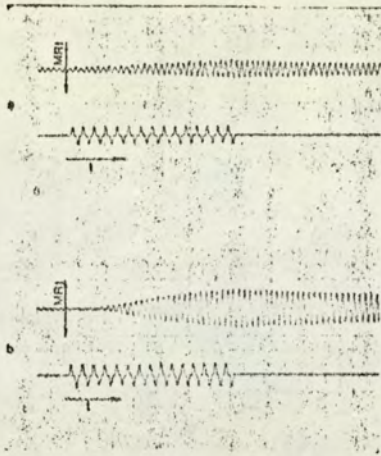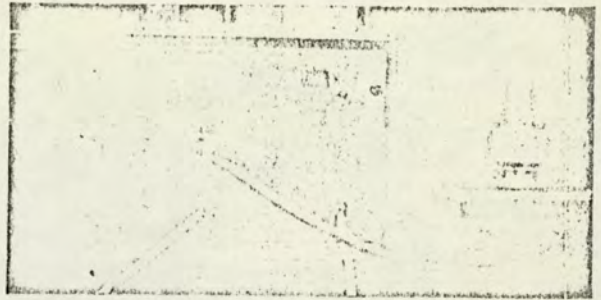
As the current is increased, the monochromatic radiant intensity increases and is recorded as a signal of higher amplitude.

(ii) With a high current, a high temperature is attained by the weld surface earlier during a weld; this is demonstrated by the earlier occurrence of the peak in the monochromatic radiant intensity curve.

Monochromatic radiant intensity recordings were also obtained by altering the welding variables such as weld time and electrode force, and other external conditions such as surface condition of the emitting weld surface. The influence of the various factors affecting temperature distribution within the weld, and therefore nugget growth, can be determined from an analysis of the monochromatic radiant intensity traces obtained for different welding conditions. Thus the monochromatic emission characteristics can be used to confirm or negate the completion of a good weld, or to establish whether the correct welding variables have been selected for a specific situation.

Finally, it may be pointed out that the experimental investigation was initially conducted without any water-cooling of the electrodes because of the complication arising from the inclusion of an aperture at the electrode tip. Since then, however, additional work has been undertaken at Aston University with a view to incorporating a suitable cooling system; a photograph of the compact electronic instrumentation system, which may subsequently be developed into a commercial monitor, is shown in Fig 8.

4. CONCLUSIONS AND COMMENTS
4.1 Welding current, weld voltage and dynamic resistance as process parameters in weld-quality monitoring

Extensive experimental investigation has been carried out to establish that the patterns of variation exhibited by voltage, current and resistance can be related to the execution of a good weld in mild steel, to variable degrees of certainty.

The use of a current meter in conjunction with a toroid is the normal practice in most metal fabrication industries, in selecting the desired welding current for a specific situation; such current meters usually register the 'peak r.m.s.' current or the r.m.s. current over the total weld time. Although an approximate estimation of the current used during a weld is of some importance in selecting the desired welding variables and, to a certain degree, in predicting the formation of a weld nugget, the current value in itself signifies very little as to the process of nugget formation because of the other factors affecting nugget growth. For example, with inadequate electrode force or large-diameter electrode tips the current values can be misinterpreted. It is, therefore, suggested that the shape of the current trace should be taken into account along with the current value for a more reliable assessment of weld quality.

The following features may be noted from an inspection of the curves of Fig 3.

Again, referring to the recordings of Fig 2 it is apparent that the sudden 'drop' in the resistance trace during a splash weld is also accompanied by a sudden 'rise' in the current trace. The voltage trace during a splash weld, although not illustrated here, shows an abrupt 'drop' in voltage similar to the resistance trace.

In the controversy regarding the choice between weld voltage and weld resistance as a parameter in monitoring and controlling weld quality the two major factors in favour of weld resistance may be summed up as below.

Firstly, in computing dynamic resistance, both weld voltage and welding current are taken into account, and therefore dynamic resistance is more meaningful than either voltage or current taken singly as a process parameter. Secondly, in spite of claims as to the successful application of weld voltage as a process parameter in controlling weld quality on the basis of Archer's 'voltage-constraint' principle, the weld temperatures predicted by Archer's equation are far in excess of experimental results[13] supported by the classical $\psi-\theta$ theorem.

4.2 Comparison of thermal condition and dynamic resistance of the weld as process parameters in monitoring weld quality
i Monitoring thermal condition is a first-order technique

As explained earlier, the thermal changes occurring in the weldment due to Joule heating are primary or first-order changes. In contrast, the process parameters such as dynamic resistance and thermal expansion are second-order effects brought about by thermal changes in the metal held between the electrode tips.

Therefore, monitoring techniques based on assessment of thermal condition of the weld can be classified as first-order techniques, and may be regarded as more effective in indicating the process of nugget formation. The monitoring techniques dependent upon second-order changes, on the other hand, may be termed second-order techniques, and are comparatively less effective in indicating the more fundamental changes which govern the formation of a weld.

II Monitoring thermal condition is preferred when spot welding stainless steel and aluminium alloys

Dynamic resistance characteristics of stainless steel and certain aluminium alloys do not suggest[14,15] the existence of any consistent pattern which can be related to the progress of nugget formation. Thus, monitoring the thermal condition of the weld may provide a more reliable indication of nugget growth when welding stainless steel and some aluminium alloys.

4.3 Effects on weld quality due to the inclusion of an aperture at the electrode tip when monitoring thermal radiation

A small protuberance or 'pip' usually appears on the weld surface due to plastic flow of weld metal into the aperture at the electrode tip, and this usually raises the question whether the
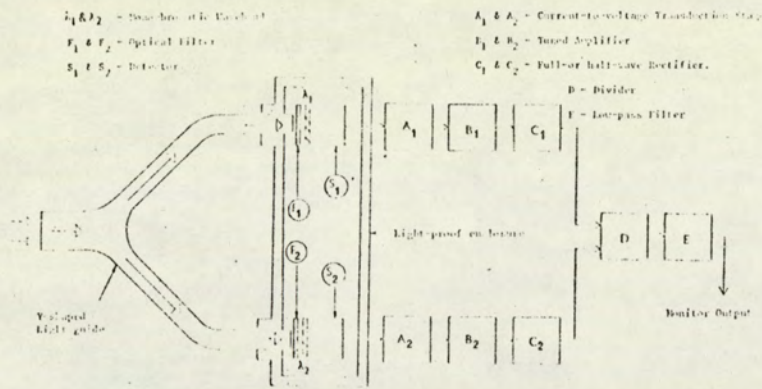
Fig 9 Block diagram of proposed monitoring system based on bichromatic response ratio measurement.

presence of the aperture itself affects the quality of the weld in any way. The results of investigation, specifically undertaken* to provide a definite answer to this question, has shown that the weld defects which usually occurred when using standard electrodes without any aperture were not in any way worsened due to the inclusion of a minute aperture; also, no noticeable reduction in the mechanical strength of the welded joint occurred due to the aperture.

4.4 Bichromatic response ratio technique of temperature measurement

The spectral radiant intensity at wavelength λ, of a thermal source at temperature T is given by $\epsilon_\lambda.J(\lambda.T)$, where ϵ_λ is the spectral emittance of the radiating source, and $J(\lambda.T)$ is defined as the spectral radiant intensity of a blackbody at temperature T. The function $J(\lambda.T)$ can be expanded according to Planck's radiation law or Wien's radiation law. Variation in spectral emittance ϵ_λ due to different surface conditions, material properties and change in temperature introduces a certain amount of inaccuracy in the indicated output of a monitoring system based on monochromatic radiant intensity measurement. To overcome such inaccuracies, it is suggested that the principle of bichromatic response ratio measurement[16, 17] be used in relating the thermal condition of the weld to the monitor output. In the bichromatic response ratio technique, the ratio of response of two detectors at two different wavebands may be related to the thermal condition of weld, thus eliminating the effects of common factors affecting ϵ. The design of a proposed monitoring system

*M.Sc. project of P. R. Ellis, entitled 'A study of the effects arising out of a change in electrode geometry upon weld quality and welding schedules in resistance-spot welding', Department of Production Engineering, University of Aston in Birmingham, October 1970.

based on bichromatic response ratio measurement is shown in Fig 9.

References ·

[1] Van Sciver, H. D., 'Spot Weld Monitoring by Resistance Change', presented at A.I.E.E. 3rd Congress, Detroit, 1952.
[2] Hayward, B. P., British Welding Journal, 1967, 14 (11), 582-91.
[3] Archer, G. R., Welding Journal, 1959, 38 (10), 987-93.
[4] Chuloshinkov, P. L., & Verdenskii, V. B., Automatic Welding, 1963, 16 (5), 9-13.
[5] Holm, R., Electric Contacts—Theory and Application, Springer-Verlag, Berlin/Heidelberg/New York, Fourth Edition, 1967.
[6] Jones, F. L., The Physics of Electrical Contacts, Oxford University Press, 1957.
[7] Harrison, T. R., Radiation Pyrometry and its underlying Principles of heat transfer, John Wiley and Sons Inc., New York, 1960.
[8] Greenwood, J. A., & Williamson, J. B. P., Proceedings of the Royal Society, 1958, 284A (12244), 13-31.
[9] Truschenko, A. A., & Sukhova, O. V., Avt. Svarka (USSR), 1958, 11 (7), 44-47.
[10] Gubenko, T. P., et al, Welding Production, 1963, 10 (2), 42-45.
[11] Bhattacharya, S., & Andrews, D. R., Welding and Metal Fabrication, 1969, 37 (11) 448-49.
[12] Smithells, C. J., Metals Reference Book, Vol. 11, Butterworths, London, Third Edition, 1962.
[13] Bentley, K. P., Greenwood, J. A., Knowlson, P. M., & Baker, R. G., British Welding Journal, 1963, 10 (12), 613-19.
[14] Roberts, W. L., Welding Journal, 1951, 30 (11), 1004-19.
[15] Towey, M., & Andrews, D. T., Welding and Metal Fabrication, 1968, 36 (10) 383-92.
[16] Herne, H., British Journal of Applied Physics, 1953, 4 (12), 374-77.
[17] Ackerman, S., 'Notes on the Design & Performance of a two-colour pyrometer', Temperature, Its Measurement & Control in Science and Industry, Vol. 3, Part 2, 849-57, Reinhold Publishing Corp, New York, 1962.